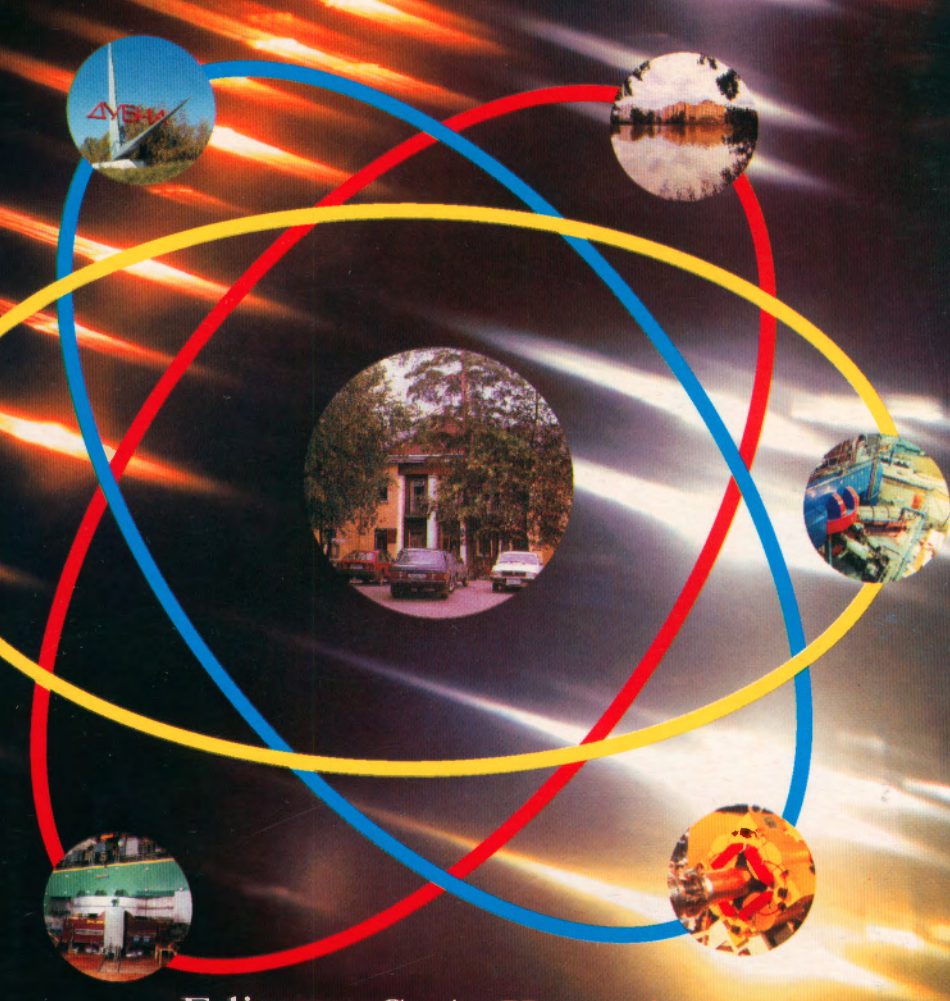






7th AFOSR Workshop

# ISOMERS and QUANTUM NUCLEONICS



Editors: S. A. Karamian

J. J. Carroll

E. A. Cherepanov

C 341:2/04) I - 85

Экз.чит.зала

# ISOMERS AND QUANTUM NUCLEONICS

### 7th AFOSR Workshop

Dubna, June 26 – July 1, 2005 Proceedings of the Workshop УДК [539.144.7+539.172.3+539.184.26+539.166] (092) ББК 22.383.4я431 22.343я431 185

The contributions are reproduced directly from the originals presented by the Organizing Committee.

Isomers and Quantum Nucleonics: Proceedings of the 7th AFOSR Workshop (Dubna, June 26 – July 1, 2005) / Eds. S. A. Karamian, J. J. Carroll, and E. A. Cherepanov. — Dubna: JINR, 2006. — 223 p.; 31 photos.

ISBN 5-9530-0105-3

The 7th International Workshop «Isomers and Quantum Nucleonics» was held at the Joint Institute for Nuclear Research, Dubna, Russia, from June 26 to July 1, 2005, extending a series of Workshops supported by the United States Air Force Office of Scientific Research. These meetings have been focused on research results that related to the promise of nuclear isomer-energy release for applications, in particular on perspectives for the creation of a gamma-ray laser and on the so-called induced, or triggered, release. Among the topics of the present Workshop were general approaches to triggering, a problem of the isomeric nuclei production, the studies of nuclear excitation with photons, electrons and plasma interactions, and nuclear decay modification by external conditions in atomic and solid-state surroundings. The Proceedings therefore collect papers into six sections that reflect these different, yet interwoven subjects.

**Изомеры** и квантовая нуклеоника: Труды 7-го рабочего совещания при поддержке AFOSR (Вашингтон) (Дубна, 26 июня – 1 июля 2005 г.) / Под ред. С. А. Карамяна, Дж. Дж. Кэрролла, Е. А. Черепанова. — Дубна: ОИЯИ, 2006. — 223 с.; 31 фото.

ISBN 5-9530-0105-3

7-е Международное совещание «Изомеры и квантовая нуклеоника» было проведено в Объединенном институте ядерных исследований (Дубна, Московская обл., Россия) с 26 июня по 1 июля 2005 г. Оно продолжило серию совещаний, организованных при поддержке Отдела научных исследований американских Воздушных сил (AFOSR). Тематика этих совещаний сконцентрирована на результатах исследований, обещающих применение изомеров в качестве источника энергии, в частности в направлении перспектив создания гамма-лазера и так называемого триггеринга или индуцированного высвобождения изомерной энергии. Среди тем настоящего рабочего совещания: общие подходы к проблеме триггеринга, возможности получения изомерных ядер, исследования возбуждений ядер под действием фотонов, электронов и при взаимодействии с плазмой, а также модификация распада ядер во внешней среде, в атомах и твердом теле. Таким образом, собранные в Трудах работы распределены по шести секциям, что отражает их различную, но внутренне взаимосвязанную тематику.

#### **PREFACE**

The 7th International Workshop on "Isomers and Quantum Nucleonics" is a continuation of the outstanding series of meetings initiated and supported by the US Air Force Office of Scientific Research (AFOSR). Initial meetings were organized in Romania between 1995 and 1997 and the international dialog and exchange of ideas were continued during the past decade with subsequent Workshops being held at various sites:

2nd AFOSR Isomer Workshop, Telluride, Colorado, USA, May 2001 3rd AFOSR Isomer Workshop, Tucson, Arizona, USA, December 2001 4th AFOSR Isomer Workshop, Albuquerque, New Mexico, USA, October 2002 5th AFOSR Isomer Workshop, Hamburg, Germany, August 2003 6th AFOSR Isomer Workshop, Nizhny Novgorod, July 2004

Traditionally, a group of Russian physicists have been quite active in exploring a number of areas of interesting research. Most recently, the 6th AFOSR Isomer Workshop was organized by the Institute of Applied Physics, RAS, Nizhny Novgorod within the International Conference "Frontiers of Nonlinear Physics." That meeting was held aboard the cruise ship "Georgy Zhukov," traveling on the Volga from Nizhny Novgorod to St. Petersburg.

For the 2005 Workshop, the international nuclear science center - Joint Institute for Nuclear Research - provided the infrastructure facilities, the organizational efforts and great hospitality from June 26 to July 01, 2005. The Workshop was supported by AFOSR and Youngstown State University (YSU) and was headed by Professors J.F. Agee (Washington) and M.G. Itkis (Dubna). The Organizing Committee included Program Co-Chairmen J.J. Carroll (Youngstown) and S.A. Karamian (Dubna), and Scientific Secretary E.A. Cherepanov (Dubna).

The Workshop program surveyed the state-of-the-art in research in fields related to mechanisms and means of inducing, or triggering, the release of energy stored in metastable isomeric states as well as selected problems of isomer production and decay. Following this general idea, six topical Sections of the Workshop are presented herein:

- Sec. 1. General perspectives on isomer triggering;
- Sec. 2. Studies with selected isomers;
- Sec. 3. Photon-induced processes;
- Sec. 4. Electron-assisted nuclear transitions;
- Sec. 5. Nuclear excitations in plasma:
- Sec. 6. Studies with Moessbauer techniques.

Among the submitted papers are reports containing new results on interactions of isomeric nuclei with electromagnetic radiation or a slow neutron bath, also being contained within plasma or in a condensed state and influenced by external fields.

Electron-assisted nuclear excitations may manifest themselves as the most promising processes for efficient isomer triggering. More general discussions are included as well, in particular on coherent wave processes and the associated gamma-ray laser concept.

A total of forty scientists from five countries took part in the 7th AFOSR Workshop on Isomers and Quantum Nucleonics. Their specializations are relatively wide and interdisciplinary and this was integral to discussions of the modern progress in the field of interest. The volume of Proceedings includes most of the presented talks, and it is hoped that this collection will give the reader a realistic view of issues presented in the Workshop. To our regret, a small number of speakers failed to submit papers for inclusion in this volume. The subjects contained in this volume nevertheless demonstrate the value of the Workshop to the participants, and in providing important communications between those participants and young colleagues and students working at JINR, Dubna for their education.

Taking this good opportunity, we would like to thank all the participants for their keen interest and valuable contributions to the meeting. We also thank the Administrations of JINR, Dubna and YSU for their support of this endeavor. Financial support by AFOSR grant via YSU is gratefully acknowledged.

Co-chairmen
Forrest J. Agee
Air Force Office of Sci. Research,
Washington
Mikhail G. Itkis
Joint Institute for Nuclear Research
Dubna, Moscow region
7th AFOSR Workshop on Isomers and
Quantum Nucleonics





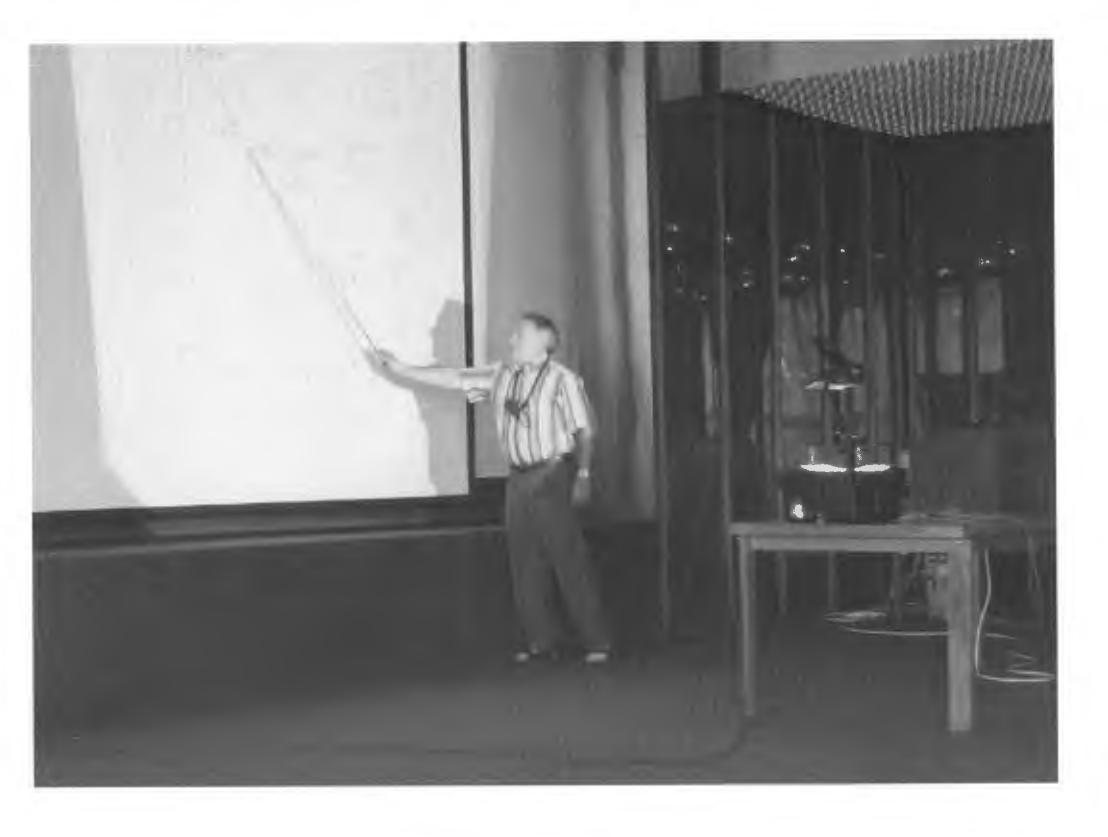


























































#### Co-chairmen:

Forrest Agee (AFOSR) Mikhail Itkis (JINR)

#### Program Vice-chairmen:

James Carroll (YSU) Sarkis Karamian (JINR)

#### **Advisory Committee**

D. Cline (Rochester)

M. Harston (Bordeaux)

O. Kocharovskaya (College Station)

M. Litz (Arlington)

A. Matsuura (Washington)

P. Regan (Surrey)

L. Rivlin (Moscow)

R. Shakhmuratov (Kazan')

P. Von Neumann-Cosel (Darmstadt)

#### **Local Organizing Committee**

S.A. Karamian

E.A. Cherepanov - Scientific secretary

A.N. Mezentsev

N.A. Dokalenko

M.I. Morozova

T.V. Mamonova

E.V. Prokhorova

#### Organized by:



Joint Institute for Nuclear Research (Dubna)



Youngstown State University (Ohio)



Air Force Office of Scientific Research (Washington)

#### CONTENTS

#### GENERAL PERSPECTIVES ON ISOMER TRIGGERING

Summary of Gamma Ray Laser and Induced Gamma Emission Research Forrest J. Agee and A.Y. Matsuura	9
Foundations of Isomer Physics for Energy Applications  James J. Carroll	15
A Few Notes on Results of Isomer Triggering Experiments $L.A.\ Rivlin$	23
Excitation of Nuclei by the Photon Beams Carrying Orbital Angular Momentum  A.A. Zadernovsky	27
Multipole Gamma-Superradiance of the Even-Even Nuclei V.V. Samartsev and A.A. Kalachev	35
STUDIES WITH SELECTED ISOMERS	
Measurement of <sup>177</sup> Lu <sup>m</sup> Triggered Isomer Burn-Up Induced by Bremsstrahlung Radiation  M. Helba, H. Roberts, M. Litz, G. Merkel and J. J. Carroll	45
Analysis of Multi-Fold Coincidence Data for Studies of Triggered Gamma Emission R. Propri, S. A. Karamian, D. Gohlke and J. J. Carroll	56
New X-Ray Induced Decay of <sup>178m2</sup> Hf Data: "Mixed J" Instead of "Mixed K" Interpretation?  E.V. Tkalya	65
Production of Long-Lived Hafnium Isomers in Reactor Irradiations S.A. Karamian, J.J. Carroll, J. Adam, E.N. Kulagin and E.P. Shabalin	68
Coulomb Excitation of the <sup>178m2</sup> Hf Isomer: Proposal S. A. Karamian and J. J. Carroll	85

#### PHOTON-INDUCED PROCESSES

Some Synchrotron X-Ray Techniques for Isomers N. R. Pereira, G. Merkel, M. Litz and J. Carroll	91
Status and Perspectives for the Experimental Investigation of <sup>178m2</sup> Hf Isomer Triggering by Low-Energy Photons  V.I. Kirischuk, P. McDaniel, C.B. Collins, J.M. Pouvesle,  N.V. Strilchuk and V.A. Zheltonozhsky	99
Excitation of <sup>113m</sup> In, <sup>195m</sup> Pt and <sup>199m</sup> Hg Isomers in the Reactions of Inelastic Gamma Scattering  Z. M. Bigan, V. I. Kirischuk, V. M. Mazur, D. M. Simochko, P. N. Trifonov and V.A. Zheltonozhsky	105
On the Possibility of Transmutation with the Low-Energy Electron Beams  D. Kamanin, and A. Matthies	110
ELECTRON-ASSISTED NUCLEAR TRANSITIONS	
Role of Autoionization States in Nuclear Excitation by an Electron Transition  I.N.Izosimov	115
To the Question of Triggering the <sup>178m2</sup> Hf Isomeric State F.F.Karpeshin and M.B. Trzhaskovskaya	121
Enhancement Mechanisms of Low Energy Nuclear Reactions F.A. Gareev, I.E. Zhidkova and Yu.L. Ratis	130
Theory of the Nuclear Decay Accompanied by the Electron Shake-off in the Crystal  A. Ya. Dzyublik	145
NUCLEAR EXCITATIONS IN PLASMA	
Nuclear Excitation by Electron Transition in Thermodynamics Equilibrium Plasmas  V.Méot, G.Gosselin, P.Morel, D.Gogny and W.Younes	153

Produced with a High Repetition Rate Laser	162
F.Gobet, F.Hannachi, M.M.Aléonard, J.F.Chemin, G. Claverie,	
M.Gerbaux, G.Malka, J.N.Scheurer, M.Tarisien, F.Blasco,	
F.Dorchies, R.Fedosejevs, C. Fourment, J.J. Santos, D.Descamps,	
V.Meot, P. Morel, B. Liesfeld, L. Robson and S.Hanvey	
Effect of Surface Cleaning on Decay of Low Energy Nuclear Isomers	171
Excited During Femtosecond Laser-Plasma Interaction	
A.B.Savel'ev, V.M.Gordienko, I.M.Lachko, A.A.Rusanov,	
D.S. Uryupina and R.V. Volkov	
STUDIES WITH MÖSSBAUER TECHNIQUES	
Experimental Observation of Laser-Induced Effects in CaF <sub>2</sub> :Eu <sup>3+</sup>	181
Single Crystals	
F. Vagizov, R. Kolesov, S.Olariu and O. Kocharovskaya	
The Influence of Magnetic Field Direction on the Resonant Absorption	191
of Long-Lived Isomer 109m Ag Gamma-rays	
V.G.Alpatov, Yu.D.Bayukov, A.V.Davydov, Yu.N.Isaev,	
G.R.Kartashov, M.M.Korotkov and D.V.L'vov	. :
Colomb Donaldon Transitor in Dolomb Donaldon Transitoria	200
Coherent Population Trapping in Ruby at Room Temperature R. Kolesov	200
Magnetic Radiofrequency Quantum Beat Approach for Test of Reversal	206
Invariance of the Electromagnetic Interaction in 99Ru	-00
A.V. Mitin and I.P. Aniskin	
Resonant Scattering of Mössbauer Photons under the Conditions of Controllable Quantum Interference	213
E.K. Sadykov, V.V. Arinin, A.A. Yurichuk and F.G. Vagizov	
Andhan Tradan	222



General perspectives on isomer triggering

## SUMMARY OF GAMMA RAY LASER AND INDUCED GAMMA EMISSION RESEARCH

#### FORREST J. AGEE & A.Y. MATSUURA

Air Force Office of Scientific Research, 875 N. Randolph St., Suite 325, Room 3112, Arlington, VA 22203USA

The potential for achieving a gamma ray laser led some decades ago to an interest in achieving induced gamma emission from spin isomers. Research has been conducted in many countries including Russia, Ukraine, Romania, US, UK, Australia, Belgium, France, and others. Many universities and scientific institutes have been in the forefront of the research. The potential for many useful applications has been widely recognized. The possibility of using substantial energy stored in isomeric states for periods of seconds to years has motivated much effort to achieve a better understanding of the field. This paper reviews the progress to date, present ongoing efforts, and suggests a way forward.

#### 1. Background

Research into gamma ray lasers and induced gamma emission (triggered release of energy stored in spin isomers) is an area with a number of interesting and potentially fruitful branches. Recent work followed the conference GARALAS 95 held in Predahl, Romania in 1995 [1]. The International Commission on Induced Gamma Emission (ICIGE) was formed at the conference and non-profit research foundation, the IGE Foundation was created to foster international cooperative research. headquartered in Bucharest, Romania. A number of useful meetings have followed including two workshops in Bucharest in 1996, and the First International Induced Gamma Emission Workshop in Predahl, Romania in 1997 [2]. More recently, The Third AFOSR Isomer Workshop was held in Tucson, AZ and the extensive international participation continued with authors from the US, Russia, Belgium, Japan, Germany and the United Kingdom [3]. Subsequent workshops have been held in Hamburg, GE and in Russia. Research has included associated studies of mechanisms and means of triggering the release of energy stored in spin isomer states as well as gamma ray laser concepts. More recently, efforts have been undertaken to achieve independent verification of the triggered release of energy from the most energetic spin isomer of Hf. Additionally, more fundamental research issues are being addressed to focus on the physical understanding of nuclear excitations in Hf and in other isomers. The goal is to develop a foundation of firm scientific data from which the potential of specific nuclear isomers may be assessed for applications.

#### 1.1. Areas of Research

The work has proceeded along a number of lines. There have been experiments performed to define better the triggering of <sup>180</sup> Ta <sup>m</sup>. Work has also been done to measure and confirm the triggering of <sup>178</sup> Hf <sup>m2</sup>. There have been efforts to study the processes for production of <sup>178</sup> Hf <sup>m2</sup> with a view to optimizing the process used at the Joint Institute for Nuclear Research at Dubna with regard to accelerator energy and feed stock. Coulomb excitation is being used to understand the nuclear structure of <sup>178</sup> Hf <sup>m2</sup>. Similar investigations are being initiated on other isomers, such as <sup>242</sup> Am, <sup>121</sup> Sn, <sup>166</sup> Ho, and <sup>177</sup> Lu. There has been work to define a new gamma ray laser concept involving laser cooled atoms. There have been studies into the use of lasers to manipulate nuclear transitions leading to electromagnetically induced (EIT) in coupled nuclear and atomic systems.

#### 1.2. Triggering the Longest Lived Isomer

The present interest in triggered gamma emission stems in part from the success in triggering release of the energy stored in the longest-lived isomer, 180 Ta m. Although the energy stored is a relatively modest 75 key, the triggered release of this most inhibited isomer has been a motivator to seek other cases in which triggered gamma emission might occur under more practically favorable circumstances. The potential for possible applications is indeed broad and extends to gamma ray lasing, high energy density storage applications such as rocket fuels, portable power sources, pulsed gamma ray sources, and a variety of potential applications in medicine [4]. Following the first measurement of triggered release of spin isomer energy [5], further work accomplished much to clarify the anomalously large transition strength associated with the triggering at 2.8 Mev [6,7,8]. The additional understanding disclosed that there were in fact a number of photon energies at work in the triggering, and that therefore, the transition strengths were not out of line [9]. The further identification of the triggering energies with energy levels determined from spectroscopy data provides as well the ability to predict outcomes from triggering events [10]. This is an important fundamental research finding that is essential to the eventual practical exploitation of induced gamma emission [11].

#### 1.3. Triggering the 31 Year Isomer of Hafnium

The isomer <sup>178</sup> Hf <sup>m2</sup>was identified as a high energy density material that might be attractive for applications over a decade ago. There was discussion and interest in the possibility of using the favorable 2.445 MeV stored energy for a variety of applications on two grounds. The first was the obviously large energy stored in a metastable state. The second was based upon the observations that systematics of lifetimes for the isomers in this mass region pointed to a possible trigger level at or below 2.8 MeV, as did other work that indicates that in this region, k no longer becomes an effective inhibitor of transitions, a so-called k-mixing level [12,13]. Following incomplete but encouraging experiments with alpha particles, emphasis

shifted to experiments with X-ray triggering. The initial experiments indicated increased radiation from the sample of <sup>178</sup> Hf <sup>m2</sup>when exposed to X-rays from a modified dental X-ray source [14.15]. Subsequent experiments have shifted for the most part to the use of spectroscopic beam lines at the Spring-8 synchrotron and at other synchrotrons, although not all with the tunable precision of the spectroscopic lines. Some experiments have reported additional information about the triggering [16.17.18.19]. Other experiments have been performed to look at various approaches to observing triggered emission without confirmation of the triggered emission [20.21.22.23]. Additional experiments are planned and others are as vet unpublished that will add more information about the status of triggering of the Hafnium 31 year isomer. In very recent work, the researchers at the University of Texas at Dallas and their colleagues have reported additional details of the triggered release of isomeric cascades based upon further experiments at SPring 8 in Japan and at the Paul Scherrer Institute. The experiments show a correlation between the photon energy and the Lshell atomic electrons, suggesting an atomic - nuclear resonance leading to a more efficient triggering than would be expected for a photon – nuclear interaction unaided by electrons. (A), (B), (C). A complication to the study of the triggering has been the lack of a sufficient supply of the isomer and the poor quality of the samples that are available. These are moreover contaminated by substantial background radiation from other radioactive nuclides, with the fraction of the isomer being measured in the lessthan 0.1% range. A much better quantity and purity of samples would greatly enhance research. In this regard, AFOSR is focusing research on other isomers that can be more easily made and that can be provided without extensive contamination by other isotopes. Such a focus is expected to provide a much faster path to better understanding of triggered gamma emission and gamma ray laser possibilities.

#### 1.4. Studies of Ways to Produce the Hafnium Isomer

Studies have been conducted at the Joint Institute of Nuclear Research at Dubna, Russia on the spallation process in making the isomer <sup>178</sup> Hf <sup>m2</sup>. The work has been focused in two directions. The first was to study the effect of accelerator energy on the process. The second was to vary the feed stock material used for spallation. The most isomer made to date was produced at Los Alamos in a beam stop. The process was obviously not optimized for Hafnium isomer production, and the resulting beam stop was highly contaminated with very radioactive isotopes that required more than a decade of cooling to reach at all usable samples. The goal of the work has been to reduce the time required for radioactive decay of contaminants and to optimize the production of the desired isomer.

The production of the high spin isomer state ( $K = 16^+$ ) in  $^{178}$  Hf  $^{m2}$ is attributed to a combined process of multi-step Coulomb excitation up from the ground state followed by  $\Box$ -decay feeding into the  $K = 16^+$  band [24]. AFOSR is investing in basic Coulomb excitation research at Gammasphere, a high resolution  $4\pi \gamma$ -ray detector facility. The result of this research performed by the University of Rochester is the observation, for

the first time, of a dramatic breakdown in the goodness of the K quantum number in low-K bands. This is in contrast to the high-K bands where K is a good quantum number. The K mixing becomes almost complete at higher angular momenta in low-K bands, whereas K remains pure for high-K bands. This result is a significant advance in understanding the structure of states in <sup>178</sup> Hf <sup>m2</sup> that has important implications regarding the population and stimulated depopulation of isomeric states.

#### 1.5. The Gamma Ray Laser

One approach to a gamma ray laser that is under investigation is an attempt to realize the concept of recoil assisted lasing with hidden inversion of a population of nuclear states in free nuclear ensembles. This work involves a consortium of Russian institutes including the International Laser Center, V. M. Lomonsov Moscow State University, Moscow State Institute for Radio Engineering, Electronics, and Automation, Lebedev Physical Institute, Russian Academy of Science, and Russian State Science Center Troitsk Institute for Innovation and Fusion Research. The work is focused on developing a demonstration gamma ray laser experiment. In this regard, MIREA is doing the theory, LPI is selecting the nucleus and developing master lasers, MSU is making the experimental arrangement including the laser cooling, using femtosecond lasers to stimulate nuclear states, and TRINITI is working on the Nd:YAG laser system [25,26,27].

#### 1.6. Electromagnetically Induced Transparency

It has been demonstrated that Nd:YAG laser radiation at 1064nm on MgO:Fe, resonant to the electronic transition of the divalent Fe in MgO, results in a new doublet structure in the Mossbauer nuclear absorption spectrum [28]. AFOSR is investing in this exciting new field of laser manipulation of nuclear transitions. Recently, the Kocharovskaya group has succeeded in demonstrating for the first time Electromagnetically Induced Transparency (EIT) in solids (ruby) at room temperature. The goal is to clarify the mechanism of the observed influence of laser radiation on nuclear transitions. Ultimately, we hope to be able to observe transparency similar to EIT in a coupled nuclear/atomic system. EIT can enhance or suppress transitions between atomic orbitals. In nuclear systems, the analogous ability to suppress a resonant nuclear transition in a coupled system using low energy lasers would greatly reduce the requirement for incoherent pumping of a potential inversion-less gammaray laser [29].

#### 1.7. Future Course of Research

The planned course of research in this area at AFOSR will focus on giving a better scientific basis for the areas of induced gamma emission and a possible gamma ray laser along the lines outlined above. Our conclusion that for a better

understanding, we need to consider other spin isomers that may be more available for study and we need to get a better understanding of the nuclear states, transition possibilities, and outcomes of such transitions. With regard to <sup>178</sup> Hf <sup>m2</sup>, we look to a better definition of the triggering both to clarify the region of low energy x-rays explored to date and to complete the work by looking at higher energies. Recent work on the gamma rays emitted in the decay of the isomer will help guide experiments that are above the energy levels explored to date [30].

There is also interest in other isomers in the same mass region A  $\sim$  180 [31,32]. The 141 y isomer <sup>241</sup> Am <sup>m</sup> is an interesting possibility for further study. Coulomb excitation research on high purity 98% enriched samples of <sup>242</sup> Am will be conducted at Argonne National Laboratory in August 2005 by researchers at the University of Rochester, Youngstown State University, and Dubna's Joint Institute of Nuclear Research. We look forward to further exploration of the best way to produce isomers, initially for research purposes and to support evaluation of possible uses for them. The ultimate goal of a gamma ray laser along lines not previously explored will take advantage of the new science of laser cooled atoms and lasing with hidden inversion. The international cooperation that is making progress possible is a pleasant and productive way of conducting research in this field as it is in others. It has much to offer for future progress, and the Air Force Office of Scientific Research appreciates the good work and interaction among the participants.

#### References

- C. B. Collins and L. A Rivlin (eds), Gamma-Ray Lasers, Proceedings of the 1<sup>st</sup> International Gamma-Ray Lasers Workshop (GARALAS '95), Hyperfine Interactions, Vol. 107 (1997).
- 2. I. I. Popescu and C. A. Ur (eds), Proceedings of the First International Induced Gamma Emission Workshop, IGE '97, Induced Gamma Emission Foundation, Bucharest Magurele, Romania (1999).
- 3. V. Baran, J. J. Carroll and L. A. Rivlin, Quantum Nucleonics and Triggered Gamma Emission, Proceedings of the 3<sup>rd</sup> ADOSR Isomer Workshop, *Hyperfine Interactions* **143** (2002).
- 4. H. Roberts, Hyperfine Interactions 107, 91-97 (1997).
- 5. C. B. Collins, C. D. Eberhard, J. W. Glesner, et al., Phys. Rev. C 37, 2267 (1988).
- 6. D. Belec, C. Arlandini, J. Besserer, et al., Phys. Rev. Lett. 83, 5242 (1999).
- 7. C. B. Collins, J. J. Carroll, T. W. Sinor, et al., Phys Rev. C 42, 1813 (1990).
- 8. D. Belec, C. Arlandini, J. Besserer, et al., Phys Rev C 65, 035801 (2002).
- 9. S. A. Karamian and J. J. Carroll, Laser Phys. 11, 23 (2001).
- 10. P. M. Walker, G. D. Dracoulis, and J. J. Carroll, Phys. Rev. C 64, 061302 (2001).
- 11. F. J. Agee, Hyperfine Interactions 143, 1-6 (2002).
- 12. C. B. Collins and J. J. Carroll, Laser Phys. 5, 209 (1995).
- 13. C. B. Collins, J. J. Carroll, and Y. T. Oganessian, Laser Phys. 5, 280 (1995).
- 14. C. B. Collins, F. Davanloo, M. C. Iosif, et al., Phys. Rev. Lett. 82, 695 (1999).

- 15. C. B. Collins, F. Davanloo, M. C. Iosif, et al., Laser Phys. 9, 8 (1999).
- 16. C. B. Collins, F. Davanloo, A. C. Rusu et al., Phys. Rev. C 61, 054305 (2000).
- 17. C. B. Collins, N. C. Zoita, A. C. Rusu et al., *Hyperfine Interactions* 135, 51 (2001).
- 18. C. B. Collins, A. C. Rusu, N. C. Zoita et al., Laser Phys. 11, 1 (2001).
- 19. C. B. Collins, N. C. Zoita, A. C. Rusu et al., Europhys. Lett. 57, 677 (2002).
- 20. I. Ahmad, J. C. Banar, J. A. Becker, et al., Phys. Rev. Lett. 87, 072503 (2001).
- 21. I. Ahmad, J. C. Banar, J. A. Becker, et al, Phys. Rev. C 67, 041305 (2003).
- 22. H. Roberts, M. Helba, J. J. Carroll, et al., Hyperfine Interactions 142, 111 (2003).
- 23. J. J. Carroll, J. Burnett, T. Drummond, et al., *Hyperfine Interactions* **143**, 37 (2003).
- 24. A.B. Hayes et al., Phys. Rev. Lett. 24, 24501 (2002).
- 25. F. J. Agee, J. J. Carroll, L. A. Rivlin, et al, *Hyperfine Interactions* 143, 7-11 (2002).
- 26. A. V. Andreev and R. A. Chalykh, Hyperfine Interactions 143, 13-22 (2002).
- 27. A. V. Andreev, O. V. Chutko, A. M. Dykhne et al., *Hyperfine Interactions* 143, 23-36 (2002).
- 28. R. Coussement et al, Phys. Rev. Lett. 89, 107601 (2002).
- 29. R. Kolesov et al, Optics Communications 179, 537 (2000).
- 30. M. B. Smith, P. M. Walker, G. C. Bell, et al., Phys. Rev. C 68, 031302 (2003).
- 31. S. A Karamian, J. J. Carroll, L. A. Rivlin, et al. *Laser Physics* **14**, no. 2, 166-174 (2004).
- 32. L. A. Rivlin, J. J. Carroll, and F. J. Agee, Laser Physics 14, No. 4, (2004).

#### FOUNDATIONS OF ISOMER PHYSICS FOR ENERGY APPLICATIONS

#### JAMES J. CARROLL

Department of Physics and Astronomy, Youngstown State University, One University Plaza, Youngstown, Ohio 44555 USA

Nuclear isomers can store significant amounts of energy for substantial periods and the potential to utilize this energy in a controllable manner has motivated considerable study. Focused attempts to produce so-called induced, or triggered, energy release from isomers have largely been carried out without explicit connection to established nuclear structure data, with mixed results. The feasibility of any application will depend on the specifics of the isomer chosen, including its decay characteristics and whether or not it is possible to cause, with high efficacy, an early loss of the stored energy. Learning the lessons of previous experimental approaches, work by the YSU Isomer Physics Project, with valued collaborations, seeks to provide a solid foundation of nuclear physics data as a guide to the search for a practical controlled energy release from isomeric nuclei. This paper surveys the present status of this effort to connect traditional nuclear physics and focused studies of possible energy-releasing processes, and looks to the future of the field.

#### 1. Introduction

Nuclear isomers, particularly those characterized as metastable states, can store up to MeV/nucleus for decades or longer, corresponding in the extreme cases to 1.3 GJoules/gram ( $^{178m2}$ Hf) and  $T_{1/2} > 10^{15}$  years ( $^{180m}$ Ta). Between these limits, a wide variety of isomers exist and just over thirty are known with halflives longer than a day [1].

The ability of isomers to store large amounts of energy at very high densities has suggested many applications [2]. For example, one could imagine a gamma-burst device, perhaps used for the cleansing of bio-contaminated environments. Should the stored energy within one gram of pure  $^{178m2}\mathrm{Hf}$  be released within 10 ns, gamma rays carrying more than 100 kW/m² could be delivered at a distance of 100 m and through a standard 4 cm Pb brick. Another possibility might be to utilize an isomer like the 141-year-lived state of  $^{242m}\mathrm{Am}$  as a form of nuclear battery. A total of 3  $\mu g$  of  $^{242m}\mathrm{Am}$  in this state would have an activity of merely 33  $\mu\mathrm{Ci}$ , but should an induced reaction be capable of transferring its population to the 16-hour ground state, an activity of 2.5 Ci would be produced. One could suppose a "battery" from this material to be stored safely until needed, then activated for use at a higher decay rate. Finally, it may

eventually be possible to produce the ultimate light source, a gamma-ray laser, utilizing an isomer as an initial storage level.

To determine the feasibility of any application, it is first necessary to obtain measured values for critical physical parameters, e. g. the cross section and interaction energy of an isomeric nucleus with some external agent. To reach such a mature state of investigation, it is valuable to assess the present stage of research and how it was attained.

#### 2. Reaching the present

A full history of the search for control of nuclear decays is beyond the scope of this paper and more detailed background may be found in Ref. [1]. Insofar as induced energy release from isomers is concerned, a major step was taken in 1987, when for the first time it was demonstrated that an external agent could cause depletion of the  $^{180m}$ Ta isomer [3]. It was shown conclusively that real photons in 6 MeV bremsstrahlung could cause this depletion, but it was not possible to determine the energy(ies) at which the reaction occurred or the corresponding cross sections. This result largely re-energized the field of study into so-called  $(\gamma, \gamma')$  reactions and led to numerous experiments on the population of isomers over the period of about 1988 – 1993 as represented [1] by about fifteen related publications. Many of these experiments were performed at the Technical University of Darmstadt, Germany, with the injector to the S-DALINAC accelerator, including the 1990 measurement of cross sections for the depletion of  $^{180m}$ Ta via mediating transitions near 2.8 and 3.6 MeV [4].

Despite this impetus, nearly a decade elapsed before a more detailed examination of the isomer-depletion reaction on <sup>180m</sup>Ta was performed. In 1998, a series of experiments [5, 6] were performed using the world's supply of enriched <sup>180m</sup>Ta and irradiations with bremsstrahlung from the Stuttgart DYNAMITRON. This experiment was a triumph of international collaboration and again demonstrated the depopulation of that isomer. The increased sensitivity of those measurements made possible the identification [5, 6] of new, lower-energy mediating transitions, with the minimum energy required being about 1 MeV. Simply put, it took a quantum input of 1 MeV to release the 75 keV stored by that isomer, which was therefore more of an energy sink than an energy source. Nevertheless, the general process was confirmed again and in greater detail. The next question would then naturally be "is there a better isomer?"

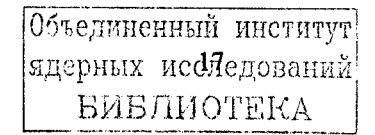
Before returning to this question, it is worthwhile to consider how these studies impacted or were impacted by more traditional types of nuclear physics studies. The field of study into nuclear structure and the underlying physics is very mature, but still growing in the breadth of techniques based on new reactions (like multi-nucleon transfer reactions [7]) and instruments [8]. Nevertheless, a new impetus came with the <sup>180m</sup>Ta results. Those results indicated that absorption of a photon by an isomeric

nucleus could excite an intermediate level that could branch into the ground-state band. This required at least some of the necessary transitions to exhibit a smaller K hindrance than would be considered typical, suggesting a mixing of the K quantum number in the participating states. The discovering of similarly K-mixed transitions in the decay of the short-lived <sup>174</sup>Hf [9] isomer contributed a parallel motivation for study of so-called "K-forbidden" transitions. It proved very difficult, however, to make the essential connections between nuclear structure and the mediating states discovered for depletion of <sup>180m</sup>Ta. In fact, only in 2001 was it possible to suggest a likely identification of nuclear levels with those intermediate states [10].

It is important to note that the initial demonstration and subsequent tests of depletion of <sup>180m</sup>Ta were made without guidance from nuclear structure data of potential mediating states – there simply was insufficient information from which to identify the weak transitions required to make the process work. And despite the everimproving quality of nuclear structure studies, their results still would not provide a priori any guidance as to what energies to try for a depletion reaction with <sup>180m</sup>Ta. This situation is the rule, not the exception, for long-lived isomers of potential value for applications.

So how then to decide what would be a "better" isomer? The <sup>180m</sup>Ta isomer, while extremely long-lived, lies at a modest excitation energy. A reasonable supposition was, therefore, to examine the possibility of induced depopulation of a higher-lying isomer. This approach was supported by systematics developed in the 1990's for related reactions [11, 12]. From this perspective, the 31-year isomer <sup>178m2</sup>Hf at 2.5 MeV became an obvious focus of attention. Spontaneous-decay transitions from this isomer are inhibited from their hypothetical single-particle values by a K hindrance on the order of  $(66)^5$  [13], leading to its long halflife – only the extremely large channel for electron conversion of the first decay transition prevents the lifetime from being much longer. Nuclear structure results suggested that the nearest likely intermediate state was 126 keV above this isomer [14], but there was more than enough motivation to just try something. After all, no structural guidance was available for <sup>180m</sup>Ta and still an important result was obtained. Thus, in 1996 began the search for an induced energy release, triggered gamma emission, from <sup>178m2</sup>Hf.

Studies into possible energy-releasing reactions on  $^{178m2}$ Hf have for the most part concentrated on real photons at energies on the order of 10 keV. This so-called low-energy triggering remains extremely controversial with the conflicting results up to early 2004 surveyed in Ref. [15]. Later, additional positive results have only served to enflame the controversy (for example, see the suggestion [16] of induced energy release through a single  $\sim 2.5$  MeV transition of  $\Delta J > 10$ ). New null results from SPring-8 [17] cast even greater doubt on claims of low-energy triggering, based on gamma-ray singles and higher-order coincidence measurements [18].





rigure 1. IJ sample within the 15U miniball array at the SPring-8 synchrotron [17,18].

In the same period, however, investigations into the nuclear structure of <sup>178</sup>Hf provided new information. Among these were the observation of new natural-decay cascades [13] and actual transitions at 331, 990 and 1,676 keV that could permit induced depletion of the 31-year isomer with unexpected strengths [19]. Those strengths were due to significant K mixing in the <sup>178</sup>Hf ground-state band at J > 14.

The study of induced (triggered) depletion of nuclear isomers has faced

significant challenges beyond that of traditional nuclear physics research. Largely this has come from the inability to find a connection between triggering results and nuclear structure, even after induced depletion was established (for <sup>180m</sup>Ta). Only now is it slowly becoming possible to create the necessary synergy by which to provide a foundation for focused depletion studies. Such a foundation is essential if this field is to mature and lead to realistic evaluations of the feasibility of nuclear isomers for applications.

#### 3. Toward the future

Maturity of the study of induced depletion of isomers must lie in a firm foundation of nuclear structure data. The YSU Isomer Physics Project has undertaken to develop this through a systematic and linked program of research. This program encompasses direct experiments of potential trigger reactions, guided where possible by available level schemes, in parallel with traditional nuclear physics studies of isomer production reactions, isomer depletion reactions and associated structural investigations. The following will summarize a few recent developments in this two-pronged approach.

#### 3.1. Enhanced study of nuclear structure of 178 Hf with gammasphere

In November 2004, a new experiment was conducted at Argonne National Laboratory using the ATLAS accelerator and gammasphere. A pulsed beam of  $^{178}$ Hf ions was incident upon an enriched  $^{208}$ Pb target producing excitations at high angular momentum for both species. Coincident gamma rays up to triples ( $\gamma$ - $\gamma$ - $\gamma$  coincidences) were recorded using the 101-detector Ge array. Lead excitations could be excluded using the high-lying first excited level of this doubly-magic nucleus. The emphasis of the experiment was to search for new  $\mu$ s isomers in  $^{178}$ Hf and transitions connecting them or known isomers to freely-radiating states such as in the ground-state band. Analysis is continuing and should be completed in 2006. At this time, there is no evidence of intermediate states for isomer depletion within 100 keV of  $^{178m2}$ Hf.

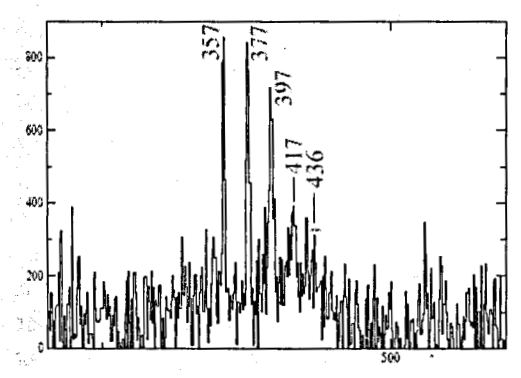


Figure 2. Transitions (in keV) feeding the 31-year isomer <sup>178m2</sup>Hf from higher-lying levels excited in the 2004 gammasphere experiment.

Collaborating institutions included the University of Surrey, TRIUMF, University of Massachusetts-Lowell, Argonne National Laboratory and YSU.

## 3.2. Initial search for new isomers at GSI/FRS

In October 2004, an initial search for new isomers was conducted at the Gesellshaft für Schwerionenforschung (GSI) using the FRS fragment separator. A beam of 670 MeV/u <sup>238</sup>U

beam was incident on a target of <sup>9</sup>Be and fragments were mass-separated with a resolution of a few hundred keV prior to obtaining correlated gamma spectroscopy on an ion-by-ion basis. Analysis is continuing. Collaborating institutions included the University of Surrey, Michigan State University, GSI and YSU.

## 3.3. GSI-RISING campaign

In 2005, the YSU Isomer Physics Project joined the GSI-RISING campaign. This is a multi-year systematic program to study the production of exotic (high-spin, isomeric) nuclei using the FRS mass separator and a Ge/BF2 array. The Rare ISotope INvestigations at GSI (RISING) collaboration includes twenty-six participating institutions: US participants are Notre Dame University, Lawrence Berkeley National Laboratory and YSU. The goal is to systematically map the landscape of K isomers and test the limits of the K quantum number.



Figure 3. FRS at GSI. Reactionfragments are analyzed by mass and gamma rays recorded ion-by-ion.

# 3.4. Measurement of production and depletion cross sections for <sup>178m2</sup>Hf using reactor neutrons

A recent experiment conducted at JINR [20] has revised the traditional cross section for production of <sup>178m2</sup>Hf by neutron capture. Also, the cross section for depletion (burn-up) of the isomer due to reactor neutrons was deduced. This work impacts the feasibility of large-scale production of this isomer.

## 3.5. Nuclear structure and isomer characterization of 174, 175 Tm at TRIUMF

In August 2005 a study of the nuclei  $^{174}$ Tm and  $^{175}$ Tm was performed at TRIUMF-ISAC (Isotope Separation and ACceleration) using the  $8\pi$  Ge array coupled

experiments focused directly on energy-releasing reactions and on the parallel development of a firm foundation of complimentary nuclear structure information. It is the nuclear structure that will (or will not) support the use of isomers in applications. The YSU Isomer Physics Project supplies the lead role in this synthesis with valued colleagues around the world and a number of experiments have been conducted or are in preparation to advance this program. A few of these efforts were highlighted herein as providing significant steps forward.

## Acknowledgments

The author wishes to recognize the hard work and dedication of undergraduate students at Youngstown State University, who have been the core of the YSU Isomer Physics Project: R. Propri, D. Gohlke, S. Ludt, S. McCann, N. Caldwell, J. Lazich, S. Smyczynski and others. Special thanks to S. A. Karamian of JINR, Dubna and to valued colleagues at other collaborating institutions. Also, thanks to YSU post-docs M. Harston and P. Ugorowski. This work was supported by the US Air Force Office of Scientific Research under contracts F49620-02-1-0187, FA9550-04-1-0270 and FA9550-05-1-0486. Additional support provided by the DCI Post-Doctoral Program under contract 2002-A061400-000.

### References

- 1. J. J. Carroll, S. A. Karamian, L. A. Rivlin, et al., Hyperfine Int. 135, 3 (2001).
- 2. H. Roberts, Hyperfine Int. 107, 91 (1997).
- 3. C. B. Collins, C. D. Eberhard, J. W. Glesener, et al., Phys. Rev. C 37, 2267 (1988).
- 4. C. B. Collins, J. J. Carroll, T. W. Sinor, et al., Phys. Rev. C 42, 1813 (1990).
- 5. D. Belic, C. Arlandini, J. Besserer, et al., Phys. Rev. C 65, 035801 (2002).
- 6. D. Belic, C. Arlandini, J. Besserer, et al., Phys. Rev. Lett. 83, 5242 (1999).
- 7. P. H. Regan, J. J. Valiente-Dobón, C. Wheldon, et al., Laser Phys. Lett. 1, 317 (2004).
- 8. I. Y. Lee, M. A. Deleplanque, and K. Vetter, Rep. Prog. Phys. 66, 1095 (2003).
- 9. P. M. Walker, G. Sletten, N. L. Gjørup, et al., Phys Rev. Lett. 65, 416 (1990).
- 10. P. M. Walker, G. D. Dracoulis, and J. J. Carroll, Phys. Rev C 64, 061302 (2001).
- 11. C. B. Collins and J. J. Carroll, Laser Phys. 5, 209 (1995).
- 12. C. B. Collins, J. J. Carroll, Y. T. Oganessian, et al., Laser Phys. 5, 280 (1995).
- 13. M. B. Smith, P. M. Walker, G. C. Ball, et al., Phys Rev. C 68, 031302(R) (2003).
- 14. T. L. Khoo and G. Løvhøiden, Physics Letters 67B, 271 (1977).
- 15. J. J. Carroll, Laser Phys. Lett. 1, 275 (2004).
- 16. C. B. Collins, N. C. Zoita, F. Davanloo, et al., Laser Phys. Lett. 2, 162 (2005).
- 17. J. J. Carroll and others, Phys Rev. C (in preparation for 2006).
- 18. P. Ugorowski, R. Propri, S. A. Karamian, et al., Nucl. Inst. Meth. A (submitted 2006).
- 19. D. Cline, J. Modern Opt. (Proc. 35th Winter Colloquium on the Physics of Quantum Electronics) 52, 2411 (2005).
- 20. S. A. Karamian, this volume (2006).
- 21. M. Helba, H. Roberts, M. Litz, et al., this volume (2006).
- 22. S. A. Karamian and J. J. Carroll, this volume (2006).

## A FEW NOTES ON RESULTS OF ISOMER TRIGGERING EXPERIMENTS

#### L.A. RIVLIN

Applied Physics Laboratory, MIREA Technical University
78 Vernadsky Ave., 119454 Moscow, RUSSIA
Phone & FAX: +7 (095) 434 9317, e-mail: rivlin140322@mccinet.ru

Possible reasons of disputability of results of isomer triggering experiments may consist in (i) unsatisfactory low spectral density of triggering radiation of broadband, as well as narrowband x-ray sources and (ii) shortage of continuous duration of triggering pulse in comparison with lifetime of upper level of trigger transition. Elimination of discrepancy (ii) shall significantly increase a running value of trigger transition and consequently a trigger efficiency itself. Another way to increase trigger efficiency is application of Moessbauer type target with isomers embedded into cooled solid matrix in conjunction with bright narrowband x-ray source.

1. The "Physics Today" reviewer had qualified results of a long set of well known experimental efforts to observe the triggering decay of long-lived nuclear isomers as "a conflicting" ones [1]. These experiments deal with perhaps one of the central problem of modern quantum nucleonics, namely with the problem of controllable energy utilization of metastable nuclear states. Current state of the art together with detail references is presented in comprehensive analytical review [1].

Triggering is a two-step process consisting radiative transition from a metastable level (m) to an auxiliary upper level (a) by absorption of an external resonant x-ray photon following by rapid spontaneous transition from (a) to a ground level. Generally speaking such a process is not forbidden by basic laws of physics. It is well known in optics and atom physics as an anti-Stokes transitions. So it is of general, as well as pragmatic importance to analyze the possible quantitative reasons of contradictious status of similar experiments in nuclear domain. The following notes present brief discussion [2] of some possible causes of quantitative experimental discrepancies, namely first of all the influence of inducing x-ray source parameters (such as total photon flux density  $\Phi$  ( $cm^{-2}s^{-1}$ ), its spectral density (brilliance)  $d\Phi/d\omega$  ( $cm^{-2}s^{-1}Hz^{-1}=cm^{-2}$ ), pulse duration  $\Delta t$  (s) and so on) on efficiency of triggering process. It should be emphasized that the types of x-ray sources used in experiments are very diverse – from dental x-ray apparatus towards relativistic electron ondulators.

2. For the sake of practical comparison of different experimental situations it is useful to introduce a quantity

$$Q = -\frac{\tau_m}{n_m} \frac{dn_m}{dt} \tag{1}$$

that is merely the ratio of rate  $-(dn_m/dt)$  of forced triggered decay of metastable states with concentration  $n_m$  to their spontaneous rate  $n_m \tau_m^{-1}$  and can be called a quality factor of trigger process (here  $\tau_m$  is spontaneous life-time of metastable level and t is time).

Disregarding transition mechanism the rate of whole triggering decay is determined by the rate of its first stage  $(m \rightarrow a)$  that generally speaking is proportional to effective absorption cross-section of inducing x-ray photons

$$\sigma_{m\to a} \sim \frac{\lambda^2}{2\pi} \frac{2J_a + 1}{2J_m + 1} \tag{2}$$

where  $\lambda$  is wavelength of inducing x-ray radiation,  $J_m$  and  $J_a$  are angular momenta of metastable and auxiliary levels correspondingly. So the quality factor is equal to

$$Q = \sigma_{m \to a} \left( \frac{d\Phi}{d\omega} \right) \tau_m \Delta \omega_a \tag{3}$$

where  $\Delta \omega_a \sim \tau_a^{-1}$  is natural width of an auxiliary level a and  $\tau_a$  is its spontaneous lifetime.

3. It is necessary to distinguish two alternative types of experimental situation: a broadband one, if the total inhomogeneous line-width  $\Delta\omega_{tot}$  of transition  $m\to a$  significantly exceeds natural width of an auxiliary level  $(\Delta\omega_{tot} >> \Delta\omega_a)$ , and a narrowband one with  $\Delta\omega_{tot}$  tending to natural width of an auxiliary level  $\Delta\omega_a$   $(\Delta\omega_{tot} \to \Delta\omega_a)$ .

In these two cases the total x-ray photon flux densities  $\Phi = (d\Phi/d\omega)\Delta\omega_{tot}$  needed to achieve fixed quality factors Q are quite different:

$$\Phi_{bb} = \frac{Q}{\sigma_{max} \tau_{m}} \frac{\Delta \omega_{tot}}{\Delta \omega_{c}} \tag{4}$$

and

$$\Phi_{nb} = \frac{Q}{\sigma_{max}\tau_{max}} \tag{5}$$

where the line-width ratio

$$\beta = \frac{\Delta \omega_a}{\Delta \omega_{co}} \tag{6}$$

is equal to  $\beta \approx 1$  in a narrowband and  $\beta << 1$  in broadband situations consequently. So that

$$\Phi_{bb} >> \Phi_{nb}. \tag{7}$$

4. At this point it is useful to give a quantitative model example. If  $\lambda = 0.124 \, nm$  (10 keV),  $\tau_m = 24h \approx 9 \times 10^4 \, s$ ,  $\sigma_{m \to a} = 2.5 \times 10^{-17} (2J_a + 1)(2J_m + 1)^{-1} \, cm^2$ ,  $\tau_a = 10 \, ns$ ,  $\Delta \omega_a / 2\pi = 10^8 \, s^{-1}$ , isotopic number = 100 and isomeric target is supported at room temperature,  $\Delta \omega_{tot} / 2\pi = 6 \times 10^{12} \, s^{-1}$ ,  $\beta \approx 2 \times 10^{-5}$ , and Q = 0.01, then  $d\Phi/d\omega \approx 300 \, photons \, per \, cm^2$ ,  $\Phi_{bb} \approx 2 \times 10^{15} \, photons \, per \, cm^2 s$ ,  $\Phi_{nb} \approx 3 \times 10^{10} \, photons \, per \, cm^2 s$ .

These estimates make it clear the irreproducible results of experiments with sources of continuous x-rays (e.g. bremsstrahlung of dental x-ray apparatus) because of their spectral densities  $d\Phi/d\omega$  and total photon flux densities  $\Phi$  are unfortunately lower than needed figures by many orders of magnitude, and the possibility to heighten them is very questionable.

Nevertheless, one can see the advantage of narrowband source with line-width  $\Delta\omega_x \to \Delta\omega_a$ . If such a source with sufficiently high spectral density would be available, the needed total flux density, according to (7), could be decreased by orders of magnitude. For this purpose the Moessbauer-type target must be used with isomers embedded into cooled solid matrix which narrows transition line-width  $\Delta\omega_{tot} \to \Delta\omega_a$ .

- 5. Another type of x-ray sources based on emission of relativistic electrons and much more bright than bremsstrahlung ones were used for triggering, but also with doubtful results [1], although their  $d\Phi/d\omega$  and  $\Phi$  seems to be sufficient for reliable observation of triggering effect. In this relation, it should be emphasized the role of continuous x-ray pulse duration  $\Delta t_x$ : x-ray irradiation time should be accurately adjusted to radiative lifetime  $\tau_{a \to m}$  of upper level of a transition  $a \to m$ . This is why running value of any transition cross-section  $\sigma_{m\to a}(t)$  possesses an asymptotic behavior:  $\sigma_{m\to a}(t)$  starts from zero value  $\sigma_{m\to a}(t=0)=0$  and approaches the final stationary value only after time delay drawing nearer to  $\tau_{a \to m}$  [3]. Thus, to achieve a satisfactory trigger efficiency, a irradiation pulse duration  $\Delta t_x$  must be close to lifetime  $\tau_{a \to m}$  [3]. In particular, this is of importance for mentioned triggering by intensive hard radiation of relativistic electrons accelerated in LINACs and similar microwave accelerators. In these types of accelerators electron pulse duration and consequently continuous duration  $\Delta t_x$  of separate x-ray pulses are situated in subnanosecond range, whereas in most cases the lifetime  $\tau_{a \to m}$  of an auxiliary level aexceeds  $\Delta t_x$  by orders of magnitude. So in these experiments running value of crosssection  $\sigma_{m\to a}(0 \le t \le \Delta t_x)$  was also lower than its asymptotic stationary value by orders of magnitude and therefore the quality factor was tending to zero  $Q \rightarrow 0$ . Perhaps, this was the main reason of disputability of results of triggering experiments with relativistic irradiation sources.
  - 6. The bottom line: to raise reliability of a new set of triggering experiments

- (a) it is necessary to increase the spectral density  $d\Phi/d\omega$  of triggering x-ray radiation of broadband, as well as narrowband sources;
- (b) in the narrowband case the Moessbauer type target with isomers embedded into cooled solid matrix seems to have significant advantages;
- (c) continuous duration  $\Delta t_x$  of triggering pulse must be adjusted with auxiliary level lifetime  $\tau_{a \to m}$  (namely,  $\Delta t_x \to \tau_{a \to m}$ ) to increase the running value of trigger cross-section  $\sigma_{m \to a} (0 \le t \le \Delta t_x)$  and the quality factor Q;
- (d) and finally, it seems to be useful to enlarge list of experimental isomers.

### Acknowledgments

This study was partially supported by the ISTC, grant #2651p and by U.S. CRDF-R.F. Ministry of Education Award, VZ-010-0.

### References

- 1. B. Schwarzschild Physics Today, 57, 21, (2004).
- 2. L.A. Rivlin Quantum Electronics (Moscow), 35, (2005) (in press)
- 3. L.A. Rivlin Quantum Electronics (Moscow), 35, 474, (2005)

# EXCITATION OF NUCLEI BY THE PHOTON BEAMS CARRYING ORBITAL ANGULAR MOMENTUM

#### A.A. ZADERNOVSKY

Applied Physics Laboratory, MIREA Technical University
78 Vernadsky Ave., 119454 Moscow, RUSSIA
Phone & FAX: +7 (095) 434 9317, e-mail: zadernovsky@mirea.ru

Drop in the efficiency of nuclear excitation through transitions of high multipolarity is related to the increase in angular momentum difference between the nuclear states involved into the excitation transition. Such transitions need the photons with high angular momentum. It is well known, that the photon beams carrying a well defined and an arbitrary high value of angular momentum about the beam axis can be produced. We discuss some features in the excitation of nuclei with the beams.

### 1. Introduction

In contrast to atomic case, in nuclei the quadrupole and higher-multipolarity electric and magnetic transitions are rather commonly found to exist in many different nuclides. As the multipolarity increases, the nuclear transition probability decreases dramatically. The drop in efficiency of the nuclear excitation through transitions of high multipolarity is related to the increase in the angular momentum difference between the nuclear states involved into the excitation transition. Such transitions need the photons with high angular momentum. Photons of an ordinary circularly polarized plane electromagnetic wave each carry only one unit (in the units of  $\hbar$ ) of angular momentum. It is well known, however, that the photon beams carrying a well defined and an arbitrary high value of angular momentum about the beam axis can be produced. Such beams, which are often referred to as the light beams with orbital angular momentum, have been extensively studied during the last decade [1]. In this paper we discuss some features in the excitation of nuclei with the beams.

## 2. Light Beams With Orbital Angular Momentum

It is well known that light can have an angular momentum. As early as in 1909 John Poynting [2] realized that circularly polarized plane electromagnetic wave must carry angular momentum. However, the polarization does not account for all of the angular momentum that can be carried by light. In addition, there is an orbital contribution. In 1992 a group at Leiden University [3] recognized that the light beams with helical phase fronts carry an angular momentum independent of the polarization state. The orbital angular momentum arises from the phase structure and can be directly deduced from the consideration of the Poynting vector. This vector gives the

direction and magnitude of the linear momentum flow. For helical phase fronts, the Poynting vector circulates about the beam axis, thus, producing an orbital angular momentum parallel to the axis. Because of the linear momentum circulation, such beams are often said to contain an optical vortex.

In terms of photons, angular momentum of a light beam is associated with the quantum state of an individual photon. Total angular momentum of a photon is a sum of spin and orbital contributions. Circular polarization relates to the intrinsic spin of photons. Circularly polarized photons of a plane electromagnetic wave each have angular momentum projection  $\pm\hbar$  on the beam axis. Light beams with an exponentional azimuthal phase dependence of  $\exp(-i\ell\varphi)$  carry an orbital angular momentum independent of the polarization state. The angle  $\varphi$  is the azimuthal coordinate in the beam cross section, and  $\ell$  can take any integer value, positive or negative. For any given  $\ell$ , the beam has  $\ell$  intertwined (left or right) helical phase front. In such a beam, the orbital angular momentum in the propagation direction has the value of  $L=\ell\hbar$  per photon.

The most common form of a helically phased beam is the so-called Laguerre-Gaussian (LG) mode. The LG modes are the solutions of the paraxial wave equation in cylindrical coordinates expressed in terms of the product of a Laguerre polynomial of radial index p and axial index  $\ell$ , a Gaussian envelope and a phase term  $\exp(-i\ell\varphi)$ . Since the mode amplitude distribution have an explicit exponentional azimuthal phase factor, that makes them the natural choice for the description of beams carrying orbital angular momentum along its propagation direction.

The LG beams can be produced in different ways. Among them are controlled production directly in a laser cavity [4], conversion of Hermite-Gaussian (HG) laser modes into LG modes with the help of cylindrical lens [5], use of spiral zone plates [6] or phase plates [7] and forked diffraction gratings [6, 8]. In practice, the most common method employed for the generation of optical beams containing vortices is the use of computer generated holograms [6]. The required hologram is formed by calculating and recording the interference pattern between a plane wave and the LG beam one seeks to produce. The result is a forked diffraction grating. Illuminating the grating with a plane wave one can produce a first-order diffracted beam carrying the desired value of orbital angular momentum.

Forked gratings can be used for production of x-rays carrying orbital angular momentum. In this case, the role of the diffraction grating might play lattice of a specially grown crystal with a fork-like dislocation. Spiral phase plates also can be used for generation of x-ray vortex beams. Recently, an experimental observation of an optical vortex in a beam consisting of 9-keV x-ray photons has been reported [9]. The vortex was created with an x-ray optical structure that imparts a spiral phase distribution to the incident wave.

Study of the excitation of nuclei through absorption of photons carrying orbital angular momentum we begin with discussion on the nuclear interaction Hamiltonian. Special attention is paid to the problem of choice of gauge for electromagnetic potentials in practical calculations of transition probabilities.

### 3. Multipole Interaction Hamiltonian

Hamiltonian of a nucleus interacting with electromagnetic field can be written as the sum

$$H = H_{\text{part}} + H_{\text{nucl}} + H_{\text{rad}} + H_{\text{int}} \tag{1}$$

containing the free-particle Hamiltonian

$$H_{\text{part}} = \mathbf{P}^2 / 2M \tag{2}$$

of the entire nucleus with mass M and momentum P, the nuclear Hamiltonian  $H_{\text{nucl}}$  describing the internal interaction of the elementary nucleons, the Hamiltonian of free electromagnetic field

$$H_{\rm rad} = \sum_{\mathbf{k}\sigma} \hbar \omega (a_{\mathbf{k}\sigma}^{\dagger} a_{\mathbf{k}\sigma} + \frac{1}{2}), \qquad (3)$$

where  $a_{\mathbf{k}\sigma}^{*}$  and  $a_{\mathbf{k}\sigma}$  are the operators for creation and annihilation of a photon with the energy  $\hbar\omega$ , momentum  $\hbar\mathbf{k}$  and polarization  $\sigma$  and, at last, the Hamiltonian  $H_{\text{int}}$  of interaction between a nucleus and electromagnetic field.

In conventional perturbation theory the sum of the Hamiltonians  $H_{\rm part}$  and  $H_{\rm nucl}$  for the material system and the Hamiltonian  $H_{\rm rad}$  for free electromagnetic field is treated as unperturbed Hamiltonian  $H_0$ . The eigenfunctions of  $H_0$  provide the basis set of states for the wavefunction of radiating system.

The interaction Hamiltonian  $H_{\rm int}$ , which is considered as a perturbation, is often expressed in terms of electromagnetic potentials, so that in the Coulomb gauge of vector potential  $\bf A$  it can be written, in single particle approximation of non-relativistic radiation theory, as

$$H_{\rm int} = -\frac{e}{mc} (\mathbf{A} \mathbf{p}) + \frac{e^2}{2mc^2} \mathbf{A}^2, \qquad (4)$$

where e is charge of a nucleon with mass m and momentum  $\mathbf{p}$  and c is the velocity of light. The vector potential in the place of a charged particle is determined by the expression

$$\mathbf{A}(\mathbf{r}) = \sum_{\mathbf{k}\sigma} \sqrt{\frac{2\pi\hbar c^2}{\omega}} \mathbf{e}_{\mathbf{k}\sigma} \left( a_{\mathbf{k}\sigma} e^{i\mathbf{k}\mathbf{r}} + a_{\mathbf{k}\sigma}^{\dagger} e^{-i\mathbf{k}\mathbf{r}} \right). \tag{5}$$

Since the interaction Hamiltonian in form (4) is obviously not gauge invariant, this approach introduce a serious concern about calculated results for nuclear transition probabilities. The expansion coefficients for the wave function look like dependent on gauge of electromagnetic potentials and therefore cannot be interpreted as probability amplitudes.

Difficulties of this type could be avoided if it is used the interaction Hamiltonian expressed in terms of electric field E and magnetic field H strengths. Already in very

early works in quantum radiation theory [10-12], the electron-photon Hamiltonian in the dipole interaction form

$$H_{\rm int} = -(\mathbf{dE}) \tag{6}$$

has been used for calculation the probabilities of atomic transitions. Afterwards, the interaction Hamiltonian in the form of multipole expansion has been established [13-15], which contains only electric and magnetic fields strengths, thus, expressing explicitly the well known gauge invariance of quantum theory. It can be represented as a sum of three terms

$$H_{\text{int}} = H_E + H_M + H_D, \tag{7}$$

where  $H_E$  describes electric multipole interaction between a nucleus and radiation field and it is given by the series

$$H_E = H_{E1} + H_{E2} + \dots + H_{EL} + \dots = -(\mathbf{dE}) + \dots$$
 (8)

with dipole electric contribution  $H_{E1}$ , quadrupole electric contribution  $H_{E2}$ , and so on, **d** - electric dipole moment of the nucleus,

$$\mathbf{E} = i \sum_{\mathbf{k}\sigma} \sqrt{2\pi\hbar\omega} \,\mathbf{e}_{\mathbf{k}\sigma} (a_{\mathbf{k}\sigma} e^{i\mathbf{k}\mathbf{R}} - a_{\mathbf{k}\sigma}^{\dagger} e^{-i\mathbf{k}\mathbf{R}}) \tag{9}$$

is electric field strength in the center of mass of the nucleus and  ${\bf R}$  - radius-vector of the center of mass.

The second term in (7),  $H_M$ , describes magnetic multipole interaction of a nucleus with radiation field and can be written as the series

$$H_M = H_{M1} + H_{M2} + \dots + H_{ML} + \dots = -(\mu \mathbf{H}) + \dots$$
 (10)

where  $H_{M1}$  - is the dipole magnetic contribution to the interaction energy,  $H_{M2}$  -quadrupole magnetic contribution, and so on,  $\mu$  - magnetic dipole moment of the nucleus and

$$\mathbf{H} = -i\sum_{\mathbf{k}\sigma} \sqrt{2\pi\hbar\omega} \left[ \mathbf{e}_{\mathbf{k}\sigma} \times \mathbf{\tau} \right] (a_{\mathbf{k}\sigma} e^{i\mathbf{k}\mathbf{R}} - a_{\mathbf{k}\sigma}^{\dagger} e^{-i\mathbf{k}\mathbf{R}})$$
 (11)

- magnetic field strength in the center of mass of the nucleus ( $\tau = k/k$  - unit vector).

The third term  $H_D$  is proportional to  $H_D \sim (H_M^2/mc^2)$  and, taking into account that  $H_M/mc^2 << 1$ , it can be neglected.

The series  $H_E$  (8) and  $H_M$  (10) are the power expansions on dimensionless parameter  $a/\lambda << 1$ , where  $a=1.2\times 10^{-13}\,A^{1/3}$  - radius (in centimeters) of a nucleus with the number of nucleons A and  $\lambda$  - is a wavelength of radiation and  $H_{EL}\sim (a/\lambda)^{L-\frac{1}{2}}$ ,  $H_{ML}\sim (v/c)(a/\lambda)^{L-\frac{1}{2}}$ , where v/c is the ratio of a velocity of nucleons to the velocity of light

Collecting all terms together, we can present interaction Hamiltonian through the multipole development

$$H_{\text{int}} = \sum_{L} \sum_{k\sigma} \left[ (V_{k\sigma}^{(EL)} + V_{k\sigma}^{(ML)}) e^{ik\mathbf{R}} a_{k\sigma} + (V_{k\sigma}^{(EL)} + V_{k\sigma}^{(ML)})^* e^{-ik\mathbf{R}} a_{k\sigma}^+ \right]$$
(12)

where both electric  $V_{\mathbf{k}\sigma}^{(EL)}$  and magnetic  $V_{\mathbf{k}\sigma}^{(ML)}$  multipole interactions can be written in the form  $V_{\mathbf{k}\sigma}^{(L)} = \left(\omega/c\right)^{L-\frac{1}{2}}V_{\tau\sigma}^{(L)}$  with  $V_{\tau\sigma}^{(L)}$  which is not dependent on frequency of emitted photon but only on the photon propagation direction assigned by the unit vector  $\boldsymbol{\tau}$ .

The equivalence of the two forms (4) and (7) of interaction Hamiltonians and the relation between the corresponding results for transition probabilities has been extensively discussed by many authors [12-23]. In a number of simple cases this equivalence can be shown [12, 16-18] by means of demonstration the formal identity between the expressions for the transition probabilities obtained with the two interaction Hamiltonians. A more general proof is obtained by applying a suitable canonical transformation [13, 14, 19, 20] or gauge transformation [15] directly to the conventional Hamiltonian (4). Since the difference between the two perturbations just corresponds to a gauge or canonical transformation under which the theory is known to be invariant, the both interactions must lead to the same physical predictions.

Nevertheless, a closer examination [18, 20-23] shows that the problem is not so simple in practical calculations of transition probabilities. Being calculated in a particular order of perturbation theory the transition probabilities turn out to be gauge dependent. The reason is that one does not use in such calculations the exact wavefunction (which differ by a phase factor in two gauges) but approximate it using perturbation theory. In addition, only a limited number of states of unperturbed Hamiltonian is usually used as a basis set for the wavefunction. As a result, transition probabilities computed with the interaction Hamiltonians in forms (4) and (7) differ by the factor of  $(\hbar\omega_1/E_1)^{2L}$  for a single photon transition with multipolarity L, by the factor of  $(\hbar\omega_1/E_1)^{2L_1}(\hbar\omega_2/E_2)^{2L_2}$  for two-photon transition and so on, where  $\omega_1$  and  $\omega_2$  represent the frequencies of photons inducing the transitions and  $E_1$  and  $E_2$  represent the energy differences between initial and intermediate or final states.

In the first order of perturbation theory the two interactions give the same results due to the fact that only initial and final states are involved and the photon energy  $\hbar\omega_1$  is equal to the energy difference  $E_1$  (see, however, the remark of Lamb [24] that only dipole interaction perturbation in form (6) gives the shape of atomic spectral line which is in agreement with experiment). In higher orders, intermediate states are involved and energy is usually not conserved in the virtual transitions to these states. For this reason, when the photon energy is much less than the energy difference between initial state and the closest intermediate state, the multiphoton transition probabilities calculated with the interaction Hamiltonians (4) and (7) may differ by many orders of magnitude [25, 26]. Thus, in this case the problem of choice between (4) and (7) becomes extremely critical.

Summarizing discussion on the problem of choice between the two forms of interaction Hamiltonian (4) and (7) we conclude that they are fully equivalent when

summation is carried out over all intermediate states and over all orders of perturbation theory. However, if only the leading term is retained it is preferable to use the gauge independent Hamiltonian in the multipole interaction form (7) which provides the most rapid convergence especially for multiquantum transitions with nonresonant intermediate states.

It should be emphasized that the interaction Hamiltonian is expressed in terms of electric and magnetic field strengths taking at the origin, that is at the place of a nucleus. We take this fact into account in the discussion, addressed in the following section, on some features in excitation of nuclei with x-ray beams carrying orbital angular momentum.

## 4. Excitation of Nuclei With X-ray Beams Carrying Orbital Angular Momentum

The existence of photon beams with a well defined projection of angular momentum  $J_z$  on the direction of its propagation is a direct consequence of the possibility to construct field modes as the eigenfunctions of the commuting set of operators for the projection of the angular momentum  $J_z$ , projection of the linear momentum  $P_z$ , energy and spin of a photon. Note that these modes do not have well defined total angular momentum, nor a definite parity.

Alternatively, one can construct field mode as the eigenstates of the four commuting operators for the square of total angular momentum  $J^2$ , its projection  $J_z$  along the z axis, energy an parity. These modes are well known as multipole waves of electromagnetic field. Photons in such states do not have well defined linear momentum, so that the beams of multipole waves with assigned direction of propagation are impossible.

The electric and magnetic field strengths at the place of a nucleus can be expanded into a set of multipole waves. The characteristic feature of the multipole waves of different orders is their different behavior in the origin: the only electric dipole wave with total angular momentum quantum number equal to unity has a nonvanishing value of the electric field strength at the place of a nucleus, the only electric quadrupole wave with total angular momentum quantum number equal to 2 has nonzero first-order gradients of the electric field strength at the place of a nucleus and so on. Such a property of the multipole waves is closely related to the low of angular momentum conservation in absorption or emission of a photon. In fact, this property ensures that the nuclear excitation through, for a example, an electric quadrupole transition, is determined by coupling of the nucleus only to the electric quadrupole wave of electromagnetic field. Therefore, the transition probability depends not on the total intensity of the electromagnetic field, but solely on the amplitude of the electric quadrupole wave. As only the quadrupole wave contributes to the quadrupole interaction, the angular momentum is conserved. If such a wave does not contribute the electromagnetic field, the excitation of a nucleus through the electric quadrupole transition becomes impossible. In this case, however, the transition may occur through a mode of higher-multipolarity and, thus, the nuclear excitation probability will be suppressed. On the contrary, the intensity of electromagnetic field strength may vanish at the place of a nucleus, this does not prevent the quadrupole and higher-order nuclear transitions to occur.

In order to illustrate this assertion we consider absorption of photons from the beam possessing a well defined projection of angular momentum  $J_z$  on the direction of its propagation. Electromagnetic field on the beam axis can be expanded into a set of multipole waves. Note, that for the beam with  $J_z$  equal to, for example, 2, only those multipole waves, which possess 2 units of angular momentum and higher, and a fixed value of the projection of angular momentum equal to 2 are involved into the expansion. This means that dipole waves do not contribute the field, so that dipole nuclear transitions are unlikely to occur. Only quadrupole and higher-order transitions can be induced by the beam. The latter becomes obvious if we take into account zero intensity of light at the beam axis. In fact, photons of the beam with  $J_z$ =2 have, along with the spin, the orbital angular momentum contribution. A feature of the beams with orbital angular momentum is that the phase singularity dictates zero field intensity on the beam axis.

Accordingly, photons with 3 units of angular momentum projection cannot be absorbed by a nucleus through quadrupole transitions. At last, photons of the beam with angular momentum projection on the beam axis equal to  $J_1+J_2+1$  and higher cannot excite at all a nucleus from an initial state with spin  $J_1$  to a final state with spin  $J_2$ , in spite of the resonance between photon energy and energy of the nuclear transition.

### 5. Conclusions

We have discussed excitation of nuclei by the photon beams carrying a well defined angular momentum projection on the beam axis. We have argued that such beams could be used for the fine tuning of the process of excitation. In particular:

- we are able to control the multipolarity of nuclear transition through which the excitation of a nucleus is going to occur;
- we are able to suppress or even forbid the absorption of photons in resonance transitions if the beam with a high enough angular momentum about the beam axis is used;
- we are able enhance or suppress absorption of photons choosing the photon beams with superposition of different angular momentum projection on the beam axis.

We have argued that improper choice of the photon beam can decrease dramatically the nuclear excitation probability. The study performed in this paper can be useful in search for the beam of an optimal configuration for excitation of nuclei through transitions of high multipolarities.

## Acknowledgments

This study was partially supported by the ISTC, grant #2651p and by U.S. CRDF-R.F. Ministry of Education Award, VZ-010-0.

### References

- 1. L. Allen, S.M. Barnett, M.J. Padgett, *Optical Angular Momentum* (Institute of Physics Publishing, Philadelphia, 2003).
- 2. J.H. Poynting, *Proc. Roy. Soc.* A82, 560 (1909)
- 3. L. Allen, M.W. Beijersbergen, R.J.C. Spreeuw, J.P. Woerdman, *Phys. Rev.* A45, 8185 (1992)
- M. Brambilla, F. Battipede, L.A. Lugiato, V. Penna, F. Prati, C. Tamm, C.O. Weiss, *Phys. Rev.* A43, 5090 (1991)
- 5. M. W. Beijersbergen, L. Allen, H.E.L.O. van der Veen, J.P. Woerdman, Opt. Commun. 96, 123 (1993)
- 6. N.R. Heckenberg, R. McDuff, C.P. Smith, A.G. White, Opt. Lett. 17, 221 (1992)
- 7. M.W. Beijersbergen, R.P.C. Coerwinkel, M. Kristensen, J.P. Woerdman, Opt. Commun. 112, 321 (1994)
- V. Yu. Bazhenov, M.S. Soskin, M.V. Vasnetsov, JETP Letters 52, 429 (1990); J. Mod. Opt. 39, 985 (1992)
- 9. A.G. Peele, P.J. McMahon et al., Optics Letters 27, 1752 (2002)
- 10. H.A. Kramers, W. Heisenberg, Z. Phys. 31, 681 (1925)
- 11. V. Weisskopf, Ann. Phys., Lpz. 9, 23 (1931)
- 12. M. Göppert-Mayer, Ann. Phys., Lpz. 9, 273 (1931)
- 13. E.A. Power, S. Zienau, *Philosophical Transactions of Royal Society* A251, 427 (1959)
- 14. J. Fiutak, Canadian Journal of Physics 41, 12 (1963)
- 15. R. Loudon, The Quantum Theory of Light (Clarendon Press, Oxford, 1973), ch. 8.
- 16. P.I. Richards, Phys. Rev. 73, 254 (1948)
- 17. F.V. Bunkin, Sov. Phys. JETP 23, 1121 (1966)
- 18. J.J. Forney, A. Quattropani, F. Bassani, Nuovo Cimento B37, 78 (1977)
- 19. E.A. Power, *Introductory Quantum Electrodynamics* (Longmans, Green, New York, 1964), ch. 8
- 20. E.A. Power, T. Thirunamachandran, American J. Phys. 46, 370 (1978)
- 21. Kuo-Ho Yang, Annals of Physics 101, 62 (1976)
- 22. F. Bassani, J.J. Forney, A. Quattropani, Phys. Rev. Lett. 39, 1070 (1977)
- 23. D.H. Kobe, A.L. Smirl, American J. Phys. 46, 624 (1978)
- 24. W.E. Lamb, Jr., Phys. Rev. 85, 259 (1952)
- 25. W. Becker, R.R. Schlicher, M.O. Scully, Physics Letters A106, 441 (1984)
- 26. S. Olariu, I. Popescu, C.B. Collins, Phys. Rev. **D20**, 3095 (1979)

## MULTIPOLE GAMMA-SUPERRADIANCE OF THE EVEN-EVEN NUCLEI\*

### V.V. SAMARTSEV

Physics Department, Kazan State University, Kremlevskaya 16, Kazan, 420008, Russia

#### A.A. KALACHEV

E.K. Zavoisky KazanPhysical-Technical Institute, Kazan Scientific Center, Russian Academy of Sciences SibirskyTtrakt 10/7, Kazan,420029,Russia

The specific features of gamma-superradiance of the inverted system of two or few closely grouped even-even nuclei (cluster) are investigated theoretically. It is determined that unlike from Dicke superradiance the intensity I of such superradiance depends on the number N of active nuclei as  $I-N^{\alpha}$ , where  $\alpha > 2$ . The attempt to explain the existing experimental data on the multipole gamma-superradiance is undertook.

### 1. Introduction

This paper is devoted to the problem of multipole gamma-superradiance by ensemble of even-even nuclei. The solution of this problem is important for a gammalaser creation, the feasibility of which was firstly shown in 1963 by L. Rivlin [1]. However a serious practical difficulty for realization of this idea is the provision for the feedback mirrors, which should be opaque in the gamma-range. Because of this very difficult technical problem the search for alternative method of the production of the strong coherent radiation was carried out. The superradiant method predicted by R. Dicke in 1954 [2] is such method, which may be realized without feedback mirrors. In 1965, the gamma-superradiance (GSR) at the electric dipole transition (E1) was theoretically studied in [3]. The corresponding expression for the intensity basically coincided with the Dicke formula except for the introduction of the Debye-Waller factor. The intensity of electric dipole GSR I is proportional to the squared number N of active nuclei:  $I \sim N^2$ . A number of later theoretical studies dwell on various aspects of GSR. One can find the corresponding references in paper [4]. A significant point established in these studies was the necessity of fitting a lattice to the Borrmann condition [5, 6]:  $k = 2\pi b$ , where k is the wave vector of a gamma-photon and b is the reciprocal lattice vector. Thus, GSR may arise only in a regular system of active

This work is supported by grant of U.S.Civilian Research and Development Foundation (no. CGP RP1-2560-KA-03) and Russian Foundation for Basic Research (project no.04-02-17082).

inverted nuclei, when the distance between nuclei (i.e. between lattice knots) is a multiple of the gamma-quant wavelength  $\lambda$ , which is of an order of  $10^{-9}$  cm. The radiation coherence length  $l_{coh} = c/\Gamma$  (where  $\Gamma$  is the multipole gamma-transition linewidth and c is the gamma-ray propagation velocity) of the first spontaneously emitted gamma photons was estimated at several tens of meters, which means that this radiation is capable of uniting the nuclei in a single ensemble by means of the common field. One can obtain the ensemble of inverted nuclei by means of the external pumping of nuclei or by thermal neutron irradiation [7]. But in gamma-optics the nuclei are often already excited as the <sup>178</sup>Hf isomer nuclei [8] and their lifetime in this state is equal to 31 years. The problem is to realize a controlled transition of such nuclei form this stable state to a shortlived state. For this purpose the nuclei were irradiated with X-ray in order to realize triggered initiation of gamma-emission [9]. One of the most detailed theoretical papers on GSR was written by B. Balko with colleagues [7], who used for his estimations the <sup>60</sup>Co nuclei prepared from <sup>59</sup>Co by thermal neutron irradiation in the isomeric level with a lifetime 637 s. The electric dipole GSR may be realized on the <sup>60</sup>Co nuclei if the thermal neutron flux with cross section of 20 b is used for the pumping of the <sup>59</sup>Co nuclei. The intensity of such GSR is proportional to  $N^2$ . The spatial diagrams of natural spontaneous decay and GSR borrowed from paper [7] are shown in Figure 1.

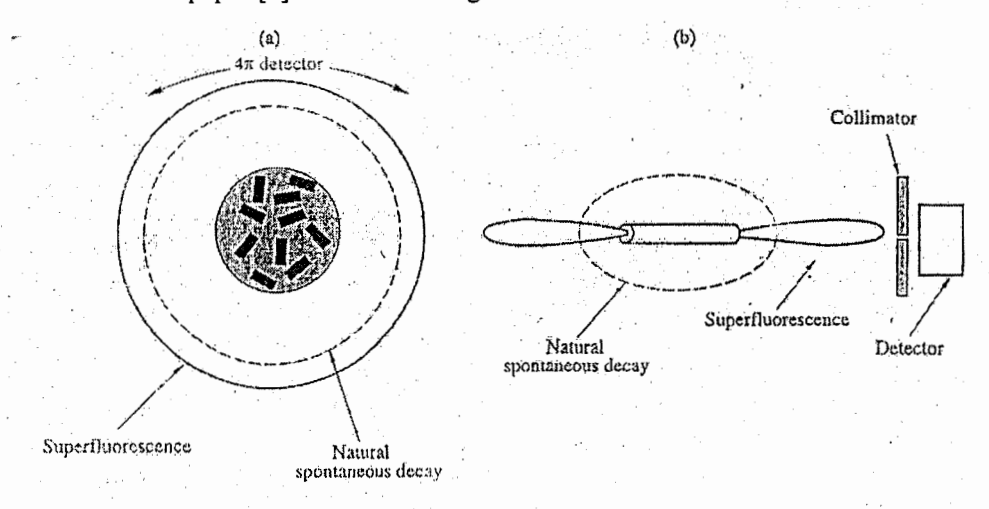


Figure 1. Cross section of a polycrystalline sample and spatial distribution of spontaneous gamma-radiation (a) and geometry of suggested experiment and main parts of experimental arrangement (b).

## 2. Quadrupole gamma-superradiance

Note that a theory of multipole superradiance was discussed as early as 1973 [10], but this paper was not connected with gamma-range. In particular, it was shown that the intensity of quadrupole superradiance at the double optical transition

frequency is proportional to  $N^4$ , where N is the number of emitters. This result may be interpreted in the following way. The collective states under consideration arise when elementary multipoles stick together, forming multipoles of a larger size. In the ideal case, N electrical multipoles with moment  $P_j = el_j$  comprise a dipole with moment  $P = e\sum_j l_j = Nel_j$ , which entails the dependence of the dipole superradiance intensity on  $N^2$ . For quadrupoles,  $Q_j = el_j^2$  and  $Q = e(\sum_{j=1}^N l_j)^2$ , so that the superradiance intensity is proportional to  $N^4$  in this case. Such a concentration dependence is typical of the superradiance from an ensemble of exchange pairs, i.e., the clusters resulting from the exchange interaction of paramagnetic ions. The clusters of three, four, etc., ions should emit multipole superradiance with an intensity proportional to  $N^6$ ,  $N^8$ , etc.

According to the above mentioned paper the intensity of the multipole GSR may be calculated by means of expression:

$$I(\Delta m\omega_0) = \left(\frac{1}{2}\right)^{\Delta m} I_0(\Delta m\omega_0) \operatorname{Sp}\left\{\rho(t) R_+^{\Delta m} R_-^{\Delta m}\right\},\,$$

where  $\Delta m = 1, 2, 3, ..., I_0(\Delta m\omega_0)$  is the intensity of spontaneous multipole radiation of isolated emitter,  $\omega_0$  is the frequency of energy transition of this emitter,  $\rho(t)$  is the density matrix of ensemble of emitters,  $R_{\pm} = R_1 \pm iR_2$ ,  $R_1$  and  $R_2$  are the transverse components of energy spin. This expression leads to the following formula for the intensity of quadrupole superradiance ( $\Delta m = 2$ ):

$$I(2\omega_0) = \left(\frac{1}{2}\right)^2 I_0(2\omega_0) \operatorname{Sp}\left\{\rho(t) R_+^2 R_-^2\right\}.$$

Note that this formula may be obtained under the semiclassical consideration of the collective spontaneous radiation by ensemble of N emitters using the following Hamiltonian of interaction of this ensemble with the radiation field:

$$H_1 = (AR_+^2 + BR_3R_+) + \text{h.c.},$$

where A and B are the constants of interaction,  $R_3$  is the longitudinal component of energy spin. The collective states of such ensemble are described by the quantum numbers  $l = \frac{N}{2}, \frac{N}{2} - 1, ..., 0$  and m = -l, -l+1, ..., +l. Then, we have

$$I(2\omega_0) = \frac{1}{4}I_0(2\omega_0)(l-m+1)(l+m-1)(l+m)(l-m+2).$$

When  $l = \frac{N}{2}$  and m = 0 for N >> 1 we have

$$I(2\omega_0) = \frac{1}{4}I_0(2\omega_0)N^4.$$

Later the quadrupole GSR was theoretically analyzed in papers [9, 11]. It was shown that quadrupole GSR may take place in even-even nuclei (<sup>114</sup>Ba, <sup>150</sup>Sm, <sup>220</sup>Ra), i.e. in nuclei with an even number of protons and neutrons. In this paper the multipole GSR is considered in terms of the cluster model.

## 3. Cluster model of nucleus and GSR

It is well known that a radioactive nucleus decays with the emission of protons, neutrons, and compound particles (alpha particles and other light and heavy nuclei) whose compositions and properties significantly differ from those of the original nucleus. These experimental facts are explainable within the nuclear cluster model [12]. According to this model the atomic nucleus may be considered both as the system of nucleons and as the reservoir of various clusters. The nucleus splits into the large number of clusters under the collision with very fast particle, which energy is equal to a few GeV. This process is shown in Figure 2 borrowed from paper [13].

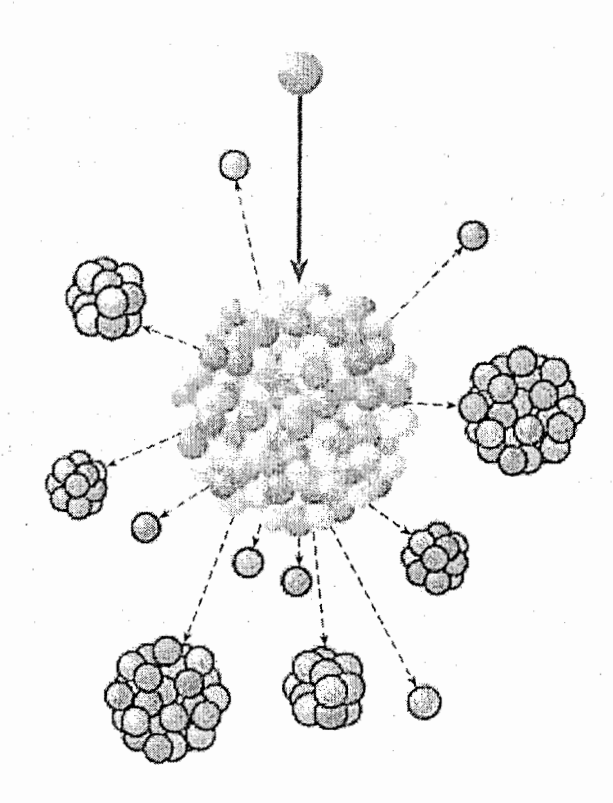


Figure 2. Illustration of nuclear cluster model in the case of collision of nucleus with fast particle [13].

A cluster is interpreted as a compact structure of two or more particles that may emerge inside a nucleus. Therefore, an atomic nucleus can be considered either as a system of nucleons or as a reservoir containing clusters with various compositions and properties. The compound particles that arise during nuclear decay are formed from the clusters that already exist in the nucleus. In terms of the modern representation of a nucleon as a three-quark combination, atomic nucleus represents a conglomeration of quark sacks containing six, nine, etc., quarks. It is also important to note that, at every instant, an individual nucleon does not belong to one and the same cluster but can with equal probability be a part of any cluster that possible in the nucleus.

The cluster model is in agreement with the idea of Bogolyubov regarding the nucleon coupling [14]. Such coupling of fermions results in the formation of bosons and makes possible Bose–Einstein condensation. The state of a Bose–Einstein condensate (BEC) represents a coherent state of all coupled nucleons. The BEC state is most readily formed by the even–even nuclei. In the BEC state, the nucleon pairs behave like waves rather than like elementary particles. Since such waves are capable of interference and this capability is the decisive sign of coherence, we consider gamma superradiance assuming that all the nucleon pairs are inphase, i.e., the system is ideally suited for the formation of cooperative effects. Along with gamma superradiance, such effects include collective gamma scattering and even gamma echo.

## 4. Generalized Dicke model of superradiance. Cluster GSR

Let us consider a system of N identical clusters in a nucleus that interact with each other both via the common field of the emitted gamma photons and by means of exchange forces, which are responsible, in particular, for the cooperative absorption or emission of gamma photons by two clusters. The size of a nucleus is substantially smaller than the gamma-ray wavelength. Therefore, the superradiance in such a system can be described using the Dicke model [2], wherein the initial Hamiltonian is supplemented with terms taking into account the cooperative effects. Thus, in the interaction representation and the rotating wave approximation, the Hamiltonian appears in the form

$$H = \sum_{k,r} g_{kr}^{(1)} a_{ks} R^{+} e^{i(\omega_{0} - \omega)t} + g_{ks}^{(2)} a_{ks} R^{+} R^{+} e^{i(2\omega_{0} - \omega)t} + \text{h.c.}.$$
 (1)

where  $a_{\mathbf{k}}$  is the photon-annihilation operator in the mode characterized by the wave vector  $\mathbf{k}$  and polarization s (at the frequency  $\omega = |\mathbf{k}|/c$ );  $R^+$  is the collective operator of the cluster transition at frequency  $\omega_0$ ; h.c. denotes the hermitian conjugate; and  $g_{\mathbf{k}}^{(1)}$  and  $g_{\mathbf{k}}^{(2)}$  are the cluster-field coupling constants corresponding to the transitions at the frequencies  $\omega_0$  and  $2\omega_0$ , respectively. These constants can be used to describe transitions of various multipolarity depending on the parity of the ground and excited states.

With regard to expression (1), the master kinetic equation for the density operator  $\rho$  of the cluster system in the Born-Markov approximation is given by

$$\frac{\partial}{\partial t} \rho = -\beta^{(1)} \left\{ R^+ R^- \rho - 2R^- \rho R^+ + \rho R^+ R^- \right\} - \\
- \beta^{(2)} \left\{ R^+ R^+ R^- R^- \rho - 2R^- R^- \rho R^+ R^+ + \rho R^+ R^+ R^- R^- \right\}, (2)$$

where  $\beta^{(n)} = \sum_{k_n} \pi \left| g^{(n)} \right|^2 \delta(n\omega_0 - \omega)$  is the rate of spontaneous transition at the frequency  $n\omega_0$ .

Let us now change to the basis of the collective Dicke states  $|l,m\rangle$ :

$$R_{3} | l, m \rangle = m | l, m \rangle,$$

$$R^{+} | l, m \rangle = \sqrt{(l-m)(l+m+1)} | l, m+1 \rangle,$$

$$R^{-} | l, m \rangle = \sqrt{(l-m+1)(l+m)} | l, m-1 \rangle.$$
(3)

Here,  $R_3$  is the operator of half-difference of the excited and ground state populations for the clusters with eigenvalues  $|m| \le l$ , where l = N/2 is the cooperative quantum number characterizing the length of the collective Bloch vector. Then, from Eq. (2), we derive the equation for populations

$$\frac{\partial}{\partial t} \rho_{mm} = -2\beta^{(1)} \left\{ g(l,m) \rho_{mm} - g(l,m+1) \rho_{m+1,m+1} \right\} - -2\beta^{(2)} \left\{ g(l,m) g(l,m-1) \rho_{mm} - g(l,m+1) g(l,m+2) \rho_{m+2,m+2} \right\}$$
(4)

where g(l,m) = (l+m)(l-m+1).

Figure 3 presents the time dependences of the correlation functions  $\langle R^+R^-\rangle = \sum_m \rho_{mm} g(l,m)$  and  $\langle R^+R^+R^-R^-\rangle = \sum_m \rho_{mm} g(l,m) g(l,m-1)$  for the system of N clusters at various N as obtained using the numerical solution to system of equations (4) with the initial condition  $\rho_{mm} = \delta_{m,l}$  (l = N/2) corresponding to the completely excited cluster system. The solution implies that  $\beta^{(1)} = 0$ , i.e., that only the pairs of clusters emit gamma photons at the frequency  $2\omega_0$ , which takes place for, e.g., quadrupole superradiance. In this case, the superradiance intensity is proportional calculations.  $\langle R^+R^+R^-R^-\rangle$ . According to numerical the ratio  $G = \langle R^+ R^+ R^- R^- \rangle / \langle R^+ R^- \rangle^2$  grows with N and the superradiance intensity is proportional to  $N^3$  (see Figure 4). This is because the superradiance signal duration is proportional to  $(\beta^{(2)}N^2)^{-1}$  (the number of pairs is proportional to  $N^2$ ) and the number of emitted photons is proportional to N/2. So, the superradiance intensity proves to be proportional to  $N^3$ , which agrees with the experimental data of paper [15]. These dependences also hold true in the general case  $\beta^{(1)} \neq 0$ , but under the condition

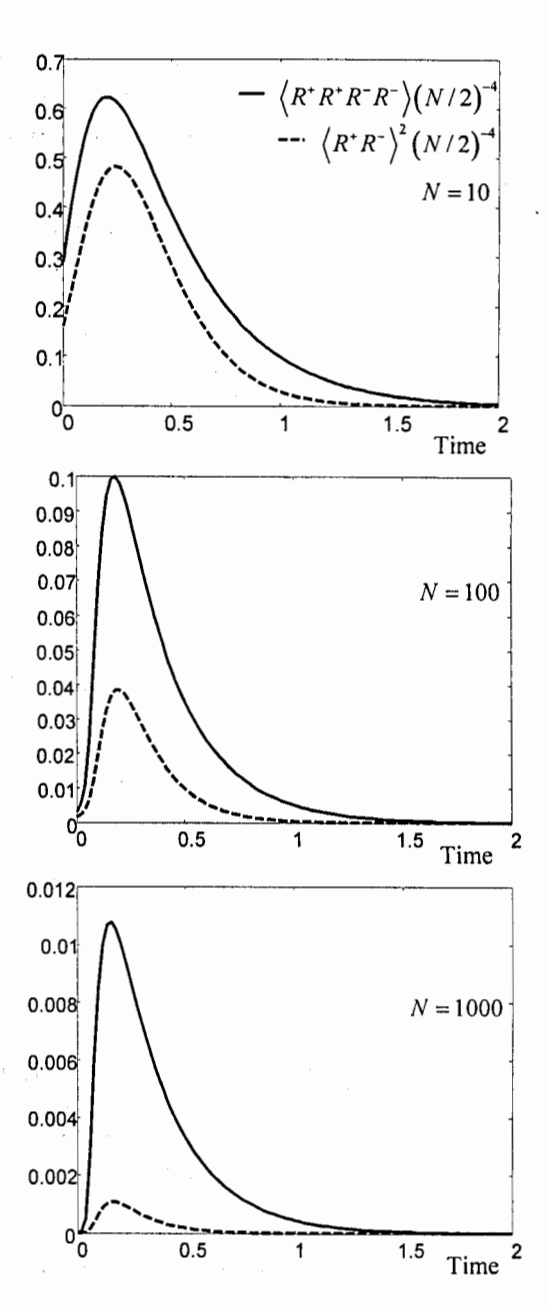


Figure 3. Time dependence of the correlation functions  $\left\langle R^+R^+R^-R^-\right\rangle$  and  $\left\langle R^+R^-\right\rangle^2$  of a N-cluster system at various N: numerical solutions to system (4) for  $\beta^{(1)}=0$  and the initial condition  $\rho_{mm}=\delta_{m,N/2}$ . The time is expressed in units of  $\left(\beta^{(2)}N^2\right)^{-1}$ .

 $\beta^{(1)} \ll \beta^{(2)} N^2$ . Then, the relationship G > 1 points to the super-Poissonian statistics of photons emitted at frequency  $\omega_0$ . In the case  $\beta^{(1)} \gg \beta^{(2)} N^2$ , the dominant superradiance signal is at the frequency  $\omega_0$  and has a duration proportional to  $(\beta^{(2)} N)^{-1}$ . With increasing N, the value of G tends to unity, and we arrive at an ordinary superradiance signal with its field staying in the coherent state.

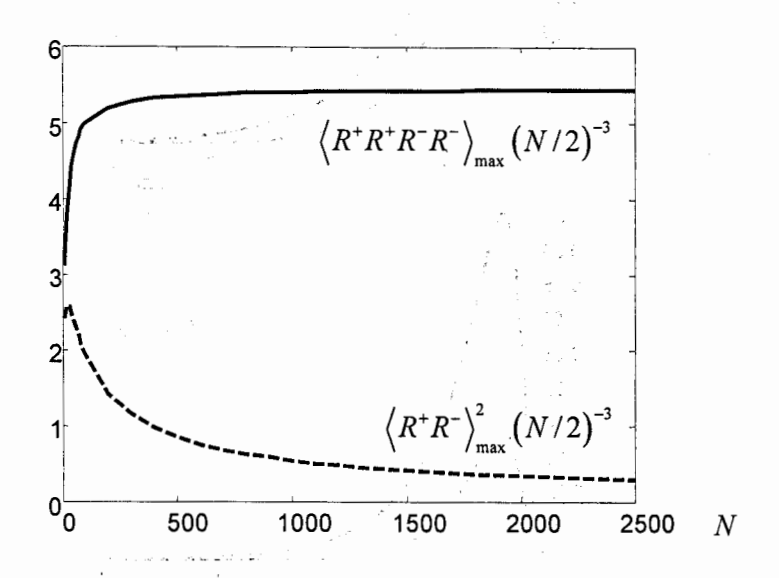


Figure 4. The peak values of correlation functions  $\langle R^+R^+R^-R^- \rangle$  and  $\langle R^+R^- \rangle^2$  divided by  $(N/2)^3$  as a function of N: the result of numerical solutions to system (4) for  $\beta^{(1)} = 0$  and the initial condition  $\rho_{mm} = \delta_{m,N/2}$ .

The above discussion gives rise to another question as to whether it is possible to observe multipole gamma superradiance in a cluster consisting of several nuclei. In our opinion, the answer is affirmative. From this viewpoint, of much interest are the nuclear highly strained molecular-type systems (nuclear molecules) that appear during the nuclear reactions (for example, <sup>12</sup>C+<sup>12</sup>C, <sup>16</sup>O+<sup>16</sup>O, and others). "Nuclear molecule" (for example, see review [16]) is a conventional term for the collective states of a nuclear system, which are usually characterized by extraordinary high spectroscopic factors (the degree of overlapping of wavefunctions) of the fragments (nuclei or clusters) comprising this system. The calculation presented above predicts an appreciable increase in the gamma-photon emission rate in nuclear molecules as compared to that in the constituent nuclei, which may prove useful for studying shortlived nuclear collective states with the methods of nuclear molecular spectroscopy.

### 5. Experiment on the multipole GSR

The experiment on the multipole gamma-superradiance (MGSR) was performed by the authors of paper [15] in the sample Mg(<sup>123m2</sup>Te), cooled to a liquid nitrogen temperature, and in the same sample at room temperature. Gamma-spectroscopic analysis was carried out by the setup consisting of the spectroscopic path based on the C<sub>3</sub>Γ-06 spectrometer (which amplified and formed a signal from preamplifier of detector) and of the analyzer of pulse amplitudes AMA-02Φ1. The samples were placed into a quartz ampoule with a length of 70 mm and a diameter of 8 mm. The length of active part of ampoule was equal to 15 mm. Mass of radioactive matter was about 2 mg, but the activity A of each nuclear isomer of Te was equal to 1.0 MBq. The sample was fixed horizontally. The gamma-quanta emitted from the side of the sample normally to the window of detector were registered. The germanium detectors ДГДК with a registration efficiency  $\eta = 0.42$  near 159 keV were used. The resolution time of detector was equal to 10 microseconds. The direct measurements of the halfdecay constant for each radionuclide were carried out both in the cooled sample Mg(123m2Te + 121m2Te) and in the uncooled sample of the same composition. Measurements of uncooled sample showed, that  $T_{1/2} = 119,15\pm0,25$  days for nuclide <sup>123m2</sup>Te. It agrees with experimental data of paper [17]. Measurements of cooled sample showed that  $T_{1/2} = 118,65 \pm 0,25$  days for the same nuclide. Thus, the decay in cooled sample became more active and the decay constant increased. The authors of experiment [15] state that the intensity of gamma-quanta emission by cooled sample is proportional to  $N^3$ , where N is the number of active nuclei. They attributed such dependence to the multipole gamma-superradiance. The spontaneous radiation of domains of polycrystalline sample is more collective at the liquid nitrogen temperature. The authors of experiment [15] think that their results may be described by means of theoretical model developed in our papers [9, 11].

## Acknowledgments

Authors would like to thank Tatiana Mitrofanova for help. This work was supported by U.S.Civilian Research and Development Foundation (grant no. CGP RP1-2560-KA-03), by the Russian Foundation for Basic Research (projects no. 04-02-17082, 04-02-81009-Bel2004 and 05-02-16003), by the Program of Presidium RAS "Quantum Macrophysics" and by Program of Department of Physical Sciences "Optical spectroscopy and standards of frequency".

### References

- 1. A.L. Rivlin, Vopr. Radioelectron. 6, 42 (1963).
- 2. R.H. Dicke, Phys. Rev. 93, 99 (1954).
- 3. J.H. Turhune, G.C. Baldwin, Phys. Rev. Lett. 14, 589 (1965).
- 4. A.A. Kalachev, V.V. Samartsev and S.S. Kharintsev, Laser Physics 15, (2005).
- 5. V.I. Goldanskii, Yu.M. Kagan, Zh. Eksp. Teor. Fiz. 64, 90 (1973) (Sov. Phys. JETP 37, 49 (1973)).

- 6. A.V. Andreev, V.I. Emelyanov, Yu.A. Illinsky, *Usp. Fiz. Nauk* **131**, 653 (1980) (*Sov. Phys. Usp.* **131**, 493 (1980)).
- 7. B. Balko, I.W. Kay, J.D. Silk, D.A. Sparrow, Laser Physics 5, 355 (1995).
- 8. C.B. Collins, S.A. Karamian, J.J. Carroll et.al. Phys. Rev. Lett. 82, 695 (1999).
- 9. V.V. Samartsev, S.N. Andrianov, Izv. Ross. Akad. Nauk, ser. fiz 65, 1044 (2001).
- 10. U.H. Kopvillem, V.R. Nagibarov, V.V. Samartsev, Phys. Lett. 42A, 399 (1973).
- 11. S.N. Andrianov, V.V. Samartsev, Laser Physics 6, 201 (1996).
- 12. K. Wildermuth, Y.C. Tang. A Unified Theory of Nucleus, F.Vieweg, Braunschweig, 1977.
- 13. S.G. Kadmensky, Soros Education Journal 6, 87 (2000).
- 14. N.N. Bogolubov, Dokl. Akad. Nauk SSSR 119, 52 (1958).
- 15. G.A. Skorobogatov, V.V. Eremin, B.E. Dzevitskii, *Izv. Ross. Akad. Nauk, ser. fiz.* 68, 1296 (2004).

eser of entral operators to the control of the cont

- 16. R.R. Betts, A.H. Wuosmaa, Rep. Prog. Phys. 60, 819 (1997).
- 17. S. Ohya, T. Tamura, Nuclear Data Sheets 70, 531 (1993).

this expression of the Silver of the

and the second of the second of the

office of the factor and the second of the second



Studies with selected isomers

# MEASUREMENT OF <sup>177</sup>LU<sup>M</sup> TRIGGERED ISOMER BURN-UP INDUCED BY BREMSSTRAHLUNG RADIATION

### M. HELBA H. ROBERTS

SRS Technologies, 500 Discovery Drive Huntsville, Alabama 35806, USA

### M. LITZ G. MERKEL

Army Research Laboratory, 2800 Powder Mill Road Adelphi, Maryland 20783, USA

### J. J. CARROLL

Youngstown State University, One University Plaza Youngstown, Ohio 44555, USA

A sample of the 160.4-day half-life <sup>177</sup>Lu<sup>m</sup> isomer was exposed to Bremsstrahlung radiation at 280 kV and 8 ma. The irradiation duration was three weeks. Gamma spectroscopy assays were conducted before and after the irradiation. Discrepancies in the <sup>177</sup>Lu<sup>m</sup> activity and the <sup>177</sup>Lu ground state activity (6.734-day half-life) before and after the irradiation would indicate an accelerated "burn-up" of isomer due to triggered decay. The experimental setup is described, and results are given. With 99% confidence, 0.10% of the isomer nuclei were lost during irradiation. An observed total integrated cross section of 10<sup>-27</sup> cm<sup>2</sup>·keV is reported.

### 1. Introduction

For two decades, nuclear isomers have been a subject of intense study, with research accelerating in the last five years. Much of this research has pursued a single isomer, Hfm², for a single application – rapid energy release through a chain reaction. While controversy may exist in the value of the triggering levels of particular gamma lines in Hfm², triggering has been shown in Hao Ta. There are other potentially useful isomers known to exist, and there are other potential applications for which a rapid chain reaction is not the optimal method of releasing the energy. Other isomers have been investigated to answer questions of nuclear structure. Astrophysical applications of tantalum isomers have been useful in dating the universe. The medical applications of isomeric materials are becoming practical as well. It is apparent that the power and energy uses of long-lived isomers are driving more interest in these materials.

The motivation for this work lies in extended use power sources, particularly long-lived energy-dense power for unattended sensors. An isomer with a radioactive daughter product could make an excellent nuclear battery. This paper describes an experiment to detect gamma induced triggering of <sup>177</sup>Lu<sup>m</sup>.

The properties of the lutetium isomer are discussed in Section 2. Experimental techniques are described in Section 3. The details and analysis process are described in Section 4. The results appear in Section 5 with conclusions identified in Section 6.

## 2. The 177Lum Isomer

<sup>177</sup>Lu<sup>m</sup> was selected as an isomer of interest for several reasons. It's half life is long enough to make it useful for applications as an isomer battery, but short enough that the decay curve can be accurately measured over the course of the experiment. The <sup>177</sup>Lu daughter product's shorter half-life is useful for applications (allowing "charging" of an isomer battery by conversion of the isomer into ground state lutetium at the depot) and can make it easier to observe an equilibrium disturbance during the burn-up experiment.

## 2.1. Decay Properties

The <sup>177</sup>Lu<sup>m</sup> isomer has a 160.4-day half-life and decays by two mechanisms. 77.6% of decays are by beta decay and proceed to the stable <sup>177</sup>Hf nuclei while the remaining 22.4% of decays are by internal transition to the <sup>177</sup>Lu ground state.<sup>8</sup> The ground state has a half-life of 6.734 days. This is shown graphically in Figure 1. The ground state is in equilibrium with the isomer parent.

The stored energy level of the isomer is 970.1749 keV. The spin of the isomer state is 23/2-. The IT decay produces 12 unique gamma rays. 36 additional gamma rays are

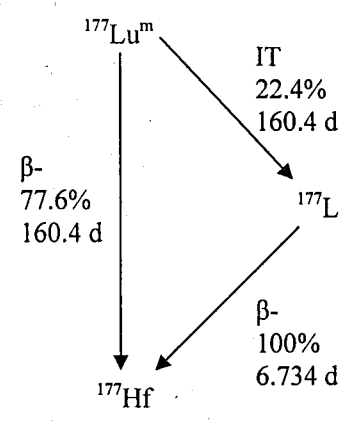


Figure 1. Decay scheme for <sup>177</sup>Lu<sup>m</sup>.

measurable as a result of the beta decay from the isomer to <sup>177</sup>Hf. The beta decay from <sup>177</sup>Lu to <sup>177</sup>Hf produces six measurable gamma rays, but these gammas are indistinguishable from six of the gammas produced in the <sup>177</sup>Lu<sup>m</sup> to <sup>177</sup>Hf beta decay.

### 2.2. Source Material

The lutetium isomer material was obtained from the University of Missouri Research Reactor (MURR). MURR produces isotopes, including the lutetium isotope  $^{177}$ Lu, for medical radiotherapy uses. One of MURR's two production methods for  $^{177}$ Lu is direct neutron activation (n, $\gamma$ ) of  $^{176}$ Lu to  $^{177}$ Lu. When this method is used, the unwanted byproduct of  $^{177}$ Lu<sup>m</sup> is formed. This byproduct was made available to SRS

Technologies for purchase in the form of seven vials with the lutetium in HCl solution.

## 2.3. Experimental Targets

Two experimental targets were assembled for this burn-up experiment. One was intended as the test article while the other was held as a control. The targets were manufactured on 28 January 2004, each with approximately 62,335 Bq of <sup>177</sup>Lu<sup>m</sup>, or 1.25×10<sup>12</sup> nuclei. The targets were created by evaporative deposition of a volume of the HCl solution on a beryllium disk. A second beryllium disk was placed over the deposit to form a "sandwich," and disks were locked into an aluminum housing. The aluminum housing was designed to mount against the beryllium window of the x-ray tube.

## 3. Experiment Overview

The burn-up experiment was conducted in three phases. In the first phase, the experimental and control targets were assayed in the SRS Technologies Spectroscopy laboratory. In the second phase, the experimental target was irradiated at the Army Research Laboratory (ARL). The control target continued to be assayed at SRS during this time. In the third phase, the experimental target was assayed again at SRS, and discrepancies in the activities were identified.

## 3.1. Expected Results

For both the <sup>177</sup>Lu<sup>m</sup> and <sup>177</sup>Lu, the decay curves measured before irradiation were extrapolated into the future. When assays were conducted after the irradiation, they were compared to the expected values from the extrapolated decay curves.

If no burn-up occurs, then the measured values after the irradiation fall along the extrapolated curves. If, on the other hand, burn-up of the isomer has occurred, then the <sup>177</sup>Lu<sup>m</sup> activity would be lower than predicted as shown in Figure 2.

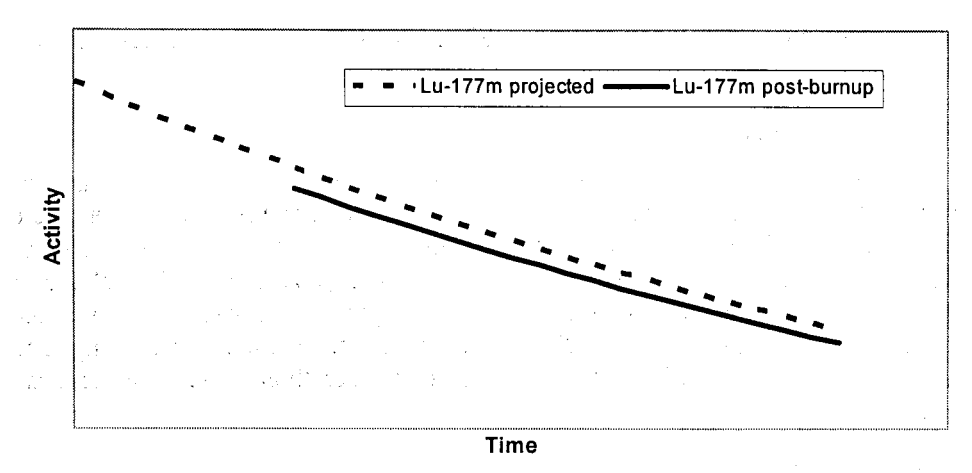


Figure 2. Sketch of expected results if the <sup>177</sup>Lu<sup>m</sup> isomer experiences significant triggered decay during the burn-up experiment.

If burn-up occurs in the form of IT decay, then the population of the ground state will increase during the irradiation. This throws the parent-daughter relationship out of equilibrium. Measurements taken immediately after the irradiation would show an increase in the <sup>177</sup>Lu activity, as shown in Figure 3. Over a couple of weeks, equilibrium would be restored, and the <sup>177</sup>Lu activity would stabilize at a value lower than that predicted by the extrapolated pre-irradiation decay curve.

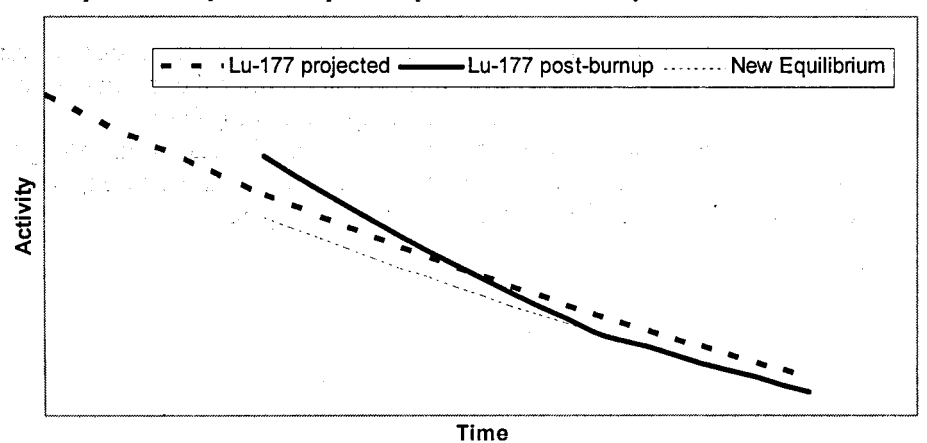


Figure 3. Sketch of expected results of the <sup>177</sup>Lu activity if the isomer experiences significant triggered decay during the burn-up experiment. An initial increase in the ground state activity will eventually reach a new equilibrium value.

## 3.2. Spectroscopy Laboratory

Activity assays were conduced at the SRS Technologies Gamma Spectroscopy Laboratory in Huntsville, Alabama. An ORTEC 10% GMX HPGe detector was used

for the measurements. Both the detector and target were located in a fixed geometry (active area 4 inches from detector crystal) inside a low-background shield. An ORTEC DSPEC Plus was used as the power supply, amplifier, and multi-channel analyzer.

Assays were conducted in 24-hour increments, with spectrum files being saved automatically. The experimental and control targets were alternated at varying intervals, with nine days per target being the most common. Approximately once per month a multi-gamma calibration source was assayed to provide independent verification of the detector performance and calibration.

## 3.3. Irradiation Laboratory

The irradiation laboratory is housed in the former Aurora Test Cell at ARL in Adelphi, Maryland. The 8 x 11 x 14 m radiation test cell volume is surrounded by 8-foot thick concrete shielding. This shielded room, designed for pulsed radiation that produced 300 krad (Si) during the 100 ns pulse width, is more that adequate for the ~45 Rads/sec dose rate from the continuous x-ray source used for the burn-up experiment. However, the danger of the present situation is perhaps larger, as the continuous x-ray source will generate enough radiation for 50% probability of death within 24 hours after just 15 seconds of exposure. For this reason, the area is interlocked.

The Norelco MG 300 bremsstrahlung source, manufactured in 1963, consists of a control console, a high voltage generator, the x-ray tube, and an oil cooler. Using the control console, we are able to vary the applied voltage (100 to 300 kV) and current (2 to 14 mA). The 240 VAC supplied from the wall is stepped up separately in two 150 kV transformers, one for the plus side (anode) and one for the minus side (filament cathode). The full 300 kV potential appears across the anode-cathode gap, accelerating the electrons towards the tungsten anode target. The electrons are stopped in the tungsten target and in decelerating produce a brehmsstrahlung spectrum of x-rays.

The experimental target was irradiated continuously from 3 May 2005 through 24 May 2005 for a total of 21 days. Expedited overnight shipping was used to minimize the downtime between the irradiation and the assays on each end. The pre-irradiation assays concluded at 1450 on 2 May 2005 and resumed at 1040 on 25 May 2005. Total flux delivered is discussed in Section 5.3.

## 4. Activity Assay Analysis

The activity of the <sup>177</sup>Lu<sup>m</sup> isomer was determined using ORTEC GammaVision analysis software. The <sup>177</sup>Lu activity was then calculated using <sup>177</sup>Lu<sup>m</sup> activity and one of the shared peaks.

## 4.1. Gamma Vision Analysis of Isomer Activity

A custom gamma peak library was created for the analysis of the <sup>177</sup>Lu<sup>m</sup> isomer activity by GammaVision. Initially, this library contained the 20 most consistent <sup>177</sup>Lu<sup>m</sup> peaks. The peaks that are shared between the <sup>177</sup>Lu<sup>m</sup> and <sup>177</sup>Lu beta decays were omitted. When the systematic error discussed in Section 4.3 was discovered, the 20-peak library was replaced by a library with only three peaks. See Section 4.3.

Scripts were written to autonomously operate GammaVision to cycle through all of the saved spectrum files and perform a peak-fitting analysis. GammaVision fit the peaks, determined the number of counts per peak, calculated the activity represented by each peak (using the number of counts, gamma intensity from the library, and detector efficiency at that energy), and finally calculated a single activity by averaging the activities for the appropriate lines. This activity is the value used to plot the <sup>177</sup>Lu<sup>m</sup> decay curves. GammaVision occasionally required the use of a deconvolution algorithm for a peak. When this occurred, the data point was omitted from the analysis.

The exponential curve fit to the data from the experimental target before irradiation corresponded to a half-life of 160.58 days. This is within 0.11% agreement with the published value of 160.4 days. The measured half-life for the control target was 160.56 days, within 0.10% agreement with the published value. After irradiation, the experimental target had a measured half-life of 161.54 days, which is within 0.71% agreement with the published value. This measured value is less precise because the decay curve is fit to only 44 data points, rather than 239 and 95 points respectively for the first two half-life calculations.

## 4.2. Ground State Activity Calculation

The <sup>177</sup>Lu activity could not be measured directly because all of the gammas evident in the <sup>177</sup>Lu beta decay are also present in the <sup>177</sup>Lu<sup>m</sup> beta decay. Therefore, the activities were calculated in the following indirect manner. For each data point, the <sup>177</sup>Lu<sup>m</sup> activity was calculated by GammaVision as described above. A single peak was selected for the <sup>177</sup>Lu activity analysis. This peak was at 112.95 keV and was selected for both it's relative prominence and it's isolation from interference by nearby peaks. Given the detector efficiency at 112.95 keV, the live time of the data collection, and the corrected gammas per disintegration for the isomer's contribution to the peak, the number of counts in the peak due to beta decay of <sup>177</sup>Lu<sup>m</sup> were calculated. These counts were subtracted from the total counts measured for the peak. Finally, the remaining counts were used with the efficiency, live time, and gammas per disintegration for the daughter's contribution to the peak to calculate the activity of the <sup>177</sup>Lu daughter. The calculation is shown in Equation 1.

of the <sup>177</sup>Lu daughter. The calculation is shown in Equation 1.
$$A_g = \frac{C_T - A_m \cdot \varepsilon_i \cdot t \cdot \gamma_{m,i}}{\varepsilon_i \cdot t \cdot \gamma_{g,i}} \tag{1}$$

m subscripts represent the m-isomer; g subscripts represent the ground state or daughter state; i subscripts represent the peak in question, 112.95 keV in this case. A

is the activity;  $C_T$  is the total measured counts;  $\varepsilon_t$  is the detector efficiency at 112.95 keV; t is the live time of the data collection;  $\gamma$  is the branching ratio or gammas per disintegration. When GammaVision required the use of a deconvolution algorithm on the 112.95 keV peak, the data point was omitted from the analysis.

These calculated activities were plotted, and exponential curves were fit to them. Since the daughter product is in equilibrium with the isomer, it should appear to have the same half-life as its parent, or 160.4 days. The experimental target before irradiation had a measured <sup>177</sup>Lu half-life of 156.81 days, which is within 2.24% of the published value. The control target had a measured <sup>177</sup>Lu half-life of 156.55 days, which is within 2.40% of the published value.

Assuming burn-up occurred, an exponential curve fit to the 44 data points taken for the experimental target after irradiation would not show the same half-life due to the disturbance of equilibrium. This was in fact the case, as the fit curve indicated a half-life of 128.03 days, a discrepancy of 20.18%.

## 4.3. Systematic Error

After the decay curves were plotted, the residuals between the measured activities and the curve fits were calculated. These residuals revealed a systematic error in the data as shown in Figure 4. The residuals are given as percentages so that data from both the experimental target and control target could be overlaid. (The two targets did not have exactly the same activity due to pipette uncertainties during the evaporative deposition.) This systematic error is attributed to the effects of temperature and humidity changes on the spectroscopy electronics over the 1.5 years of measurements.

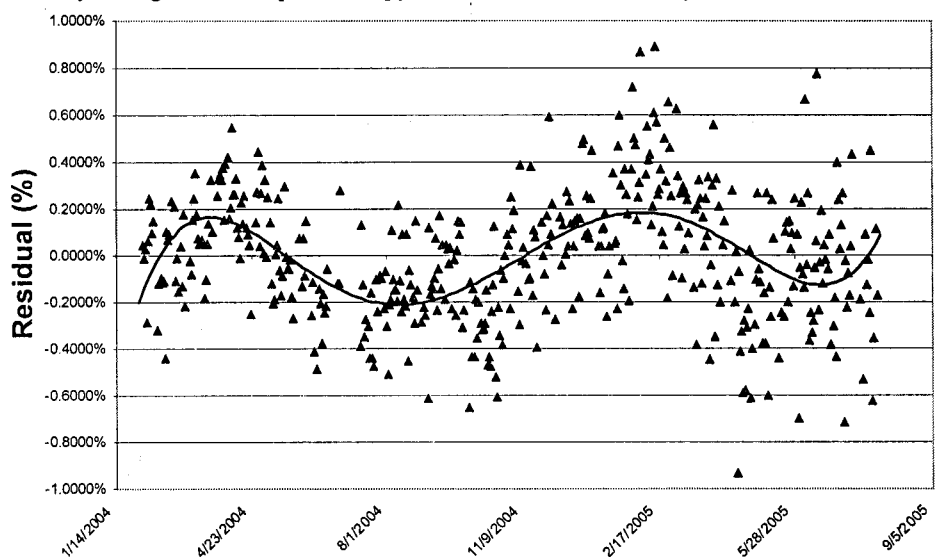


Figure 4. Residuals from all data collected. A 5th order polynomial fit is added.

Because temperature and humidity effects on spectroscopy equipment often manifest themselves in an energy-dependent manner, the first mitigation step taken was to change the <sup>177</sup>Lu<sup>m</sup> library from 20 peaks to three peaks as indicated in Section 4.1. The three peaks chosen were 105.36 keV, 121.62 keV, and 128.50 keV. These peaks were chosen for their proximity to the 112.95 keV peak used for the <sup>177</sup>Lu activity calculation so that any systematic error would be expected to have the same effect on all analyzed peaks on a given date.

A proper analysis of the residuals is vital for this burn-up experiment because the residuals are essentially where a burn-up effect would be identified. If <sup>177</sup>Lu<sup>m</sup> nuclei are "missing" after irradiation then the activities measured after the irradiation will tend to be lower than the projection of the decay curve fit to the data taken before the irradiation, i.e. they will appear as negative residuals. However, the chart in Figure 4 shows a fluctuation in the residuals (including data from the control target) that dips below zero in the area where the post-irradiation assays of the experimental target were taken. It would be fallacious to report a systematic error as evidence of burn-up.

A 5<sup>th</sup> order polynomial curve was fit to the residual data as given in Equation 2. The contribution of this systematic error as represented by the polynomial curve is removed from the residuals (missing nuclei) before the final burn-up results are presented. Full details are given in Section 5.2.

$$y = 1.74 \times 10^{-14} x^5 - 3.33 \times 10^{-9} x^4 + 2.55 \times 10^{-4} x^3 - 9.77 x^2 + 1.87 \times 10^5 x - 1.43 \times 10^9$$
 (2)

### 5. Results

Preliminary and detailed results are presented below.

### 5.1. Initial Results

At first glance, the results are indicative of triggered isomer decay. Figure 5 and Figure 6 compare favorably to Figure 2 and Figure 3, although the magnitude of the change is small.

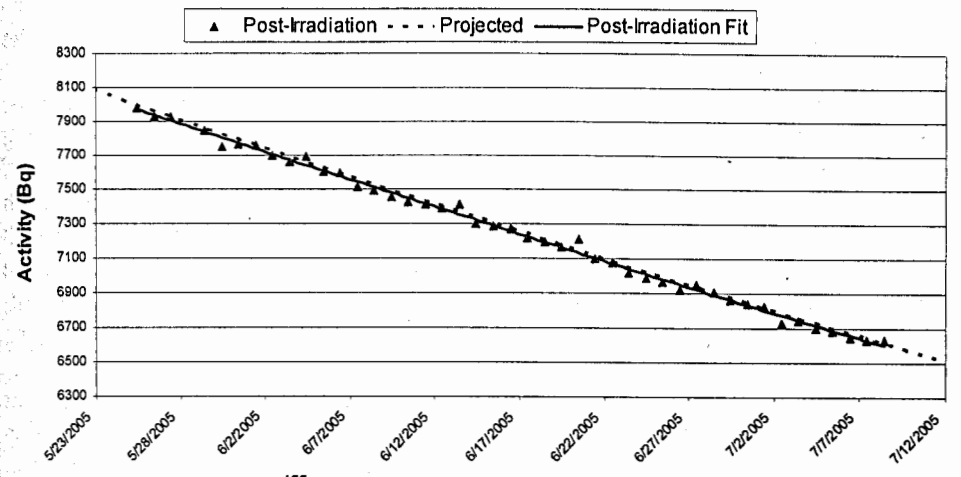


Figure 5. Post-irradiation  $^{177}Lu^m$  assay data showing a slight decrease from the projected activity. 1- $\sigma$  error bars are too small for visibility.

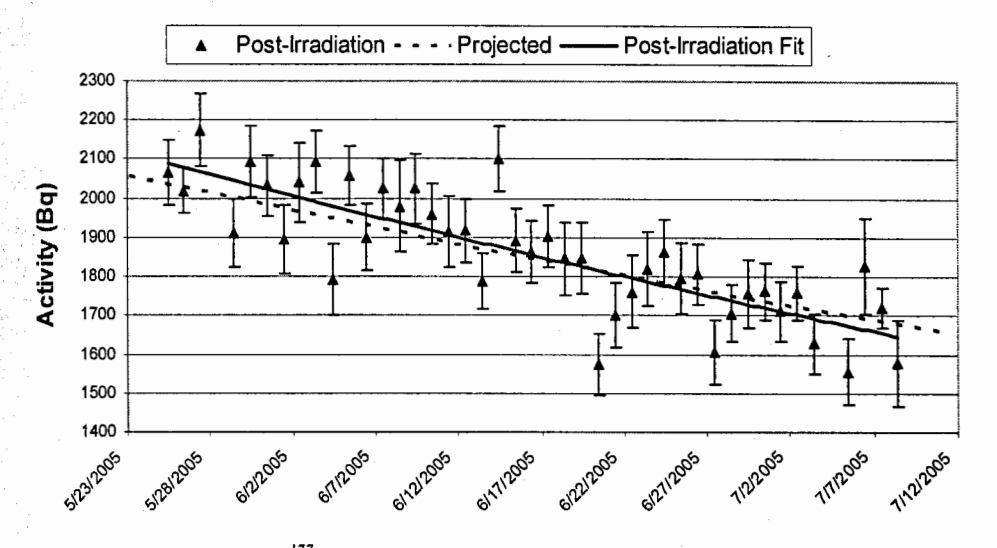


Figure 6. Post-irradiation  $^{177}$ Lu assay data showing an initial increase over projected activity followed by a decline to a new equilibrium point. Error bars show 1- $\sigma$  counting uncertainty.

## 5.2. Detailed analysis of Isomer Activities

The actual number of <sup>177</sup>Lu<sup>m</sup> nuclei can be calculated from the measured activity, and the projected number of nuclei can be calculated from the projected activity. The difference between these values represents the number of nuclei lost due to triggered isomer decay during irradiation. For these 44 data points, the mean loss is  $3.36 \times 10^8$  nuclei with a standard deviation of  $5.01 \times 10^8$ . Applying a confidence test to the null hypothesis that the mean nuclei change equals zero and the alternate hypothesis that

the mean nuclei change is less than zero (a decrease) gives a one-sided Z-statistic of -4.45. This corresponds to a confidence of 99.9996% that the shift occurs, although the shift is only 0.67 standard deviations.

However, a significant portion of this measured change in the activity is due to the systematic error discussed in Section 4.3. This error is accounted for in the following way. For each data point, the systematic error as a fraction is calculated from the 5<sup>th</sup> order polynomial. This value is subtracted from the fractional loss calculated at each data point. The result is a new set of nuclei change values that represent how far each measurement deviates from the systematic error polynomial curve rather than the projected value (which appears as the "0" line on Figure 4). For the region of interest, this is a conservative adjustment, reducing the magnitude of the shift and the statistical confidence discussed above.

After adjusting for the systematic error, the data set shows a mean loss of  $1.76 \times 10^8$  nuclei with a standard deviation of  $5.00 \times 10^8$ . The Z-statistic is -2.34 which corresponds to a confidence of 99.0% that a shift of 0.35 standard deviations occurred.

At the beginning of the irradiation period, the experimental target had  $1.76\times10^{11}$  Lu<sup>m</sup> nuclei. A loss of  $1.76\times10^8$  nuclei would indicate that 0.10% of the initial nuclei were burned up by triggered decay over the three-week irradiation period. The natural decay over this same period removed  $1.52\times10^{10}$  nuclei, or 8.67% of the initial nuclei.

### 5.3. Triggering Cross Section Calculation

The total flux produced by the x-ray tube was  $3.00\times10^{12}$  photons/sec/cm<sup>2</sup>. The active area of the target was 11 mm<sup>2</sup>. Therefore, the total flux through the isomer material was  $3.30\times10^{11}$  photons/sec. The total irradiation time was 1.823,040 seconds, resulting in a total flux through the isomer material during the experiment of  $6.02\times10^{17}$  photons. The cross section analysis conservatively assumes that the trigger energy is at the peak of the flux spectrum, 85 keV. A trigger energy width of 1 keV is assumed. The integrated area over this region is 0.573% of the total flux. This results in a flux through the isomer at the trigger energy of  $3.45\times10^{15}$  photons.

The cross section observed for this reaction can be determined from Equation 3.

$$N_f = N_i \Phi \int \sigma(E) F(E_1, E_0) dE \qquad (3)$$

where  $N_f$  is the number of triggered nuclei,  $N_i$  is the number of initial isomer nuclei,  $\Phi$  is the flux of the x-ray, and  $\sigma$  is the absorption cross section. From the method of Collins, *et al.*<sup>3</sup>, the balance of the equation simplifies as Equation 4.

$$\int F(E_1, E_0) dE = 1 \qquad (4)$$

The absorption cross section is calculated as  $3\times10^{-19}$  cm<sup>2</sup>keV. The total integrated Breit-Wigner cross section for this transition is  $\sigma\Gamma_{\gamma}$ .  $\Gamma_{\gamma}$  is given in Equation 5.

$$\Gamma_{\gamma} = \frac{\Gamma_{Tot}}{1 + \alpha} \tag{5}$$

Where  $\alpha$  is the internal conversion coefficient, taken as 0.5 for this calculation.  $\Gamma_{Tot}$  is calculated from the lifetime of the m-isomer state as shown in Equation 6.

$$\Gamma_{Tot} = 0.22 \cdot \frac{\ln(2)}{T_{1/2}} \tag{6}$$

For  $^{177}$ Lu<sup>m</sup>,  $\Gamma_{Tot}$  is  $1.1 \times 10^{-8}$  and  $\Gamma_{\gamma}$  is  $7.3 \times 10^{-9}$ . The total integrated cross section,  $\sigma \Gamma_{\gamma}$ , is on the order of  $10^{-27}$  cm<sup>2</sup>keV, or 1 eV barn. This compares to an estimate by Carroll, *et al.*<sup>1</sup> of an upper bound for the cross section of about 100 eV barn.

### 6. Conclusions

Triggered decay of the <sup>177</sup>Lu<sup>m</sup> isomer is indicated by the results of this burn-up experiment, but with a small magnitude and with less confidence than desired. A repeat of the experiment with greater irradiation flux and less systematic error in the detector system is desirable. Systematic error could be reduced through more rigorous climate control and use of the gain stabilization features of the DSPEC Plus. Once greater triggering magnitude and confidence is established, additional experiments with lower endpoint energies can be conducted to narrow down the candidate triggering energies.

A repeat experiment with a higher x-ray tube voltage is also recommended to search for a higher triggering energy that might have a larger cross section.

## Acknowledgments

The authors acknowledge the U.S. Air Force Office of Scientific Research for support that led to the identification of the source for the isomer stock.

### References

- 1. J. J. Carroll, S. A. Karamian, L. A. Rivlin, A. A. Zadernovsky, *Hyperfine Interactions* 135, 3-50 (2001).
- 2. A. Lal, J. Blanchard, "The Daintiest Dynamos," *IEEE Spectrum Online*, 29 Jun 2005.
- C. B. Collins, J. J. Carroll, T. W. Sinor, M. J. Byrd, D. G. Richmond, K. N. Taylor, M. Huber, N. Huxel, P. v. Neumann-Cosel, A. Richter, C. Spieler, W. Ziegler, *Physical Review C* 42, R1813 (1990).
- 4. H. Roberts, Hyperfine Interactions 107, 91 (1997).
- 5. P. Walker, G. Dracoulis, "Energy traps in atomic nuclei," *Nature*, 399, p35-40.
- 6. A. A. Pustovalov, "Nuclear thermoelectric power units in Russia, USA and European space agency research programs," *Thermoelectrics*, Proceedings ICT '97, 26-29 Aug. 1997, Pages 559 562.
- 7. P. Walker, J. J. Carroll, "The ups and downs of nuclear isomers," *Physics Today*, June 2005.
- 8. V. Hnatowicz, Czech J. Phys. B 31, 260 (1981).

# ANALYSIS OF MULTI-FOLD COINCIDENCE DATA FOR STUDIES OF TRIGGERED GAMMA EMISSION

R. Propri, S. A. Karamian, D. Gohlke, and J. J. Carroll

<sup>a</sup>Department of Physics and Astronomy, Youngstown State University, One University Plaza, Youngstown, OH 44555 <sup>b</sup>Flerov Laboratory of Nuclear Reactions, Joint Institute for Nuclear Research, 141980 Dubna, Russia

#### Abstract

In recent years, considerable attention has been focused on attempts to trigger a controlled energy release from long-lived nuclear isomers. The study of  $^{178}Hf^{m2}$  has been of particular interest due to its attractive properties. In light of the controversial nature of some experimental results, issues regarding methods of data analysis have become extremely important. This article discusses analysis of multi-dimensional data recorded at the SPring-8 synchrotron facility with the YSU miniball detector array, including timing characteristics,  $\gamma$ - $\gamma$  and higher-fold coincidences, and the development of software tools for the analysis.

## 1. Introduction

Over the past two decades, several experiments have been performed in an attempt to demonstrate the controlled release of excess energy stored in long-lived nuclear isomers. This process, called triggering, was successfully demonstrated for an isomer of tantalum from 1989 – 1999 (as surveyed in Ref. [1]). A more attractive candidate for applications may be <sup>178</sup>Hf<sup>m2</sup>, storing tremendous amounts of energy and having a 31-yr half life. In light of the controversial nature of some experimental results (see the review of Ref. [2]), issues regarding data analysis have become extremely important. Experiments with the YSU miniball have been carefully conducted in order to investigate the claims of triggering success. The analysis has received a great deal of careful attention and general techniques are discussed here.

# 2. Detector Array and Data Structure

The YSU miniball detector array consists of one high-purity Ge detector and six BGO scintillators. The system is intended to perform time-resolved calorimetry measurements of  $\gamma$ -ray energies released in the decay of  $^{178}$ Hf $^{m2}$ . The system has been characterized in detail as discussed in Ref. [3]. The decay of  $^{178}$ Hf $^{m2}$  leads to separate cascades of transitions on time scales shorter than that of the detection system. The transitions within each of these cascades are therefore considered to be simultaneous.

In order to ensure that at least one transition in the cascade was detected with high energy resolution, Ge detection served as the master gate trigger. Every Ge detection triggered a 5 µs master gate for digitization of each detector's energy and time information. For each master gate, a total of nineteen parameters were digitized and recorded and then inserted into the data stream for storage. Each group of nineteen parameters recorded within a gate is referred to as an event. The final output of the data acquisition (DAQ) system is a series of files each containing roughly 48,000 events. A tabulated representation of the data structure within a file is given in Fig. 1.

Amadan din Kili I Mal	event Ge abs. header time		Ge energy	BGO 1-6 energies	not used	BGO 1-6 time stamps		
Parameter -	1	23	4	5 6 7 8 9 10	11	12 13 14 15 16 17		
AFREST SI	49407	10 12999	1069	0 0 00 0 0	0	3955 3955 3955 3955 3955 3955		
304 . · · · · · 2	49407	20 30709	1604	0 106 0 468 0 0	0	3956 3956 3956 1197 3956 3956		
3. 5. 5. 7 1 1 1 1 1 3 1 1 1 1 1 1 1 1 1 1 1 1 1	49407	22 8530	863	0 0 0 0 0 665	0	3957 3957 3957 3957 3957 150		
l event 4	49407	28 15277	1702	391 0 0 574 0 437	0	3958 3958 3958 1223 3958 3958		
14 1 W. W. S.	49407	30 4700	1560	0 0 0 181 0 0	0	3959 3959 3959 3959 3959 3959		
6	49407	33 12841	1603	0 2322 0 0 0 0	0	3960 1586 3960 3960 3960 3960		
7	49407	33 30324	2475	0 0 0 1003 0 0	0	3961 3961 3961 1511 3961 3961		
8	49407	34 25124	1054	0 0 0 130 0 0	0	3962 3962 3962 3962 3962 3962		
9	49407	35 7915	1052	185 332 0 0 650 0	o	3963 3963 3963 3963 1426 3963		
<b>J</b> 0	49407	35 11979	1071	0 0 0 0 0 478	0	3964 3964 3964 3964 3964 1480		

Fig. 1: Tabulated representation of YSU miniball data structure showing parameter designations and ten example events. Parameters 11, 18, and 19 were not used in the raw data.

## 3. Data Sorting

In the summer of 2004 about 70 GB of data were collected at Japan's SPring-8 synchrotron facility. Analysis of the data required the ability to sort through them and to extract useful information. A software suite has been developed at YSU in order to perform the sorting necessary for the analysis with the program ProSort<sup>©</sup> being the main tool in the suite. The suite is FORTRAN-based featuring a windows-style graphical user interface (GUI), made possible by Winteracter<sup>©</sup> software [4]. Also included is a tool called DataGin<sup>©</sup> designed to inspect each event to ensure that the structure is correct, i.e. each event has the correct number of parameters. Minor instabilities in the data handling hardware caused roughly 0.3% of the recorded events to be incomplete. DataGin removes the incomplete events from the data files prior to sorting and analysis.

# 3.1. ProSort®

ProSort<sup>©</sup> is the tool used to extract useful information from stored miniball data. Its GUI (see Fig. 2) allows a user to choose the conditions on which subsequent output is generated. Miniball data contain information about gamma energy and time. The user can choose any combination of conditions upon these parameters to focus on important events. Conditions are entered as ranges, such as on individual detector time

stamps. The program also calculates additional information including the sum of the energies of the BGO detectors and the total detected fold (how many scintillators fired). Sorting conditions may also be entered based on these calculated parameters, e.g. to output events having a particular detected fold. The user may request output of singles energy and time spectra as well as bi-dimensional histograms (matrices) of any two parameters and projections of those histograms. The output files only contain counts from those events which satisfy all the conditions chosen by the user. Sorting may be done in steps, saving intermediate data subsets for later, additional sorting.

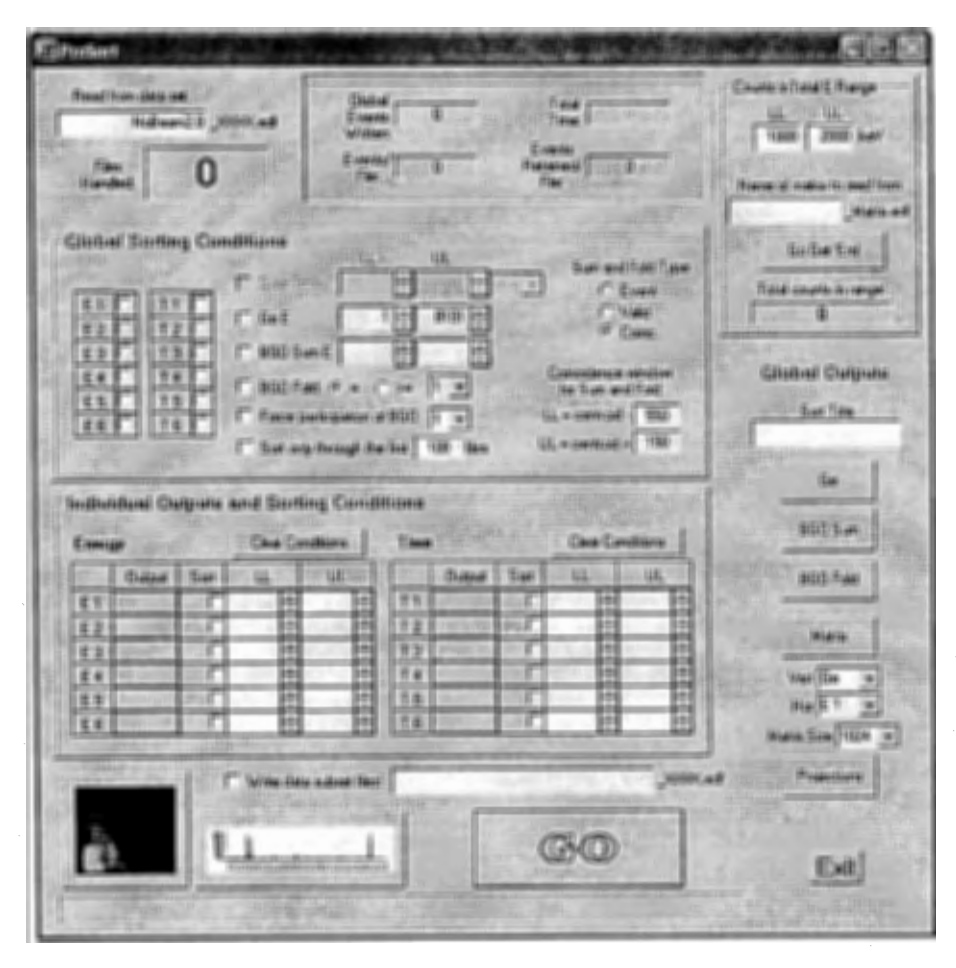


Fig. 2: GUI for ProSort<sup>©</sup>.

In addition to simple sorting of existing parameter values and of calculated values based on them, ProSort® has been designed to handle compound conditions. This occurs when the outcome of one conditional test depends on the outcome of another. For example, suppose one desires output containing only events in which three BGO scintillators fired in coincidence with the Ge detector. The program

calculates a BGO fold that is based not only on how many of the detectors fired (had non-zero energy value), but also on the timing characteristics of each detector; the BGO fold depends on the time condition.

Another tool in the suite allows the inspection of BGO – BGO coincidences without regard to the Ge. Since the peak in each BGO time-stamp histogram corresponds to coincidence with the Ge detection, it is of no use in searching for coincidences among BGOs. Instead, the entire histogram range must be examined for time stamps occurring within some range of each other. To accomplish this, the program uses a width, chosen by the user, and scans it across each histogram counting the number of BGOs containing a time stamp within the width at each position. If two or more BGOs contain a time stamp within the width at the same position then they are said to be in coincidence. The highest number of time stamps occurring in coincidence is taken as the detected BGO fold. Although available, this feature was not part of the standard analysis procedure since it was desired that all events reflect a gamma-ray detected by the Ge.

The software is also equipped with tools for quickly viewing graphs of the output. The 'Histogram Viewer' button on the GUI launches a dialog containing a histogram engine. The user can view any histogram by specifying the type of histogram (e.g. Ge energy, BGO 2 time, etc.) and the name that was chosen for the sort that produced it. The histogram display is controllable by zooming in and out and scrolling left and right and is auto-scaled to the highest peak in view.

It is also useful, although more difficult, to have quick access to graphical display of the bi-dimensional histograms. The 'Bi-dimensional Histogram Viewer' button on the GUI implements a simple routine that assigns different colors to different value ranges and then plots a color map of the histogram values in a window. It is not as useful as a 3-dimensional graphing engine, but it's certainly more convenient for quick checks of output details.

# 4. Data Analysis

The purpose of this paper is to illustrate some of the tools and methods being used to obtain the detailed results presented elsewhere [3]. As such, the following consists of examples of such tools and methods.

# 4.1. Example 1: γ-γ and Higher Fold Coincidences

The aim of the miniball is to separate prompt triggered events from natural decay with the use of calorimetry [3]. Figure 3 shows part of the energy level diagram for <sup>178</sup>Hf. The 31-yr m2 isomer lies 2.44 MeV above the ground state. Due to the 4-s m1 isomer in the 8 band, the total energy released in natural decay on a coincident time scale will not be 2.44 MeV, but will be split into two parts. A coincident cascade from the m2 isomer to the m1 isomer will release about 1.3 MeV, and a cascade from the m1 isomer to the ground state will release about 1.1 MeV. Prompt triggering, as suggested in some reports (see the review of Ref. [2]) would, however, release the full

2.44 MeV plus the energy that triggered the decay. An example illustrates how the miniball would separate natural decays from prompt triggered decays.

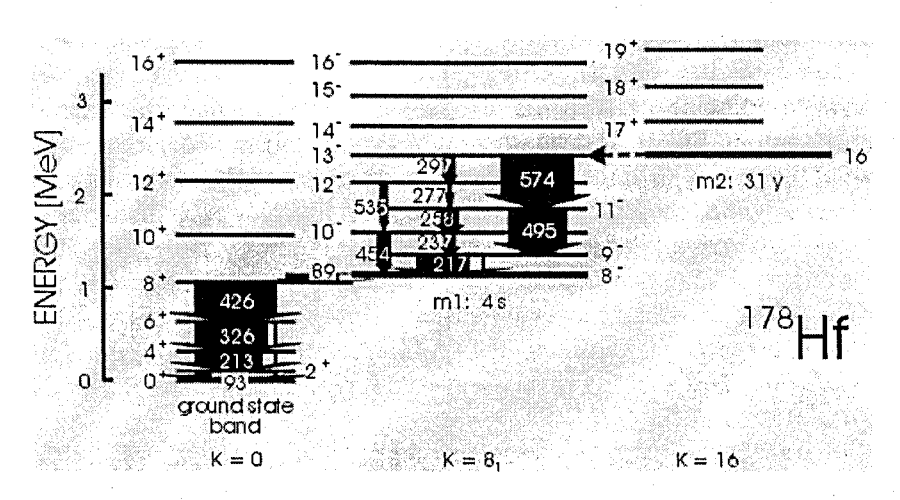


Fig. 3: Partial energy level diagram for <sup>178</sup>Hf. Arrows indicate main natural-decay transitions from the 31-yr m2 isomer.

Consider a pair of transitions emitting gammas from one nucleus within one cascade such that they occur in coincidence. We will consider the Ge and one BGO for detection of the pair. There are four ways that the total energy of the pair can be deposited in the two detectors (neglecting Compton effects). If we label the two distinct gammas  $y_1$  and  $y_2$ , then we can list the four detection possibilities. 1) Ge detects  $\gamma_1$  and BGO detects  $\gamma_2$ ; 2) BGO detects  $\gamma_1$  and Ge detects  $\gamma_2$ ; 3) Ge detects  $\gamma_1$ and  $y_2$ ; 4) BGO detects  $y_1$  and  $y_2$ . In each case a total of the sum of the two energies is detected. A bi-dimensional histogram of Ge energy vs. BGO energy could be used to display the counts for all four cases as in Fig. 4a. Each case is plotted at a different location according to the energies caught in each detector, but they all share a common total sum energy since they all represent the same pair of gammas. The peaks plotted in the histogram all lie along a diagonal locus of constant sum energy. Figure 4b shows such a histogram created using real data taken during a <sup>178</sup>Hf<sup>m2</sup> background run. Circled in the histogram are two peaks resulting from a pair of gammas from the ground state band, namely the 325 keV and 426 keV pair. The diagonal line upon which they lie represents a constant energy locus of 325 + 426 = 751 keV. The case in which both gammas are caught by the Ge (case 3) is not shown here because the 0<sup>th</sup> channel has been excluded from the sort. The case in which both gammas are caught by the BGO (case 4) does not appear because a Ge detection is needed to produce a master gate. Since every event must include a Ge detection, the detected fold is written as 1 + F, where F represents the number of BGO scintillators that fired. Therefore, cases 1 and 2 correspond to a detected fold of 1 + 1, and case 3 corresponds to a detected fold of 1 + 0 (since only the Ge reports a signal).

The example above involved only two gammas for simplicity, but the same idea applies to higher folds of gamma detection. For higher folds, the bi-dimensional histogram would plot Ge energy vs. the sum energy of all BGO detections. As stated above, the total energy released in a coincident burst of gammas in prompt triggering differs from that of natural bursts and would therefore appear along a different constant energy locus. It is in this way that prompt triggered events may be identified apart from natural decays. In a histogram of Ge energy vs. BGO sum energy, assuming all gammas are detected, the peaks from each burst of gammas will appear along their respective constant energy loci – one corresponding to 1.1 MeV and one to 1.3 MeV from natural decays, and one corresponding to ~2.44 MeV from any prompt triggered emission.

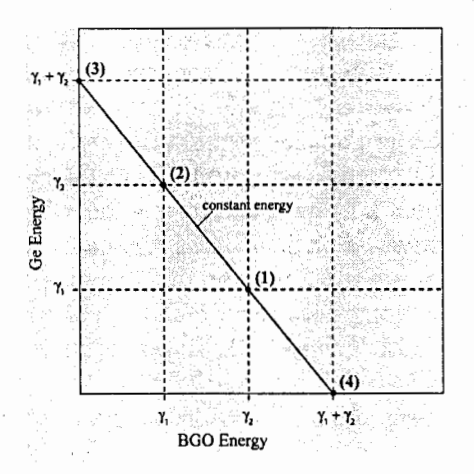


Fig. 4a: Illustration of count placement hypothetical bi-dimensional in the detection histogram for four possibilities discussed above. The numbers correspond the cases to considered in the text.

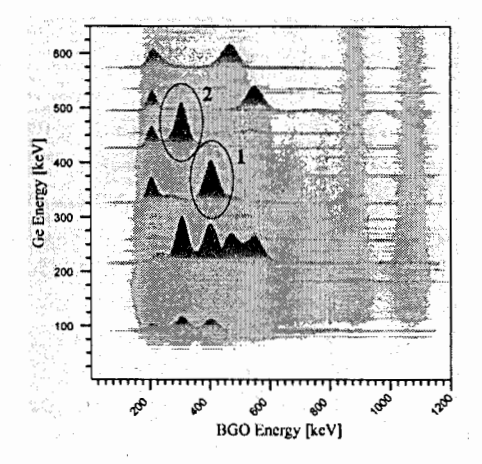


Fig. 4b: Bi-dimensional histogram of real data showing gamma pairs along constant energy loci. Circled are the 325, 426 keV gamma pair, which lie along a constant energy locus of 751 keV. The numbers correspond to the cases considered in the text where  $\gamma_1$  = 325 keV and  $\gamma_2$  = 426 keV.

# 4.2. Example 2: Focusing on Coincident Gammas

In any recorded event, it is known that the Ge detector fired, for this is the origin of the master gate and nothing would be recorded without it. This gate remains open for 5 µs and allows anything entering the BGO detectors to be recorded. In such a system random background radiation and decays from other nuclei will inevitably enter the data stream. Because analysis is most interested in decays from single nuclei, one desires only the BGO detections of gammas that originated in the same nucleus as the gamma that was detected by the Ge. Although there is nothing in the data to

identify a gamma's origin, many unwanted data can be eliminated based on timing information.

Again, consider a pair of transitions from one nucleus emitted within one cascade such that they occur in coincidence. For this example, let the Ge detector catch  $\gamma_1$  and let a BGO catch  $\gamma_2$ . When the Ge crystal captures  $\gamma_1$ , the master gate is opened and the system's CAMAC driver inserts a time stamp into the data stream for this particular event. This detection also triggers a START signal in a TDC. The BGO caught  $\gamma_2$  at the same time as the Ge detection, but in order for the BGO's signal to be processed it must fall within the master gate and therefore must be delayed a few  $\mu$ s. The signal is split for energy and time information and the timing pulse makes its way to the TDC to produce a STOP signal. In this way the BGO detection is time stamped relative to the master gate, or equivalently, to the Ge detection.

Each BGO time signal can be placed into one of two categories, those from gammas originating in the nucleus whose decay triggered the gate, and those from gammas not originating in that nucleus. The former will ideally all have a constant TDC value due to the preset delay and will therefore appear in the time histogram at some specific location (walk of START and STOP signals will produce shoulders on a coincidence peak for real instruments). The latter will have no correlation with the gamma that triggered the master gate and will therefore be distributed randomly across the time histogram. The expected time histogram is a superposition of these two, a flat background across the histogram with a spike at some location which represents real coincidences with the gamma that triggered the gate. Using ProSort<sup>©</sup>, it is possible to require that parameters only be included in calculations and output when their time value falls within some range, chosen by the user. This allows the user to exclude detections of non-coincident gammas from the output although it is impossible to exclude the small number of random coincidences falling within the time-sort range.

## 4.3. Example 3: Matrix Cuts

The system's detectors were chosen to achieve a balance of performance, portability, and cost. The high-purity Ge detector was chosen to insure at least one gamma in each event with good energy resolution, while the BGO detectors provide the higher efficiency needed for calorimetry. Determining BGO system efficiencies is complicated by the poor resolution of the scintillators. The efficiency calculations involve the areas of peaks in the BGO energy histograms, but the many poorly resolved peaks in the <sup>178</sup>Hf spectrum overlap making them very difficult, if not impossible, to fit in the pure BGO singles spectrum. By projecting onto the BGO axis all the counts within a given range on the Ge axis (Figs. 5a, 5b), the peaks can be separated out and fit with appropriate software, such as TV [5] which was used in this work. This process is called a "cut" or a software gate.

The ability to separate peaks out in cut projections stems from the fact that only certain sets of gammas are emitted in coincidence with each other. For example, a study of the energy level scheme in Fig. 3 reveals that only four specific gammas are likely to be emitted with the 213 keV gamma in the ground state band (gsb).

Therefore, if one makes a cut around the Ge energy of 213 keV, the BGO projection will only include the peaks of those four specific gammas.

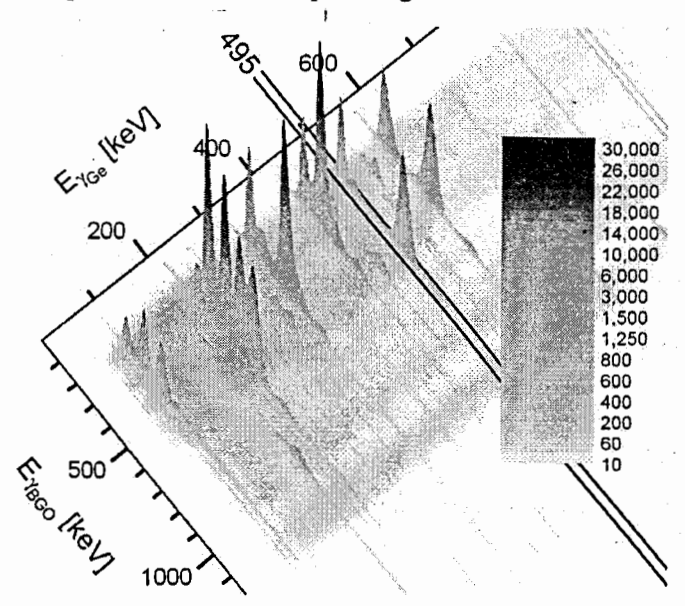


Fig. 5a: Illustration of a cut selection. All counts within the black lines will be projected onto the BGO axis and everything else will be discarded.

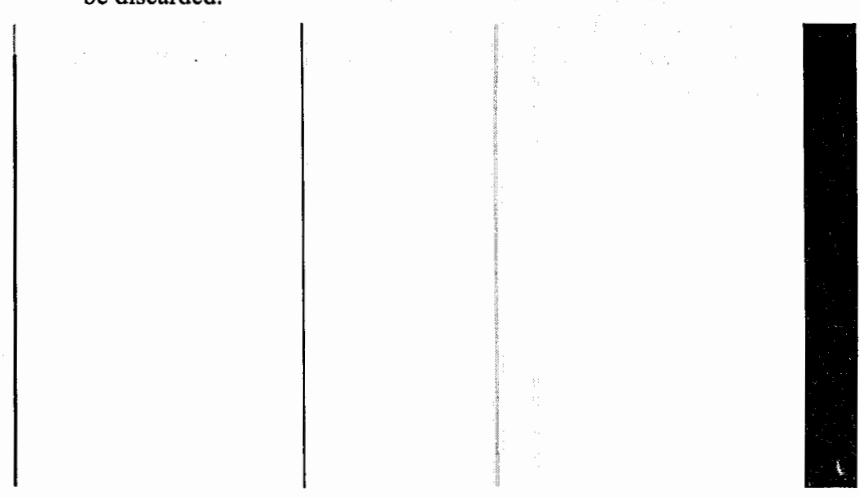


Fig. 5b: Illustration of a cut projection (bottom pane). All counts within the black lines in 5a have been projected into a one-dimensional histogram in BGO energy. The narrow top pane shows a portion of the Ge spectrum with the cut.

In practice, the lower energy gammas are filtered out by discriminators and some transitions are heavily converted. This leaves only three main gammas in the gsb that are significantly detected, 213, 325, and 426 keV. A cut on any of these three peaks will include peaks at the other two energies. Therefore, cuts on each of these three energies in the Ge projection yield two efficiency values at each BGO energy. The same technique applies to the 8 band.

## 5. Summary

With the need for increasingly more careful examinations of triggering claims, several techniques have been utilized to increase the quality of data analysis. The YSU miniball was designed to perform calorimetry measurements on <sup>178</sup>Hf<sup>m2</sup> and the techniques described here maximize the potential for extracting useful information from its data.

## Acknowledgments

This work was supported by the US Air Force Office of Scientific Research under contract F49620-02-1-0187.

## References

- 1. J. J. Carroll, S. A. Karamian, L. A. Rivlin, et al., Hyperfine Int. 135, 3 (2001).
- 2. J. J. Carroll, Laser Phys. Lett. 1, 275 (2004).
- 3. P. Ugorowski, R. Propri, S. A. Karamian, et al., Nucl. Inst. Meth. A (submitted 2006).
- 4. Winteracter, Interactive Software Services Ltd., www.winteracter.com, (2006)
- 5. TV, Institute of Nuclear Physics, University of Cologne, Germany, www.ikp.uni-koeln.de/~fitz/, (2003)

# NEW X-RAY INDUCED DECAY OF <sup>178M2</sup>HF DATA: "MIXED J" INSTEAD OF "MIXED K" INTERPRETATION?\*

#### E.V. TKALYA

Institute of Nuclear Physics, Moscow State University, 199999, Vorob'evy Gory, Moscow, Russia

This report reviews intriguing experimental result published by C.B.Collins et al., at Laser Phys. Lett. **2**, 162 (2005) about induced decay acceleration of long-lived isomer <sup>178m2</sup>Hf (16<sup>+</sup>, 2.446 MeV, 31 yr) by the low energy synchrotron radiation and registration of the 2.457 MeV γ-emission. Theoretical analysis shows that experimentalists have to wait for the 2.457 MeV γ-photon more than 10<sup>50</sup> years. It was established, that there is only one way to explain of the origin of these photons - to proclaim the intermediate nuclear level is not "mixed K", but is "mixed J".

In the experiment with a beam of synchrotron radiation [1], where the isomeric nuclei <sup>178m2</sup>Hf were irradiated by photons with the energy 9567 eV (which is 6 eV higher than the binding energy of an electron on the  $2p_{3/2}$  shell of the hafnium atom,  $E_{L_{III}}=$ 9561 eV), a new gamma line with the energy  $\omega_r = 2457.20(22)$  keV was detected (see Figure 1). This result appears to be highly improbable. The induced decay in the experiment described in Ref. [1] occurred in approximately the same conditions as the one described in Ref. [2]. (No value of the cross section was given in Ref. [1], but the figure for the gamma emission is roughly the same as the one reported in Ref. [2], while the synchrotron-radiation flux is more than 30 times higher: 2×10<sup>12</sup> cm<sup>-2</sup> s<sup>-1</sup> in the 1 eV range against  $3\times10^{10}$  cm<sup>-2</sup> s<sup>-1</sup> in the 0.5 eV range.) For effective excitation, the spin of the intermediate state must be  $J^{\pi} = 15$ . We assume else, following to authors of Refs. [1-2], that the intermediate "mixed K" level is connected to all other nuclear states by K-allowed transitions. The multipolarity of the gamma radiation, which in Ref. [1] is interpreted as the result of the decay of the intermediate state into the ground state  $0^+$  of the  $^{178}$ Hf nucleus, must then be E15. The ratio of the radius of the nucleus  $R = 1.2\sqrt[3]{A}$  fm = 6.8 fm to the wavelength  $\lambda_{\gamma} = 2\pi/\omega_{\gamma} = 505$  fm is small:  $R/\lambda_{\nu} = 0.013$ . Hence, the probability of the E15-transition, e.g., in the Weisskopf model amounts to only 2.5×10<sup>-49</sup> s<sup>-1</sup>.

<sup>\*</sup> This work is supported by grant no. 2651 of the International Center for Science and Technology.

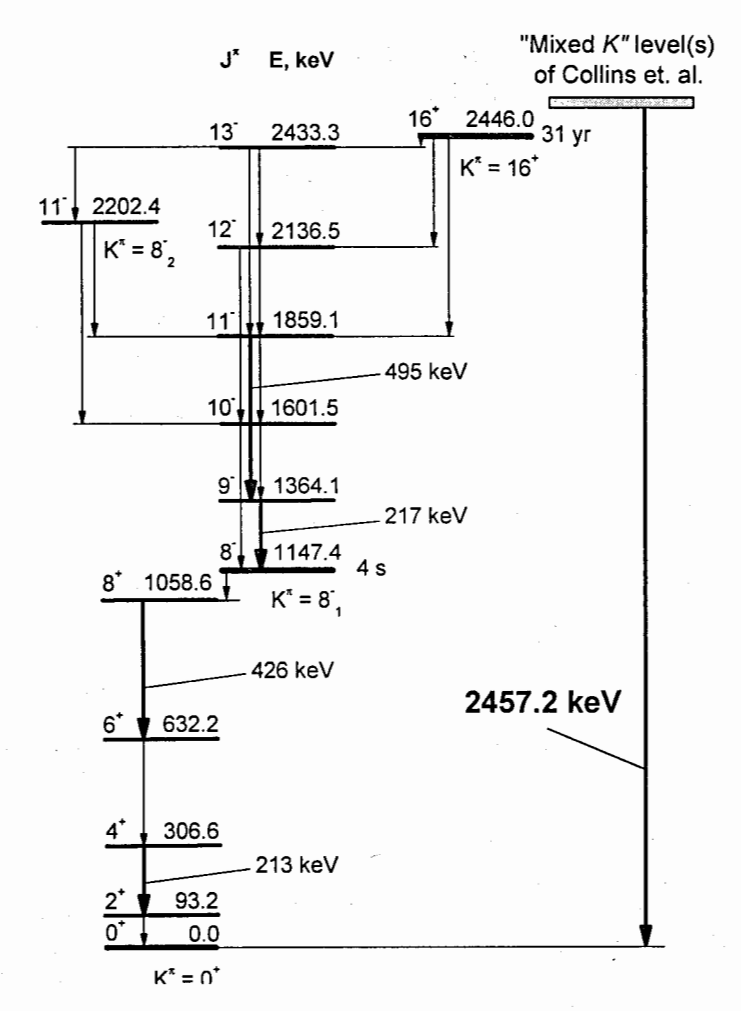


Figure 1. Decay scheme of <sup>178m</sup>Hf. Depicted are transitions in the spectrum of <sup>178</sup>Hf in which, according to [1,2] and other works of Collins's team an increase in the gamma-radiation intensity exceeding the measurement errors were detected. The 2457.2 keV line was discovered by Collins et al. in 2004 [1].

The equation describing the excitation and decay of the "mixed K" state in an irradiated target containing  $N_{\rm m2}$  <sup>178m2</sup>Hf nuclei has the simple form (where we ignore the natural decay of <sup>178m2</sup>Hf nuclei)

$$\frac{dN_{Mixed K}}{dt} = N_{m2}\sigma\varphi - (\lambda + \lambda_{E15})N_{Mixed K}, \qquad (1)$$

where  $\lambda$  is the decay constant, which ensures the observed enhancement of ordinary gamma transitions (see Figure 1) in previous experiments of Collins's team (the list of corresponding references see in Ref. [3]), and  $\lambda_{E15}$  is the probability of the emission of an E15 (2457.2 keV) gamma quantum in Ref. [1]. The activity of the target along the indicated second channel is

$$Q_{E15} \approx N_{m2} \sigma \varphi \frac{\lambda_{E15}}{\lambda + \lambda_{E15}} . \tag{2}$$

We take the value of the cross section of excitation of the intermediate state obtained in the first experiment of Collins's group involving a beam of synchrotron radiation [2]:  $\sigma \approx 2 \times 10^{-22}$  cm<sup>2</sup>. We estimate  $\lambda$  in accordance with the hypothesis, that its value must be comparable to the width of the Isomeric State  $\rightarrow$  "mixed K" transition. (This assumption reduces the probability of the nucleus returning to the isomer level and creates conditions for maximum population of the states from which enhancedintensity transitions were recorded in the experiments of Collins's team.) In this case, it will take more than 10<sup>50</sup> years (!) of continuous irradiation of a target with about 10<sup>13</sup> <sup>178m2</sup>Hf isomers in an experiment similar to the one described in Ref. [1] for at least one transition to occur from the intermediate state to the ground state of the nucleus accompanied by emission of an E15 (2457.2 keV) photon. The result speaks for itself. Actually, in such a situation, it is irrelevant what multipolarity the transition has, E15 or, e.g., E13 (in the latter case, the cross section of excitation of the intermediate level is much smaller). It is also irrelevant what the synchrotron-radiation flux was or how many 178m2Hf nuclei the target actually contained. Modern physical theories provide no explanation for this experimentally observed fact of the given transition.

Possibly the simplest way to remove this contradiction is to pronounce the intermediate level a "mixed J" level and to assign to it all the properties that the authors of Refs. [1-2] assigned to "mixed K" states.

### References

- 1. C.B. Collins et al., Laser Phys. Lett. 2, 162 (2005).
- 2. C.B. Collins et al., Europhys. Lett. 57, 677 (2002).
- 3. E.V. Tkalya, Physics-Uspekhi 48, 525 (2005).

# PRODUCTION OF LONG-LIVED HAFNIUM ISOMERS IN REACTOR IRRADIATIONS

# S. A. KARAMIAN, 1\* J. J. CARROLL, 2 J. ADAM, 1† E. N. KULAGIN, 1 AND E. P. SHABALIN 1

<sup>1</sup>Joint Institute for Nuclear Research, Dubna 141980, Russia <sup>2</sup>Youngstown State University, Youngstown, Ohio 44555, USA

Metal <sup>nat</sup>Hf samples were activated in the Dubna IBR-2 reactor at positions corresponding to different neutron fluxes. Samples were bare or shielded by Cd and CB<sub>4</sub> layers. The gamma activity of the samples was analyzed with Ge gamma spectrometers during a two-year period following their irradiation. In the presence of the dominant activation products <sup>175</sup>Hf and <sup>181</sup>Hf, the high-spin isomers <sup>178m2</sup>Hf and <sup>179m2</sup>Hf were also detected despite relatively low levels. The isomer-to-ground-state ratios and cross-sections were determined from the measured yields. For <sup>178m2</sup>Hf, the cross section for burnup (destruction) by neutron capture after its production was also estimated, clarifying the results from earlier experiments. In the context of suggestions for use of <sup>178m2</sup>Hf for applications, the results confirm that large-scale production of this isomer by reactor irradiations is not feasible. In contrast, the efficiency of production for <sup>179m2</sup>Hf is much higher and an amount of about 10<sup>16</sup> atoms may be produced in standard reactor irradiations.

#### I. Introduction

Total and activation cross-sections as well as resonance parameters for slow neutron radiative capture may be found for stable Hf isotopes in the tabulations of Refs. [1, 2]. It is well-known that the main activity induced in natural hafnium targets is due to the production of <sup>175</sup>Hf (70-day halflife) and <sup>181</sup>Hf (42-day halflife) after  $(n, \gamma)$  reactions. In addition, the short-lived first metastable  $(m_1)$  isomers of <sup>178</sup>Hf, <sup>179</sup>Hf and <sup>180</sup>Hf are also formed with cross-sections that are sufficient for successful detection. However, the production of high-spin second metastable  $(m_2)$  isomer via  $(n, \gamma)$  reactions in isotopes like <sup>178</sup>Hf and <sup>179</sup>Hf are more problematic. Only recently has a measurement appeared in the literature for the production of  $J^{\pi} = (25/2^{\circ})^{179m^2}$ Hf [3]. The production of the famous  $J^{\pi} = 16^{+}$  isomer <sup>178m2</sup>Hf was reliably detected from its activity in 1973 [4], but the cross section was deduced using some assumptions that deserve additional investigation.

The population of high-spin states following neutron capture may be expected to have a rather low probability due to the need for their population by stretched cascades of many  $\gamma$  rays. This type of cascade is characterized statistically by a relatively low yield. High-fluence irradiations are normally required in order to

E-mail address: karamian@nrmail.jinr.ru

<sup>†</sup> Permanent address: Inst. Nuc. Phys., Rez., CZ-25068, Prague, Czech.Rep.

produce an observable activity for such low-yield products, but this introduces another complication in that a significant "burnup," or depletion, of the produced nuclei may occur. For some products the destruction cross-section can be higher than 1,000 barns. Therefore, fluences above  $0.5 \times 10^{21}$  n/cm² should be avoided to produce negligible burnup or the remaining activity after irradiation would suggest a production cross-section that was significantly underestimated.

Fast neutrons within a reactor spectrum are sometimes useful for isomers production via  $(n, n'\gamma)$  reactions. These reactions may complicate the analysis of experiment and must be kept in mind when designing experiments for the measurement of low-yield exotic radionuclides by reactor irradiations. In the present work, the production of the high-spin isomers  $^{178m2}$ Hf and  $^{179m2}$ Hf isomers was observed and quantitatively characterized, taking into account such factors. These measurements therefore serve to augment the existing data obtained in high-flux irradiations for the former isomer [4] and to provide new information for the latter [3]. The burnup of  $^{178m2}$ Hf by  $(n, \gamma)$  reactions was also investigated, expanding the results of Ref. [5].

## II. Experimental detail

In a first series of experiments, metal Hf samples of about 20 mg were irradiated in an outer channel of the IBR-2 Dubna reactor of the Frank Laboratory of Neutron Physics, Joint Institute for Nuclear Research. Metal Hf targets of natural isotopic composition are advantageous as compared to an enriched target in their chemical purity and lower resonance-absorption factors. The standard method of Cd difference was applied for the isolation of the separate effects of thermal and epi-Cd neutrons. The neutron spectrum at the location of the targets was well-known from previous experiments, but NiCr-alloy samples were nevertheless irradiated as spectators. The activity of  $^{51}$ Cr served to calibrate the slow neutron flux while  $^{58}$ Co was produced in a reaction with fast neutrons at  $E_n > 0.8$  MeV and was used for calibration of the fast neutron flux.

Following their irradiation, the activity of the samples was studied using a 20% efficiency HPGe gamma detector. The spectroscopic system allowed a count rate up to 15 kHz while preserving a reasonable dead time less than 25% and a spectral resolution on a level of 1.8 keV for the  $^{60}\text{Co}$  lines. Standard test sources ( $^{152}\text{Eu}$  and others) were used for energy and efficiency calibrations of the  $\gamma$  spectrometer.

In measured spectra from the activated Hf samples,  $\gamma$  lines were observed and their peak areas quantitatively determined for the following radionuclides: <sup>175</sup>Hf, <sup>179m2</sup>Hf, <sup>180m</sup>Hf and <sup>181</sup>Hf. The bulk of the activity was due to <sup>175</sup>Hf (70 d) and <sup>181</sup>Hf (42.4 d) formed in  $(n, \gamma)$  reactions. Negligible activity was contributed from admixtures of other elements in the Hf material. Only Zr was present in a quantity of about 3%, while the concentration of other elements was estimated to be on the level

of less than 1 ppm. The detected yields of  $^{175}$ Hf and  $^{181}$ Hf were used as additional, intrinsic calibrators of the neutron fluxes and then the thermal cross-section  $\sigma_{th}$ =(0.44±0.02) b and resonance integral  $I_{\gamma}$ =(5.8±0.7) b were deduced for  $^{180m}$ Hf production in the  $^{179}$ Hf( $n, \gamma$ ) reaction. The resulting values were in good agreement with the tabulated data [1], confirming the accurate calibration of the neutron flux in these irradiations.

A yield of the high-spin  $^{179m2}$ Hf isomer was detected and clearly originated from reactions with fast neutrons, since the effect of thermal neutrons was found to be insignificant for its production. This conclusion was definite because bare and Cd-shielded samples showed the same activity of  $^{179m2}$ Hf within the standard error. No  $\gamma$  lines from  $^{178m2}$ Hf were observed in this first series of irradiations, reflecting its low production yield and the presence of much higher activities of other nuclides.

A second series of experiments was performed in order to significantly improve the sensitivity of the measurements for detection of the low-yield isomers. At the same position in the outer channel, a larger Hf sample was placed for a longer duration. The sensitivity was improved by three orders-of-magnitude, but this was still insufficient for observation of <sup>178m2</sup>Hf. A strong increase in the neutron flux was then sought to increase the production of this isomer. In the reactor, an inner channel was available that allowed an irradiation near, but outside, the active core within a cylindrical region shielded by a 3-mm layer of CB<sub>4</sub>. A Hf sample was exposed there for eighteen days, after which decay of the resulting activity was followed for two years. Finally, activity of <sup>178m2</sup>Hf was successfully observed and its yield determined after the third series of irradiations.

At the inner location, the thermal flux was determined in earlier experiments to be about  $0.5 \times 10^{12}$  neutrons/(cm² s), thus during the eighteen-day irradiation a fluence near  $10^{18}$  n/cm² could be accumulated. In the present experiments, the value of flux was not used explicitly since all measurements were carried out in a relative mode by comparing the activities of  $^{178m2}$ Hf,  $^{179m2}$ Hf and  $^{180m}$ Hf nuclei to those of spectators and intrinsic calibrators  $^{175}$ Hf,  $^{181}$ Hf and  $^{95}$ Zr which were present within the targets. Such a method is reliable and accurate in the presence of shields. Data processing requires special care for high-sensitivity measurements of neutron-production cross sections. The burnup of isomeric nuclei produced during the irradiation must be taken into account when the neutron fluence exceeds  $10^{20}$  n/cm². In the present irradiations, however, even in the inner channel the fluence was 100 times lower. This is due to the fact that IBR-2 is a pulsed reactor constructed specially for time-of-flight spectroscopy, not to achieve a high mean power. With this fluence, burnup of high-spin hafnium isomers or other double neutron-capture reactions may be expected to have a probability below  $10^{-3}$  compared to the probability for single neutron capture. Nevertheless, some excess activity of  $^{182}$ Ta was detected beyond that which could be attributed to single neutron capture on a small admixture of  $^{181}$ Ta in the target. This excess production of  $^{182}$ Ta was likely due to the double neutron capture process:  $^{180}$ Hf(n,  $\gamma$ )  $^{181}$ Hf  $\rightarrow$   $^{181}$ Ta(n,  $\gamma$ )  $^{182}$ Ta.

Also, in order to achieve a higher absolute yield of <sup>178m2</sup>Hf in the second and third experimental series, relatively thick metal samples were used. Self-absorption of thermal and resonance neutrons could not be neglected for these thicker samples, which were rods of 1-mm cross-sectional dimension.

The well-known equation describing the reaction rate per target nucleus when exposed to comparable fluxes of thermal and resonance neutrons is

$$r = (\sigma_{th} + \frac{I_{\gamma}}{k})F_{th} \quad , \tag{1}$$

where  $F_{th}$  is the thermal neutron flux. The coefficient k reflects the particular characteristics of the spectrum of irradiating neutrons, being a fixed constant for a definite location of each irradiation station in a specific reactor. It may be defined approximately as

$$k = \frac{F_{th}}{F_{res}} \ln(E_2 / E_1) \qquad (2)$$

where  $E_1$  and  $E_2$  define the "resonance" range of neutron energies and  $F_{res}$  is the flux of resonance neutrons. For simplicity, one can introduce the notation:

$$\sigma_{eff} = (\sigma_{th} + \frac{I_{\gamma}}{k}) \quad . \tag{3}$$

In the first series of experiments, the numerical value k=5 was determined and this was in agreement with extensive previous measurements carried out in the outer channel of the IBR-2 reactor. The outer and inner channels used in this work are separated by only air and a shutter which is opened when the outer channel is used. Thus, the same value of k was used for irradiations at the inner location, while the effect of CB<sub>4</sub> and self-shielding was considered separately as described below.

The production rate of some nuclide in a target of definite composition and mass can be expressed as follows:

$$\frac{dN}{dt} = \frac{N_A \cdot c \cdot a \cdot m}{M} (\sigma_{th} \cdot \tau_{th} + \frac{I_{\gamma}}{k} \tau_{res}) F_{th} \quad , \tag{4}$$

where  $N_A$  is Avogadro's Number, c is the mass concentration of the element of interest in g/g, a is the abundance of a particular isotope of that element, m is the total mass of

the irradiated target and M is the atomic mass of the element. The  $\tau_{th}$  and  $\tau_{res}$  factors are dimensionless attenuation coefficients reflecting self-absorption in the target layer for thermal and resonance neutrons, respectively. Each may reach a maximum value of unity for targets of negligible thickness or be significantly smaller for thick targets.

Equation (4) describes the  $(n, \gamma)$  capture reaction with slow neutrons. The  $F_{lh}$  and k parameters represent characteristics of the reactor, while all but one of the other parameters must be specified for a definite nuclide in the target, i. e. the capturing isotope. The lone exception is the factor  $\tau_{lh}$ , which is a unique parameter characteristic of all reactions with thermal neutrons in a target of specific composition and thickness and is independent of the particular capturing isotope. Unlike  $\tau_{lh}$ ,  $\tau_{res}$  is individualized because the resonance energies and peak cross-sections are extremely specific to each isotope and vary irregularly from one nuclide to another. Strong absorption near the resonance peak for one isotope may produce absolutely no influence on the resonances of other nuclides. The partial thickness of the target corresponding to the individual isotopes will also depend on c, a and b, and this is important for resonance neutron absorption.

In the outer channel, neither the first nor the second series of irradiations were sufficiently intense to produce a detectable yield of  $^{178m2}$ Hf. However, the dominant activities of  $^{175}$ Hf,  $^{181}$ Hf and  $^{95}$ Zr were measured with high accuracy. Using Eq. (4), the concentration of Zr was evaluated numerically, as well as the  $\tau_{th}$  coefficient specific to the target and the resonance absorption coefficient  $\tau_{res}$  specific to  $^{181}$ Hf production via the  $^{180}$ Hf( $n, \gamma$ ) reaction. For  $^{175}$ Hf and  $^{95}$ Zr, resonance absorption was insignificant due to the low concentration of  $^{174}$ Hf and  $^{94}$ Zr nuclides within the target. These evaluated parameters were then employed in the analysis of the measurements carried out following the irradiation near the active core that had much higher flux.

In this inner location, the thermal neutron flux was strongly attenuated (almost absorbed entirely) by the 3-mm thick CB<sub>4</sub> shield, while the transmission of neutrons was also influenced at other energies below 20 eV. No sharp cut-off occurs since the total cross-section of boron varies smoothly with neutron energy. Therefore, activation by thermal neutrons could be excluded and the effect of resonance neutrons was characterized by a corrected resonance integral *I<sub>s</sub>(corr)* as follows:

$$I_{\gamma}(corr) = I_{\gamma} \frac{\int_{0}^{E_{max}} E_{n}^{-1} \chi(E_{n}) g \Gamma_{n} dE_{n}}{\int_{0}^{E_{max}} E_{n}^{-1} g \Gamma_{n} dE_{n}},$$
(5)

where  $I_{\gamma}$  is the tabulated resonance integral,  $\chi(E_n)$  is the calculated transmission function through the CB<sub>4</sub> filter, and  $g\Gamma_n$  is the resonance strength obtained from the

data of Ref. [1]. Using so-calculated  $I_2(corr)$  values, one can calibrate the resonance neutron flux inside the CB<sub>4</sub> shield, again determined from the measured activities of high-yield <sup>175</sup>Hf and <sup>181</sup>Hf. For both isotopes the self-absorption coefficients  $\tau_{res}$  are known from the outer-channel experiment described above, but the  $\tau_{res}$  value corresponding to production of <sup>178m2</sup>Hf in the <sup>177</sup>Hf( $n, \gamma$ ) reaction was not calibrated. Although one may assume stronger absorption for <sup>177</sup>Hf than for <sup>180</sup>Hf, taking into account the resonance strengths for both nuclides. A more precise estimate for the  $\tau_{res}$  of <sup>177</sup>Hf was obtained on the basis of the resonance excitation function given in Ref. [2], as compared to <sup>180</sup>Hf.

Finally, the total number of resonance neutron capture events by  $^{177}$ Hf nuclei in the target was deduced. From this value the isomer-to-ground state ratio  $\sigma_m/\sigma_g$  may be determined for  $^{178}$ Hf whenever activity of  $^{178m^2}$ Hf is measured.

### III. Results

In gamma spectra measured after two-years cooling of the Hf sample exposed to a fluence of about 10<sup>18</sup> n/cm<sup>2</sup> (in the inner channel), characteristic lines from <sup>178m2</sup>Hf decay were found as shown in Fig. 1. Their intensities were still much lower than the lines resulting from the dominant <sup>175</sup>Hf and <sup>181</sup>Hf activities. This could be expected for the 31-year-lived isomer, which should be produced with a low yield that is suppressed by its high angular momentum and resulted in an isomer-to-ground state ratio on the level of about 10<sup>-8</sup> or less. The spectrum contains many lines of different origin, including those from activated admixtures within the sample, from natural background and from summations of the gamma rays with characteristic X- rays of the emitting atoms within the sample and the Pb within the detector shield. The panels in Fig. 1 show gamma lines from <sup>178m2</sup>Hf decay as well as some other lines that are not related to this analysis.

Table 1 gives the number of counts detected for gamma transitions from  $^{178m2}$ Hf decay at 426.4, 495.0 and 574.2 keV, in comparison with the major lines of  $^{175}$ Hf and  $^{181}$ Hf. Lines from  $^{178m2}$ Hf at lower energies were completely obscured by the large Compton background despite the cooling period. The statistical error in the peak area of the line at 574.2 keV is poor because this lies near the strongly-manifested Compton ridge due to  $\gamma$  lines from  $^{95}$ Zr and  $^{95}$ Nb detected at energies of about 750 keV. Better accuracy was reached for the other two lines and the observed intensities were sufficient to define the number of  $^{178m2}$ Hf nuclei within the activated target, taking into account all necessary factors of efficiency and decay. By comparing this number to the calculated total number of  $^{177}$ Hf(n,  $\gamma$ ) events, as described above, this gave the experimentally measured  $\sigma_{m2}/\sigma_g$  ratio for  $^{178}$ Hf. The latter value was determined for resonance neutrons transmitted through the CB<sub>4</sub> filter. However, a similar  $\sigma_{m2}/\sigma_g$  ratio should be valid for slow neutrons in general, including thermal neutrons. Such regularity has been experimentally confirmed in many cases when the

 $\sigma_m/\sigma_g$  ratio was determined both from measured  $\sigma_{ih}$  and  $I_{\gamma}$  values, e. g. the case of the <sup>180m</sup>Hf isomer [1].

Taking the  $\sigma_{m2}/\sigma_g$  ratio so-obtained and then using the known [1]  $\sigma_{th}$  and  $I_{\gamma}$  parameters for the <sup>177</sup>Hf(n,  $\gamma$ ) reaction, the partial  $\sigma_{th}$  and  $I_{\gamma}$  for population of <sup>178m2</sup>Hf were deduced. The accuracy of this result cannot be expected to be very high due to the modest statistics (see Table 1). In principle, however, the present data were taken under more clean conditions than in previous measurements reported in the literature and should be reliable.

Neutron capture cross-sections for Hf nuclides are summarized in Table 2 with literature data taken from Ref. [1]. The present results are given for the reactions of particular interest,  $^{177}$ Hf(n,  $\gamma$ ) $^{178m2}$ Hf,  $^{178}$ Hf(n,  $\gamma$ ) $^{179m2}$ Hf and  $^{178m2}$ Hf(n,  $\gamma$ ) $^{179g,m2}$ Hf. The latter reaction which is responsible for  $^{178m2}$ Hf destruction (burnup) may be especially exotic and is discussed in more detail below.

More than thirty years ago, activity of the  $^{178m2}$ Hf isomer was observed [4] from isotopically-enriched hafnium targets irradiated within a high-power reactor. Gamma spectra of this isomer were carefully studied using state-of-the-art techniques available at that time. However, the production cross section given in Ref. [4] may not be very accurate because it was determined by only considering the effect of thermal neutrons, neglecting the resonance neutron flux, and assuming that the "burnup" (destruction) cross section was at a rather low level of less than 20 b. It is well-known that a purely thermal flux does not exist in any reactor near its active core and the presence of resonance neutrons changes the yields of reaction products. Also the  $^{178m2}$ Hf yield could be strongly reduced due to the burnup process at the fluences applied in the work of Ref. [4],  $\geq 10^{21}$  n/cm<sup>2</sup>. The degree of burnup definitely depends on the values of  $\sigma_{th}$  and  $I_{\gamma}$  for the isomeric nucleus, but the relatively low  $\sigma_{th}$  given in Ref. [4] was unexpected.

Values of  $\sigma_{th}$  and  $I_{\gamma}$  for neutron capture show for many nuclei a correlation with the level density of neutron resonances. Standard estimations using the Gilbert-Cameron formula [6], verified by known neutron resonance densities for various nuclides, predict a much higher resonance density for <sup>178m2</sup>Hf than that known for the <sup>178g</sup>Hf nucleus. The former nucleus may be characterized by a level density comparable with the measured resonance density for <sup>177</sup>Hf, or perhaps even larger. Thus, similar values of  $\sigma_{th}$  and  $I_{\gamma}$  can be expected for <sup>178m2</sup>Hf and <sup>177</sup>Hf nuclei and these are much larger than the 20 b used in Ref. [4]. Recently, the burnup cross-section due to thermal neutrons was measured in Ref. [7] for the <sup>177m</sup>Lu isomer and a value of  $\sigma_{th} = 590$  b was obtained, including both neutron capture and superelastic scattering components. Noting that <sup>177m</sup>Lu also possesses high spin and excitation energy similar to <sup>178m2</sup>Hf, one may expect them to have comparable burnup cross-sections. Such arguments motivated the present independent measurements of the <sup>178m2</sup>Hf production cross section in reactor irradiations and an evaluation of the role of burnup which depends on neutron flux.

There is no doubt that the number of produced <sup>178m2</sup>Hf nuclei was determined correctly in the earlier experiment [4], although the cross-section was underestimated by a factor of 10 using an incorrect approximation. Now that yield [4] may be taken and combined with appropriate corrections so that it can be compared with the present cross-sections. To make this recalculation of the cross section corresponding to the earlier experiment, the following assumptions are made:

- 1. The effective cross-section of Eq. (3) is, in general, appropriate to account for the contribution of resonance neutrons.
- 2. An effective, or net, production cross-section,  $\sigma_{pro}$ , calculated with the  $\sigma_{th}$  and  $I_{\gamma}$  from the current experiment, should be valid for the conditions of Ref. [4] when an appropriate value of k = 20 (suitable for a well-thermalized spectrum as would be expected for that experiment) is taken.
- 3. The yield of  $^{178m^2}$ Hf measured in Ref. [4] in a high-fluence irradiation may then be reproduced with the calculated  $\sigma_{pro}$  by taking into account a much larger burnup effect than was assumed in the earlier work.

Following this approach, the effective cross-section for burnup in the  $^{178m^2}$ Hf(n,  $\gamma$ ) reaction was deduced. The accumulation of a given product nucleus in the presence of burnup is given by

$$N_{net}(\Phi) = \frac{N_t \sigma_{pro}}{(\sigma_t - \sigma_{burn})} \left[ e^{-\sigma_{burn}\Phi} - e^{-\sigma_t \Phi} \right] , \qquad (6)$$

where  $N_{net}$  and  $N_t$  are the net number of product nuclei and the number of target nuclei at the start of the irradiation, respectively,  $\Phi$  is the neutron fluence,  $\sigma_{burn}$  and  $\sigma_t$  are the capture cross-sections that take into account the burnup of the product and target nuclei, respectively. The  $\sigma_{pro}$  value is the physical production cross-section without burnup. All  $\sigma$  values are defined to be effective, as in Eq. (3).

Combining the present production cross-section results with the yield measurements of Ref. [4] as described above, the effective burnup cross-section,  $\sigma_{burn}$ , was deduced for the <sup>178m2</sup>Hf isomer using Eq. (6). This effective cross-section is a linear combination of  $\sigma_{th}$  and  $I_{\gamma}$  values summed for two exit channels of the capture reaction, together corresponding to the formation of <sup>179</sup>Hf product nuclei in either its ground state (g) or its 25-day-lived  $m_2$  state.

Fortunately, decomposition of  $\sigma_{burn}$  was possible because  $\sigma_{th}$  and  $I_{\gamma}$  parameters have already been directly measured for production of  $^{179m2}$ Hf after irradiation of  $^{178m2}$ Hf in Ref. [5]. The ground-state yield may also be determined by subtraction of the  $^{179m2}$ Hf contribution from the total burnup yield of  $^{178m2}$ Hf. It was assumed that the

ratio  $\sigma_{m2}/\sigma_g$  for production of  $^{179m2}$ Hf and  $^{179g}$ Hf nuclei in neutron capture by  $^{178m2}$ Hf should be approximately the same for both thermal and resonance neutrons. The partial  $\sigma_{th}$  and  $I_\gamma$  for the  $^{178m2}$ Hf(n,  $\gamma$ )  $^{179g}$ Hf branch are therefore deduced and should be added to the previously known values for the branch of the reaction that populates  $^{179m2}$ Hf. Thus, the burnup of  $^{178m2}$ Hf due to neutron capture reactions is now characterized by the total  $\sigma_{th}$  and  $I_\gamma$  values, although with only modest accuracy. Nevertheless, the general behavior of production and burnup processes has been clarified by the present experiment.

Table 3 compares the cross-sections for  $^{178m2}$ Hf production in reactions with slow and fast neutrons. The upper limit therein for the  $^{178}$ Hf(n,  $n'\gamma$ ) reaction was determined based on the present measurements. Fast neutrons with  $E_n \geq 3$  MeV could, in principle, activate the  $^{178m2}$ Hf state located at a 2.446-MeV excitation energy. Fast neutrons can certainly penetrate through the CB<sub>4</sub> shield without significant absorption and their flux was measured by activation of a Ni spectator. Thus, a cross-section can be deduced for fast neutron production of  $^{178m2}$ Hf if its production is attributed to the  $(n, n'\gamma)$  reaction. However, the values of  $\sigma_{m2}$  and  $\sigma_{m2}/\sigma_g$  obtained in such a manner are unphysically large when the reaction's the spin deficit of  $\Delta I = 31/2$  is considered for a hypothetical  $^{178}$ Hf(n,  $n'\gamma$ )  $^{178m2}$ Hf reaction. Recall that  $\Delta I = J_m - J_t - 1/2$ . Finally, it was assumed that the deduced cross-section for fast-neutron production of  $^{178m2}$ Hf is just an upper limit, while the dominant means of producing this isomer is due to slow neutron capture. The  $^{179}$ Hf(n, 2n) reaction with 14.5-MeV neutrons was characterized in Refs. [8, 9]. The efficient production of  $^{178m2}$ Hf in that reaction makes it one of the best methods for accumulation of this isomer, but the achievable flux of 14-MeV neutrons restricts the real use of this reaction for large-scale manufacture. In the case of reactor irradiations, neutrons with energies greater than 10 MeV appear with very low probability.

Table 4 summarizes cross-sections for  $^{179m2}$ Hf production which are described in more detail in Ref. [3]. In that work it was explained that the main production mechanism was the  $(n, n'\gamma)$  reaction, unlike the situation found now for  $^{178m2}$ Hf production. The difference may be attributed primarily to the spin deficit  $(\Delta J)$  values, which causes a preference in the  $(n, \gamma)$  reaction for  $^{178m2}$ Hf, but in the  $(n, n'\gamma)$  reaction for  $^{179m2}$ Hf. The absolute cross-section for  $^{179m2}$ Hf production is not particularly low and in standard reactor irradiations quantities as large as  $\mu g$   $^{179m2}$ Hf could be accumulated. Nanogram amounts are achievable for  $^{178m2}$ Hf, but this would appear to be insufficient for applications or for using the isomer as target or beam nuclei in experiments.

### IV. Discussion

The results summarized in Tables 2 - 4 permit the plot of Fig. 2, showing the systematics of the isomer-to-ground ratio versus spin-deficit for production of hafnium isomers. This plot leads to some interesting points and, perhaps, a general conclusion. It can be seen in Fig. 2 that the  $\sigma_m/\sigma_g$  ratio follows a regular exponential decrease with

increasing  $\Delta I$ . The  $(n, \gamma)$ ,  $(n, n'\gamma)$  and (n, 2n) reactions demonstrate separate curves with individual slopes in the log plot. A natural explanation for the appearance of different curves is that the projectile angular momentum increases with the neutron kinetic energy. In general, the systematics does not demonstrate any unexpected behavior, but the plot allows a quantitative definition of real values for specific reactions. It can, therefore, be used to make estimates of  $\sigma_m/\sigma_g$  values for other cases. It is important to note is that the systematics cover a wide range in angular momentum, as high as J=16 for isomers populated in the  $(n, \gamma)$  reaction and corresponding to a  $\sigma_m/\sigma_g$  ratio lower than  $10^{-8}$ . Such values are not typical in comparison with other measurements known in the literature for neutron-induced reactions.

The conclusion that  $^{179m2}$ Hf is produced in via  $(n, n'\gamma)$  reactions while, conversely,  $^{178m2}$ Hf is produced via  $(n, \gamma)$  reactions is supported by Fig. 2 in addition to the arguments given above. In this plot the upper limits determined for  $^{178m2}$ Hf production via the  $(n, n'\gamma)$  reaction and for  $^{179m2}$ Hf production in the  $(n, \gamma)$  reaction deviate from the systematic pattern, both lying far above the curves corresponding to the respective reactions. Following the systematic trends, it appears that the real cross-section for production of  $^{179m2}$ Hf via  $(n, \gamma)$  reactions is negligible in reactor irradiations as compared with the much larger cross section for  $(n, n'\gamma)$  reactions, and vise versa for  $^{178m2}$ Hf.

The present result that there are significant cross sections for burnup of  $^{178\text{m}2}\text{Hf}$  in the  $^{178\text{m}2}\text{Hf}(n, \gamma)^{179\text{m}2,g}\text{Hf}$  reaction equal in total  $\sigma_{th}$ =235 b and  $I_{\gamma}$ =5600 b is worth further discussion. Such large values are known for many other nuclei, e. g. the  $^{177}\text{Hf}$  nucleus with odd neutron number is characterized by even higher values, as is known from Ref. [1]. In the even-even  $^{178}\text{Hf}$  nucleus, a pair of neutrons is decoupled in the m2 state, so that the isomeric nucleus can manifest itself for as equivalent in behavior to an odd-neutron nucleus. Thus, the observed large burnup cross-section is not out of scale [1], unlike the extremely large  $(n, \gamma)$  cross-section for burnup of  $^{178\text{m}2}\text{Hf}$  reported in Ref. [10]. That value was not reproduced by the present measurements.

Table 2 shows that the population of the ground state appears with  $4\times$  higher probability than the m2 state, but stronger selectivity was not manifested. This can be understood in the following way. Figure 3 shows a partial level scheme for <sup>179</sup>Hf, the daughter of the burnup reaction on <sup>178m2</sup>Hf. Compound-nucleus states of <sup>179</sup>Hf are excited after neutron capture by <sup>178m2</sup>Hf and possess  $J^{\pi} = 31/2^+$  or  $33/2^+$  and a fixed excitation energy near 8,546 keV. For the lower-lying structure, the important features are the  $m_2$  isomer in <sup>179</sup>Hf with  $J^{\pi} = 25/2^-$  at 1,106 keV and the two rotational bands built on the ground and isomeric states. Many other bands exist [11] and the population of  $m_2$  and g states may initially proceed via such bands near the top of the cascade that follows neutron capture. However, these decay paths will eventually reach the bands shown in Fig. 3. Direct transitions can also take place from the

compound-nucleus state to the ground or m2 bands, but, of course, many different cascade paths contribute to the population of a given final state because the level density above  $E^* = (4-5)$  MeV is high in hafnium nuclei.

There is no spin deficit for the burnup reaction on  $^{178m2}$ Hf leading to the highspin  $^{179m2}$ Hf state and it should be strongly populated. It is possible that some preference for this final state may arise due to its high K value and the fact that there is a similar structure of the target and product m2 isomers. However, this experiment demonstrated a preference for population of the ground state. A first conclusion is that the K quantum number and structure tagging do not survive past neutron capture at  $E^*$  above 8 MeV. This may explain the nearly equal population of the  $m_2$  and ground states.

A similar lack of selectivity to structure details at  $E^* > B_n$  was concluded from the measurements of Ref. [12] on depopulation of the <sup>180m</sup>Ta isomer by fast neutron inelastic scattering, in accordance with the basic ideas of the statistical model. In that work, no preferential population of the ground state was observed, unlike the present case of capture on <sup>178m2</sup>Hf. The question remains why there exists even a modest preference for ground-state population following the  $(n, \gamma)$  reaction on <sup>178m2</sup>Hf. One must take into account the presence of many levels of appropriate spin near and below the compound-nucleus state and these will be populated after neutron capture with equal probability without any influence of structure effects. Thus, selectivity for reaching either the ground or m2 states cannot appear near the top of the cascades. One must speculate that the modest preference for the ground state arises due to the position of the m2 level at 1.1 MeV. Some cascades proceeding to the ground state may obtain a higher probability simply because they possess a larger reserve of energy above the ground state than those reaching the isomer, thus providing more possibilities for branching. This idea has not yet been developed in detail.

The above interpretation can be modified if superelastic scattering (SES) [13] contributes a significant part of the observed total burnup cross-section. Until now, SES for <sup>178m2</sup>Hf was not measured and theoretical estimates allow a wide range for this cross-section. This process was not accounted for in the present analysis. There is a lack of sufficiently-developed simulation procedures for reactions with high-spin isomers, despite interesting experimental data may be found in the literature [14-16].

# V. Summary

Production of the high-spin  $^{178m2}$ Hf isomer in  $^{nat}$ Hf targets was successfully observed after their activation with the reactor neutrons at fluences lower than  $10^{18}$  n/cm². It was established that  $^{178m2}$ Hf is mainly produced due to the capture of slow neutrons in  $(n, \gamma)$  reaction, while  $^{179m2}$ Hf is produced in the  $(n, n'\gamma)$  reaction with fast neutrons. The production cross-sections are very different, so that it is possible to accumulate  $^{179m2}$ Hf in a microgram amount after standard irradiations, but only nanograms of  $^{178m2}$ Hf. Comparing the present measurements with the published data, the destruction (burnup) cross-section was deduced for  $^{178m2}$ Hf due to a second neutron

capture from the reactor flux. The partial  $\sigma_{th}$  and  $I_{\gamma}$  values were specified for the burnup process leading to both  $m_2$  and g states in <sup>179</sup>Hf. Also, the isomer-to-ground state ratios for hafnium isomers in neutron-induced reactions were systematized. The potential application of the <sup>178m2</sup>Hf isomer as a reservoir for energy storage and pulsed release has already been discussed extensively in the literature. However, the present results, as well as those in the literature, do not support an optimistic view of reactors as a source of large-scale manufacture of this long-lived isomer. Other reactions may prove more efficient for production of <sup>178m2</sup>Hf.

## Acknowledgements

The authors gratefully acknowledge support from the United States Air Force Office of Scientific Research under contract F49620-02-01-0187.

### References

- 1. S. F. Mughabghab, Neutron Cross Sections, Volume 1. Neutron Resonance Parameters and Thermal Cross Sections, Part B, Z= 61-100 (Academic Press, 1984).
- 2. V. McLane, C. L. Dunford, and P. F. Rose, *Neutron Cross Sections, Volume 2. Curves* (Academic Press, 1988).
- 3. S. A. Karamian, J. J. Carroll, J. Adam, et al., Laser Phys. 14, 438 (2004).
- 4. R. G. Helmer and C. W. Reich, Nuclear Physics A211, 1 (1973).
- S. A. Karamian, Y. T. Oganessian, J. Adam, et al., in VI International School-Seminar "Heavy-Ion Physics", Dubna, Russia, (World Scientific, Singapore, 1998), p. 565.
- 6. A. Gilbert and A.G.W. Cameron, Canadian J. Phys. 43, 1446 (1965).
- 7. O. Roig, G. Bélier, J.-M. Daugas, et al., Nucl. Inst. Meth. A 521, 5 (2004).
- 8. M. B. Chadwick and P. G. Young, Nucl. Sci. Eng. 108, 117 (1991).
- 9. Y. Weixiang, L. Hanlin, and Z. Wenrong, Chinese J. Nucl. Phys. 14, 326 (1992).
- 10. G. V. Muradian, O. Y. Shatrov, M. A. Voskanian, et al., Phys. Atomic Nucl. **66**, 6 (2003).
- 11. S. M. Mullins, G. D. Dracoulis, A. P. Byrne, et al., Phys Rev. C 61, 044315 (2000).
- 12. S. A. Karamian, C. B. Collins, J. J. Carroll, et al., Phys. Rev. C **59**, 755 (1999).
- 13. G. Reffo and M. H. MacGregor, Nucl. Sci. Eng. 114, 124 (1993).
- I. A. Kondurov, Y. V. Petrov, E. M. Korotkikh, et al., Phys. Lett. B 106, 383 (1981).
- 15. Y. T. Oganessian and S. A. Karamian, Hyperfine Int. 107, 43 (1997).
- 16. D. Belic, C. Arlandini, J. Besserer, et al., Phys. Rev. C 65, 035801 (2002).

Table 1. Number of peak counts in the γ lines from <sup>178</sup>m<sup>2</sup>Hf compared to the lines of <sup>175</sup>Hf and <sup>181</sup>Hf (see Fig. 1). The gamma spectrum was taken after two-years "cooling" of a metal <sup>nat</sup>Hf sample activated with reactor neutrons.

Nucleus	$E_{\gamma}$	Counts .	Statistical
179m2	[keV]		error
<sup>178<i>m</i>2</sup> Hf	426.4	19,321	6.3 %
	495.0	12,461	7.6 %
	574.2	16,627	10. 4%
<sup>175</sup> Hf	343.4	$1.086 \times 10^9$	0.2 %
	432.8	$1.599 \times 10^7$	0.3 %
<sup>181</sup> Hf	482.0	$1.487 \times 10^{8}$	0.3 %

Table 2. Neutron capture cross-sections for hafnium isotopes.							
Target	$J^{\pi}_{_{t}}$	Product	$J^{\pi}_{\ p}$	$\sigma_{ih}$ [barn]	$I_{\gamma}[barn]$	$\sigma_m/\sigma_g$	Reference
<sup>174</sup> Hf	0+	<sup>175</sup> Hf	5/2	561	436		[1]
<sup>176</sup> Hf	0+	<sup>177</sup> Hf	7/2	23.5	880	_	[1]
<sup>177</sup> Hf	7/2-	<sup>178g</sup> Hf	0+	373	7,173	_	[1]
		<sup>178m</sup> /Hf	8	0.96	_	$1.6 \times 10^{-3}$	[1]
		<sup>178<i>m</i>2</sup> Hf	16 <sup>+</sup>	2.6 ×	$5 \times 10^{-5}$	$(7\pm2)\times10^{-9}$	Present
				10 <sup>-6</sup>			
<sup>178</sup> Hf	0+	<sup>179g</sup> Hf	9/2+	84	1,950	<del></del>	[1]
		<sup>179ml</sup> Hf	1/2	53		0.63	[1]
		<sup>179<i>m</i>2</sup> Hf	25/2	≤2× 10 <sup>-4</sup>	$\leq 1.3 \times 10^{-3}$	$\leq 2.4 \times 10^{-6}$	Present
<sup>178<i>m</i>2</sup> Hf	16 <sup>+</sup>	<sup>179g</sup> Hf	9/2+	190	4,500	(0.24±0.07)	Present*
		<sup>179m2</sup> Hf	25/2 <sup>-</sup>	45±5	1,060±60		[5]
<sup>179</sup> Hf	9/2+	<sup>180g</sup> Hf	0+	41	630	_	[1]
		<sup>180</sup> mHf	8-	0.45	6.9	1.1 × 10 <sup>-2</sup>	[1]
<sup>180</sup> Hf	0+	<sup>181</sup> Hf	1/2-	13.04	35.0		[1]
* Obtain	* Obtained by comparison of present results with those of Ref. [4].						

Table 3. Summary of the production of <sup>178m2</sup> Hf via different neutron-induced								
reactions.	reactions.							
Reaction	Energy	$\Delta J$	Cross-section	$\sigma_m/\sigma_g$	Reference			
	·		[mb]					
$^{177}\mathrm{Hf}(n,\gamma)$	Thermal	12	$2.6 \times 10^{-3}$	_	Present			
	Resonance	12	$I_{\gamma} = 5 \times 10^{-1}$	$(7\pm2)\times10^{-9}$	Present			
			2		ļ			
$^{178}\mathrm{Hf}(n,n\dot{\gamma})$	$E_n \ge 3 \text{ MeV}$	31/2	$\leq 7 \times 10^{-3}$	$\leq 2.5 \times 10^{-6}$	Present			
<sup>179</sup> Hf(n,2n)	$E_n = 14.5 \text{ MeV}$	11	7.3	$3.5 \times 10^{-3}$	[8]			

Table 4. Su reactions.	immary of the p	roduction	n of <sup>179m2</sup> Hf vi	a different neut	ron-induced
Reaction	Energy	ΔJ	Cross- section [mb]	$\sigma_m/\sigma_g$	Reference
$^{178}$ Hf( $n,\gamma$ )	Thermal	12	≤ 0.2	≤ 2.4 × 10 <sup>-6</sup>	Present
	Resonance	12	$I_{\gamma} \leq 13$	$\leq 7 \times 10^{-6}$	Present
<sup>179</sup> Hf(n,n 'γ)	$E_n \ge 1.5 \text{ MeV}$	15/2	4.5±0.5	(1.6±0.2) × 10 <sup>-3</sup>	Present
<sup>180</sup> Hf(n, 2n)	$E_n = 14.8$ MeV	12	25	7 × 10 <sup>-3</sup>	[8]

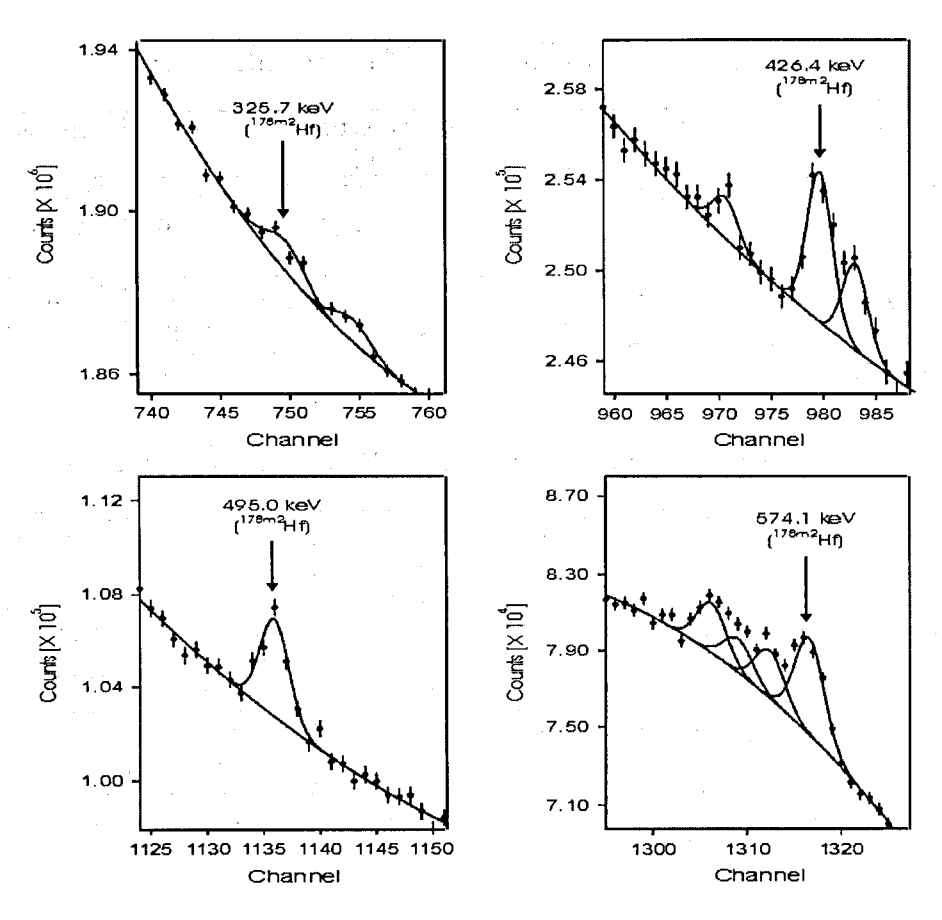


Figure 1: Panels show sections of the gamma spectrum collected from the metal <sup>nat</sup>Hf sample after neutron irradiation in the inner channel of the IBR-2 reactor, and after two-years cooling time. Lines corresponding to decay of the <sup>178m2</sup>Hf isomer are identified and peak fits are shown from which the counts of Table 1 were determined.

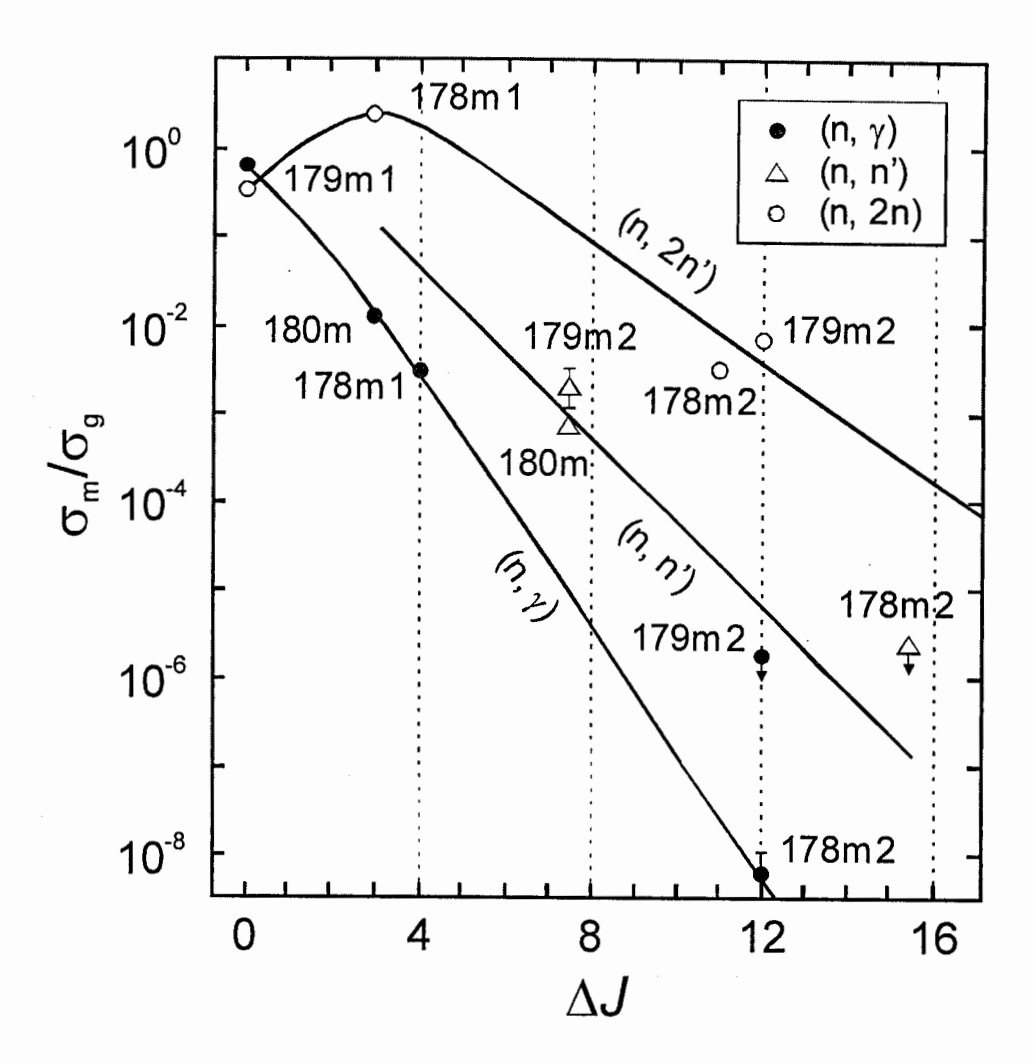


Figure 2: Measured values of the isomer-to-ground-state ratio versus spin deficit ( $\Delta J$ ) parameter for hafnium isomers produced in neutron-induced reactions. Numerical data and references are given in Tables 2 – 4. For simplicity, points according to the literature are given without error bars.

# $^{178m2}$ Hf(n, $\gamma$ ) $^{179m2,g}$ Hf

c. n. resonances

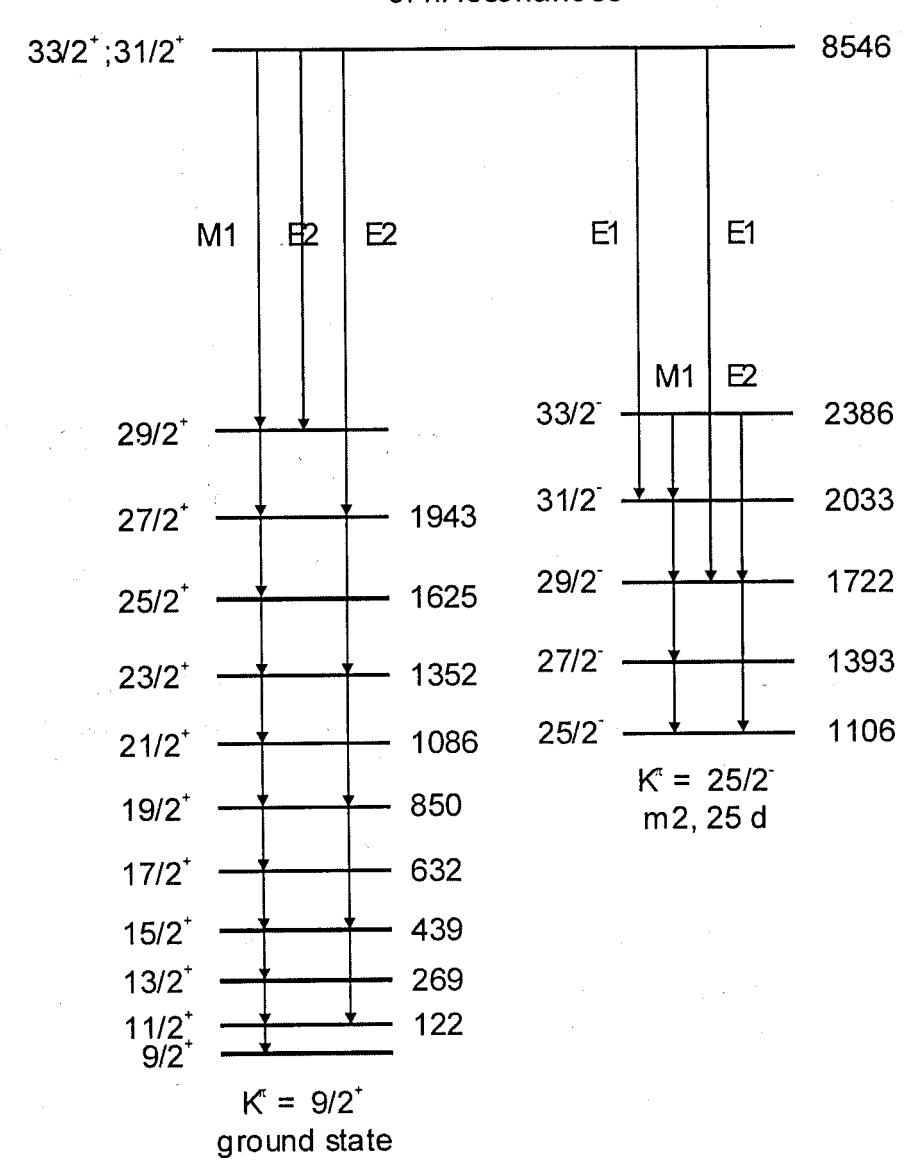


Figure 3: Partial level scheme depicting population of the  $m_2$  and ground states in  $^{179}$ Hf after the  $^{178m_2}$ Hf(n,  $\gamma$ ) reaction with slow neutrons. The cascades shown illustrate the discussion in the text.

# COULOMB EXCITATION OF THE <sup>178M2</sup>HF ISOMER: PROPOSAL

#### S. A. KARAMIAN

Joint Institute for Nuclear Research, Dubna, 141980, Russia

#### J. J. CARROLL

Youngstown State University, Youngstown, Ohio, OH-44555, USA

Possible experiment on Coulomb excitation of the <sup>178m2</sup>Hf isomeric nuclei is discussed in some detail. A key role should play use of the isomeric material in a form of the accelerated ion beam, not in a form of target. In this version, the effect-to-background ratio should be improved by an order of magnitude. High-sensitivity detecting system, like the combination of Gamma-Sphere and Chico detectors should be applied. It will provide selection of events corresponded to the projectile excitation. Accounting an available amount of <sup>178m2</sup>Hf, one can estimate a number of events in gamma-spectra of the isomer Coulomb excitation. It should be enough for observation of the isomer triggering via transitions to the ground-state band in <sup>178</sup>Hf. Thus, a value of reduced matrix element for triggering would be the main result of this experiment.

#### 1. Introduction

The problem of isomer triggering, which may release the energy stored in long-lived nuclear excited states, has attracted increased attention in recent years both in terms of general scientific interest and for potential applications. In all cases, an important parameter is the cross-section for triggered isomer depopulation by exposing a metastable nucleus to some external stimulus, i.e. a flux of photons or particles. The cross-sections of triggering reactions are generally reduced from their ideal values by strong hindrance factors arising from a high multipolarity and/or a nuclear structure mismatch for electromagnetic transitions between isomeric and triggering levels. In the experiment described in Ref. [1], the population of levels in bands built on isomers was successfully observed via Coulomb excitation reactions acting on the stable <sup>178</sup> Hf isotope in its ground state. Surprisingly, the cross-section for this population was moderately high and this was attributed to strong K mixing of different structure configurations at high angular momentum.

This observation suggests a special experiment by which to observe triggering of the <sup>178m2</sup>Hf isomer into the levels of the ground state band via Coulomb excitation, essentially as an inverse of the reaction observed in Ref. [1]. Specific transitions are implied for triggering and their energies are known, making possible experimental

design and for quantitative estimations of the reaction rate. The magnitude of the cross-section for the population of <sup>178</sup>Hf isomers [1, 2] promises likewise significant probabilities for the reversed process of triggering. A successful new experiment will quantify parameters such as the energies, multipolarities and reduced matrix elements for energy-releasing trigger transitions. These parameters are needed to assess the feasibility of inducing a release of isomeric energy under an intense photon flux as suggested for some applications [3].

At this time, technical challenges restrict the availability of samples containing  $^{178m2}$ Hf in an amount sufficient for preparation of a target suitable for standard inbeam  $\gamma$ -spectroscopic experiments. Therefore, it is necessary to consider the possibility of performing an experiment with  $^{178m2}$ Hf nuclei as projectiles. Radioactive ion-beam facilities operate routinely at many laboratories and the long-lived  $^{178m2}$ Hf nuclide should not be extraordinarily difficult for beam production.

### 2. Acceleration of isomeric ions

The most critical issues which define the cost of an experiment and the quality of the measurements are the consumption rate for and total available amount of  $^{178m2}Hf$ . The isomeric material can be produced using the  $^{176}Yb$  ( $^4He,\,2n)^{178m2}Hf$  reaction, as described in Ref. [4]. With a 100- $\mu A$  beam of  $^4He^{++}$  ions at 35 MeV, one can accumulate  $10^{15}$  atoms of  $^{178m2}Hf$  during an irradiation time of about one month. An isomer-to-ground state ratio for  $^{178}Hf$  nuclei as high as  $\sigma_m/\sigma_g=0.05$  could be reached using this reaction with  $^4He$  ions. Other reactions are characterized by lower  $\sigma_m/\sigma_g$  values and are less suitable for in-beam spectroscopic measurements. In the proposed Coulomb excitation experiment, the accumulated isomeric material would be spent for acceleration of ions of  $^{178m2}Hf$ .

It would be difficult to separate the isomeric and ground-state  $^{178}$ Hf nuclei during acceleration. Some methods to do so have been discussed in principle, but they would result in a reduction of the beam intensity by orders-of-magnitude due to losses of the isomeric ions. One may assume that a realistic total efficiency of the source-accelerator system is on the level of 1 %. This modestly-good value represents the ratio between the number of ions reaching the target and the total number of atoms consumed in the ion source. With such an efficiency, a total number of about  $10^{15}$  isomeric atoms will be spent during 10 hours of beam with an intensity of approximately  $3 \times 10^8$  ions/s. The full current of the  $^{178}$ Hf ion beam will be about 1 particle nA, taking into account  $\sigma_m/\sigma_g = 5$  %.

As indicated above, only about 10 hours of irradiation time will be available at a beam intensity of  $3 \times 10^8$  ions/s. The beam current can be reduced to extend the irradiation time, but the integral number of ions reaching the target will be conserved near  $10^{13}$  ions containing  $^{178\text{m}2}$ Hf. It is necessary to determine if this is sufficient for a successful experiment. Theoretical estimates may be conducted based on the idea of K mixing for the interband transitions of Ref. [2] and they show in first approximation

that such experiment may be possible. An estimation of the count rate is discussed below. However, only the successful detection of triggering can lead to the real cross sections for Coulomb depopulation of the <sup>178m2</sup>Hf isomer.

## 3. Choice of target and beam parameters

A schematic of the experiment can be given as follows. A target made of low-background material (Pb) will be irradiated by a  $^{178}$ Hf ion beam at an energy much lower than the Coulomb barrier of interaction. The projectile-target spectrum due to Coulomb excitation should be recorded in coincidence with the scattered ions. Use of a multi-detector  $\gamma$  array is needed to obtain  $\gamma$ - $\gamma$  and higher coincidences. The spectra collected with the "isomeric" (5%) beam will need to be compared with a pure ground-state  $^{178}$ Hf beam and the difference spectrum obtained. This difference spectrum may contain cascades corresponding to population of high-spin levels both within the band built on the isomer and within the ground-state band (g.s.b.). The latter case, population of high-spin members of the g.s.b may take place due to single-step Coulomb excitation from the isomer, if K mixing is indeed significant as discussed in Refs. [1, 2]. Observation of the corresponding  $\gamma$ -cascades would then serve as a signal of isomer triggering.

As is the usual case in any experiment, the background intensity plays a significant role. One may analyze some restrictions on the scheme that accrue from the presence of different backgrounds:

- 1. The beam energy should be relatively low, about 3.5 MeV/nucleon, in order to prevent population of  $J \ge 14$  members of the g.s.b. due to excitation from the J = 0 ground state of <sup>178</sup>Hf within the beam. The probability for such multiple Coulomb excitation is drastically reduced at this low beam energy [2] and triggering can therefore be clearly isolated.
- 2. A Pb target should be used because it will produce an insignificant Coulomb excitation spectrum and does not contribute to the background. This is particularly the case if an enriched target of <sup>208</sup>Pb, for example, can be used.
- 3. The need to obtain coincidences between  $\gamma$  signals and scattered ions does not allow the use of a thick target that stops the beam.
- 4. Doppler-correction is absolutely necessary. Otherwise it would be impossible to distinguish narrow  $\gamma$  lines when those gammas are emitted in flight.
- 5. Detection of the scattered projectile defines the direction of the emitter motion, but the absolute speed varies due to energy losses in the target. The target thickness should be optimized for successful Doppler correction.
- Scattered radioactive nuclei produce an insignificant pollution in the detectors, however the beam damp content should be added to the ion source elements for the recuperation of isomeric nuclei past irradiation.

### 4. Count rate estimation

According to Ref. [2], it is assumed that safe background conditions will occur with a beam energy lower than 4.6 MeV/nucleon. Successful Doppler correction requires that the emitter velocity should not vary more than  $\pm$  5 % along its stopping path in the target from entrance to exit. This corresponds to projectile energy losses in the target of about 20 %. The Doppler correction procedure should be performed in event-by-event processing with a velocity dependent on the scattering angle in the laboratory system. With the known dE/dx parameter, one deduces that the Pb target should have a thickness of about 4 mg/cm². A realistic intensity for the <sup>178m²</sup>Hf beam was already introduced to be about  $3 \times 10^8$  ions/s. Thus, the Coulomb excitation cross section can be estimated and the rate of excitation events can be deduced in a straightforward manner therefrom.

Here the single-step E2 Coulomb excitation from the 16+ isomeric level to the 14<sup>+</sup>, 16<sup>+</sup> and 18<sup>+</sup> levels of the g.s.b. are calculated. The respective transition energies are known to be 331, 990 and 1,675 keV. Weisskopf strength was assumed for these transitions due to the observance in Ref. [2] of strong K mixing in the g.s.b. at spins  $J \ge 10$ . Following Ref. [5],  $B_w(E2) \uparrow = 0.0297 \ e^2 \ b^2$  is taken as the Weisskopf value for all transitions. With a mean projectile energy of 740 MeV, one finds values of the Coulomb excitation parameter of  $\xi = 0.489$  for 331 keV,  $\xi = 1.46$  for 990 keV and  $\xi = 2.47$  for 1.675 keV transitions. Thus, the excitation of the projectile nuclei should occur with a relatively large cross section. This will depend on the assumed solid angle for detection of the scattered projectiles.

The CHICO detector developed at the University of Rochester, as often utilized at Argonne National Lab and at other accelerator facilities, provides wide-angle detection of scattered projectiles over nearly  $2\pi$  solid angle in the forward direction. Selecting c.m.s. scattering angles between  $60^{\circ}$  -  $140^{\circ}$ , these correspond to laboratory system angles from  $32^{\circ}$  -  $85^{\circ}$ . Smaller angles are not useful due to the reduced probability of Coulomb excitation. However, the given interval covers a solid angle of 4.8 sr or 75 % of  $2\pi$ .

Using the above-described parameters, an excitation rate of about 245 events/s is found for the 331 keV transition, about 3.2 events/s for the 990 keV and of about 1.5·10<sup>-2</sup> events/s for 1.675 keV transition. The 14<sup>+</sup> level can be successfully excited even using a lower beam energy of 3 MeV/nucleon.

A multiple gamma-detector system, coupled with CHICO for Doppler correction and background suppression, should provide reliable detection of g.s.b. excitation events in the form of multiple gamma cascades from the 14<sup>+</sup>, 16<sup>+</sup> and 18<sup>+</sup> levels after

their single-step excitation from the  $16^+$  isomer. The gamma background due to Coulomb excitation starting from the  $0^+$  ground state would not be significant and, in addition, can be removed by subtracting a spectrum taken under the same conditions, but with a pure <sup>178</sup>Hf ground-state beam. Thus, the triggering events can be reliably selected and the corresponding cross section deduced. The excitation rate would be sufficient to accomplish an experiment with an integral number of  $10^{13}$  <sup>178m2</sup>Hf ions incident on a Pb target during a run, until a total of  $10^{15}$  isomeric atoms are spent. Indeed, with an excitation rate of 250 events/s,  $10^7$  events can be accumulated during 10 hours of data acquisition. The efficiency of  $4\pi$  gamma arrays is typically very large, especially for the detection of high-multiplicity gamma cascades as needed in this proposed experiment.

# **Summary**

Transitions beginning on the 16+ isomer and leading to states in the ground-state band in <sup>178</sup>Hf would serve to trigger a release of energy stored in the metastable level. Direct observation of such transitions and characterization of their cross sections is essential for basic scientific knowledge and to assess the feasibility of applications. While standard Coulomb excitation experiments are not possible with <sup>178m2</sup>Hf as a target due to the small amounts of isomeric material likely to be available, an experiment using <sup>178m2</sup>Hf nuclei as a beam is promising and should be pursued.

## References

- 1. A. B. Hayes, D. Cline, C. Y. Wu, et al., Phys. Rev. Lett. 89, 242501 (2002).
- 2. D. Cline, J. Modern Opt. (Proc. 35th Winter Colloquium on the Physics of Quantum Electronics) (in press for 2005).
- 3. J. J. Carroll, S. A. Karamian, L. A. Rivlin, et al., Hyperfine Int. 135, 3 (2001).
- 4. Y. T. Oganessian, S. A. Karamian, Y. P. Gangrski, et al., J. Phys. G 18, 393 (1992).
- 5. D. Cline, A. B. Hayes, C. Y. Wu, et al., Proposal to Argonne National Laboratory, ATLAS/Gammasphere facility: K conservation, octupole correlations, and induced depopulation of the 141 year K = 5 isomer in <sup>242</sup>Am, (April 2005).



Photon-induced processes

## SOME SYNCHROTRON X-RAY TECHNIQUES FOR ISOMERS

N. R. PEREIRA<sup>†</sup>

Ecopulse, Inc, PO Box 528, Springfield, VA 22150, USA

G. MERKEL AND M. LITZ

Army Research Laboratory, Adelphi, MD 02783, USA

#### J. CARROLL

Youngstown State University, Youngstown, OH 44555, USA

While the earliest attempts to affect the decay of isomers with x-rays applied broad-band bremsstrahlung sources, many more recent studies of isomers have used x-rays from third-generation synchrotrons. This paper highlights some synchrotron techniques that may be useful for use with isomers but have not yet been applied. One is concentrating the x-rays with x-ray optics, notably Ecopulse's lithium refractive x-ray lens, the other is usage of the synchrotron radiation's time structure. The techniques are offered as is, without adding any special considerations of how they might be applied to a specific measurement on a particular isomers. This should be done in a more complete experimental design that was planned for the future.

### Introduction

In physical measurements of radiation-induced processes there are often two principal and mutually contradictory issues: the desired signal is often proportional to a driving influence, hence one difficulty is to get a large enough driver. In cases when the driver must be large the signal tends to be relatively small, and the second difficulty is then to suppress a background that is, in general, also proportional to the driving signal. For isomer studies a synchrotron is often the most appropriate x-ray source because of its well-controlled characteristics.

In this paper we highlight one way to increase the x-ray fluence on a synchrotron,, with a refractive lens Ecopulse has made with lithium metal. In tests at Argonne's Advanced Photon Source (APS) this lens increases the fluence of 10 keV x-rays 50-fold. We also mention a technique, developed by others at the APS, that suppresses the radiation background relative to the signal associated with nuclear transitions by a time delay.

## X-ray refractive lens from lithium metal

The advent of highly collimated x-ray beams from synchrotrons has allowed practical use of x-ray refraction, in x-ray lenses that are conceptually identical to the standard refractive lenses, used for radiation from microwaves to UV light. Together with its colleagues at Argonne's Advanced Photon Source, Ecopulse has developed x-

ray refractive lenses made from lithium metal. The motivation for the use of non-traditional lithium is, of course, lithium's low x-ray attenuation: for 10 keV x-rays the attenuation length in solid lithium is 60 mm. Since attenuation is dominated by the photoelectric effect, which scales as the cube of the photon energy, for 5 keV x-rays Li's attenuation length shrinks to 7.5 mm. Something similar is true for all materials used in refractive lenses, e.g., beryllium, plastics, or even aluminum or silicon, suggesting that refractive lenses have an optimum energy range. For lithium the useful energy range is the lowest, around 10 keV and exactly where the oft-touted isomer <sup>178m2</sup>Hf may have an interesting transition that could, according to some reports, be triggered and make 178-Hf suitable for some applications.

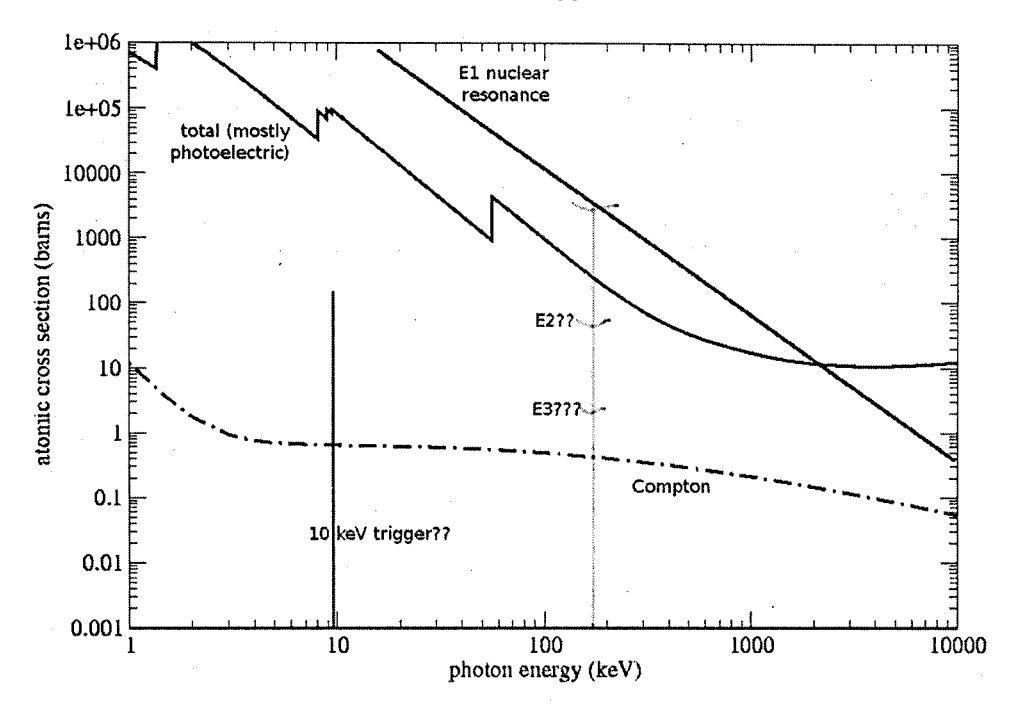


Figure 1: Atomic and nuclear cross sections for Hf.

Figure 1 shows some of Hf's cross sections. The top straight line is the theoretical cross section for excitation of the nucleus in an E1 transition as function of energy. For Hf this transition is expected at the light vertical line, at 126 keV. Along this line are indicated the expected cross sections for the higher order transitions E2 and E3. The solid line is the total atomic cross section for Hf's 72 electrons, and the dashed line is the Compton cross section for a single electron. The vertical line at 10 keV is the nuclear trigger cross section as claimed for Hf. The figure illustrates the principal difficulty in exciting nuclear transitions: they are very narrow. In fact, they are much narrower than suggested by the line width at the resonance energy. Obviously, their

integrated cross section is minute compared to the photoelectric and even the Compton cross section of the many (72 for unionized Hf) electrons that surround the nucleus.

Ecopulse's lithium lens may be useful in experiments aimed at verifying triggering of 178-Hf at about 10 keV, but it is not particularly useful for experiments at the E1-transition at 126 keV.

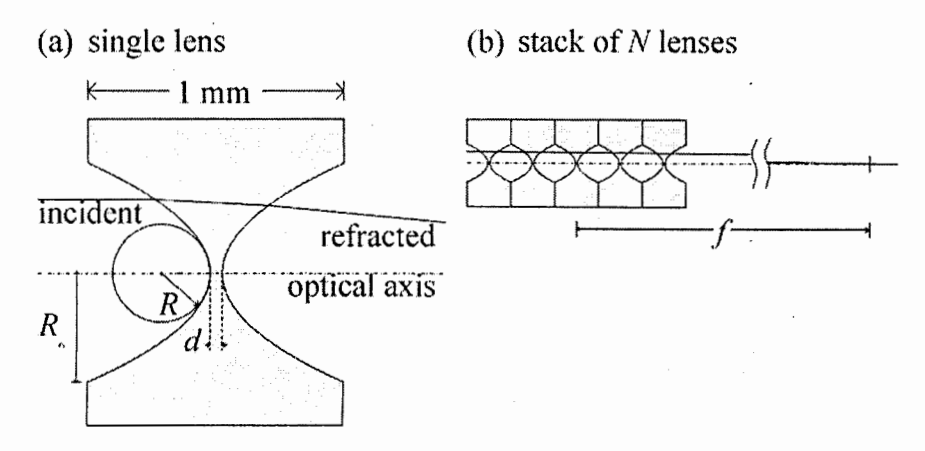


Figure 2: Aachen-style parabolic lenses as used by Ecopulse [1].

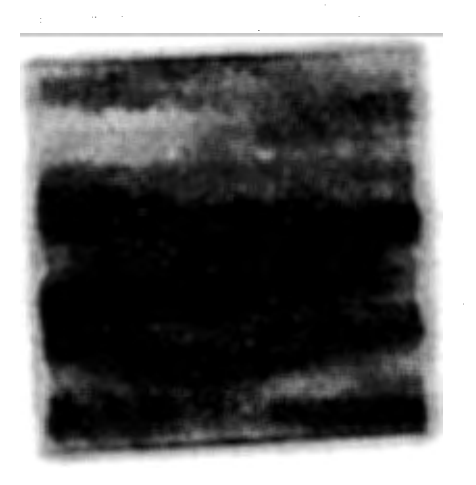
Figure 2 is the design of Ecopulse's lithium lens [1]. Its geometry is identical to that of the aluminum and beryllium lenses built by the x-ray lens group at Aachen University. For a single refractive parabolic lens with radius of curvature r, the focal length f is  $f = r/(2\delta)$ , and for N lenses in series the focal length is N times smaller,

$$f = r/(2N\delta) . (1)$$

Here  $\delta=1-n=(\omega_0/\omega)^2/2$  is the refractive index decrement,  $\omega_0$  is a characteristic frequency of the electrons, and  $\omega$  is the frequency of an x-ray with energy  $h\omega/2\pi$ . For lithium at 10 keV the refractive index decrement is about 1/1,000,000. Since the radius of our lenses is 0.26 mm, the focal length of a single parabolic lens from lithium is then 130 m. This is long, but not excessive: it is on the same order as the typical 50 m distance to the x-ray source at the APS. Putting 80 lenses in series makes the focal length 1.6 m and this lens can focus 10 keV x-rays in a useful manner.

Figure 3 is one result. To the left is an intensity plot of the unfocused 10 keV x-ray beam that goes into the lens. It is square, 0.5 mm on a side, with intensity striations that have since been largely suppressed through enhancements of the x-ray optics upstream, by the scientists at the MHATT?XOR beam line where the measurements were done. To the right is the x-ray intensity in the focal plane behind the lens. Its intensity is reduced by x-ray filters in the beam to make the beam more visible. The filters preferentially attenuate the 10 keV component, leaving unaffected the small harmonic contribution at 30 keV that accompanies the fundamental x-rays at

10 keV. As a result, the 10 keV x-rays focused in the center are visible together with 30 keV x-rays. For these harder x-rays the index of refraction decrement is 1/9 of that for 10 keV x-rays, so that they are only slightly bent by the lens and they form a slightly contracted version of the original beam. The 20 micron by 30 micron focal spot in 10 keV x-rays is in its peak about 50 times more intense than the unfocused beam. The focused beam contains about half the 10 keV photons in the original beam. However, some of them are in a halo that surrounds the focus and is not separately visible in Figure 3. Additional work can suppress the halo, and mitigate small-angle scattering that is a principal reason why the focus is not as small as it should be theoretically.



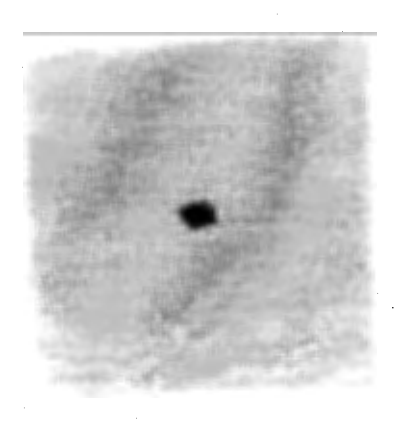


Figure 3: Unfocused x-ray beam (left) and focused but attenuated beam (right).

There are two reasons to consider focusing x-rays for isomer studies, either with a refractive lens or with other x-ray optics (mirrors, zone plates). One is to have additional flexibility to match the x-ray spot size to the sample size, the other is to give additional options for time-resolved diagnostics.

### Match spot size.

When the attenuation in a material is so large that the x-rays do not reach the sample's back side, the atoms located there do not participate in the measurement. They may just as well be absent. When the material is exceedingly expensive, as any isotopically or especially isomerically enhanced material would be, samples that are too thick are therefore wasteful. On the other hand, a sample that is too thin wastes precious x-rays. The optimum is a sample with a thickness in between the two extremes. As can be expected the optimum thickness is an attenuation length. A sample with N atoms with cross section  $\sigma$  then has an area A of

$$A = N\sigma \tag{2}$$

Of course, if the cross sections for the different processes differ many orders of magnitude, as they do for 178-Hf, there is substantial freedom in the choice of cross section, and therefore in the sample area (which is often limited by other factors such as fabrication requirements anyway).

When only a few interesting atoms are available the optimum sample size is quite small. One of the Hf samples has about 10<sup>14</sup> of the 178m2 isomer. If the trigger cross section at 10 keV were to be as sketched, about 100 barns or 10<sup>-22</sup> cm<sup>2</sup>, the optimum area would be sub-micron, about 10<sup>-7</sup> cm<sup>2</sup>. The same sample with the 100 kb atomic cross section would be just about as large as the x-ray focus in Figure 2, 20 by 30 microns. However, the actual sample contains the isomer only as a minor impurity, perhaps 1/100,000. Then the optimum sample size is on the order of 1 cm<sup>2</sup>, as is the size of the actual sample. Since the unfocused x-ray beam is about 1 mm high and a few mm wide, the sample is too large. In measurements on a synchrotron the sample is therefore put under an angle so that the beam illuminates it more or less uniformly, the opposite of what the lens would do. However, samples with higher concentration of the active isomer would be smaller and could make good use of x-ray optics.

#### Suppress radiation background by using the synchrotron's time structure.

The synchrotron's x-rays come in sub-ns short pulses at a rapid clip, at a MHz or so. Some measurements can benefit from the time structure, including some that use nuclear resonances. The reason is the resonance itself, which implies a typical time scale  $\Delta t$  over which the resonance builds up or decays. Heisenberg's uncertainty principle  $\Delta E$ .  $\Delta t = h/2\pi = 10^{-34}$  Js relates a time scale to an uncertainty in energy, an energy width  $\Delta E$ . As an example, the well-known nuclear resonance of <sup>57</sup>Fe has a 140 ns decay time that corresponds to a very narrow width, 5 neV.

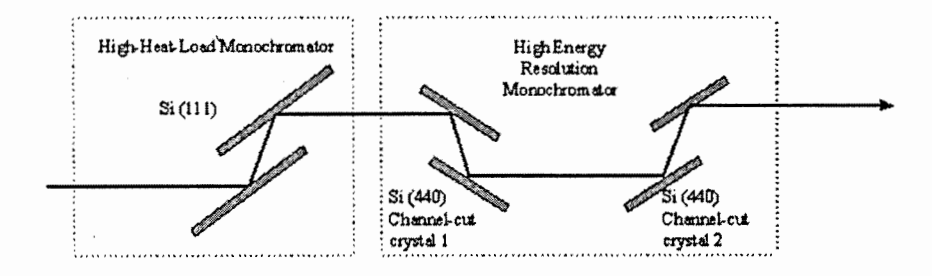


Figure 4: Monochromator chain needed to get x-ray beams with micro-eV width.

Figure 4 and Figure 5 show some of the x-ray optics elements that are needed to take advantage of the synchrotron's time structure in using nuclear resonances for

measurements. The left side of Figure 4 sketches the usual monochromator that slices out of the polychromatic (white) powerful (sub-kW) x-ray beam only a small energy range of interest. The first monochromator crystal must withstand the full power of the x-rays directly from the synchrotron, up to 1 kW. It is therefore cooled, to 77 K. The second crystal narrows the width further, and redirects the beam so that it remains horizontal.

For the lithium lens the desired x-ray energy is around 10 keV, and the width is not particularly important: the high heat load monochromator's standard width around 1 eV is perfectly acceptable. However, the nuclear resonance is so much narrower that further monochromatization is essential. The right side of Figure 4 shows how to do this conceptually: two additional channel-cut crystals reduce the intensity of unwanted energies with four additional higher order reflections. While conceptually straightforward, the demands on the hardware to get the energy slices within a desired meV band are extremely severe, and aligning all these monochromators is very time-consuming: it is not something to be attempted by the weak.

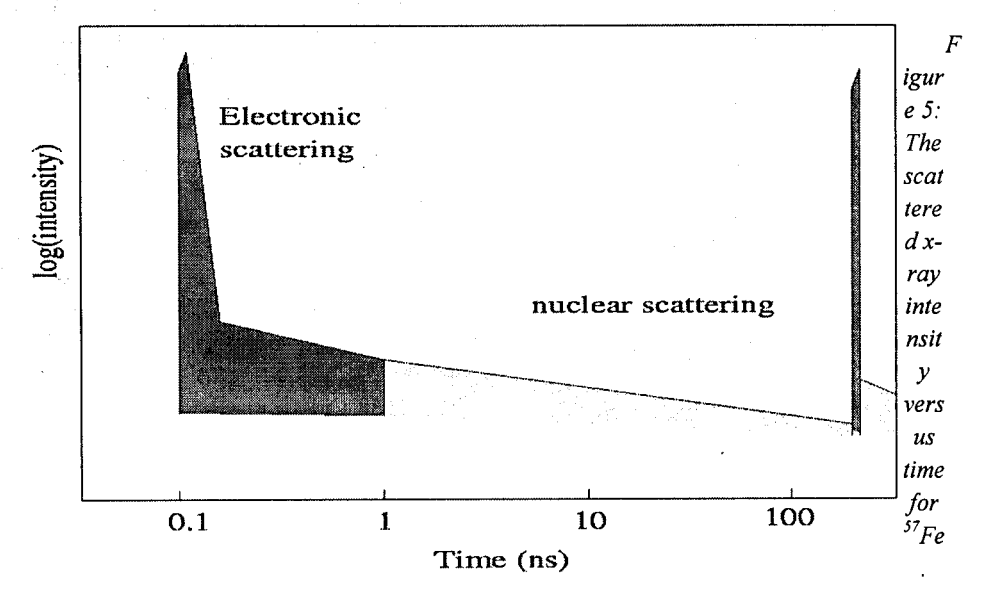


Figure 5 shows schematically the intensity as function of time for a sample containing <sup>57</sup>Fe, 26 electrons surrounding a Moessbauer nucleus from which the numbers in this section are taken [2]. The nucleus <sup>57</sup>Fe has a decay time of 140 ns, corresponding to a width of 4 neV.

The APS's x-ray pulses are about 0.1 ns wide and, depending on the operational mode, can come as sketched in the figure, every few 100 ns or so. While the x-rays are in a very narrow energy band, some meVs wide, most immediately scatter off the electrons and appear as an intense peak that coincides in time with the 0.1 ns wide x-ray pulse. A few photons are in the 5 neV wide band that can excite the nuclear resonance. These photons are stored temporarily in the nucleus, and reappear as decay

radiation with a characteristic decay time around 140 ns. The instantaneously scattered radiation, the background, is suppressed by turning on the photodetectors only after the x-ray pulse is gone: Figure 5 shows this as 1 ns. Suitable x-ray detectors are amplified photodiodes, ADPs, for which a reference is given in [2].

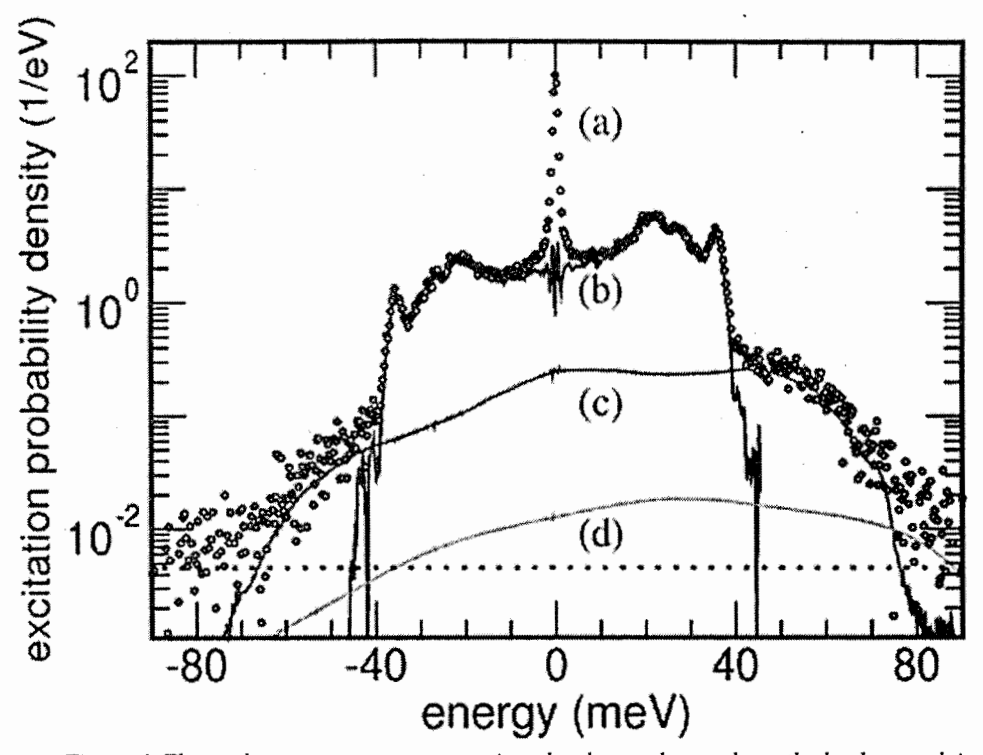


Figure 6. The nuclear resonance cross section clearly stands out above the background, in a measurement of solid state properties (from [2]).

Figure 6 illustrates what can be achieved. The figure shows the intensity of the scattered x-rays from an iron sample, in which the Moessbauer nucleus <sup>57</sup>Fe is affected by the phonons in the material. The shift in energy can be measured with an accuracy of meVs, sufficiently to see the various components of the lattice vibrations that are the subject of the investigation (see [2]). Contrast this figure with what has sometimes been claimed to constitute proof of a nuclear resonance in <sup>178m2</sup>Hf, and the difference is obvious: a strong peak as in Figure 6 convinces every reasonable physicist that the measurement makes sense, and that the results can be trusted. Conversely, a glitch in a bunch of data points that could equally well be caused by statistics causes at best controversy and at worst destroys reputations if the glitch is steadily mis-interpreted as signal.

It seems very worthwhile to measure isomeric triggering cross sections with the help of the techniques highlighted here, and any other techniques that contribute to suppressing the radiation background. Doing this may be more difficult for naturally radioactive materials such as <sup>178m2</sup>Hf, where the natural decay supplies an additional background that can not be suppressed in the manner suggested here.

Other difficulties abound. While a high resolution monochromator would work at 10 keV, so that Hf- triggering measurements with ~10 keV x-rays can be done better with additional monochromatization and time delays, the narrower the energy spectrum the more difficult it is to find the correct energy. And, triggering at higher energy where the transition is known to exist, around 126 keV, would be more difficult because monochromators and detectors at higher energies don't work so well.

Opportunities abound too. For example, a much slower nuclear transition than the 140 ns for <sup>57</sup>Fe might make it possible to move the sample far enough away from the x-ray beam so that it can be counted in a quiet environment. In principle it is possible to move materials with a speed around 1 km/s, or 10 cm in 0.1 ms. A nuclear transition that takes 68 microseconds, as the E1-transition in <sup>178m2</sup>Hf might, could give enough time to take the sample to a remote counter in less than a decay time. In this time perhaps half of the decays could have happened, but the other half would still be there. The advantage is negligible background.

The purpose of this presentation is achieved if you will consider doing measurements that might use these or other advanced techniques.

#### Acknowledgments

Part of this work was conducted at the MHATT-CAT insertion device beamline at the Advanced Photon Source and was supported in part by the U.S. Department of Energy, Grant No. DE-FG02-03ER46023. Use of the Advanced Photon Source was supported by the U.S. Department of Energy, Office of Science, Office of Basic Energy Sciences, under Contract No. W-31-109-Eng-38.

#### References

- 1. N. R. Pereira, E. M. Dufresne, R. Clarke and D. A. Arms, *Parabolic lithium refractive optics*, Rev. Sci. Instrum. 75, 37 (2004); and earlier papers as referenced therein.
  - 2. e.g., W. Sturhahn, *Nuclear Resonant Spectroscopy*, J. Phys. Cond. Matter, **16** 497-530, (2004). This is a review paper that discusses the use of nuclear resonance spectroscopy and the Moessbauer effect in solid state measurements.

# STATUS AND PERSPECTIVES FOR THE EXPERIMENTAL INVESTIGATION OF <sup>178M2</sup>HF ISOMER TRIGGERING BY LOW-ENERGY PHOTONS

V.I. KIRISCHUK <sup>1</sup>, P. MCDANIEL <sup>2</sup>, C.B. COLLINS <sup>3</sup>, J.M. POUVESLE <sup>4</sup>, N.V. STRILCHUK <sup>1</sup> AND V.A. ZHELTONOZHSKY <sup>1</sup>

<sup>2</sup> Sandia National Laboratories, Albuquerque, NM, USA

All the experimental data available on <sup>178m2</sup>Hf triggering are investigated in detail. An attempt is made to define what mechanism could be responsible for the triggering of <sup>178m2</sup>Hf isomeric state and how at least some of the problems of the first experiments can be solved. While the main positive results of previous experiments on x-ray stimulated decay of <sup>178m2</sup>Hf isomer continue to be reliably confirmed, such experiments could be replicated now by other teams and perhaps it would help not only to find all missing links in the chain of the triggering phenomenon understanding, but to expand the research to other long-lived nuclear isomers and nuclides suitable for such purposes as well.

#### Introduction

The pioneering experiments on  $^{178m2}$ Hf isomer triggering did produce a sort of confusion throughout the scientific community since the observed high efficiency of the triggering with low-energy x-rays stressed all models, which might have been able to predict such an effect [1-6]. Moreover, there appeared to be not only one but at least two distinct reaction branches for triggering. Different trigger energies in different series of experiments produced absolutely diverse deexcitation channels, one that included  $^{178m1}$ Hf isomer ( $T_{1/2} = 4$  sec.) and another one – not. And though the experimental investigation of  $^{178m2}$ Hf triggering phenomenon has been continued using not only portable x-ray machine [7-9], but synchrotron radiation (SR) sources as well /10 - 12/, significant efforts are still being applied to find both proper explanations and correct mechanisms responsible for such unexpectedly high efficiency of the triggering as well.

One of such mechanisms is Nuclear Excitation by Electron Transition (NEET), the process inverse to internal electron conversion, when energy of one of the atomic transitions that follow the ionization of atomic shells during the irradiation of  $^{178m2}$ Hf isomeric target by soft x-rays can resonantly be transferred into the nucleus taking simultaneously away some of its quantum momentum and softening greatly the hindrance of corresponding nuclear transition. In such an event one or even a number of additional nuclear transitions not observed in the spontaneous decay of  $^{178m2}$ Hf isomer should be detected and some indications of such new transitions as in the single spectra [8] and as in the coincidence spectra [9 – 12] have already been reported. Unfortunately, all the newly observed transitions have been acquired with rather poor statistics, moreover they are not numerous enough to propose any unambiguous scheme for the triggered decay of  $^{178m2}$ Hf isomer.

<sup>&</sup>lt;sup>1</sup> Institute for Nuclear Research, 03680, Prospect Nauki 47, Kiev, Ukraine

<sup>&</sup>lt;sup>3</sup> Center for Quantum Electronics, University of Texas at Dallas, TX 75083-0688, USA

<sup>&</sup>lt;sup>4</sup> GRAMI, CNRS, Universite d'Orleans, Orleans, France

Another perspective mechanism is Inelastic Electronic Bridge (IEB), the process similar to internal Compton effect, when the electron is shaken up to a discrete state, the vacancy in which can be produced during the irradiation of  $^{178m2}$ Hf sample by soft x-rays, rather than being emitted into the continuum. In this event atomic electrons could take away extra quantum momentum of the nucleus and relax significantly the forbiddenness of corresponding nuclear transition as well. From the experimental point of view, if IEB mechanism is responsible for  $^{178m2}$ Hf triggering, then one can hardly expect any additional nuclear transitions and the only effect that could be registered is the accelerated decay of  $^{178m2}$ Hf isomeric state at certain energies of incident x-rays when necessary electron holes are generated with high efficiency and such the accelerated decay has already been experimentally observed also [11-13].

At the same time, one should not forget that  $\beta$ -processes could be stimulated by x-ray radiation as well. The point is that excitation energy of  $^{178m2}$ Hf is high enough to allow  $\beta$ -decay to  $^{178}$ Ta and EC-decay to  $^{178}$ Lu, though no such decay was ever been detected in the spontaneous decay of  $^{178m2}$ Hf isomer. Recent calculations of weak processes stimulation by synchrotron radiation have clearly shown [14] that the more forbidden a  $\beta$ -decay the more accelerated decay should be observed and, for instant in the case of fourth forbidden  $\beta$ -decay the decay rate can be changed by about two orders of magnitude. The most intriguing is that in the event of x-ray stimulated either  $\beta$ - or EC-decay of  $^{178m2}$ Hf isomer the same 8 level at 1479 keV of  $^{178}$ Hf should be populated, though this level is not populated during the spontaneous decay of  $^{178m2}$ Hf isomer. It means that a new  $\gamma$ -ray line at the energy of 332 keV could be detected and the most interesting is that such  $\gamma$ -ray line has been registered though with not high confidence in the initial  $^{178m2}$ Hf experiments when baseline spectra were recorded just after x-ray irradiation of the isomeric target. Moreover,  $^{178m2}$ Hf triggering can be of the same nature as the triggering of  $^{176}$ Lu [15].

# Experimental investigation of <sup>178m2</sup>Hf isomer triggering by low-energy photons

### X-rays energies above L-edges

In the experiments at SPring8 [11 – 12] the accelerated decay of  $^{178m2}$ Hf has been registered when the isomeric target was irradiated by x-rays with energy about 6.4 eV and 12.8 eV above L<sub>3</sub> edge, respectively. It could mean that  $^{178m2}$ Hf triggering happens while the ionization of L<sub>3</sub> shell goes with the photon energy high enough to ionize resonantly O<sub>4</sub> atomic shell also, the binding energy of which is 6.4 eV, furthermore either once or twice (Hf atom has only two electrons at O<sub>4</sub> atomic shell), respectively. In such occasion the strongly K-forbidden E3 transition, through which the spontaneous decay of  $^{178m2}$ Hf isomeric level proceeds (mostly by L<sub>3</sub> internal conversion), might go through IEB. As a result, L<sub>3</sub> electron fills a hole in O<sub>4</sub> atomic shell taking away some part of quantum momentum and additionally monoenergetic photon with an energy E<sub>7</sub> given by E<sub>7</sub> = E<sub>0</sub> – (B<sub>L3</sub> - Bo<sub>4</sub>), where E<sub>0</sub> is the isomeric transition energy and B<sub>L3</sub> and Bo<sub>4</sub> are the binding energies of the initial and final electronic states, is emitted as well taking away remaining part of quantum momentum. In such event, the total angular momentum and parity hindrance can be relaxed and the isomeric state will decay by E2 or E1 transition instead of E3 one. Anyway, the corresponding nuclear transition would not be so highly hindered and

K-forbidden as in the case of the decay by internal electron conversion and it could explain the observed high efficiency of the triggering.

In fact  $^{178m2}$ Hf triggering has been detected when the isomeric target is irradiated by x-rays above L<sub>1</sub> edge as well [10], however due to very poor statistics now it is impossible to determine precisely the triggering energies. On the other hand,  $^{178m2}$ Hf triggering has obviously been registered when the isomeric target is irradiated by x-rays with the energy about  $11275 \div 11310$  eV and  $11650 \div 11660$  eV and it is just  $5 \div 40$  eV and  $380 \div 390$  eV above L<sub>1</sub> edge, respectively. The first energy interval corresponds to the binding energies of O<sub>1-5</sub> and N<sub>6-7</sub> shells, though what is the most surprising is that the second energy interval corresponds exactly to the binding energy of N<sub>3</sub> shell (B<sub>N3</sub> =380.3 eV) or, taking into account that the triggering energy cannot be determined precisely, even to the sum of binding energies for N<sub>3</sub> and O<sub>4</sub> shells.

#### 20.825 keV x-rays

In 2002 experiments at SPring-8 a new and very significant result has been obtained that seems to resolve the main and especially crucial discrepancies of the initial Hf triggering experiments [16]. On the contrary to the case of incident x-rays energies above L-edges when the acceleration of gamma emission rate is immediate, in the event of more energetic x-rays having energies near 20.825 keV a channel for deexcitation resulting in a cascade of gamma transitions that includes a Hf isomer has been observed. Moreover, taking into account that Hf atomic electron binding energies are 11.2707 keV, 9.5607 keV and 1.7164 keV for  $L_1$ ,  $L_3$  and  $M_4$  shells respectively, it is very exciting and simultaneously surprising that the energy of x-rays at which the effect has been registered is 20.825 keV – just about 6.4 eV and 12.8 eV below the sum of atomic electron binding energies for  $L_1$  +  $L_3$  and  $L_3$  +  $L_3$  +  $M_4$  shells, respectively. Naturally, having the continuous and not well-controlled spectrum of incident x-rays in the initial Hf triggering experiments one could stimulate any of the possible decay channels and with different efficiency and it seems to explain why in several experiments absolutely different results were obtained, though full understanding of such triggering mechanism has not been reached yet.

#### Irradiation Process Control

Simultaneously with the acquiring a huge amount of experimental information on <sup>178m2</sup>Hf isomer triggering, essential efforts have been applied to investigate all the irradiation process and control it as much as possible, on the contrary to the initial experiments when only scattered x-rays were recorded by heavily shielded Ge detectors. First of all, a procedure for the alignment of the active part of the isomeric target with the incident beam of SR x-rays has been developed in detail and it allows knowing very precisely the target position relative to the beam spot center. At the same time, it has been confirmed that there are harmonics in the beam, moreover their content comprised 10% of all incident photons and odd harmonics were "on axis", while even harmonics propagated "off axis".

Secondly, very simple and as it happened to be very effective method of irradiation control has been used as well. The total counting rate for the detection of all  $\gamma$ -rays above

100 keV collected with Ge detector can be considered as a signature of the accelerated  $^{178m2}$ Hf isomer decay induced by incident x-rays. Obviously, such technique should work since in the case of about 10 keV x-rays and properly shielded Ge detector there are no chances for the scattered x-rays to be registered at all and  $\gamma$ -ray spectra above 100 keV would surely be absolutely identical either the beam is on or off.

As a result, the confidence that incidence for the monochromatic x-rays upon the isomeric content of the target caused an enhanced acquisition of  $\gamma$ -rays is 91  $\sigma$  [17], a strong confirmation for the triggering of the decay. Furthermore, the levels of confidence for the positive results being published considerably exceed those for the negative results - only 2.6 sigma being reported for a negative SR experiment at Argonne [18].

This result can happen to be even much more important and explain many discrepancies and problems of the previous experiments on  $^{178m2}$ Hf isomer triggering. The point is that such high level of confidence for the triggering obtained from total counts above 100 keV can surely support an idea that the triggering goes through numerous paths. It may be a reason why at such large effect one cannot detect all the  $\gamma$ -ray transitions with confidence enough to construct the decay schemes of triggered  $^{178m2}$ Hf isomer while they are spread over too many paths. And although such idea should obviously be checked experimentally as well, it sounds quite reasonable.

#### Triggering level at 2457.2 keV

If the mechanism of the direct interaction of a photon and nucleus or NEET is still working, then a previously unobserved level of  $^{178}$ Hf in close proximity of  $^{178m2}$ Hf isomer must exist. Such a level at 2457.2 keV has already been found [17] when the gain of the spectroscopy amplifier was decreased enough to register  $\gamma$ -rays in the range of energies up to 2500 keV, moreover one branch of its subsequent decay has been identified populating the ground state of  $^{178}$ Hf.

At the same time, though the confidence that this is a new line at 2457.20 (22) keV in the spectrum of the induced decay is  $6.5 \, \sigma$ , the proposed level at 2457.2 keV that decays directly to the ground state of <sup>178</sup>Hf can hardly explain how the triggering occurs. Moreover, this level is surely populated by the first harmonic of x –rays and it means that a loss of  $(19.13 - 11.15) = 7.98 \, \text{keV}$  should be explained as well. On the other hand, it looks very intriguing that this level seems to lie at the energy around 11.15 (27) keV above <sup>178m2</sup>Hf isomeric level, while the binding energy for L<sub>1</sub> atomic electron of Hf is 11.2707 keV – too close to the energy gap between these two levels to be accidental.

#### Discussion and conclusions

Since 1998 a great variety of experiments using both a dental x-ray machine and synchrotron radiation sources were performed. As a result, γ-emission from the 31-yr isomer of <sup>178</sup>Hf induced by x-ray irradiation has been observed with very high level of significance. The use of monochromatic SR sources did allow showing that the induced decay of <sup>178m2</sup>Hf isomer can be detected at a number of x-ray energies, moreover at different energies absolutely different paths of <sup>178m2</sup>Hf isomer induced decay can

registered: some of them populate the 4-s isomer of <sup>178</sup>Hf and other ones – bypass the <sup>178ml</sup>Hf isomer.

At the same time, experimental observation of <sup>178m2</sup>Hf isomer triggering when the outer atomic shells are ionized opens a new direction of the isomer triggering research. And although, on the one hand in order to use low energy x-rays one needs to have very thin targets, on the other hand in the case of O<sub>4</sub> atomic shell ionization one could exploit lasers as well, since it should be the energy range of eximer lasers. As a result, much more intense laser irradiation can compensate a need to use the thin targets and allow studying the triggering phenomenon experimentally as well.

Another very interesting observation is that no conductive target has ever triggered and no insulating target has ever failed to trigger. It could mean that half-lives of the holes in the outer atomic shells are of the great importance since in the case of insulators the hole half-lives can be orders of magnitude longer than in the event of conductors. Moreover, according to recent theoretical estimates due to extremely high Debye temperature a target in which the isomer was deposited in a bedding of insulating, diamond-like carbon opens another interesting direction of the isomer triggering research as well.

For all such experiments one needs to have a target with the maximal concentration of  $^{178m^2}$ Hf isomers and it arises with the new force a problem of isotope separation. Moreover, all the available  $^{178m^2}$ Hf isomeric material has been produced decades ago and in not the optimal nuclear reactions so taking into account that there is a need to use picogram quantities of  $^{178m^2}$ Hf isomers one could use the most effective way of production, namely  $^{175}$ Lu  $(\alpha, p)$   $^{178m^2}$ Hf,  $^{176}$ Yb  $(\alpha, 2n)$   $^{178m^2}$ Hf and  $^{181}$ Ta  $(p, \alpha)$   $^{178m^2}$ Hf nuclear reactions with the energy of projectiles up to 100 MeV [19].

As often happens in new directions of research, such measurements are complex and efforts do not always succeed. At the same time, the levels of confidence for the positive results being published considerably exceed those for the negative results. While the main positive results of previous experiments on x-ray stimulated decay of <sup>178m2</sup>Hf isomer continue to be reliably confirmed, any team could replicate such experiments now and perhaps it would expand the research to other long-lived nuclear isomers and nuclides suitable for such purposes as well. At the same time, further theoretical analysis is obviously needed since it could help to plan much more effectively all future experiments saving time, efforts and money.

#### References

- [1] C. B. Collins, F. Davanloo, R. Dussart, M. C. Iosif et al., *Phys. Rev. Lett.*, 1999, **82**, 695.
- [2] C. B. Collins, F. Davanloo, R. Dussart, M. C. Iosif et al., Laser Phys., 1999, 8, 9.
- [3] Silviu Olariu and Agata Olariu, Phys. Rev. Lett., 2000, 84, 2541.
- [4] D. P. McNabb, J. D. Anderson, J. A. Becker and M. S. Weiss, *Phys. Rev. Lett.*, 2000, **84**, 2542.
- [5] P. von Neumann-Cosel and A. Richter, Phys. Rev. Lett., 2000, 84, 2543.
- [6] C. B. Collins, F. Davanloo, M. C. Iosif, R. Dussart et al., *Phys. Rev. Lett.*, 2000, 84, 2544.
- [7] C. B. Collins, F. Davanloo, M. C. Iosif et al., *Physics of Atomic Nuclei*, 2000, **63**, 2067.
- [8] C. B. Collins, F. Davanloo, A. C. Rusu, M. C. Iosif et al., *Phys. Rev. C*, 2000, **61**, 054305.
- [9] C. B. Collins, A. C. Rusu, N. C. Zoita et al., Hyp. Interact., 2001, 135, 51.
- [10] C. B. Collins, N. C. Zoita, A. C. Rusu et al., Europhys. Lett., 2002, 57, 677.
- [11] C. B. Collins, N. C. Zoita, F. Davanloo et al., Laser Phys., 2004, 14, 1.
- [12] C. B. Collins, N. C. Zoita, F. Davanloo et al., Rad. Phys. And Chem., 2004, 71, 619.
- [13] V. I. Kirischuk, N. V. Strilchuk and V. A. Zheltonozhsky. *The Proceedings of the II International Conference "Frontiers of Nonlinear Physics"*, Nizhni Novgorod, Russia, 2004, 119.
- [14] I. V. Kopytin and K. N. Karelin. The Proceedings of the LV International Conference "Frontiers in the Physics of Nucleus", S. Petersburg, Russia, 2005, 295.
- [15] V. I. Kirischuk, V. P. Khomenkov, N. V. Strilchuk et al., Laser Phys. 2004, 14, 1169.
- [16] N. C. Zoita, F. Davanloo, C. B. Collins et al., *Proc. Int. Conf.* "7ème colloque sur les SOURCES COHERENTES ET INCOHERENTES UV, VUV ET X APPLICATIONS ET DEVELOPPEMENTS RECENTS" (St. Etienne, France, 7-11 June 2004), *J. Phys. IV France*, 2005, **127**, 163.C. B. Collins, N. C. Zoita, F. Davanloo et al, *Laser Phys. Lett.* 2005, **2**, 162.
- [18] I. Ahmad, J. C. Banar, J. A. Becker et al, Phys. Rev. C 2005, 71, 024311.
- [19] V. I. Kirischuk, V. A. Ageev, V. P. Khomenkov et al, Laser Phys. 2004, 14, 1173.

# EXCITATION OF <sup>113M</sup>IN, <sup>195M</sup>PT AND <sup>199M</sup>HG ISOMERS IN THE REACTIONS OF INELASTIC GAMMA SCATTERING

Z. M. BIGAN<sup>2</sup>, V. I. KIRISCHUK<sup>1</sup>, V. M. MAZUR<sup>2</sup>, D. M. SIMOCHKO<sup>2</sup>, P. N. TRIFONOV<sup>1</sup> AND V.A. ZHELTONOZHSKY<sup>1</sup>

> Institute for Nuclear Research, National Academy of Sciences, Kiev, Ukraine
>  Institute of Electron Physics, National Academy of Sciences, Uzhgorod, Ukraine

#### Abstract

The yields curves and reaction cross-sections were measured for reactions  $^{113} \text{In}$  ( $\gamma, \gamma'$ )  $^{113m} \text{In}$  ( $T_{1/2} = 1.7 \text{ h}$ ,  $J^{\pi} = 1/2^{-}$ ),  $T_{1/2} = 1.7 \text{ h}$ ,  $T_{1/2} = 1.7 \text{ h}$ ,

#### Introduction

The photon scattering by atomic nuclei is the universal process that occurs in all nuclei and at any energy. In all cases the process of inelastic gamma-ray scattering associates with the radiative transitions. These transitions de-excite a nucleus and may be separated into several groups. First, there are CC'-transitions between highly excited compound states which lie in the continuous spectrum (C' – initial state, C – final state). Secondly, there are transitions between highly excited C-states and low-lying S-states (CS-transitions). And thirdly, there are SS'-transitions between the ordinary low-lying states (S' – initial state, S – final state). Metastable (isomeric) states are excited by gamma-transitions of all three types.

The investigation of isomer excitation in  $(\gamma, \gamma')$  reactions is relevant due to works on the stimulated decay of isomeric states [1-3]. Now there is no theoretical explanation for significant acceleration of <sup>178m</sup>Hf decay during its  $\gamma$ - or electron irradiation. The understanding of isomer production mechanism during  $\gamma$ -ray irradiation is very important for the astrophysical purposes as well.

Bearing in mind all the stated above, we have carried out the study of <sup>113m</sup>In, <sup>195m</sup>Pt and <sup>199m</sup>Hg isomer excitation. The choice of Pt and Hg nuclei is topical for the understanding of isomer excitation mechanism, since significant increase of the isomer excitation probability is observed in this atomic mass region. The data on <sup>113m</sup>In are very limited, so it is important that during the irradiation of natural indium target <sup>115m</sup>In isomer is excited as well. Since <sup>115m</sup>In has been well investigated in many works, it may be used as a sort of the calibration sample.

This paper is dedicated to the investigation of cross-sections for the production of isomeric states in <sup>113</sup>In, <sup>195</sup>Pt and <sup>199</sup>Hg nuclei during the inelastic gamma-ray scattering in 4 - 12 MeV energy range. And though the isomeric states excitation in  $(\gamma, \gamma')^m$ -reactions was studied rather extensively [1], the corresponding cross sections for mentioned above nuclei at the threshold of  $(\gamma, n)$ -reactions have not been investigated sufficiently yet.

The isomeric states photo-excitation in all investigated nuclei was studied earlier during the photoactivation analysis for samples of different composition [2]. The  $(\gamma, \gamma')^m$ -cross sections for <sup>113</sup>In, <sup>195</sup>Pt and <sup>199</sup>Hg were studied at 1 - 3 MeV energies using as the isotopic sources [3], as the bremsstrahlung radiation [4].

#### Measurement technique and results

These investigations were carried out at the bremsstrahlung beam of M-30 microtron in the Institute of Electron Physics.  $^{113}\text{In}(\gamma,\gamma')^{113m}\text{In}, ^{195}\text{Pt}(\gamma,\gamma')^{195m}\text{Pt}$  in  $^{199}\text{Hg}(\gamma,\gamma')^{199m}\text{Hg}$  reaction yields were measured with a step of  $\Delta E=0.5$  MeV.  $^{113m}\text{In}, ^{195m}\text{Pt}$  and  $^{199m}\text{Hg}$  isomer production was defined using 391.7 keV; 98.8 keV, 129.7 keV and 158 keV, 374 keV gamma-line intensities, correspondingly.

The spins and parities of isomeric  $J_m^{\pi}$  and ground  $J_g^{\pi}$  levels, their differences  $\Delta J = J_m - \Delta J_g$ , half-lives  $T_{1/2}$  of the isomeric states, energies  $E_{\gamma}$  of the detected gammalines and their intensities taken from [5, 6] are shown in Table 1.

Table 1. Spectroscopic properties of the investigated isomers.

Isotope	$J_m^\pi$	$J_{\mathrm{g}}^{\pi}$	ΔJ	T <sub>1/2</sub>	Eγ, keV	I, %
<sup>113</sup> In	1/2	9/2 <sup>+</sup>	4	99.4 m	391	64.2
<sup>195</sup> Pt	13/2+	1/2	6	4.02 d	98.8; 129	11.0; 2.7
<sup>99</sup> Hg	13/2+	1/2-	6	42.6 m	158; 374	52; 14

The induced activity measurements were carried out using the spectrometer with Ge(Li)-detector of 100 cm<sup>3</sup> volume. The fragment of indium target gamma-spectrum is given at Fig. 1. The targets of natural isotopic composition were irradiated at the maximum energy  $E_{\gamma max} = 12$  MeV of the bremsstrahlung spectrum. The cross sections of  $^{113}$ In( $\gamma$ ,  $\gamma'$ ) $^{113m}$ In,  $^{195}$ Pt( $\gamma$ ,  $\gamma'$ ) $^{195m}$ Pt and  $^{199}$ Hg( $\gamma$ ,  $\gamma'$ ) $^{199m}$ Hg reactions are shown at Fig. 2.

All the obtained cross sections in 4-12 MeV range have one-hump nature with a maximum at  $(\gamma, n)$ -reaction threshold. For <sup>195</sup>Pt  $(\gamma, \gamma')^m$ -cross section maximum is found at 6.1 MeV, for <sup>199</sup>Hg - at 6.5 MeV and for <sup>113</sup>In - at 9.2 MeV, while  $(\gamma, n)$ -thresholds for these nuclei are 6.12 MeV, 6.50 MeV and 9.2 MeV, respectively. As one can see, within experimental uncertainties these values are practically the same.

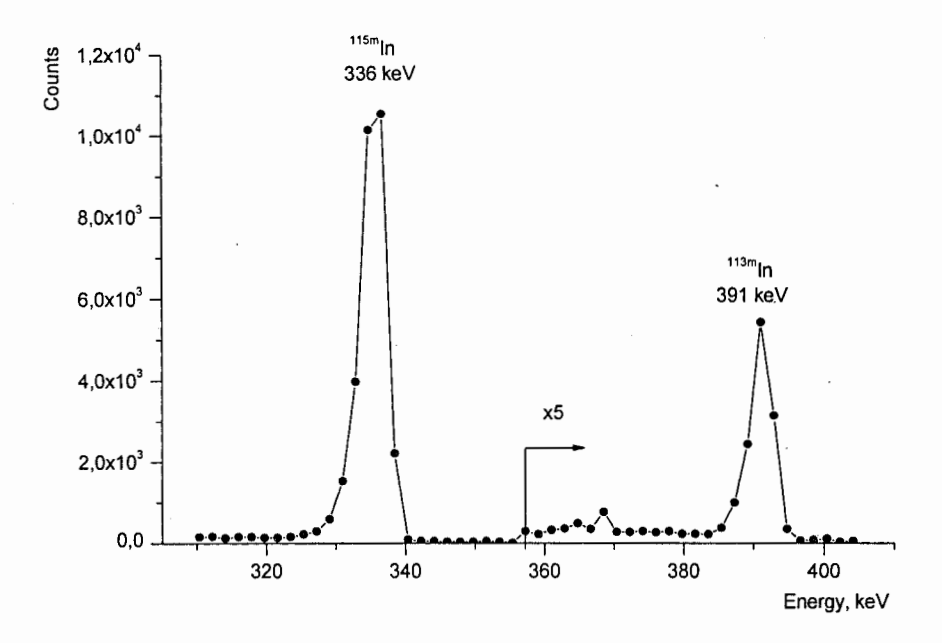


Fig. 1. The fragment of natural indium target gamma-spectrum.

The obtained cross sections allow us to find, using the total photoabsorption cross section  $\sigma_{tot}$ , the experimental isomeric ratios  $r = \sigma_m / \sigma_{tot}$ . The experimental isomeric ratios r were calculated at  $(\gamma, \gamma')^m$ -reaction maximum, where the relative mean-square errors are minimal and reach  $\sim 15\%$  for the obtained isomer ratios.

Lorentzian values, which approximate  $\sigma_{tot}$ , were taken as the total photoabsorption cross sections at and below  $(\gamma, n)$ -reaction thresholds. To determine the r value for <sup>113</sup>In,  $\sigma_{tot}$  parameters obtained for <sup>115</sup>In [8] were taken since  $\sigma_{tot}$  for <sup>113</sup>In was not measured at all, on the other hand due to the proximity of masses for these nuclei the giant dipole resonance parameters should be quite similar.  $\sigma_{tot}$  value for <sup>199</sup>Hg was taken from [9].

As a result, the following isomeric ratio values were obtained: for  $^{113}$ In at E = 7.0 MeV r = 0.057, at E = 8.0 MeV r = 0.069 and at E = 9.0 MeV r = 0.065; for  $^{195}$ Pt r = 0.014 at E = 5.5 MeV and r = 0.018 at E = 6.0 MeV; for  $^{199}$ Hg r = 0.0146 at E = 6.0 MeV and r = 0.013 at E = 6.5 MeV.

To estimate r value theoretically the isomeric ratios for investigated reactions in 5.5-9 MeV range were calculated. The calculation was carried out for the Fermigas model [10]. In the calculations it was supposed that dipole gamma quantum is absorbed by a nucleus and forms the compound nucleus, then it de-excites by E1 gamma-transition cascade and last of these transitions populates the isomeric or ground state. Bethe-Bloch formula was used for the description of nuclear level density and spin J distribution [11]:

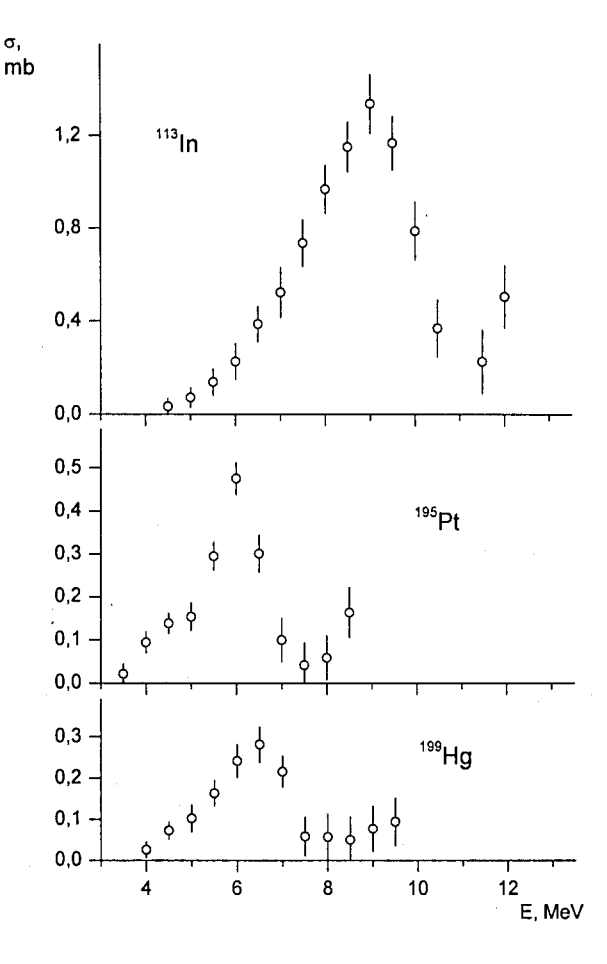


Fig. 2. Cross sections of  $(\gamma, \gamma')$ -reactions for the investigated nuclei.

$$\rho(U,J) = \frac{2J+1}{24\sqrt{2}a^{\frac{1}{4}}U^{\frac{5}{4}}\sigma^{3}} \exp\left\{2\sqrt{aU} - \frac{(J+\frac{1}{2})^{2}}{2\sigma^{2}}\right\}$$

where  $\sigma$ - spin limiting parameter, which may be written down as [12]:

$$\sigma^2 = 0.0899 \sqrt{aU} \cdot A^{\frac{1}{3}}$$

where A – mass number, a – level density parameter, U – excitation energy that should be understood as the effective energy [12]. The calculation procedure is described in more detail in [13].

The calculations were carried out as without free parameters as by fixing the spin limiting parameter  $\sigma$ . The agreement between calculated isomeric ratios and experimental data can be reached for <sup>195</sup>Pt and <sup>199</sup>Hg at  $\sigma = 2.5$ -3.0, while for <sup>113</sup>In - at  $\sigma = 4.5$ . Such  $\sigma$  values agree within uncertainties with  $\sigma = f(A)$  dependence given in [14].

In conclusion, it should be noted that the isomeric states population in inelastic scattering processes looks quite simple. If all the levels are equivalent, then the statistical mechanism should work and sequential calculations should agree with the experimental results.

However, in 0 - 2 MeV energy region the excited states are discrete and their structure may be essentially different even for the neighboring nuclei. Thus, in general the statistical approach is not applicable and we are formally compelled to extend it to this region. Furthermore, for the nuclei at  $(\gamma, n)$ -reaction threshold other mechanisms, such as direct or semidirect population of the isomeric states, can make significant contribution as well.

#### References

- 1. Yu. P. Gangrsky, V. M. Mazur, Phys. of El. Part. and Atom. Nucl. 33 158 (2002) [in Russian].
- 2. Ph. Breban, G. Blondiaux, M. Valladon, Nucl. Instr. and Meth. 158, 205 (1979).
- 3. A. Veres, I. Pavlicsek, M. Csürös, L. Lakosi, Acta Phys. Hung. 34, 97 (1973).
- 4. E. C. Booth, J. Brownsow, Nucl. Phys. A98, 529 (1967).
- 5. N. G. Gusev, P. P. Dmitriev, *Quantum radiation of radioactive nuclides*, (Atomizdat, Moscow, 1977) [in Russian].
- 6. R. B. Firestone et al., *Table of Isotopes* (CD edition, Version 1.0, JWiley Interscience, March, 1996)
- 7. A.V. Varlamov et al., *Atlas of Giant Dipole Resonances*, (IAEA Nuclear Data Section, Austria, Vienna, 1999).
- 8. A. Lepretre et al., Nucl Phys. A219, 39 (1974).
- 9. A. Veyssière, H. Beil, R. Bergère, J. Phys. 36, 267 (1975).
- 10. L. Ya. Arifov, B. S. Mazitov, V. G. Ulanov, j. Nucl. Phys. 34, 1028 (1981) [in Russian].
- 11. A. V. Malyshev, Levels density and atomic nuclei structure, (Atomizdat, Moscow, 1969) [in Russian].
- 12. V. M. Stavinsky, Phys. of El. Part. and Atom. Nucl. 3, 839 (1972) [in Russian].
- 13. Z. M. Bigan, M. V.. Goshovsky, V. M. Mazur, Z. Z. Torich, Preprint No. 85-15, KIYaI (Kiev Institute for Nuclear Research, Kiev, 1985) [in Russian].
- 14. N.S. Biryukov et al., J. Nucl. Phys. 30, 26 (1979) [in Russian].

# ON THE POSSIBILITY OF TRANSMUTATION WITH THE LOW-ENERGY ELECTRON BEAMS

#### DMITRI KAMANIN<sup>†</sup>

Flerov Laboratory for Nuclear Reactions, JINR Dubna, 141980, Russia

#### **ANDREJ MATTHIES**

Hans Wälischmiller GmbH, Dresden, D-01328, Germany

The use of the bremsstrahlung gamma-rays produced by low energy electron beams of about 30 MeV can provide effective transmutation due to a specific shape of the photonuclear cross-section around the giant resonance. Such a method of transmutation could be alternative to the accelerator driven systems utilizing high energy protons.

The general understanding of the nuclear waste "transmutation" of RIAR and IPPE, the ones of leaders in the reactor technologies in Russia, consist in separation and collecting the of fuel burning products, first of all of Np, Am, I, Tc in development of the reactor conceptions of incineration of the fission products (FP) and minor actinides (MA). In spite of our obvious success in application of fast reactors [1, 2], the desired way of the waste disposal could be essentially improved by introducing the Electron Driven Afterburner (EDA), the initiative project of the FLNR JINR. The idea to drive fission by bremsstrahlung had become obvious since giant dipole resonance has been found. Also the application of  $(\gamma,xn)$  reactions for transmutation of FP is not new, however, on the contrary to some other projects [3] we propose to use low energy electron beams (LEEB) around the energy of 30 MeV.

Although it is difficult to imagine all the details of the construction nowadays, but some general features of EDA can be proposed. A LEEB itself advantages in high stability, in easy handling meaning also a simplified beam transport, in compactness of the burning module, in absence of the radiotoxic products of the beam-target interaction as well as in low activation of the constructional materials. The target technologies for LEEB are already enough developed [4]. The further attractive properties of EDA are given in a favor of the comparison with that of the ADS projects based on high-energy proton beams [5]. Due to the application of the electron accelerators one can assume a multi-modular structure of the afterburner providing such properties as a high serviceability, an optimized maintenance expenses, and, perhaps, a portability of the entire system.

<sup>†</sup> Corresponding author. Email: kamanin@fobos.jinr.ru

Another anticipated feature of EDA at the electron energy around 30 MeV consist in the low beam power consumption per transmuted nucleus. In particular, our simple estimates for the neutron production calculated for 1 kW of the beam power are given in the table 1 below.

Table 1 Estimated neutron flux

Project	Beam	Neutron flux		
IBR-30	e 40 MeV	2*10 <sup>14</sup>		
ADS	p 1 GeV	$1.8*10^{14}$		
IREN	e 200 MeV	10 <sup>14</sup>		

Even in the given table the neutron flux per 1 kW of the beam power for 40 MeV is higher than that for ADS. Taking also into account that the result for ADS is calculated for infinite target, on the contrary the range of gamma-quanta is very short; this comparison will be even more obvious in the favor of EDA.

Main minor actinides are characterized by the so-called threshold fission cross-section. Therefore their transmutation can be reached using only a small part of neutrons available in the power reactors. The use of the bremsstrahlung produced by LEEB can provide much more effective transmutation due to a specific shape of the photonuclear cross-section around the giant resonance. Summarizing, EDA could be alternative to the ADS utilizing high energy protons.

We have calculated the MA-transmutation efficiency of EDA by means of the well known MCNP Monte-Carlo code using the cross-sections  $(\gamma,F) = (\gamma,f) + (\gamma,nf)$  and  $(\gamma,n)$  from the EXFOR (Berman) library for the electron energies of 20 and 30 MeV [6]. We took <sup>237</sup>Np as the MA representative due to the lack of photonuclear data for other MA (Figure 1). On the other hand, the results for Cm and Am should be similar to <sup>237</sup>Np, because their photofission cross-sections near giant resonance which contribution is dominating should not drastically vary from that for <sup>237</sup>Np. In our calculations the 2 mm thick tungsten target served as the converter, because it is optimal value for the production of the photons.

We have calculated the direct fission rate in an idealized 10% water solution of <sup>237</sup>Np placed into the sphere of 30 cm in the diameter. The total rate per 10<sup>6</sup> incident electrons amounted to 308 nuclei at 20 MeV. Increasing the electron energy by 50% leads to doubling the transmutation rate due to the shape of the bremsstrahlung spectrum given in the Figure 2.

The transmutation rate due to the direct reactions at 30 MeV found for the metallic neptunium amounts to 15 kg per year counted for 1 GW of the beam power. However, photofission alone provides only 30 % of the burning rate due to a high flux of the secondary prompt neutrons from fission in the transmutation area. The total fission rate inside the cylinder reaches more than 0.016 per 1 incident electron. This intensity is enough to burn more than 40 kg of  $^{237}$ Np per GW per year. Taking into consideration such processes like  $(\gamma,n)$  and (n,2n) delivering short-lived  $^{236}$ Pu, the total efficiency of Np-transmutation turn to be even larger than 50 kg/GW/year. This value

is already comparable with that amounting to 70-140 kg for the thermal and fast power reactors. Our conclusions are in the good agreement with the independent calculations implemented for the metallic <sup>238</sup>U [7].

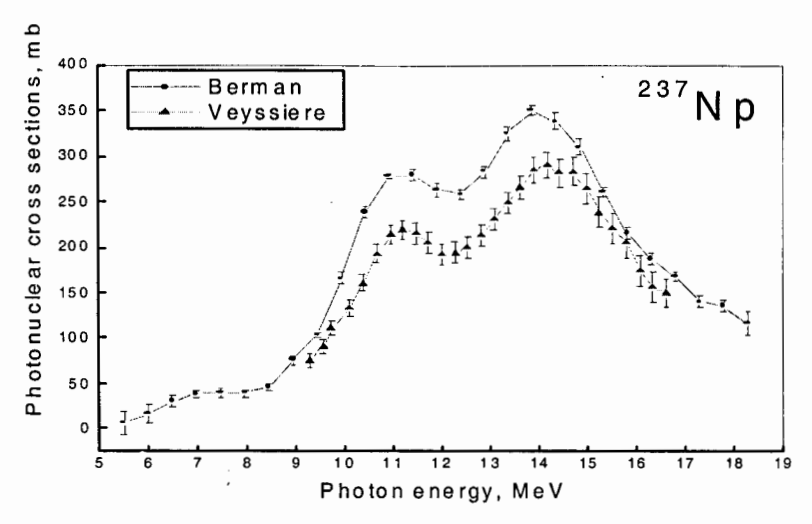


Figure 1. While the individual photonuclear data are measured with the acceptable quality level they vary from each other significantly.

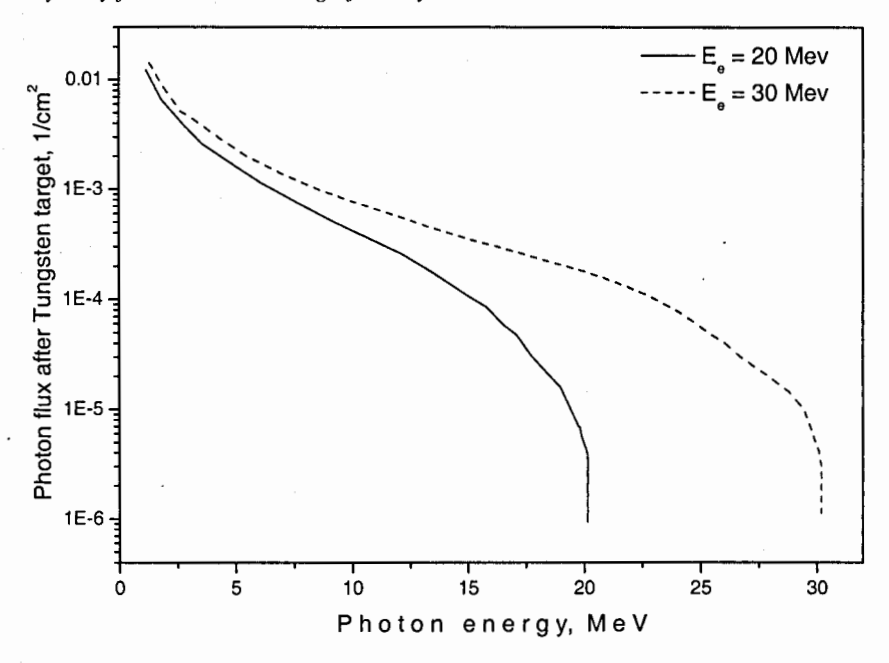


Figure 2. The shape of the bremsstrahlung spectra per one incident electron.

Compared to <sup>237</sup>Np, which can serve as a fuel component, the feasibility study of transmutation of FP in EDA is even more desirable since any significant amount of FP could not be loaded into BR. As an example two radioactive isotopes which should be

transmuted into less hazardous forms are <sup>99</sup>Tc and <sup>129</sup>I. Both of these isotopes are very long-lived and require disposal strategies that will isolate them from the environment for long periods of time. Both iodine and technetium are considered difficult to isolate because they dissolve readily in groundwater and move easily throughout the ecosystem.

The reactions like those given below lead to production of stable isotopes with the reasonable cross-sections.

 $\begin{array}{c} 129I~(\gamma,n)~128I~(T_{1/2}\text{=}25~\text{min}) \to 128\text{Xe (stable)} \\ 129I~(\gamma,2n)~127I~(\text{stable}) \\ 90\text{Sr}(\gamma,n)~89\text{Sr}~(T_{1/2}\text{=}50~\text{d}) \to 89\text{Y (stable)} \\ 90\text{Sr}(\gamma,2n)~88\text{Sr (stable)} \end{array}$ 

The calculated cross-sections of  $^{129}\text{I}$  ( $\gamma$ ,xn) in dependence of the photon energy are given in the Figure 3. For the reactions of interest with emission of one or two neutrons the most effective photon energy window is 12-22 MeV. Such the energy of bremsstrahlung quanta can be provided most effectively by the incident electrons of the energy of 30-40 MeV. The increase of the electron energy will increase number of photons in the given energy window, but the non-effective beam power consumption will also raise simultaneously.

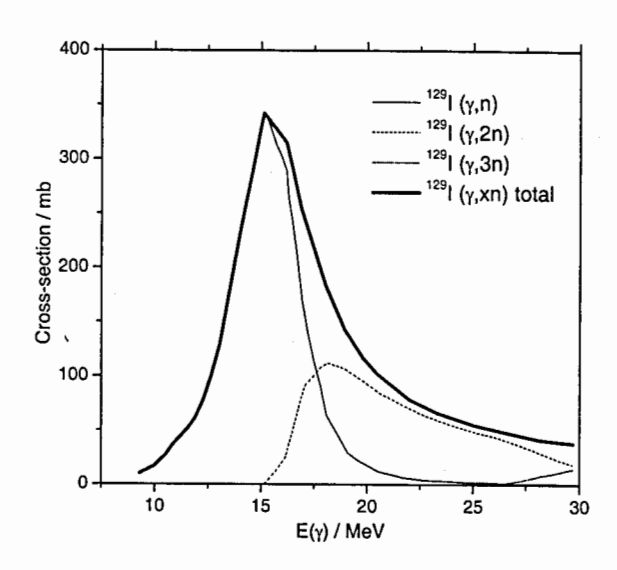


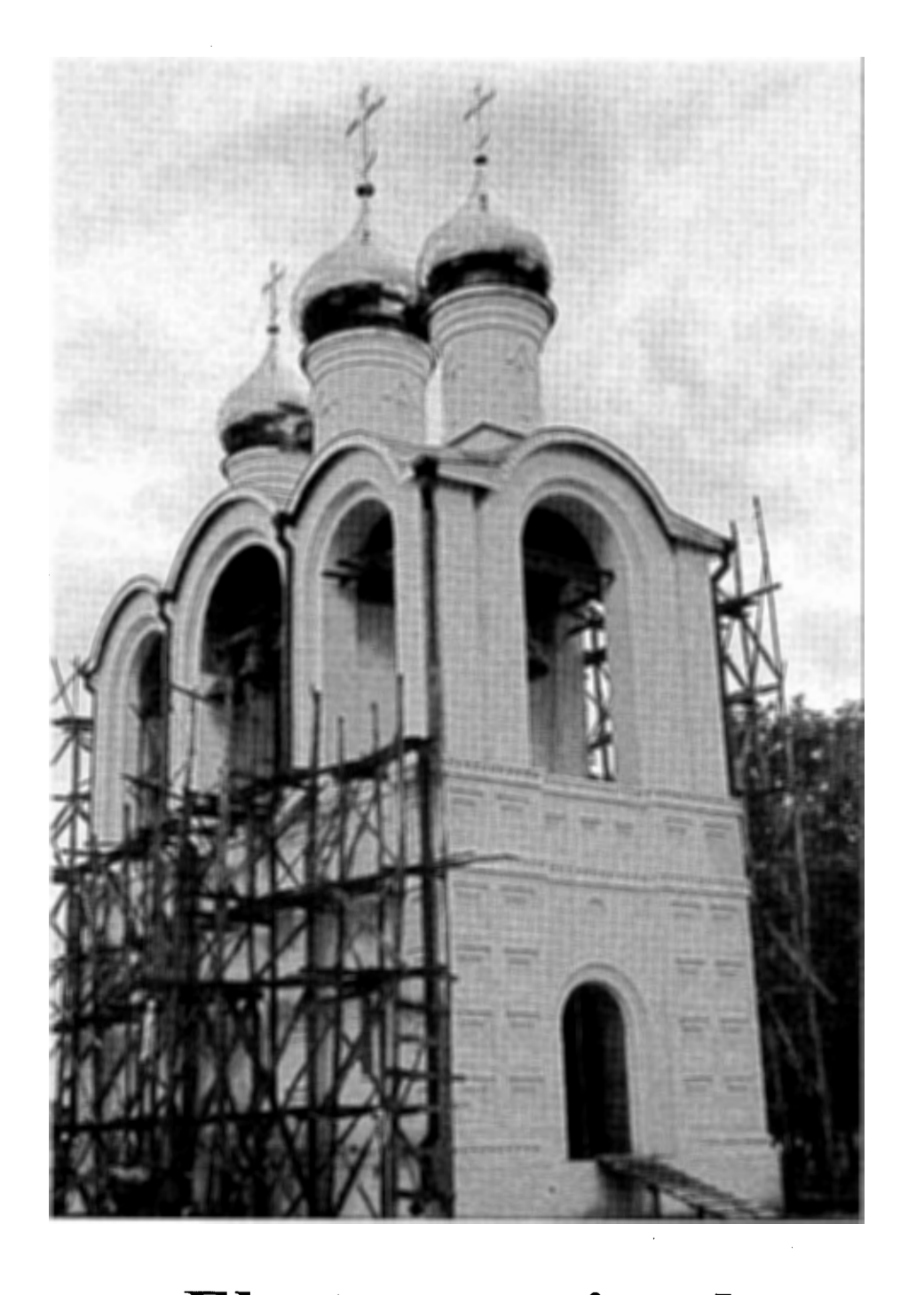
Figure 3. The calculated cross-sections of  $^{129}I(\gamma,xn)$  in dependence of the photon energy.

The simple arguments presented above demonstrate the real possibility and efficiency of the low-energy electron accelerators in resolving the problem of a nuclear waste. Taking into account their briefly listed advantages and commercial availability of the high-power low energy electron-accelerators one could assume also comparatively low costs and short implementation times of the probe EDA device. Nowadays the main difficulty of the EDA project consist in the lack of photo-nuclear

data. This obstacle, however, can be overcame incomparably faster and cheaper than the development of the missing technologies for the high-energy ADS.

#### References

- 1. Bychkov A.V., Vavilov S.K. et al. Pyroelectrochemical reprocessing of irradiated FBR MOX fuel. III. Test on high burn-up BOR-60 fuel. / Paper on GLOBAL-97 Conferences, 5-10 Okt., Yokohama, Japan.
- 2. Mayorhsin A.A., Kisly V.A., Shishalov O.V. et al. Calculative-experimental validation of minor actinides transmutation in the BOR-60 reactor. Experience on vibropac UNpO2 fuel irradiation./ GLOBAL 2001 International Conference "Back-end of the fuel cycle: from research to solutions" Paris, France, 9-13 Sept. 2001
- 3. http://nfdfn.jinr.ru/flnph/iren/iren.html and refs. therein
- 4. Skiba O.V. et al. Experience of development and operation of Semi-Industrial Complex for BN-600/800 reactor FAs. In Russian. Int. Conference "Nuclear Energy and Fuel Cycles", Moscow-Dimitrovgrad, Russia, 1-5 Dec. 2003
- 5. W.Gudowski. Accelerator-driven Transmutation Projects. The Importance of Nuclear Physics Research for Waste Transmutation. *Nucl. Phys.* **A654**, 436c (1999); S.Matsuura. Future Perspective of Nuclear Energy in Japan and the OMEGA Program, *Nucl. Phys.* **A654**, 417c (1999).
- 6. D.V. Kamanin, A. Matthies, A.A. Goverdovski, A.D. Rogov "Transmutation of minor actinides at high-current low-energy electron accelerators" Heavy Ion Physics, *FLNR JINR Scientific Report* 2001-2002, 308 Dubna 2003.
- 7. S.G. Yavshits et al., Experimental Investigations of Electron-Accelerator-Driven Transmutation Technology in KRI: Results and Perspectives. Report at the Int. Sci. Seminar "Low and Intermediate Energy Electron Beams" March 5-6, 2003, Dubna, FLNR JINR, Russia.



Electron-assisted nuclear transitions

# ROLE OF AUTOIONIZATION STATES IN NUCLEAR EXCITATION BY AN ELECTRON TRANSITION

#### I.N.IZOSIMOV

Khlopin Radium Institute, 2<sup>nd</sup> Murinski avn. 28 St. Petersburg, 194021, Russia

e-mail: izosimov@atom.nw.ru

In this report the nuclear excitation by an electron transition (NEET) is considered for resonance excitation of electrons to the autoionozation (AS) states which have energies higher than ionization potential (IP). For AS the excitation energy concentrate on two or more electrons and at the decay of AS states simultaneously one electron escape from atom (ionization) and other one go to the ground state (photon emission or NEET). Emission of e may compensate the difference in the energy and multipolarity for NEET. Specific quantum characteristics of the AS open new possibilities for different kinds of nuclear isomers excitation and triggering driven by AS and NEET effect. Possible experiments are discussed.

#### 1. Autoionization states

It is very attractive to use nuclear excitation by an electron transition [1-3] (NEET) because of high cross section for electron shells excitation in different processes. The process consists in that the electron shell excitation energy is transferred to the nucleus without photon radiation. But for effective NEET scheme realization it is necessary compensate the differences in the multipolarity and energy between electron shell and nuclear transition. One of the possible mechanism of such compensation using NEET via autoionization states is suggested in the present paper.

Autoionization states (AS) are unstable related to ionization of atomic state (escape of electron) with two or more excited electrons [4,5]. AS are the quasi stationary states and were observed as a resonances. For external electron shells excitation AS are well known and were observed practically for all elements up to Pu [6,7]. Multistep laser excitation schemes [4] may be very effective for AS excitation with the energies up to 15 eV. For internal electron shells excitation AS may have energies up to 10-100 keV and electron or ion impact may be used for such AS excitation. AS for internal electron shells excitation practically were not studied. Because of electron-electron interaction at the AS decay simultaneously one electron escape from atom (ionization) and the other one go to the ground state by photon emission (electron shell transition). At a suitable conditions instead of photon emission the nuclear excitation by an electron transition (NEET) may take place. For NEET via AS decay the excitation energy is distributed between emitted electron and NEET (similar as energy is distributed between electron and antineutrino in  $\beta$  decay).

Emission of e may compensate the difference in the energy and multipolarity for NEET and it is not necessary to have the precise coincidence between energy and multipolarity of electron shell transition and nuclear transition.

For example let us consider the AS of two electrons atoms or ions connected with configurations nlnl' and n=2. The energy of such states  $(E_{AS,n=2}\approx -Z^2/4)$  is higher than the energy of single charged ion  $(E\approx -Z^2/2)$  and nlnl' states with n=2 are the unstable AS states. Due to electron-electron interaction AS may decay (Figure 1) with simultaneously escape of one electron from atom and other electron transition to the 1s state.

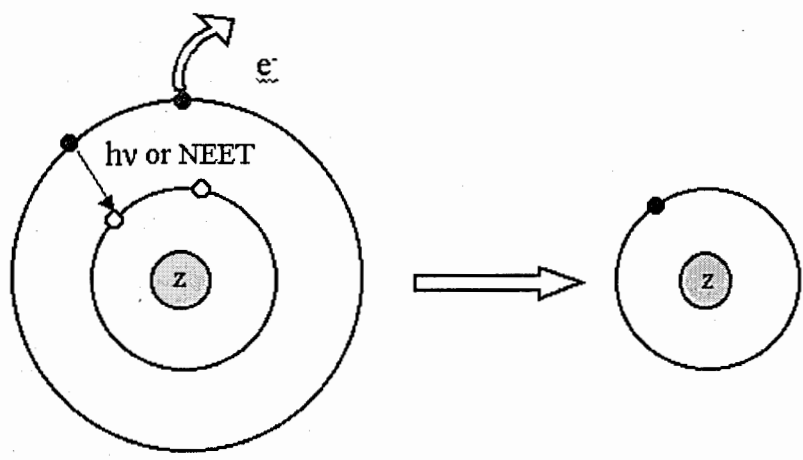


Figure 1. Scheme of autoionization states (AS) structure and decay. Simultaneously one electron escape from atom (ionization) and the other one go to the ground state by photon emission or by transfer the energy to the nucleus without radiation (NEET). Emission of e may compensate the difference in the energy and multipolarity for NEET.

For electron configuration  $2s^2$  we will have  $^1S^+$  autoionization state, for 2s2p configuration –  $^{1,3}P^-$  AS states and for  $2p^2$  –  $^1S^+$ ,  $^1D^+$ ,  $^3P^+$  AS states. Electron-electron interaction mixed  $^1S^+$  states from  $2s^2$  and  $2p^2$  configurations and one of  $^1S^+$  (with more weight of  $2s^2$  configuration) AS will have the lowest energy and other  $^1S^+$  ( with more weight of  $2p^2$  configuration) AS will have the highest energy.

The decay width  $\Gamma$  is different for different AS and weekly depend on Z. For lowest  $^1S^+$  AS state  $^1D^+$  and  $^1P^-$  AS states  $\Gamma{\approx}0.2\text{eV}$ . For highest  $^1S^+$  and  $^3P^-$  AS states  $\Gamma{\approx}(0.02{\text -}0.005)\text{eV}$ . Decay of  $^3P^+$  AS states to 1s state is forbidden as E1 and its decay width may be much smaller compare to other AS. So the width and half-life for AS may change in wide range and  $\Gamma{\leq}0.2\text{eV}$ ,  $T_{1/2}{\geq}10^{-14}\text{s}$ .

## 2. NEET via AS in eV region (229mTh 3.5eV isomer excitation)

Scheme of the autoionization states excitation using laser radiation is presented in the Figure 2. Ionization potential (IP) for Th is 6.08eV. Using three step excitation

scheme ( $hv_1+hv_2+hv_3 \le 12eV$ ) it is possible to study NEET via AS for nuclear isomers with excitation energy  $E \le 6eV$ .

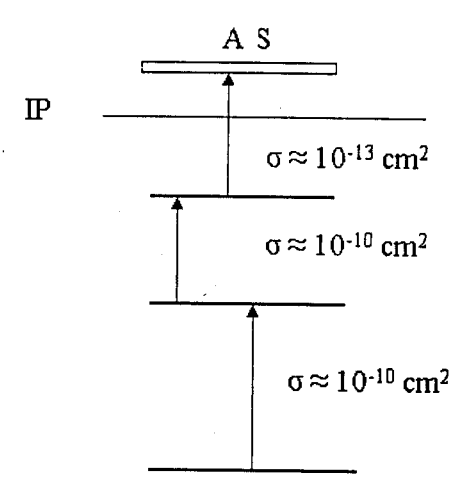


Figure 2. Three steps scheme of autoionization states (AS) excitation in atom using laser radiation. Efficiency of AS excitation in atoms during three synchronized lasers pulses  $\geq 10\%$ .

<sup>229</sup>Th is believed have a nuclear ground state corresponding to the  $5/2^+$ [633] rotational band head [8] and a low-lying (3.5±1 eV) isomer [9] corresponding to the  $3/2^+$ [631] rotational band head. <sup>229m</sup>Th 3.5eV isomer is indicated in the decay schemes of <sup>233</sup>U, <sup>229</sup>Pa and <sup>229</sup>Ac [10]. Decay scheme of <sup>229</sup>Pa and <sup>229m</sup>Th energy [10] are shown in Figure 3.

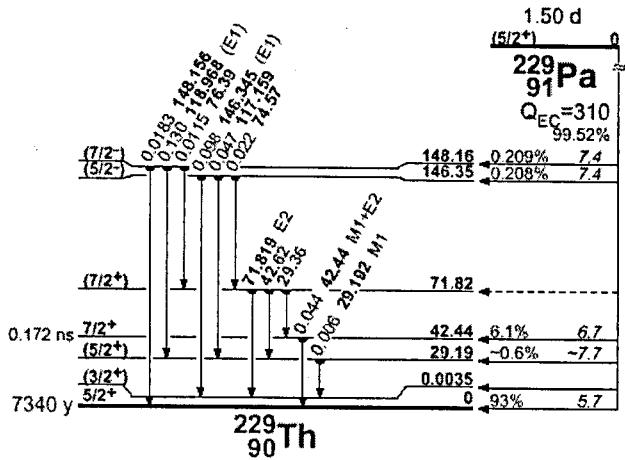


Figure 3. <sup>229</sup>Pa decay scheme [10] and <sup>229m</sup>Th energy.

<sup>229m</sup>Th can decay by direct M1 photon emission (nuclear light) to the ground state or by alpha decay to <sup>225</sup>Ra. It is hard to predict quantitatively  $T_{1/2}$  and partial widths for isomer decay. Alpha decay measurements indicate that if the isomer exist, its half-life must be  $T_{1/2} \le 6h$  or  $T_{1/2} \ge 20d$  [11]. Theoretical estimations for M1 photon emission depends on nucleus-electron interaction and isomeric state energy. Results are:  $T_{1/2} \approx 3s$ -9min [12] and  $T_{1/2} \approx 20$ -200 hours [9]. Up to now, there is no direct evidence for the identification of <sup>229m</sup>Th.

via AS. For AS excitation three step laser scheme plan to be used (Figure 2). We plan to find optimal scheme for NEET isomer excitation via AS. Isomer will be excited only at definite laser radiation wavelengths and its decay may be detected with high selectivity. Only when three lasers radiation wavelengths are in resonance with <sup>229</sup>Th atomic transition one may observed signal from <sup>229m</sup>Th decay with proper half-life.

For NEET via AS the energy of emitted electron  $(E_e^*)$ , AS excitation energy  $(E_{AS})$ , ionization potential (IP), electron energy  $(E_e)$  when instead NEET photon with energy  $E_{hv}$  is emitted and isomer excitation energy  $(E_{NEET})$  are connected as:

$$E_{AS} - IP - E_e^* \approx E_{NEET},$$
 (1)

$$E_{hv} + (E_e - E_e^*) \approx E_{NEET}. \tag{2}$$

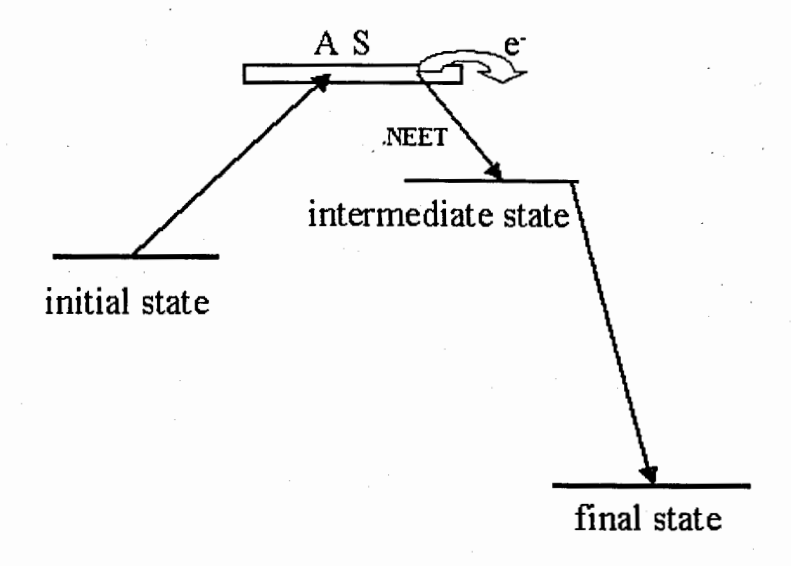
Due to electron emission for NEET the differences between  $E_{h\nu}$  and  $E_{NEET}$  may be compensated. Also electron emission may compensate the differences in multipolarity between electron shell transition and nuclear transition. For M1 nuclear transition ( $^{229m}$ Th) it is not necessary to compensate multipolarity, because for NEET the proper AS (for which E1 transition is forbidden, similar to  $^3$ P $^+$ AS) may be used.

# 3. NEET via AS in keV region (178m2Hf isomer triggering)

When the direct transition between initial (isomeric) and final state has a low probability than excitation to the intermediate (trigger) state may deexcite the isomeric state. The trigger level may be excited by X-ray [13-20] and X-ray triggered gamma emission may take place in the process initial-to-intermediate-to-final state transitions. <sup>178m2</sup>Hf 31-year isomer is interesting for triggering because its high energy accumulation (1.2 gigaJoules per gram, excitation energy 2.445MeV) and a pure gamma-burst applications (stable ground state). The autoionization states may be used for an intermediate state excitation in NEET via AS. For <sup>178m2</sup>Hf isomer the possible trigger levels may be near 10keV and 100keV [13-20]. Autoionization states excitation in the 10keV – 100keV energy region and NEET process may solve the problem of <sup>178m2</sup>Hf isomer triggering. In the case NEET via AS the compensation of the energy and multipolarity differences, due to specific of NEET via AS, may play a key role.

For excitation of the AS in the 10 keV - 100 keV energy region it is necessary to create two or more holes in internal electron shells of Hf atoms or ions. Simultaneous

emission of one electron and transition of the second electron to the atomic ground state without photon radiation (NEET) at AS decay may compensate the differences in energy and multipolarity with the corresponding energy transformation into the excitation of a nuclear intermediate state (NEET via AS). Schematic diagram showing the triggering emission of  $\gamma$ -ray driven by NEET via AS is presented in Figure 4 (initial-to AS-to-intermediate-to-final state transitions).



Figur4. Scheme of the NEET via AS triggered gamma emission.

For AS excitation in internal electron shells the electron or ion impact may be used. Now there is no detail experimental data on AS excitation in internal electron shells and the finding of effective mechanism of such AS excitation may allow to make the next step in triggered gamma emission processes study and applications both for <sup>178m2</sup>Hf and other long-lived isomers. The other problem is the ability to mass produce of <sup>178m2</sup>Hf is remain a question at this moment [21,22]. One if the possible way for produce <sup>178m2</sup>Hf is to use Coulomb excitation to the trigger level.

#### 4. Conclusion

Nuclear excitation by an electron transition (NEET) via autoionization states may be an effective instrument for both nuclear isomers excitation and for triggering of  $\gamma$ -ray emission and depopulation of isomers driven by NEET via AS. For eV isomer excitation ( $^{229m}$ Th) the laser radiation may be effectively used for proper AS excitation with high efficiency and selectivity. For the triggering emission of  $\gamma$ -ray driven by NEET via AS it is necessary to find an effective way to excite AS in tens keV energy region.

#### References

- 1. M. Morita, Prog. Theor. Phys. 49, 1574 (1973).
- 2. D.F.Zaretsky and F.F.Karpeshin, Sov. J. Nucl. Phys. 29, 151 (1979).
- 3. F.F.Karpeshin, Proceedings of the V Int. Workshop Applications of lasers in atomic nuclei research. Poland, 2001. Ed.JINR, Dubna, E15-2002-84, p.176.
- 4. V.S.Letokhov, Laser photoionozation spectroscopy. Academic Press (London), 1987.
- 5. V.M. Galitsky, B.M. Karnakov and V.I.Kogan, *Problems in quantum mechanics*. Textbook, Second Edition. Moscow, Nauka, 1992.
- 6. P.Peuser, at el, Appl. Phys. B38, 249 (1985).
- 7. B.A.Bushaw, W.Nortershauser, K.Blaum and K.Wendt, *Spectrochimica Acta.* **B58**, 1083 (2003).
- 8. R.G.Burke, et al, *Phys. Rev.* C42, R499 (1990).
- 9. R.G.Helmer and C.W.Reich, Phys. Rev. C49, 1845 (1994).
- 10. R.B.Firestone and C.M.Baglin, *Table of Isotopes*. Update Eight Edition on CD-ROM,1998.
- 11. E.Browne, et al, Phys. Rev. C64, 014311 (2001).
- 12. F.F.Karpeshin, et al, Proceedings of the Int. Conf. Nuclear Shapes and Nuclear Structure at Low Excitation Energies. ANTIBES, France, June 20-25, 1994. P.181.
- 13. C.B.Collins and J.J.Carroll, Hyp. Int. 107, 3 (1997).
- 14. C.B.Collins, et al, Phys. Rev. Lett. 82, 695 (1999).
- 15. J.J.Carroll, et al, Hyp. Int. 135, 3 (2001).
- 16. J.J.Carroll, et al, Hyp. Int. 143, 37 (2002).
- 17. C.B.Collins, et al, Phys. Rev. C61, 054305 (2000).
- 18. C.B.Collins, et al, Laser Phys. 11, 1 (2001).
- 19. C.B.Collins, et al, Phys. Atomic Nucl. 63, 2067 (2000).
- 20. C.B.Collins, et al, J. de Phys. IV. 11, 437 (2001).
- 21. S.A.Karamian and J.Adam, Czech.J.Phys. 53, B381 (2003).
- 22. S.A.Karamian, *Proceedings of International Symposium on Exotic Nuclei, EXON 2004*, Peterhof, Russia, July 5-12, 2004. World Scientific (in press).

# TO THE QUESTION OF TRIGGERING THE <sup>178m2</sup>Hf ISOMERIC STATE

### F.F.KARPESHIN

Fock Institute of Physics, St. Petersburg State University 198904 St. Petersburg, Russia

# M.B.TRZHASKOVSKAYA

Petersburg Nuclear Physics Institute, Gatchina Leningrad district, 188300 St. Petersburg, Russia

#### Abstract

Many aspects of studies of NEET and TEEN processes in <sup>229</sup>Th and <sup>178m2</sup>Hf atoms are undertaken. Experiments on induced photo-deexcitation of <sup>178m2</sup>Hf are reviewed. Theoretical description of possible triggering channels is presented. Influence of the ionization of the electron shell on ICC and nuclear lifetimes is studied. Values of internal conversion coefficients and transition ebergies are presented from relativistic self-consistent-field Dirac-Fock (DF) calculations.

# 1 Introduction

Recent experiments on photo-induced deexcitation of <sup>178</sup>Hf and some other isomers arose a wave of great interest [1, 2, 3, 4]. Earlier, the isomer of <sup>180m</sup>Ta was successfully triggered [5, 6, 7, 8]. The deexcitation was induced by irradiating a sample with gamma-ray beam. In the case of Hf, the results obtained are rather contradictious, which arose discussion. Spesifically, the magnitude of the measured cross-section of triggered <sup>178m2</sup>Hf was doubted [1, 9, 10, 11]. Some of the criticism remains however to be of purely speculative character. Specifically, it was argued in [9] that the value of the reported cross-section exceeds the upper limit derived from the sum rules for the nuclear photoabsorption.

Our present purpose is to demonstrate that such a consideration should not be conducted without due account of the role played by the electron shell [12, 13, 14]. The shell drastically afects the nuclear deexcitation rates through internal and, specifically, resonance internal conversion process. In this relation, consider diagram of Fig. 1 for a nuclear transition of multipo-

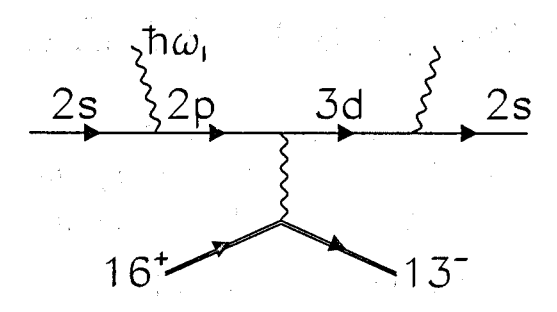


Figure 1: Feynman graph of the photo-induced deexcitation of the  $^{178}Hf$  isomer through the E2 transition in resonance with the electron shell.

larity E3. The role of transitions of high multipolarity in internal conversion was pointed out in refs. [12, 15]. We shall calculate the electron transitions from the 2s level, supposing  $E_{2s} = 0$ . For simplicity, we assume that the energy of the nuclear transition  $\omega_n$  is less than the atomic 3d energy  $E_{3d} = 10.2$  keV. As an example, let us consider the 2433.328-keV  $13^-$  level, lying 12.7 keV below the isomeric one, as a nuclear triggered level. This can also be some unknown level, as it was suggested in ref. [1]. In contrast with the  $^{180m}$ Ta case [5, 6, 7, 8, 16, 17, 18], we consider the situation when the triggered nuclear level lies below the isomeric one. In this case, irradiation acts as to induce the deexcitating transition of the isomer directly to the low-lying nuclear level, from where it cascades down.

Moreover, in our case, the nuclear transition energy  $\omega_n$  turns out to be more than the energy of the related two-photon electron transition. Consequently, the excess energy is taken away by an induced emission process, instead of absorbing energy from the external radiation. The consideration in both cases is conducted, however, in a similar way, with essentially the same results [19], by means of the induced resonance conversion.

The isomer can also undergo the radiative decay via the nonlinear process of the two-photon resonance conversion. This decay mode is represented by the same Feynman diagram, but in another cross-symmetric channel [20, 21]. In the above case of induced resonance conversion, the vertex corresponding to the radiative  $2s \rightarrow 2p$  transition is stimulated by externally applied radiation. Therefore, its effect can be considered in terms of the related cross-section, which is obtained from the transition probability per unit time by dividing it by the incoming radiation flux. As the transition probability is proportional to the intensity, due to the Einstein's coefficients,

the division gives an invariant value. Note that experimental search for this decay mode can be conducted apart from test triggering, as the energy of the emitted dipole photon is represented by a line at the energy of

$$\omega_1 = \omega_n - \omega_{3d-2s} \quad , \tag{1}$$

derived from the energy conservation. Observation of such line would offer a calculable tool of triggering the  $^{178m2}$ Hf energy.

# 2 Method of calculation

Let us calculate the diagram of Fig. 1. By virtue of the resonance twoquantum transition, a 2s electron undergoes excitation to the 3d state. The corresponding amplitude is

$$F_{ind}(\omega_{\ell}) = \bar{\Psi}_{2s}(\mathbf{r}_{3})A_{\omega}^{\mu^{\bullet}}(\mathbf{r}_{3})\gamma^{\mu}G_{\mu\nu}(r_{2}, r_{3})\gamma^{\nu} \times G_{\nu\lambda}(\mathbf{r}_{1}, \mathbf{r}_{2})A_{\omega_{\ell}}^{\lambda}(\mathbf{r}_{1})\Psi_{2s}(\mathbf{r}_{1})J_{\nu}(\mathbf{R}), \qquad (2)$$

where  $\Psi_{2s}(\mathbf{r})$  is the electron wave function in both the initial and final states,  $G_{\nu\lambda}(\mathbf{r}_1,\mathbf{r}_2)$  is the electron Green's function,  $\gamma^{\mu}$  – the Dirac matrices, and  $J_{\nu}(\mathbf{R})$  is the four-vector of the nuclear transition current.

We make use of the spectral representation of the Green's function:

$$G_E(r_1, r_2) = \sum_n \frac{\Psi_n(r_1) > \langle \bar{\Psi}_n(r_2) \rangle}{E - E_n + i\frac{\Gamma_n}{2}}.$$
 (3)

Summation in eq. (3) extends to the full basis of the electron states, including those occupied by the other atomic electrons [22].

Assume that  $\omega_{\ell} \approx E_{2p}$ ,  $\omega_{\ell} + \omega_n \simeq E_{3d}$ . Then one can omit the contribution from the other terms in expansion (2). As a result, one arrives at the following expression for the amplitude (2):

$$F_{ind}(\omega_{\ell}) = F_{\gamma}^{(a)}(3d \to 2s) \frac{1}{\Delta_{3d} + i\frac{\Gamma_{3d}}{2}} F_{c} \frac{1}{\Delta_{2p} + i\frac{\Gamma_{2p}}{2}} F_{\gamma}^{(a)}(\omega_{\ell}), \qquad (4)$$

where  $\Delta_{3d} = \omega_{\ell} + \omega_n - E_{3d}$ ,  $\Delta_{2p} = \omega_{\ell} - E_{2p}$ , and  $\Gamma_i$  is the total width of the corresponding level. Furthermore,  $F_c$  is the discrete conversion amplitude, corresponding to the energy transfer from the nucleus to the electron. Finally,  $F_{\gamma}^{(a)}$  is the electron photoabsorption amplitude.

Squaring amplitude (4) in a usual way, and averaging over the initial and summing over the final magnetic quantum numbers, one gets the expression for the cross-section of the induced isomer deexcitation as follows:

$$\frac{d\sigma_{ind}(\omega_{\ell})}{d\omega_{\ell}} = \sigma_{a} \frac{\alpha_{\partial} \Gamma_{\gamma}^{(n)} / 2\pi}{\Delta_{2p}^{2} + \left(\frac{\Gamma_{2p}}{2}\right)^{2}} \frac{\Gamma_{\gamma}^{(a)} (3d \to 1s) / 2\pi}{\Delta_{3d}^{2} + \left(\frac{\Gamma_{3d}}{2}\right)^{2}}.$$
 (5)

The discrete conversion width  $\Gamma_c$  is factorized into the product of the radiative nuclear width  $\Gamma_{\gamma}^{(n)}$  and the discrete conversion coefficient  $\alpha_{\partial}(E3)$  [13, 19, 23, 24]:

$$\Gamma_c \equiv \alpha_{\partial}(E3)\Gamma_{\gamma}^{(n)}. \tag{6}$$

Expression (5) has two poles. The first pole corresponds to  $\Delta=0$ . That is the electron virtually turns out in the 2p real state. This does not bring about any new physics, therefore, as there are already six atomic electrons in that state. Normal discrete conversion can take place in these electrons, as shown in section 4.

New physics is related to the condition  $\Delta_{3p} = 0$ , which corresponds to the second pole. In this case, we lift up the electron to a nearly real 3d state. It is the Pauli principle which does not allow the electron to dwell in this state [22], and makes him to perform a radiative transition back to the 2s state, with the corresponding width  $\Gamma_{\gamma}(3d \to 1s)$ . Thus again, as in [22], the radiative width of the back transition generically enters the formula, involving the corresponding next order term into the overall cross-section.

Integrating the expression (5) over  $d\omega_{\ell}$  within the interval of  $\Delta\omega$  around the second pole, we arrive at the following expression for the mean cross-section in the interval:

$$\sigma_{ind}(\omega_{\ell}) = \frac{1}{\Delta\omega} \int \frac{d\sigma_{ind}(\omega_{\ell})}{d\omega_{\ell}} d\omega_{\ell} = \frac{1}{\Delta\omega} \sigma_{a}(\omega) \frac{\alpha_{\partial} \Gamma_{\gamma}^{(n)} / 2\pi}{\Delta_{2p}^{2} + \left(\frac{\Gamma_{2p}}{2}\right)^{2}} \times \frac{\Gamma_{\gamma}(3d \to 1s)}{\Gamma_{3d}}.$$
 (7)

After summation over all the  $3d \rightarrow 1s$  transition channels, the last fraction in eq. (7) becomes unity. We therefore omit it below.

It is then convenient to express the photoabsorption cross-section in terms of the radiative width  $\Gamma_{\gamma}$  of the inverse transition [25]:

$$\sigma_a(1s \to 2p) = \left(\frac{\pi}{\omega}\right)^2 \Gamma_{\gamma}^{(a)}(2p \to 1s). \tag{8}$$

The final expression reads as follows:

$$\sigma_{ind}(\omega_{\ell}) = \frac{1}{\Delta\omega} \left(\frac{\pi}{\omega_{\ell}}\right)^{2} \frac{\Gamma_{\gamma}^{(a)}(2p \to 1s)}{\Delta_{2p}^{2}} \frac{\alpha_{\partial}\Gamma_{\gamma}^{(n)}}{2\pi}.$$
 (9)

For illustrative purposes, eq. (9) may be compared to the photoabsorption cross-section for the inverse nuclear transition  $13^- \rightarrow 16^+$ :

$$\sigma_{ph}^{(n)} = \frac{1}{\Delta\omega} \left(\frac{\pi}{\omega_n}\right)^2 \Gamma_{\gamma}^{(n)}. \tag{10}$$

Dividing eq. (9) by 10, we get the enhancement conversion factor R as f as follows:

$$R = \left(\frac{\omega_n}{\omega_\ell}\right)^2 \frac{\alpha_\partial \Gamma_\gamma^{(a)}}{2\pi \Delta_{2p}^2} \,. \tag{11}$$

# 3 Numerical results and discussion

Values of the radiative widths  $\Gamma_{\gamma}^{(a)}$ , atomic energies  $E_n$ , and discrete conversion coefficients  $\alpha_{\partial}(E3)$  were calculated within the framework of the Dirac-Fock method, using package of the computer codes RAINE [27, 28, 29]. The

Table 1: Calculated energies, transition probabilities and discrete ICC  $\alpha_{\partial}(E3)$  in <sup>178</sup>Hf atom. Decimal order is indicated in brackets behind the number. Nuclear transition energies are used for the  $\alpha_{\partial}$  values.

Transition	Multipolarity	$\omega_a, \mathrm{keV}$	$\Gamma_{\gamma}^{(a)}$ , eV	$\alpha_{\partial}(E3)$ , eV
$2p_{1/2} \rightarrow 2s$	E1	0.536	1.6	_
$2p_{3/2} \rightarrow 2s$	E1	1.730	0.13	_
$3d_{3/2} \rightarrow 2s$	E2	9.618	0.64(-2)	
$3d_{5/2} \rightarrow 2s$	E2	9.674	0.95(-2)	
$2p_{1/2} \to 3d_{5/2}$	E3	12.7	-	0.70(10)
$2p_{3/2} \to 3d_{5/2}$	E3	12.7	_	0.37(10)

calculated values are represented in Table 1.

A reasonable value for the averaging interval  $\Delta\omega$  in eq. (9) is around the total atomic width of all the related virtual states [?]:

$$\Delta\omega_{\ell} \gtrsim \Gamma_{2s} + \Gamma_{2p} + \Gamma_{3d} \quad . \tag{12}$$

In view of the values presented in Table 1 for the radiative widths, we put with a considerable reserve  $\Delta\omega\gtrsim 1$  eV. (The less is  $\Delta\omega_\ell$  the more the R value). We put the value of  $\omega_\ell=E_{3d}-\omega_n\simeq 1$  keV. The discrete conversion coefficient  $\alpha_{\partial}(E3)$  value, as one can see from Table 1, is  $\alpha_{\partial}(E3)\simeq 10^{10}$  eV. Substituting those values into eq. (10), one arrives at the enhancement R-factor value of about

$$R \simeq \left(\frac{\omega_n}{\omega_\ell}\right)^2 \frac{\alpha_\theta \Gamma_\gamma^{(a)}(2p \to 1s)}{2\pi \Delta_{2p}^2} \simeq \frac{10^{10} \cdot 0.01 eV}{2\pi \cdot 10^6 eV} \simeq 10^3. \tag{13}$$

That is making use of the resonance properties of the electron shell enhances the cross-section by three orders of magnitude in comparison with what would be expected in the case of triggering bare nucleus.

### Isomer deexcitation via discrete conver-4 sion

The isomer can also undergo the resonance conversion decay via the elastic electron-bridge mechanism, shown by the Feynman graph in Fig. 2. Nuclear quanta are resonantly scattered in the 2p electron shell, with virtual excita-

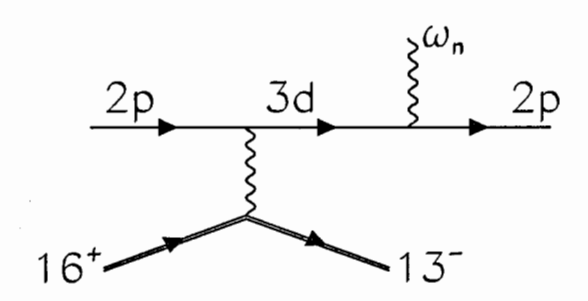


Figure 2: Feynman graph of the  $^{178}Hf$  isomer deexcitation through the resonance electron bridge mechanism.

tion of the 2p electrons to the 3d state, and re-emitted with the same energy  $\omega_n$  in the course of back electron transition to the primary 2p position. The expression for the bridge probability reads as follows [19, 24]:

$$R = \frac{\alpha_{\theta} \Gamma_{\gamma}^{(a)}}{2\pi \Delta^{2}} \,. \tag{14}$$

Using in eq. (14) values from Table 1, we arrive at the R value of approximately  $R \approx 1$ . Account of this channel leads to renormalization of the experimental internal conversion coefficient by R times [26], like in the case of the 76-eV E3 transition in <sup>235</sup>U. Study of the electron bridge mechanism is of great interest, and can be performed with beams of heavy ions [30, 31].

# References

- [1] C. B. Collins, F. Davanloo, R. Dussart, M. C. Iosif, J. M. Hicks, S. A. Karamian, C. A. Ur, I. I. Popescu, V. I. Kirischuk, J. J. Carroll, H. E. Roberts, P. McDaniel, and C. E. Crist, Phys. Rev. Letters, 82, 695 (1999).
- [2] C. B. Collins, F. Davanloo, A. C. Rusu, M. C. Iosif, N. C. Zoita, D. T. Camase, J. M. Hicks, S.A.Karamian, C. A. Ur, I. I. Popescu, R. Dussart, J. M. Pouvesle, V. I. Kirischuk, N. V. Strilchuk, P.McDaniel, and C. E. Crist, *Phys. Rev.* C61, 054305 (2000).

- [3] F. J. Agee, in: Proceedings of the International Conference on Lasers 97, 393 (1998).
- [4] C. B. Collins, A. C. Rusu, N. C. Zoita, M. C. Iosif, D. T. Camase, F. Davanloo, C. A. Ur, I. I. Popescu, J. M. Pouvesle, R. Dussart, V. I. Kirischuk, and F. J. Agee, Hyperfine Interactions, 135, 51-70 (2001).
- [5] C. B. Collins, J. J. Carroll, T. W. Sinor, M. J. Byrd, D. G. Richmond, K. N. Taylor, M. Huber, N.Huxel, P. v. Neumann-Kosel, A. Richter, C. Spieler, and W. Ziegler, *Phys. Rev.* C42, 1813 (1990).
- [6] A. G. Belov, Yu. P. Gangrsky, A. P. Tonchev, and P. Zuzaan, Hyperfine Interactions 107, 167 (1997).
- [7] I. Bikit, L. Lakosi, J. Safar, and L. Concik, Phys. Rev. C59, 2272 (1999).
- [8] I. Bikit, L. Lakosi, J. Safar, and L. Concik, Astrophys. J. 522, 419 (1999).
- [9] S.Olariu and A.Olariu, Phys. Rev. Lett. 84, 2541 (2000).
- [10] D.P.McNabb, J.D.Anderson and J.A.Bocker. Phys. Rev. Lett. 84, 2542 (2000).
- [11] P. von Neumann-Cosel and A.Richter. *Phys. Rev. Lett.*, **84**, 2543 (2000).
- [12] F.F.Karpeshin. Hyperfine Interactions, 143, 79 (2002).
- [13] F.F.Karpeshin, M.R.Harston, F.Attallah, J.F.Chemin, and J.N.Scheurer, Phys. Rev. C53, 1640 (1996).
- [14] F.F.Karpeshin, M.B.Trzhaskovskaya, M.R.Harston, and J.F.Chemin, in: Applications of Lasers in Atomic Nuclei Research, Proceedings of the Vth International Workshop on "Prospects for the development of Laser Methods in the Study of Nuclear Matter". May 28-31, 2001, Poznan, Poland. Dubna, 2002, p. 187.
- [15] F.F.Karpeshin, in: Applications of Lasers in Atomic Nuclei Research, Proceedings of the V International Workshop on "Prospects for the development of Laser Methods in the Study of Nuclear Matter", May 28-31, 2001, Poznan, Poland. Dubna, 2002, p. 176.

- [16] D. Belic, C. Arlandini, J. Besserer, J. de Boer, J. J. Carroll, J. Enders, T. Hartmann, F.Kappeler, H. Kaiser, U. Kneissl, M. Loewe, H. J. Maier, H. Maser, P.Mohr, P. von Neumann-Cosel, A. Nord, H. H. Pitz, A. Richter, M.Schumann, S. Volz, and A. Zilges, *Phys. Rev. Lett.* 83, 5242 (2000).
- [17] D.Belic, C. Arlandini, J. Besserer, J. de Boer, J. J. Carroll, J. Enders, T. Hartmann, F. Kappeler, H. Kaiser, U. Kneissl, E. Kolbe, K. Langanke, M. Loewe, H. J. Maier, H. Maser, P. Mohr, P. von Neumann-Cosel, A. Nord, H. H. Pitz, A. Richter, M. Schumann, F.-K. Thielemann, S. Volz, and A.Zilges, Phys. Rev. C65, 035801 (2002).
- [18] S.A.Karamian, in: Physics of Isomers, Proceedings of the 1st International Workshop, Saint-Petersburg, 18-21 June 2000. Eds.: F. F. Karpeshin, S. N. Abramovich, Yu. P. Gangrsky. Sarov, VNIIEF, 2001, p. 164.
- [19] B.A.Zon, F.F.Karpeshin. Zh. Eksp. i Teor. Fiz., 97, 401, 1990. (Engl. transl. Sov. Phys. JETP (USA), 70, 224, 1990.)
- [20] F.F.Karpeshin, Particles and Nuclei, Dubna, 2006, at press.
- [21] F.F.Karpeshin, Prompt Fission in Muonic Atoms and Resonance Conversion, St. Petersburg: Nauka, 2005.
- [22] F.F.Karpeshin, M.B.Trzhaskovskaya, M.R.Harston, and J.F.Chemin. Phys. Rev. C65, 034303 (2002).
- [23] D.F.Zaretsky and F.F.Karpeshin. Yad. Fiz. 29, 306 (1979). (Engl. transl. Sov. J. Nucl. Phys., 29, 151, 1979.)
- [24] F.F.Karpeshin, I.M.Band and M.B.Trzhaskowskaya. NEET revisited in connection with the resonance radiative pumping of Th-229m.—
   In: Nuclear Shapes and Nuclear Structure at Low Excitation Energies.
   Antibes (France) 20 25 June, 1994. Abstracts of the Contributed Papers, p. 50; Proceedings of the International Conference.
- [25] F.F.Karpeshin, I.M.Band and M.B.Trzhaskovskaya, Nucl. Phys. A654, 579 (1999)).
- [26] V.A.Krutov, Izv. Akad. Nauk SSSR, ser. fiz., 22, 171 (1958).
- [27] Band I.M., Listengarten M.A., and Trzhaskovskaya M.B., Izv. Akad. Nauk SSSR, Ser. Fiz. 53, 910 (1989). (Engl. transl.: Bull. Acad. Sci. USSR, Phys. Ser. 53, 85 (1989)).

- [28] Band I.M., Listengarten M.A., and Trzhaskovskaya M.B., Izv. Akad. Nauk SSSR, Ser. Fiz. 54, 15 (1990). (Engl. transl.) Bull. Acad. Sci. USSR, Phys. Ser. 54, 14 (1990).
- [29] Band I.M. and Trzhaskovskaya M.B., ADNDT 55, 431 (1993).
- [30] F.F.Karpeshin, Yu.N.Novikov and M.B.Trzhaskovskaya. Internal conversion in hydrogen-like ions. PIYaF report No. 2470. Gatchina: PIYaF RAS, 2002; Yad. Fiz., 66, 234 (2004) (English transl. Phys. At. Nucl. (USA), 66, 217 (2004).
- [31] F.F.Karpeshin and M.B.Trzhaskovskaya, Izv. Rossiisk. Akad. Nauk, Ser. Fiz., 67, 1526 (2003). (English transl. Bull. Russian Acad. Sci., Phys. Ser. (USA), 67, 2003).

# ENHANCEMENT MECHANISMS OF LOW ENERGY NUCLEAR REACTIONS

#### GAREEV F.A.

BLTPH, Joint Institute for Nuclear Research, 141980, Dubna, Russia, gareev@thsun1.jinr.ru

#### ZHIDKOVA I.E.

LIT, Joint Institute for Nuclear Research, 141980, Dubna, Russia, zhidkova@jinr.ru

#### RATIS Yu.L.

Physics Department, Samara Aerocosmic State University, 443086, Samara, Russia, ratis@samtel.ru

We have concluded that transmutation of nuclei at low energies is possible in the framework of the known physical laws - excitation and ionization of atoms and universal resonance synchronization principle are responsible for it Investigation of this phenomenon requires knowledge of different branches of science: nuclear and atomic physics, chemistry and electrochemistry, condensed matter and solid state physics,...

#### 1. Introduction

One of the fundamental presentations of nuclear physics since the very early days of its study has been the common assumption that the radioactive process (the half-life or decay constant) is independent of external conditions. Rutherford, Chadwick and Ellis [1] came to the conclusion that:

ullet wthe value of  $\lambda$  (the decay constant) for any substance is a characteristic constant independent of all physical and chemical conditions».

This very important conclusion (still playing a negative role in cold fusion phenomenon) is based on the common expectation (P. Curie suggested that the decay constant is the etalon of time) and observation that the radioactivity is a nuclear phenomenon since all our actions affect only states of the atom but do not change the nucleus states. We cannot hope to mention even a small part of the work done to establish the constancy of nuclear decay rates. For example, Emery G.T. stated [2]:

 $\bullet$  «Early workers tried to change the decay constants of various members of the natural radioactive series by varying the temperature between  $24^{\circ} K$  and  $1280^{\circ} K$ , by applying pressure of up to  $2000 \, atm$ , by taking sources down into mines and up to the Jungfraujoch, by applying magnetic fields of up to 83,000 Gauss, by whirling sources in centrifuges, and by many other ingenious techniques. Occasional positive results were usually understood, in time, as result of changes in the counting geometry, or of the loss of volatile members of the natural decay chains. This work was reviewed by Meyer and Schweider [3], Kohlrausch [4], and Bothe [5]. Especially interesting for

its precision is the experiment of Curie and Kamerlingh Onnes [6], who reported that lowering the temperature of radium preparation to the boiling point of liquid hydrogen changed its activity, and thus its decay constant, by less than about 0.05%. Especially of Rutherford and Petavel [7], who put a sample of radium emanation inside a steel-encased cordite bomb. Even though temperatures of  $2500^{\circ}C$  and pressures of 1000 atm were estimated to have occurred during the explosion, no discontinuity in the activity of the sample was observed».

It seems (in that time) that this conclusion was supported by the following very clean and strong arguments (Common Sense):

- Nuclear processes have characteristic energies ≈ 1 MeV, whereas chemistry
  has a few eV per atom, molecules have a part of eV. The inner atomic shells
  are bound with many keV in the medium and heavy elements.
- 2. The localization of electrons in atoms is  $\approx 10^{-8}$  cm, whereas the localization of nucleons in nuclei is  $\approx 10^{-13}$  cm.

Therefore, the nucleus should be unaffected by superficial atomic changes: nuclear processes should not be influenced by the surroundings. The constancy of nuclear decay rates was firmly established, confirming evidences from experimental studies of  $\alpha$  – and  $\beta$  – decays and theoretical estimations.

The constancy of nuclear decay rates acquired the strength as a classical law. Any papers contradicting this law were ignored by all the scientific journals as erroneous ones.

The history of science has own laws. The ground of the  $\beta$ -decay of nuclei was given by E. Fermi in 1934 year. It was very easy to prove that certain processes of radioactive decay should be intimately connected with the presence of atomic electrons and may be affected by the changes in the electronic structure produced by chemical compounds. It took 13 years to understand this very simple phenomenon. The possibility of altering the decay rate of  $Be^7$  was suggested in 1947 by Segre [8] and by Dodel [9, 10]. In the case of electron- capture decays the decay rate is directly related to the density of atomic electrons in the nucleus and that the effects of different chemical environments should be measurable. The theoretical foundation was the following [8]:

• «The radioactive decay constant of a substance decaying by orbital electron capture is proportional to  $|\psi(0)|^2$  of the electrons. In the case of a light element like  $^7Be$  it may be possible to alter this quantity by an appreciable amount by putting the Be in different chemical compounds. We would then have a slight change of the radioactive half-life of the Be in different compounds, the magnitude of the effect may be in the neighborhood of one percent, but it is practically impossible to give quantitative estimate because the total change of  $\psi(0)$  is affected by certain factors such as the density of the crystal, nature of the chemical bond, etc. they are both positive and negative, and have comparable magnitudes. To obtain a reliable estimate of the effect we require a more detailed knowledge of the wave functions for various compounds than is at present available. Experiments are in progress to detect the effect by comparing the half-life of  $^7Be$  in Be metal with that in BeO or  $BeF_2$ ».

The confirmed altering decay rate for  $^{7}Be$  in different chemical compounds were of the order 0.1% [2]. The 6-hr isomer  $^{99m}Tc$  decays by internal conversion of a 2.2-keV E3 transition. The observed effects in different chemical forms were of the order 0.3% [2]. The greatest chemically induced half-life changes of the order 3.5% were established in [11].

The half-life of  ${}^7Be$  electron capture was measured [12] in endohedral fulleren  ${}^7Be @ C(60)$  and  ${}^7Be$  metal:  $T_{1/2} = 52.68 \pm 0.05$  and  $T_{1/2} = 53.12 \pm 0.05$  days, respectively. This 0.83% difference between the electron capture in  $C_{60}$  and in  ${}^7Be$  metal represents a strong environment effect on the  ${}^7Be$  EC capture rate, caused by the different electronic wave functions near the  ${}^7Be$  nucleus inside a  $C_{60}$  cage and inside Be metal.

A weak interaction which is responsible for electron capture and other forms of beta decay are of very short range. So the rate of electron capture and emission (internal conversion) is proportional to the density of electrons at the nucleus. It means that we can manage the electron-capture (emission) rate by the change of the total density in the nucleus. It can be carried out with in the different macroscopic ways using available environmental effects. These questions were highlighted in different reviews and books [2, 13-19] at the end of the seventies of the 20 the century. The reader should compare the common accepted conclusions about the decay rates in the thirties and seventies of the 20 the century.

Data on pleochroic halos led to the conclusion [20] that those data do not provide a convincing proof that the laws of radioactive decay are constant in time. Shnol S. and coauthors [21] came to the conclusion that the decay rates of radioactive nuclei change in time with the period of 24 hours, 27, and 365 days. Periodic variations in  $\beta$  – decay rates of  $^{60}Co$ ,  $^{90}Sr$  and  $^{137}Cs$  were discovered [22-25]. The 27-day and 24-hour period in these changes were found.

The aim of this talk is to discuss the possibility of inducing and controlling the nuclear reactions at low temperatures and pressures by using different low energy external fields and various physical and chemical processes. Main question is following: is it possible to enhance LENR rates by using the low and extremely low energy external fields?

#### 2. Cold fusion and transmutation

In 1989 Fleishmann M. and Pons S. reported about their observation of nuclear products and excess heat on a palladium electrode during the electrolysis of solutions in heavy water. The electrochemical experiments were interpreted by the authors as a result of nuclear fusion reaction (named cold fusion) but the scientific community rejected this interpretation. More than 3000 papers in the field of cold fusion and transmutation (further the low-energy nuclear reaction LENR) were published. Various anomalous results were observed at low temperatures and pressures which are beyond the framework of modern theoretical paradigm. The theoretical models are not

able even qualitatively describe these anomalies. The reader can find the history and problems of cold fusion in the Proceedings of the International Conferences on Condensed Matter Nuclear Science, the Russian Conferences on Cold Nuclear Transmutation of Chemical Elements and Ball Lighting, and also in a recent review of the Department of Energy of the USA [26] and books [27, 28]. The Russian experimental data on the low energy nuclear reactions are published in [29-32] and their new theoretical interpretation were given in [33-36].

The general important conclusion can be drawn from the studies performed during 15 years:

• The poor reproducibility of experimental results and extreme difficulties of their interpretation in the framework of modern standard theoretical physics are the main reasons of the persistent non-recognition of cold fusion and transmutation phenomenon.

Recent progress in both direction is remarkable (see Abstracts ICCF-11, Marseille: France: 2004, 31 October - 5 November) nevertheless the understanding of rejection by physical society this phenomenon is a key point for further success corresponding fundamental research.

## 2.1. Reproducibility of Low Energy Nuclear Reaction Experiments

Reproducibility of experiments within and between laboratories is a fundamental requirement and cornerstone for any scientific investigations. There are many fundamental factors that are relevant to the issue of reproducibility (see details in [37]).

Everybody with a perfect ear will say that the play, for example, on viola will have never be reproducible: it dependent on too many factors (resonance conditions) which is impossible to repeat. The semiconductor effect in a transistor is extremely sensitive to damages and impurities of crystal which were impossible to control in the initial experiments. The degree of reproducibility was increasing over the years when the properties of used materials were improved and standardized, and the process was optimized and controlled with high accuracy. The same would happen for reproducibility of LENR [27]. We will show that this expectation for LENR is correct only partly<sup>1</sup>.

The targets in standard nuclear physics using accelerators are the substances in the ground states: the gases, amorphous solids or crystalline solids. The projectile particle interaction with

target nuclei has taken place in vacuum. Therefore, the influence of the surrounding matter (say, atomic electrons) on the velocity of such nuclear processes (especially at high energies) should be negligible. It seems these expectations supported by estimations of energy and size differences  $(10^{-5} - 10^{-6})$  atoms and nuclei and experiments show almost a full reproducibility.

References to original and review cold fusion literature are not given in our talk. They are available in Proceedings of ICCF.

We come to the following conclusion:

• A greater part of processes in nuclear physics takes place in closed systems. Reproducibility of such experiments should be independent of the place and time of measurements - a cornerstone of the modern scientific method.

LENRs occur in the surroundings (gases, condensed mater, water, solutions,...) which are induced by low-energy external fields as ultrasounds, electromagnetic fields, lasers, .... So atoms, molecules in the surroundings and atoms of interacting nuclei are in excited states or ionized. Nuclei, atoms, the surrounding medium and external fields representing interacting subsystems are form a dynamical open system. Frequencies and phases of subsystem motions may be coordinated according to the universal resonance synchronization principle (see Appendix) and the result may be a creation collective (coherence) state for the whole system. We will call such a system an auto-oscillation system in which the frequency of an external field and frequencies of the all subsystem are commensurable. The demand for frequency commensurability means that all motions in a system are in co-ordination (in resonance) which is difficult to fulfil. This is the cause of poor reproducibility of LENR.

We formulate as a working hypothesis the following assumption:

• LENRs take places in open systems in which all frequencies and phases coordinated according to the universal resonance synchronization principle - main reason of poor reproducibility. Poor reproducibility and unexplained results do not mean that the experiment is wrong.

## **2.2.** The Bound State $\beta$ – Decay

Bound state  $\beta^-$  decay  $(\beta_b)$ , in which the decay electron remains in an electron bound state of the daughter atom and the monochromatic antineutrino carries the total decay energy Q, was first predicted by R. Daudel, M. Jean, and M. Lecoin [38] in 1947 and discussed in [39-43].

This new decay mode, the bound state  $\beta^-$  decay, was for the first time experimentally observed for bare  $^{163}Dy$  [44] (Bare means that the atom  $^{163}Dy$  is ionized fully. We will use designation for this case as  $^{163}Dy^{66+}$ ) and  $^{187}$ Re [45]. Nuclei  $^{163}Dy$  are stable as a neutral atom  $(Q_{\beta}=-2.565\,keV)$  and become radioactive when fully ionized atoms (bare nuclei  $^{163}Dy^{66+}$ ) decay to  $^{163}Ho^{66+}$  ( $Q_{\beta_b}^K=+50.3$  keV) via the bound state  $\beta_b$  decay with a half-life of 47 days. Nucleus  $^{163}Ho$  is unstable and it is transferred to  $^{163}Dy$  by electron capture with a half-life of  $4.6\cdot10^3$  yr. Difference of masses  $m(^{163}Ho)-m(^{163}Dy)=2.6$  keV, therefore the electron capture is only possible from M- or higher orbits. Unstable nuclei  $^{163}Ho$  became practically stable due to ionization of atoms  $^{163}Ho$  up to these orbits because the electron capture in such cases is only possible from continuum states which have an extremely small probability. The ionization of atoms changes the beta decay direction of nuclei: in

neutral atoms  $^{163}Ho$  ( $^{163}Dy$ ) the electron capture lead to the transition  $^{163}Ho \rightarrow ^{163}Dy$  ( $^{163}Dy$  are stable), in fully ionized atoms bare nuclei  $^{163}Ho^{67+}$  ( $^{163}Dy^{66+}$ ) are stable (unstable).

• General conclusion: in neutral atoms the some ground state nuclei are decay via orbital electron capture, for bare nuclei (fully ionized atoms) the electron capture branches are blocked. In such cases (if in addition the positron decays are lacking) bare nuclei became stable. This conclusion is a very strong and well-known in nuclear society.

For neutral  $^{187}$  Re $^{0+}$  only a unique, first forbidden transition to the  $^{187}$ Os ground state is energetically possible. The small matrix element and the small  $Q_{\beta}$  value of  $Q_{\beta} = 2.663(19)$  keV lead to the long half-life of 42 Gyr. The measured half-life [45] for bare  $^{187}$  Re $^{75+}$ 

 $(Q_{\beta}^{K} = +72.97 \text{ keV})$  of  $T_{1/2} = (32.9 \pm 2.0)$  yr is billion times (BILLION-9 ORDERS of MAGNITUDE) shorter than that for neutral <sup>187</sup> Re.

• The ground state  $\beta$  - decay (orbital electron capture) properties of nuclei cardinally change when all electrons of the atomic shells are removed: stable (unstable) nuclei become unstable (stable) and a half-life may decrease up to billion times - 9 orders of magnitude. The interpretation is very simple: magnitude of  $Q_{\beta}$  ( $T_{1/2} \approx AQ_{\beta}^{-5}$ ) and phase volume increase for the ionized atoms rather than for neutral ones and it is evident that the Pauli principle plays a different role in neutral and fully ionized atoms.

## 2.3. The Nuclear Decay of Coulomb Excited and Isomeric States for Fully Ionized Atoms

The half-lives of isomeric states of fully ionized  $^{144m}Tb^{65+}$ ,  $^{149m}Dy^{66+}$  and  $^{151m}Er^{68+}$  have been measured [46]. The increase was observed of the half-lives of bare isomers by factors of up to 30 to their neutral counterparts. The authors [46] give the correct and evident interpretation of experimental results:

• This is due to the exclusion of the strong internal conversion and electron-capture channels in the radioactive decay of these bare nuclei.

Experiments with highly -ionized  $^{57}Fe^{q+}$  (q=19-25) (q=19-25) projectiles at 6 MeV [47] and  $^{125}Te^{q+}$  q=46-48) projectiles at 27 MeV/u [48] have demonstrated a growth (ranging from a few 10% up to 670%) of nuclear half-lives of Coulomb excited levels due to the direct influence of the electronic configuration on the internal-conversion coefficients.

## 2.4. The Effect of Host on the Half-life of <sup>7</sup>Be

Norman E.B. et al. [49] measured  $^{7}Be$  decay rates in gold (Au), graphite, boron nitride and tantalum (Ta). Among these materials, they found that the  $^{7}Be$  half-life

was the longest in Au and the shortest in graphite. According to their experiments, the decay rate of  $^{7}Be$  in Au is lower than that in graphite by  $(0.38 \pm 0.09)\%$ .

Ray A. [51] measured the difference  $^7Be$  decay rates in Au and  $Al_2O_3$  and found that the decay rate in Au was lower than that in  $Al_2O_3$  by  $(0.72\pm0.07)\%$ .

Ray A. et al. [50] pointed out that the apparent disagreement between the two sets of experimental results was most likely due to the choice of different reference samples with which the comparisons were carried out. Indeed, Norman E.B. et al. [49] used  $^7Li$  beam for their implantation studies, whereas Ray A [51] used proton beam. The radiation damage by  $^7Li$  on gold lattice sites, where  $^7Be$  nuclei stop, would be much larger [52] ( $3 \cdot 10^{-4}$  vacancies/Angstrom/ion) than the corresponding damage ( $10^{-5}$  vacancies/angstrom/ion) for proton. Therefore, the radiation damage effects on lattice due to heavy ion irradiation might also be partly responsible for apparent discrepancies. It means that to speak about reproducibility in this case we should take into account at least atomic physics effects that are usually ignored.

The ratio of L to K-shell electron capture in  ${}^{7}Be$  bare nucleus shows [53] that the measured ratio is less than half of the existing data for free  ${}^{7}Be$ .

ullet These discrepancies are most likely due to the distortions of L and K-shell orbitals by the host medium.

## 2.5. Controlled Gamma-Decay of Excited Nuclei

According the modern theory, the spontaneous gamma-decay of excited nuclei in free space without any material bodies is a noncontrolled process. Probability  $A_{eg}$  of this decay

$$A_{eg} = \frac{1}{\tau} = \frac{4\pi^{2}\omega_{eg} |\vec{d}_{eg}|^{2} \rho(\omega_{eg})}{3\hbar} = \frac{4\omega_{eg}^{3} |\vec{d}_{eg}|^{2}}{3\hbar c^{2}}$$

is fully determined by the matrix element  $\left| \vec{d} \right|_{eg}$  of the nucleus dipole moment and energy of the nuclear transition  $h\omega_{eg} = E_e - E_g$ .

The total lifetime  $\tau_{tot} = \frac{\tau}{(1+\alpha)}$  and radiative lifetime  $\tau$  of this excited nucleus in free space are the constants. Here  $\alpha$  is the coefficient of internal electron conversion for the nuclear transition  $E_e - E_g$ .

Problems become very complicated in the important case when material bodies are present in the surrounding space. Vysotskii V.I. [54] considered the general system which included the

excited atom nucleus, the system of atom electrons, the system of zero-energy (in vacuum state) electromagnetic modes and the screen-the system of N resonant or

nonresonant atoms situated at the distance  $d >> \lambda_{eg} = \frac{2\pi c}{\omega_{eg}}$ . The authors of [55] concluded that

• It is usually stated that in all cases with the presence of any material bodies at a macroscopic distance  $d >> \lambda_{eg} = \frac{2\pi c}{\omega_{eg}}$  from the excited nucleus the expression

for the lifetime  $\tau$  and  $\tau_{tot}$  remains the same or changes by an unmeasurable small value. Such a supposition is erroneous. It was shown [54] that a spontaneous gammadecay is a process of an excited nucleus relaxation, the phase promise of which is caused by interaction with a fluctuating state of the thermostat at the distance  $d >> \lambda_{eg}$  from the nucleus. The phenomenon of a controlled nucleus gamma-decay is a result of interaction of the nucleus with zero-energy modes, interaction of these modes with the atoms of controlled (and controlling) screen, and interaction of the nucleus with the system of atom electron.

The increase in radiative lifetime  $\tau$  of an excited nucleus by 10-40% and total lifetime  $\tau_{tot}$  by 1% was observed in the experiments [55-57] with gamma-source  $^{57}Co(^{57*}Fe)$  and with gamma-absorber made of stable  $^{57}Fe$  isotope. So these results prove the possibility of controlled essential influence of a thin resonant screen on the amplitude, space and temporal characteristics of a spontaneous decay and excited nuclei radiation.

## 2.6. Okorokov Effect

Let us consider the interaction of an incoming particle (atom or nucleus having the ground state  $E_g$  and the excited state  $E_e$ ) with the crystal target. It is possible to choose the conditions [58,59] when the frequency of a collision particle with the atoms of crystal  $\nu_{col} = V_0/a_0$  (the velocity  $V_0$  of a particle motion  $a_0$  is the distance between the atoms in the crystal) will be commensurable with the transition frequency  $\nu_{in}$  of the particle

$$v_{tr} = \frac{E_e - E_g}{h} = \frac{n_1}{n} v_{col},$$

where  $n_i$  - integer numbers. It is clear that at such conditions the interaction between the particle and atoms of the crystal should have a resonance character.

If the particle interacts with the n atoms of the crystal, then the probability to excite the particle is equal to

$$W(n) = W(1)n^2,$$

where W(1) is the probability of excitation of the particle by one atom of the crystal. This is a collective (coherent) amplification mechanism of the excitation for the projectiles in the periodic field of the crystal predicted first by Okorokov V.V. [58,57] and observed experimentally by Okorokov V.V. too [60-62].

The resonance and coherent amplification of atoms and nuclei excitations by the periodic fields of crystals is now well established and recognized by the physical society and is used in different applications but is not known for the cold fusion society.

From a modern point of view water has a very complicated geometrical structure as a collection of quasicrystal clusters (see [63] and references in it). The hydrogen atom, atoms and molecules, water and solutions, solid states and condensed matter have the same homology in the geometric structure where the de Broglie wave length of electron in the ground state of hydrogen atom plays the role of the standard one [64].

The puzzle of poor reproducibility of experimental data of LENR is now evident:

- Electrolysis in solutions, discharge in gases and any external influence on atoms means
- 1. The atoms are ionized thus changing radioactive rates by bound state  $\beta_b$  decay of nuclei.
- 2. The ions can be accelerated a such way that they come to resonance conditions to intensify of excitation of nuclei, atoms, ....
- 3. Even small external fields can induce large responses as an avalanche in the mountains stimulated, say, by an accident cry.

A mechanical analogue of the observed phenomenon is the synchronization of oscillations of the pendulum clock suspended from the moving girder - the Huygens synchronization principle [65]. The universal resonance synchronization principle for a microsystem (for nuclei, atoms, molecules for living and nonliving sells,...) was established in [66].

The decrease and increase radioactivity of tritium with increasing temperature in small titanium particles was observed [67] that current experiment and theory overlooked this effect.

#### 2.7. Nuclei and Atoms as Resonators

In 1953 Schwartz H.M. in 1953 [68] proposed to consider the nuclear and the corresponding atomic transitions as a unified whole process. This process contains the  $\beta$ - decay which represents the transition of nucleon from one state to another with emission of electron and antineutrino and simultaneously the transition atomic shell from the initial state to the final one. A complete and strict solution of this problem is still waiting its another time (see, for example, review paper [69]).

The division of decay energy into nuclear and atomic energies has only a conditional sense, especially, in the resonance case. The process has a resonance charter and its probability is large when energy differences of nuclear and atomic transitions become close to zero. The drastic acceleration of decay time in H-like ions of  $^{229m}Th$  may be up to  $10^5$  [69], the electron shell serves as a trigger, reducing the lifetime of the isomer by up to five orders of magnitude.

The probability of the resonance transfer of energy by electrons from the nuclei can be increased by application of laser, which compensates the defect of resonance. The corresponding enhancement factor in some cases may be 10<sup>3</sup>. It is important to note

that the knowledge of isomer energy is not necessary, the laser should be synchronized on the atomic frequency.

- This is a real phenomenon of resonance synchronization (see Appendix) of nuclear, atomic, and laser frequencies to control the decay processes.
- It is also predicted [70] that the lifetime of the hindered photo-fission can be reduced up to  $10^3 10^4$  by application of laser. Laser in a such case changes the angular momentum of decaying state by unity practically without altering its energy.
- Low energy external fields in LENR can play a role of a trigger changing the quantum numbers of the hindered or forbidden processes so that the first should be enhanced and the second should be allowed. This mechanism inducing LENR may be the main reason for poor reproducibility of LENR experiments and main mechanism of geo- and biotransmutations.

#### 2.8. Geo-, Bio- and Alchimical Transmutations

All the above-described mechanisms of LENR are grounded on the universal resonance synchronization principle (see Appendix). The main requirement of this principle is that the frequencies  $v_i(ext)$  of external fields should be commensurable with the frequencies  $v_j(in)$  of subsystems making a whole system:  $v_i(ext) = v_j(in) n(j)/n(i)$ . We strongly emphasize that the frequencies of an external field can be infinity small in comparison with the corresponding frequencies of subsystems. The frequencies  $v_i(ext)$  are as a triggers starting emission of internal energy. The enhancement (resonance) effect on LENR induced by external fields can be extremely large (small) when maximal values of density distributions for external fields and the corresponding distributions of a subsystem coincide (do not coincide). It means that:

• Even extremely low-energy external fields may induced nuclear transmutations with emission of internal high-energies according to the universal resonance synchronization principle.

Natural geo-transmutations in the atmosphere and earth occur at the points of strong change in geo- and electromagnetic fields [71-73]. V.I. Vysotsky and A.A. Kornilova published an excellent book: «Nuclear Fusion and Transmutation of Isotopes in Biological System» [74], we refer a reader to this book.

It seems (for F.A.Gareev) that some alchemists may [75] «change base metals into noble ones, silver or gold» do not contradict with the mechanisms of LENR described above.

## 2.9. Ball lightning as macroscopic low energy nuclear reactor

All internal contradictions of the previous theories of a ball lightning were based, by default, on an assumption that the ball lightning is a plasmoid. In order to maintain the macroscopic volume of air (the mixture of nitrogen, oxygen, water vapour, etc.) in ionized condition it is necessary to provide a great amount of energy from some kind of a source. Many experimenters, among them such well-known experts as P.L.

Kapitsa, made repeated attempts to create a long-living spherical plasmoid in laboratory conditions. However, no efficient ways of supplying the isolated plasma clots with energy and maintaining them in a stationary condition for a few minutes (that is the lifetime of a natural ball lightning) could be found.

The purpose of this paper is to substantiate a hypothesis that the natural ball lightning is an area of space where the chain nuclear reaction of the bound-state  $\beta$ -decay of radioactive phosphorus nuclei takes place. It is shown that the analyzed phenomenon is related to the physics of electrical discharge in gases indirectly. Therefore the term globular lightning is not sufficiently correct.

The main hypothesis which is asserted hereinafter, was formulated for the first time in [76]. The logic of the creation of this hypothesis is as follows:

- 1. Ball lightning always leaves a smell of sulphur, ozone and nitrogen oxide after itself [77].
- 2. Sulphur can be generated only as a result of phosphorus  $\beta$ -decay [78].
- 3. Rate constant of  $\beta$ -decay depends on a lot of the ionization degree of decaying radionuclide [33]. The half-life of ionized radiophosphorus is approximately 1-2 minutes and is comparable with the lifetime of ball lightning in natural conditions.
- 4. Radiophosphorus is abundant in nature. It is found in rain-water in macroscopic amounts [79].

This model was proved in [76] and we can say, that it is now confirmed. Thus ball lighting is a type of a natural low energy nuclear reactor.

#### 3. Conclusions

We have concluded that LENR is possible in the framework of the modern physical theory - the universal resonance synchronization principle and based on its different enhancement mechanisms of reaction rates are responsible for it<sup>2</sup>. Investigation of this phenomenon requires the knowledge of different branches of science: nuclear and atomic physics, chemistry and electrochemistry, condensed matter and solid state physics, .... The results of this research field can provide a new source of energy, substances and technologies.

The puzzle of poor reproducibility of experimental data is due to the fact that LENR occurs in open systems and is extremely sensitive to parameters of external fields and systems. Poor reproducibility and unexplained results do not mean that the experiment is wrong<sup>3</sup>.

<sup>&</sup>lt;sup>2</sup> Intensification of LENR using superwave excitation [80] is based on this principle.

<sup>&</sup>lt;sup>3</sup> Solutions of salts, electrolytes and living systems contain a large amount of ions. In these cases the bound state  $\beta_b$ -decay and other described above enhancement mechanisms of LENR can play an essential role. Unfortunately we do not know the works devoted to this problem.

#### Appendix. Atoms as open systems

The conservation laws fulfill for a closed systems. Therefore, the failure of parity in week interactions means that the corresponding systems are the open systems. Periodic variations (24 hours, 27, and 365 days [21-25]) in  $\beta$ -decay rates indicate that failure of parity in week interactions have a cosmophysical origin.

The charged particles moving with acceleration should radiate (absorb) electromagnetic waves – the fundamental classical electrodynamics low. The stable orbits of electrons in atoms are exist, but electrons do not radiate on them according to third Bohr's postulate (third Bohr's postulate in 1913 - "Despite the fact that it is constantly accelerating, an electron moving in such an allowed orbit does not radiate electromagnetic energy. Thus, its total energy E remains constant."). Why electrons do not radiate on the stable state of atoms – nobody knows it. We formulate as a working hypothesis the following assumptions:

- The classical lows of physics are valid for macro- and microsystems. Contradiction between classical electrodynamics and quantum theory should be solved a very simple way. Proton and electron in hydrogen atom move with the same frequency, their motions are synchronized. A hydrogen atom represents radiation and accepting antennas (dipole) interchanging of energy with the surrounding substance. This energy is the relict radiation energy.
- The relict radiation (T=2.725 K) should play a role of conductor for proton and electron motions in the hydrogen atom due to the universal resonance synchronization principle. The external field relict radiation field and hydrogen atom form an auto-oscillation system in which the frequencies of an external field and frequencies of the whole subsystem are commensurable. The demand for frequency commensurability means that all motions are in a co-ordination (in resonance).
- The sum of radiate and absorb energies by electron and proton moving in an allowed orbit is equal to zero. THUS, ITS TOTAL ENERGY E REMAINS CONSTANT only the last part of the third Bohr's postulate is correct.
- The relict radiation is a result of the selforganization of stable hydrogen atom according to the universal resonance synchronization principle.

#### References

- 1. Rutherford E., Chadwick J., and Ellis C.D. Radiations from Radioactive Substancs, Cambridge Univ. Press, 1930.
- 2. Emery C.T. Annual Rev. Of Nucl. Sci. 1972, V.22, p.165.
- 3. Meyer S., Schweidler E. Radioactivitat. Leipzig: B.G. Teubner, 2nd ed., 1927.
- 4. Kohlrausch K.W.F. Radioactivitat, Handbuch der Experimentalphysik, V.15, Leipzig: Akademische verlagsgesellschaft mbH, 1928.
- Bothe W. Handbuch der Physik, ed. H. Geiger, K. Scheel, Berlin: Springer 2nd ed., 1933, V.22-1, p.201.
- 6. Curie M., Kamerlingh Onnes M., Le Radium, 1913, V.10, p.181.
- 7. Rutherford E., Petavel J.E., Brit. Assoc., Advan. Sci., Rep.A, 1907, p.456; Rutherford E. Collected Papers, New York: Interscience, 1963, V.2, p.36.

- 8. Segre E., Phys. Rev., 1947, V.71, p.274.
- 9. Daudel R., Rev. Sci., Paris, 1947, V.85, p.162.
- 10. Bouchez R., Daudel R., Daudel P., Muxart R., J. Phys. Radium, 1947, V.8, p.336.
- 11. Cooper J.A., Hollander J.M., Rassmusen J.O., Phys. Rev. Let., 1965, V.15, p.680.
- 12. Ohtsuki T., Yuki H., Muto M., Kasagi J., Ohno K., Phys. Rev. Lett., 2004, V.93, p.112501-1.
- 13. DeBenedetti S., Des. Barros., Hoy G.R. Ann. Rev. Nucl.Sci., 1966, V.16, p.31.
- 14. Starodubchev C.B. Transmutations of nuclei and atomic shells (in Russian). Book 1. Tashkent 1969.
- 15. Konopinski E.J. The Theory of Beta Radioactivity. London: Oxford Univ. Press, 1966.
- 16. Schopper H.F. Weak Interactions and Nuclear Beta Decay. Amsterdam: North-Holland, 1966.
- 17. Wu C.S., Moszkowski S.A. Beta Decay. New York: Interscience-Wiley, 1966.
- 18. Bouchez R., Depommier P., Rep. Prog. Phys., 1960, V.23, p.395.
- 19. Berenyi D., Rev. Mod. Phys., 1968, V.40, p.390.
- 20. Spector R.M., Phys. Rev., 1972, A5, p.1323.
- 21. Shnol S.E. et al., UFN (in Russian), 1998, V.168, p.1129.
- 22. Baurov Yu.A., Shutov V.L., Prikladnaja Fizika (in Russian), 1995, V.1, p.40.
- 23. Baurov Yu.A., Kondratov A.A., Kushniruk V.F., Sobolev Yu.G., Scientific report 1995-1996, "Heavy Ion Physics", Preprint JINR E7-97-206, p.354, Dubna, 1997.
- 24. Baurov Yu.A., Konradov A.A., Sobolev Yu.G., E-print hep-ex/9809014, 16 September, 1998.
- 25. Baurov Yu.A., et al., Modern Phys. Lett., 2001, A16, p.2089.
- 26. Hagelstein P.I., McKubre M.C.H., Nagel D.J., Chubb T.A. and Hekman R.J., New Physical Effects in Metal Deuterides. 2004.
- 27. Krivit S.V., Winocur N. The Rebirth of Cold Fusion, Los Angeles, 2004.
- 28. Kirkinski v.A., Novikov Yu.A. Theoretical Modeling of Cold Fusion, Novosibirsk, 2002.
- 29. Urutskoev L.I., Liksonov V.I., Tsinoev V.G., Prikladnaja Fizika (in Russian) 2000, V.4, p.83.
- 30. Urutskoev L.I., Liksonov V.I., Tsinoev V.G., Annales de la foundation de Broglie, 2002, V.27, p.701.
- 31. Balakirev V.F., et al., Transmutations of Chemical Elements, Ekaterinberg, UrO RAN, 2003.
- 32. Kuznetzov V.D. et al., Annalesde la fondation de Broglie. 2003, V.28, p.173.
- 33. Gareev F.A., Zhidkova I.E., Ratis Yu.L., Preprint JINR P4-2004-68 (in Russian), Dubna, 2004.
- 34. Gareev F.A., Zhidkova I.E., Ratis Yu.L., Proceedings of the 11-th Russian Conference on Cold Nuclear Transmutation of Chemical Elements and Ball Lighting, Dagomys, city of Sochi, September 28 October 5, 2003, Moscow 2004, p.169.
- 35. Gareev F.A., Gareeva G.F., Zhidkova I.E., Geoinformatika (in Russian), 2003, V.1, p.51.
- 36. Gareev F.A., Ratis Yu.L., Science, Economy and Management, Samara, 2002, V.3, p.103.

- 37. Nagel D.J., Godick J., Proceedings of ICCF-10, 2003.
- 38. Daudel R., Jean M., Lecoin M., J. Phys. Radium, 1947, V.8, p.238.
- 39. Bahcall J.N., Phys. Rev., 1962, V.124, p.495.
- 40. Batkin I.S., Izv. AN SSSR, ser. fiz. (in Russian), 1976, V.49, p.1279.
- 41. Kopytin I.V., Doktorskaja dissertachija (in Russian), Voronezh, 1986.
- 42. Takahashi K., Yokoi K., Nucl. Phys., 1983, A404, p.578.
- 43. Takahashi K., Boyd R.N., Mathews G.J., Yokoi K., Phys. Rev. 1987, C36, p.1522.
- 44. Jung M., et al., Phys. Rev. Lett., 1992, V.69, p.2164.
- 45. Bosch F., et al., Phys. Rev. Lett., 1996, V.77, p.5190.
- 46. Litvinov Yu.A., et al., Phys. Lett., 2003, B573, p.80.
- 47. Phillips W.R., et al., Phys. Rev., 1993, A47, p.3682.
- 48. Attallah F., et al., Phys. Rev., 1997, C55, p.1665.
- 49. Norman E.B., et al., Phys. Rev. Lett., 2001, B519, p.15.
- 50. Ray A., Das P., Saha S.K., Das S.K., Phys. Lett., 2002, B531, p.187.
- 51. Ray A. et al., Phys. Lett., 1999, B455, p.69.
- 52. Ziegler I.F., Bierserk J.P., Littmark U., The Stopping range in Solids, Pergamon, New York, 1985.
- 53. Voytas et al., Phys. Rev. Lett., 2002, V.88, p.012501.
- 54. Vysotskii V.I., Phys. Rev., 1998, C58, p.337.
- 55. Vysotskii V.I., Kornilova A.A., Sorokin A.A., Komisarova V.A., Reiman S.I., Riasnii G.K., Laser Physics, 2001, V.11, No.3, p.1.
- Vysotskii V.I., Bugrov V.P., Kuzmin A.A., et al., Hyperfine Interactions, 1997, V.107, p.277.
- 57. Vysotskii V.I., Bugrov V.P., Kornilova A.A., Reiman S.I., International Conf. on the physics of Nuclear Science and Technology, Proceedings 1998, V.2, p.1739.
- 58. Okorokov V.V., Sov. J. Nucl. Phys. 1965, V.2, p.719; Jadernaja Fizika (in Russian), 1965, V.2, p.1009.
- 59. Okorokov V.V., JETP Lett. (in Russian), 1965, V.2, p.111.
- 60. Okorokov V.V., et al., JETP Lett. (in Russian), 1972, V.16, p.588; JETP Lett., 1972, V.16, p.415; 1973, A43, p.485.
- 61. Okorokov V.V., et al., Preprint ITEP No19, 1973.
- 62. Okorokov V.V., Proceedings of FPV-2002, Novosibirsk, 2002, p.48.
- 63. Senin S.V., The Water, Moscow, 2004.
- 64. Gareev F.A., Gareeva G.F., , in: FPB 2000, Novosibirsk, 2000, p.161.
- 65. Blechman I.I., Synchronization in Nature and Technology (in Russian), 1981, Moscow, Nauka.
- 66. Gareev F.A., Gareeva G.F., in Proc. of the 1<sup>st</sup> Intern. Workshop, Saint Petersburg, 18-21 June 2000, Sarov, 2001, p.179.
- 67. Reifenschweiler O., Phys. Lett., 1994, A184, p.149.
- 68. Schwartz H.M., J. Chem. Phys., 1953, V.21, p.45.
- 69. Karpeshin F.F., Hyperfine Interaction, 2002, V.143, p.79.
- 70. Gangrski Yu.P., Markov B.N., Nuclei on ray of laser (in Russian), Moscow, 1984.
- 71. Krivizski V.A., Transmutations of Chemical Elements in Evalutions of Earth (in Russian). Moscow, 2003.
- 72. Jones S.E., Ellsworth J.E., 10th Intern. Conf. on Cold Fusion, 2003, Cambridge, Ma: LENR-CANR.org.

- 73. Mamyrin B.A., Tolstixin I.N., Isotops of He in Nature (in Russian), Moscow, 1981.
- 74. Vysotskii V.I., Kornila A.A., Nuclear Fusion and Transmutation of Isotopes in Biological Systems, Moscow, 2003.
- 75. Perez-Pariente J., J.Scientific Exploration, 2002, V.4, p.593.
- Ratis Yu.L. Natural Science. Economy. Management. Special Issue. Samara. SSAU, 2003, p.4.; Ratis Yu.L. Ball lightening as macroscopical quantum phenomena, monography, Samara, SSC RAS, 2004, 132 p., Preprint JINR P4-2004-67, Dubna 2004, 16 p.
- 77. Smirnov B.M., UFN, 1990, V.160, N.4, p.1.
- 78. Selinov I.P. Isotopes, V.1, M: Science, 1970.
- 79. Lal D., Narasappaya N., Zutshi P.K., Nucl. Phys., 1957, V.3, p.69.
- 80. Dardik I., et al., in: Tenth Intern. Conf. On Cold Fusion. 2003, Cambridge, MA: LENR-CANR.org.
- 81. Schrodinger E. Brit. J. Philos. Sci., 1952, V.3, p.233.
- 82. Gareev F.A. Preprint No 13-98 (in Russian), Institute of Nuclear Physics, Alma-Ata, 1998, p.115.
- 83. Schrodinger E., WHAT IS LIFE? The Physical Aspects of the Living Cell, 1955.
- 84. Gareev F.A. In: ISINN-VII, Dubna, May 25-28, 1999, p.71.
- 85. Gareev F.A. JINR Communications E4-97-25, Dubna, 1997; JINR Communications E4-96-456, Dubna, 1996.
- 86. Gareev F.A. In: FPB-98, Novosibirsk, June 1998, p.92.; Gareev F.A., Gareeva G.F. In: FPB-00, Novosibirsk, July 2000, p.161.; Gareev F.A., Zhidkova I.E. In: FPB-02, Novosibirsk, July 2002.
- 87. Alon U., Surette M.G., Barkai N., Leibler S., Nature 397(1999), V.397, p.168.
- 88. Bornhold S., Sneppen K.. NORDITA preprint 99/83 CM, Copenhagen, 1999.
- 89. Pauling L. The Nature of the Chemical Bond. Cornell University Press, 1960.
- 90. Gryzinski M., In: FPB-2000, Novosibirsk, July 2000, p.89, 2001; Sprawa Atomu, Hamo-Sapiens, Warszawa, 2002.
- 91. Gryzinski M., Preciesly about Atom (in Russian), Novosibirsk, 2004.
- 92. Gryzinski M., Jour. Chem. Phys., 1975, V.62, p.2629; Phys. Lett., 1972, A41, p.69.

# Theory of the nuclear decay accompanied by the electron shake-off in the crystal

## A.Ya. Dzyublik <sup>a</sup>

Institute for Nuclear Research, Kiev, Ukraine

#### Abstract

The nuclear exponential decay accompanied by the output of shake-off atomic electrons with the energies of the order 1 eV is analyzed in the framework of the unified theory. We analyzed the shape of the energy spectra of shake-off electrons as well as of the satellite peaks in the internal conversion spectrum, associated with this shake-off. The role of the of the electron wave reflection on the frontier crystal and vacuum is studied.

#### 1. Introduction

Migdal [1] and Feinberg [2] have been the first to indicate that sudden alteration of the nuclear charge  $Z \to Z \pm 1$ , caused by the  $\beta$  decay, gives rise to emission of the atomic electrons with low energies, which are called "shake-off electrons". The same shake-off is provided also by another nuclear decays and reactions (the electron conversion or capture,  $\alpha$  decay etc.), which can be treated as sudden processes [3-9]. The shake-off probability is determined by familiar squared overlapping integral [10]. The same magnitude of such a probability is provided by the perturbation theory, if an abrupt alteration of the Hamiltonian can be regarded as a small perturbation [10]. This is valid for nuclei with large charge number Z. However, all the calculations for the shake-off of electrons are being done only in the

<sup>&</sup>lt;sup>a</sup>E-mail: dzyublik@ukr.net

first order of the perturbation theory, not taking into account the previous nuclear decay. Naturally, it would be desirable to consider the nuclear decay and subsequent shake-off as an unified process in all the orders of the perturbation theory.

Always the energy distribution of the shake-off electrons has the form of a peak centered at the energy  $\sim 1$  eV, having the width of the same order of magnitude with a smooth tail, expanding up to the energies of  $\sim 20$  eV [8, 9]. On the other hand, Porter et al. [6] investigated the distortion of the high-energy internal conversion spectrum for K electrons, caused by the emerging of the complementary shake-off electrons from the upper shells. They discovered a weak additional spectral line, shifted with respect to usual K line by the binding energy of the L electron. They interpreted this satellite as a complementary spectrum to the shake-off one.

Here we shall represent a two-step decay theory, which describes on an equal footing first the nuclear transition and then the emission of the shake-off electron. We discuss also the influence of the crystal medium on the shake-off.

## 2. Basic equations

For definiteness, below we shall talk about the internal conversion with emission of the K electron followed by the shake-off of the L electron. Their radius-vectors are **r** for the K electron and **r'** for the L one.

The Hamiltonian of the whole system (nucleus+ two electrons) is written down as

$$\hat{H}(t) = \hat{H}_0 + \hat{V}(t). \tag{1}$$

The unperturbed Hamiltonian is given by

$$\hat{H}_0 = \hat{H}_N - \frac{Ze^2}{r}g(r) - \frac{Z'e^2}{r'}g(r') + U,$$
(2)

where  $H_N$  is the Hamiltonian of the nucleus with the charge Ze; the mean field "seen" by the L electron is approximated by the Coulomb field of the nucleus with an effective charge Z'e. The factor g(r) describes the screening, having the radius R (see also [11]),

$$g(r) = \begin{cases} 1, & r < R, \\ 0, & r \gg R \end{cases} \tag{3}$$

The unperturbed Hamiltonian includes also the effective potential U, caused by the atoms of the crystal affecting on the electrons. This potential is taken to be  $U_0$ , when the shake-off electron moves inside the crystal

 $(ReU_0 < 0)$  and 0 otherwise. Since the energy of the conversed electros largely exceeds  $|U_0|$ , this potential is not significant for them.

The perturbation Hamiltonian is taken in the form

$$\hat{V}(t) = \hat{V}_c(\mathbf{r}) + \Delta \hat{H}(\mathbf{r}', t). \tag{4}$$

The first term  $\hat{V}_c$  is responsible for the internal conversion. In the Coulomb gauge it reads

$$\hat{V}_c(\mathbf{r}) = -e^2 \sum \frac{1}{|\mathbf{r} - \mathbf{r}_i|} + \frac{Ze^2}{r},\tag{5}$$

where  $\mathbf{r}_i$  are the radius-vectors of the protons in the nucleus. The second one determines the shake-off of the L electron. Following [6], we assume the K electron to screen one unit of the nuclear charge, so that after its removal from the atom at the moment  $t_1 > 0$  the Hamiltonian of the L electron suddenly attributes the additional term

$$\Delta \hat{H}(\mathbf{r}',t) = -\frac{e^2}{r'}e^{-t/\tau_R}\theta(t), \tag{6}$$

where

$$\theta(t) = \begin{cases} 1, & t > 0, \\ 0, & t < 0. \end{cases}$$
 (7)

and  $\tau_R$  is the recovery time of the hole in the K shell due to transitions of electrons from the upper levels with emission of X-Rays.

The eigenvalues  $E_b$  and eigenfunctions  $\varphi_b$  of the operator  $\hat{H}_0$  are determined by the equation

$$\hat{H}_0 \varphi_b = E_b \varphi_b. \tag{8}$$

The functions  $\varphi_b$  form a complete orthonormal set, i.e.

$$\langle \varphi_b | \varphi_b' \rangle = \delta_{bb'}. \tag{9}$$

Let at the initial moment t = 0 the system be described by the wave function

$$\varphi_a = \psi_{I_e M_e}^N(\xi) \chi_K(\mathbf{r}) \chi_L(\mathbf{r}'), \tag{10}$$

where the function  $\psi_{I_e M_e}^N(\xi)$  describes the nucleus in the excited state, while  $\chi_K(\mathbf{r})$  and  $\chi_L(\mathbf{r}')$  the electrons, moving in the K and L orbits respectively. Then the corresponding eigenvalue is

$$E_a = E_0 - A_K - A_L, (11)$$

where  $E_0$  denotes the transition energy in the nucleus,  $A_K$  and  $A_L$  the binding energies of the atomic electrons. In the intermediate state  $|c\rangle$  one has the nucleus in the ground state  $\psi^N_{I_gM_g}(\xi)$  and K electron, emitted into the continuous spectrum with the energy E. The corresponding energy equals

$$E_c = E - A_L. \tag{12}$$

In the final state  $|b\rangle$  there is also L electron, ejected from the atom as a result of the shake-off. It has the wave vector  $\vec{\kappa}$  inside the medium in the region, where the Coulomb field of the parent atom is completely screened, and k in the vacuum. This electron energy is given by

$$E' = \frac{\hbar^2 k^2}{2m} = \frac{\hbar^2 \kappa^2}{2m} + U_0. \tag{13}$$

The final energy of the whole system will be

$$E_b = E + E'. (14)$$

The wave functions of the electrons in the Coulomb field are well-known (see, e.g. [10, 11]). In particular, for the L1 electron bound in the atom, whose equilibrium position is determined by the radius-vector  $\mathbf{R}$ , the wave function has the form

$$\chi_{L1}(\mathbf{r}') = \frac{1}{\sqrt{2}} (1 - \rho/2) \exp(-\rho/2),$$
(15)

where

$$\rho = (\mathbf{r}' - \mathbf{R})/a \tag{16}$$

and

$$a = \hbar^2 / me^2 \tag{17}$$

represents the Bohr radius of the atom.

At  $\rho < R$  the radial part of the continuous wave function for the electron with the orbital angular momentum l is

$$\psi_{\kappa,l}^+(\mathbf{r}') \sim \exp(-z/2)z^l \Phi(l+1-i\xi, 2l+2; z),$$
 (18)

where  $\Phi(a,c;z)$  is the confluent hypergeometric function,  $z=2i\kappa'r$  and  $\xi$  is the so-called Coulomb parameter:

$$\xi = \frac{mZe^2}{\hbar^2\kappa}. (19)$$

## 3. Two-step decay

Since the Hamiltonian  $\hat{H}(t)$  depends on time, we cannot apply standard decay theory [11], developed for the stationary Hamiltonians. Instead one must solve time-dependent Schrödinger equation for the wave function  $\Psi(t)$  of the system

$$i\hbar \frac{\partial \Psi(t)}{\partial t} = \hat{H}(t)\Psi(t).$$
 (20)

For this aim we expand the wave function  $\Psi(t)$  in basis functions  $\varphi_b$ :

$$\Psi(t) = \sum_{b} c_b(t) \varphi_b e^{-iE_b t/\hbar} \tag{21}$$

and reduce Eq. ( ) to equation for the expansion coefficients

$$i\hbar c_b(t) = \sum_{b'} V_{bb'}(t)e^{i(E_b - E_{b'})t/\hbar} c_{b'}(t).$$
 (22)

It is useful to break the time axis by the intervals of large duration T and impose periodic boundary conditions for the Hamiltonian

$$\hat{H}(t) = \hat{H}(t+T). \tag{23}$$

and respectively for the wave function. Such procedure is quite analogous to that with quantization box, frequently used in three-dimensional space x, y, z especially in solid-body physics. Then the matrix element  $V_{bb'}(t)$  can be expanded in the Fourier series:

$$V_{bb'}(t) = \sum_{n=-\infty}^{\infty} V_{bb'}(n)e^{in\Omega t},$$
(24)

where the circular frequency  $\Omega = 2\pi/T$ , and

$$V_{bb'}(n) = \int_{-T/2}^{T/2} dt e^{-in\Omega t} V_{bb'}(t).$$
 (25)

The initial condition at t = 0 is

$$c_b(0) = \delta_{ba}. (26)$$

For the exponential decay law

$$c_a(t) = \exp\left(-\Gamma t/2\hbar\right),\tag{27}$$

where  $\Gamma$  is the width of the excited nuclear level. Following [12], we substitute (27) into Eq. (22) and replace the energies of the intermediate states  $E_c$  by their complex values  $E_c - i\Gamma'/2$ , where  $\Gamma'$  determines the attenuation

of the intermediate levels. As a result, we arrive at the following expression for the expansion coefficients:

$$c_{b}(t) = \sum_{n,m=-\infty}^{\infty} \frac{V_{bc}(n)V_{ca}(m)}{E_{c} - E_{a} + m\hbar\Omega + i(\Gamma - \Gamma')/2} \times$$

$$\left\{ \frac{1 - \exp[i(E_{b} - E_{c})t/\hbar + in\Omega t - \Gamma't/2\hbar]}{E_{b} - E_{c} + n\hbar\Omega + i\Gamma'/2} - \frac{1 - \exp[i(E_{b} - E_{a})t/\hbar + i(n+m) - /2\hbar]}{E_{b} - E_{a} + (n+m)\hbar\Omega + i\Gamma/2} \right\}$$
(28)

In our case the matrix element  $V_{ca}$ , responsible for the internal conversion, does not depend on time. Therefore at  $t \to \infty$  one has

$$c_b(\infty) = \sum_{n=-\infty}^{\infty} \frac{V_{bc}(n)V_{ca}}{\left(E_b - E_c + n\hbar\Omega + i\Gamma'/2\right)\left(E_b - E_a + n\hbar\Omega + i\Gamma/2\right)}. \tag{29}$$

For  $T \to \infty$  and  $\omega_n = n\Omega \to \omega$  we pass from the Fourier summation over n to Fourier integration:

$$\frac{1}{T} \sum_{n=-\infty}^{\infty} \to \frac{1}{2\pi} \int_{-\infty}^{\infty} . \tag{30}$$

Let us take into account that at  $T \to \infty$ 

$$V_{bc}(n) = M_{bc} \frac{1}{T} \int_0^\infty dt e^{-i\omega t - \gamma t/\hbar}, \tag{31}$$

where  $\gamma = \hbar/\tau_R$  defines the recovery width of the hole in the K shell,

$$M_{bc} = -\langle b|e^2/\rho|c\rangle. \tag{32}$$

This shake-off matrix element on the Coulomb wave functions has been calculated in a lot of papers (see, e.g., [1-4]).

Combining Eqs. (29)-(32), one easily gets

$$c_b(\infty) = \frac{V_{bc}V_{ca}}{[e' + A_L + i(\Gamma' + \gamma)/2][E + E' + A_k + A_l - E_0 + i(\Gamma' + \gamma)/2]}.$$
(33)

The transition probability to the final state  $|b\rangle$  is determined by

$$P_b(\infty) = |c_b(\infty)|^2. \tag{34}$$

## 4. Energy and angular distribution

In order to obtain the probability  $\Delta P$  of ejection of the conversed K electron and shake-off L electron in the energy intervals  $\Delta E$  and  $\Delta E'$ , respectively, within the solid angles  $\Delta \Omega_{\mathbf{k}}$  and  $\Delta \Omega_{\mathbf{k}'}$  one has to multiply  $P_b(\infty)$  by the number of final states in these intervals, namely by

$$\Delta \rho = \frac{\Delta \mathbf{k}}{(2\pi)^3} \frac{\Delta \mathbf{k}'}{(2\pi)^3} = \frac{1}{(2\pi)^6} \frac{2m^3}{\hbar^6} \sqrt{E} \Delta E \Delta \Omega_{\mathbf{k}} \sqrt{E'} \Delta E' \Delta \Omega_{\mathbf{k}'}.$$
(35)

In order to find the energy distribution of the shake-off electrons  $W_{sh}(E')$  we should integrate  $\Delta P$  over the energy of conversed electrons E. As a result one has

$$W_{sh}(E') \sim \frac{|M_{bc}(E')|^2}{(E' + A_L)^2} \sqrt{E'}.$$
 (36)

This expression describes the peak, observed in energy distribution of the shake-off electrons.

In addition, we should multiply this quantity by the transmission coefficient T(E) of the low-energy shake-off electrons through the surface of the crystal slab, containing radioactive nuclei. Let the crystal occupy the region z < 0 and the axis z be perpendicular to its surface. The wave vectors of the electron inside the crystal  $\vec{\kappa}'$  and outside it  $\mathbf{k}'$  are related by the expression (see, e.g., [13])

$$\kappa'_{x} = k'_{x}, \quad \kappa'_{y} = k'_{y}, \quad \kappa'_{z} = \sqrt{k'_{z}^{2} + 2mU_{0}/\hbar^{2}}.$$
 (37)

The penetration coefficient of the electron wave through the surface jump of the potential at z=0 is given by

$$T = \frac{4\kappa_z' k_z'}{(\kappa_z' + k_z')^2}. (38)$$

Note that  $k_z' = k' cos\theta$ , where  $\theta$  is the angle between the direction of the shake-off electron beam, emitted from the crystal, and the normal to the crystal surface. Then we see that  $T \to 0$  if  $\theta \to \pi/2$ . Recently similar angular distribution of the shake-off electrons yield has been observed experimentally by Kupryashkin et al. [9].

In order to find the energy spectrum  $W_{ic}(E)$  of the electrons, which suffered the internal conversion, followed by the shake-off electron emission, one must integrate  $\Delta P$  over E'. Such integration gives

$$W_{ic}(E) \sim \frac{|M_{bc}(E_{max} - E)|^2}{(E_{max} - E + A_L)^2} (E_{max} - E)^{1/2} T(E_{max} - E),$$
(39)

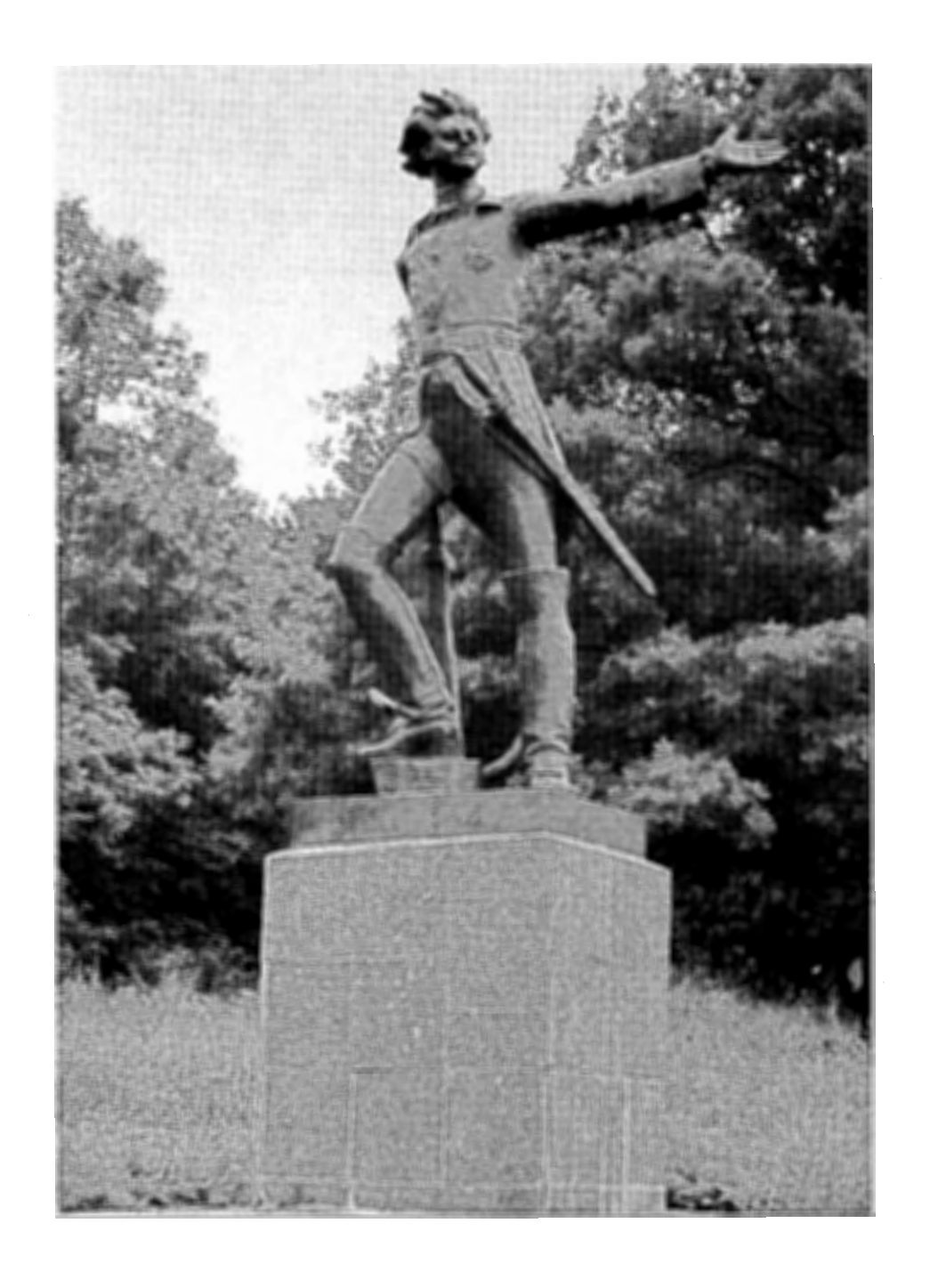
where  $E_{max}$  denotes the maximum energy of the complementary electron spectrum provided by the internal conversion,

$$E_{max} = E_0 - A_K - A_L. \tag{40}$$

The curve  $W_{ic}(E)$  describes the satellite in the spectrum of internal conversion, which is concentrated at the energy  $E_{max}$  and is shifted with respect to the central line by the binding energy  $A_L$  of the L electron. Its shape is a mirror image of that for the shake-off electrons, which occupy initially the L level. Our Eq. (39) is consistent with more intuitive calculations of Porter at al. [6].

#### References

- [1] A.Migdal, J. Phys. (USSR) 4, 449 (1941).
- [2] E.L.Feinberg, J. Phys. (USSR) 4, 424 (1941).
- [3] J.S.Levinger, Phys. Rev. 90, 11 (1953).
- [4] H.Primakoff and F.T.Porter, Phys. Rev. 89, 930 (1953).
- [5] M.S.Freedman, F.T.Porter, F.J.Wagner, and P.P.Day, Phys. Rev. 108, 836 (1957).
- [6] F.T.Porter, M.S.Freedman, and F.Wagner, Jr., Phys. Rev. C 3, 2246 (1971).
- [7] B.V.Bobykin, S.K.Lyubov, Yu.A.Nevynni, Zh. Tech. Fiz. 58, 1524 (1988).
- [8] V.T.Kupryashkin, L.P.Sydorenko, A.I.Feoktistov and I.P.Shapovalova, Izv. Russian Acad. Nauk (ser. physics) 67, 1467 (2003).
- [9] V.T.Kupryashkin, L.P.Sydorenko, A.I.Feoktistov and I.P.Shapovalova, Izv. Russian Acad. Nauk (ser. physics) 68, 1208 (2004).
- [10] L.D.Landau, E.M.Lifshitz, Quantum Mechanics (Moscow, Nauka, 1974).
- [11] M.Goldberger, K.Watson, Collision Theory (New York, J.Wiley, 1964). [12] L.D.Landau, E.M.Lifshitz, Relativistic Quantum Theory, part 1 (Moscow, Nauka, 1968).
- [13] V.I,Ignatovich, Physics of Ultracold Neutrons (Moscow, Nauka, 1986).



Nuclear excitations in plasma

# NUCLEAR EXCITATION BY ELECTRON TRANSITION IN THERMODYNAMICS EQUILIBRIUM PLASMAS

## V.MÉOT, G.GOSSELIN, P.MOREL

Département de Physique Théorique et Appliqué, Service de Physique Nucléaire CEA/DAM Ile de France BP12 91680 Bruyères-le-Châtel France

#### D.GOGNY, W.YOUNES

Lawrence Livermore National Laboratory
Livermore, California 94551, USA

A NEET model in plasma at Local Thermodynamic Equilibrium (LTE) has recently been developed. In this model, the microscopic NEET probability is described by a dynamic model. The atomic spectrum is assimilated to a gaussian distribution around the mean value of the transition energy given by an average atom model, which allows us to derive a transition rate as a function of the temperature and the density of the plasma. A complete calculation of nuclear excitation by NEET rate of the first excited state of <sup>235</sup>U in LTE plasma is presented and compared to experimental results. The variations of nuclear lifetime under LTE plasma conditions will be discussed.

#### 1. Introduction

The Nuclear Excitation by Electronic Transition (NEET) [1], observed in <sup>197</sup>Au and <sup>189</sup>Os [2], [3], is both the excitation of the nucleus and the de-excitation of the atomic system. The NEET process becomes resonant when the energy of the nuclear excited state matches the energy separation between two atomic bound states. The main difficulties in observing this effect are, on one hand, that the coupling matrix element between atomic and nuclear systems may be very low because it strongly depends on the presence of the electrons near the nucleus. On the other hand, the matching between the nuclear and electronic transitions may be poor. Because both quantities depend on the electronic configuration, the NEET and its inverse process the TEEN, probabilities could be enhanced by modifying the atomic environment of the nucleus. The hot dense plasmas where the ions undergo large changes by means of the thermodynamic conditions are ideal laboratories to observe these modifications of nuclear rates. We report here the calculation of the NEET and TEEN transition rates in thermodynamic equilibrium <sup>235</sup>U plasma.

The first state,  $J^{\pi} = \frac{1}{2}$ , of <sup>235</sup>U, located at 76.8 eV, is a good candidate to test that mechanism because it may be possible to create, through plasma ionization, an excited atomic configuration in uranium that relaxes towards the excitation of the isomeric

level. However characterizing the phenomena requires counting the excited nuclei produced in the process, and this can only be done if the lifetime of the nuclear state is long enough. This is the case for the isomeric state of the <sup>235</sup>U, with a lifetime of 26.8 minutes which allows a measurement after the system has cooled down.

Many attempts were made to observe the excitation of this isomeric level in plasma. In 1979, a Japanese group [4] claimed that they excited the nuclear level using a CO<sub>2</sub> laser. The excitation rate obtained was greater than 1 s<sup>-1</sup>. A Russian group attempted to reproduce the experiment without success, although they used a more enriched <sup>235</sup>U [5]. More recently, in a French collaboration between the CEA/DAM and the university of Bordeaux , some experiments, dedicated to the excitation of the <sup>235</sup>U isomeric nuclear level, have been performed using various lasers: a one shot Neodymium laser (300 J), called PHEBUS, located at Limeil-Brevannes (France), and a high rate YaG laser (1 J) at the CENBG (University of Bordeaux). The intensities were 10<sup>12</sup> W/cm<sup>2</sup> and 10<sup>13</sup> W/cm<sup>2</sup>. No signal could be extracted although the experimental limits for the excitation rate are appreciably lower than the previous ones [6], [7]. It is why we think that the nuclear excitation of the <sup>235m</sup>U in plasma is still an open question and need to be calculated.

In the framework of the formal theory of reaction, we described the NEET process. A crucial point in the understanding of such a process in plasma holds in a good description of characteristic times of the different physical phenomena to take into account: the NEET process itself, the atomic widths, the plasma evolution and the duration of the LTE regime. The most relevant hydrodynamic parameters, such as charge state, density or temperature were calculated under the hypothesis of Local Thermodynamic Equilibrium (LTE) using a relativistic average atom model. To get an accurate description of the statistical nature of the electronic spectrum we went beyond this model assuming a Gaussian distribution of the electronic transition around the average transition. From this approach, we derived NEET and TEEN rates depending on density and temperature.

## 2. Dynamics of the NEET process

The probability to populate a long lived nuclear excited state through its coupling with electronic transitions was calculated using the formalism presented in reference [8]. It allows describing the properties of decaying states as a function of time. The details of the calculation of the probability are made in reference [8]. We are content to give here the probability of exciting the isomeric level by NEET after a time t is:

$$P_{NEET}(\delta,t) = \frac{\left|R_{1,2}\right|^{2}}{\delta^{2} + \left(\frac{\Gamma_{1} - \Gamma_{2}}{2}\right)^{2}}$$

$$\left[1 - e^{-\frac{\Gamma_{2}t}{\hbar}} + \frac{\Gamma_{2}}{\Gamma_{1}}\left(1 - e^{-\frac{\Gamma_{1}t}{\hbar}}\right) - \frac{\Gamma_{2}\left(\Gamma_{1} + \Gamma_{2}\right)}{\delta^{2} + \left(\frac{\Gamma_{1} + \Gamma_{2}}{2}\right)^{2}} + \frac{2\Gamma_{2}e^{-\frac{(\Gamma_{1} + \Gamma_{2})t}{2\hbar}}\cos\left(\frac{\delta}{\hbar}t + \varphi\right)}{\sqrt{\delta^{2} + \left(\frac{\Gamma_{1} + \Gamma_{2}}{2}\right)^{2}}}\right]$$
with  $\tan \varphi = \frac{2\delta}{\Gamma_{1} + \Gamma_{2}}$ 

where  $\Gamma_1$  and  $\Gamma_2$  are the widths of the electronic configurations and  $\delta$  is the mismatch energy between the atomic and nuclear transition.

This expression reaches an asymptotic value after a characteristic time, given by the exponentials, lying around:

$$\tau_{\infty} = \frac{\hbar}{2} \left( \frac{1}{\Gamma_1} + \frac{1}{\Gamma_2} \right)$$

This asymptotic probability is in fact the usual expression:

$$P_{\text{NEET}}(\delta, t = \infty) = P_{\text{NEET}}^{\infty}(\delta) = \frac{\left|R_{1,2}\right|^2}{\delta^2 + \left(\frac{\Gamma_1 + \Gamma_2}{2}\right)^2} \left(1 + \frac{\Gamma_2}{\Gamma_1}\right)$$
(2)

The coupling matrix element  $\left|R_{1,2}\right|^2$  is slightly different from that of internal conversion because it depends on the energy mismatch. Its expression is:

$$\left|R_{1,2}\right|^{2} = 4\pi\alpha\omega_{N}^{2}\left(\omega_{N} + \frac{\delta}{2}\right)^{2L} \frac{2j_{2} + 1}{L^{2}[(2L+1)!!]^{2}} \left(\frac{j_{1}}{1/2} \frac{j_{2}}{-1/2} \frac{L}{0}\right)^{2} \left|R_{n_{1}\kappa_{1},n_{2}\kappa_{2}}\right|^{2} B(EL)$$

where  $R_{n_1\kappa_1,n_2\kappa_2}$  is the radial electronic matrix element and B(EL) is the reduced nuclear matrix element.

#### 3. Atomic calculations

The mismatch  $\delta$ , which characterizes the resonance, could be obtained with a relativistic average atom model. This model, first proposed by B.Rozsnyai [9], solves the Dirac-Fock equation for bound electrons, assuming the atom is in a spherical box with a radius dictated by the density. The self-consistent treatment starts with the relativistic Thomas-Fermi-Dirac model in the iterative procedure. The free electrons

are treated statistically by means of the Fermi-Dirac distribution. In such a model, the occupation numbers of electronic orbital may be non-integer and are given by the Fermi-Dirac statistics.

We applied this calculation to the excitation of the first isomeric state of  $^{235}$ U and found two atomic transitions in resonance with the nuclear transition: the  $(6d_{5/2}-6p_{1/2})$  and  $(6p_{1/2}-5d_{5/2})$ . This result is in agreement with the work presented in reference [10].

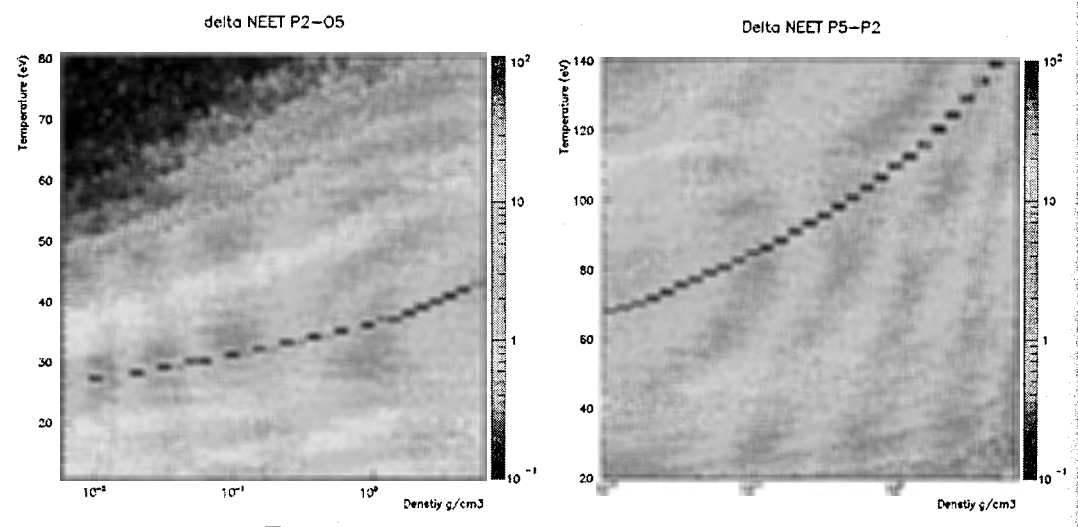


Figure 1. Mismatch  $\bar{\delta}$  for the  $(6p_{1/2}-5d_{5/2})$  and  $(6d_{5/2}-6p_{1/2})$  versus the temperature and density of the plasma

We have plotted, on figure 1 the isovalues of  $\overline{\delta}$  in the density-temperature map, for the  $(6d_{5/2}-6p_{1/2})$  and  $(6p_{1/2}-5d_{5/2})$  atomic transitions of an uranium ion. The average atom model is the first step to extract the region of interest in terms of density and temperature. On figure 1, two valleys corresponding to the  $(6d_{5/2}-6p_{1/2})$  and  $(6p_{1/2}-5d_{5/2})$  transitions under matching conditions  $(\overline{\delta}\sim 0)$  can be extracted.

The coupled atom-nucleus matrix elements  $\left|R_{1,2}\right|^2$  are also calculated in the framework of the average atom model. The coupled atom-nucleus matrix element is a slowly varying function of the density along the resonance valley observed in figure 1. It is worth around 1.9  $10^{-18}$  eV<sup>2</sup> for the  $(6d_{5/2}$ - $6p_{1/2})$  transition and around 0.6  $10^{-18}$  eV<sup>2</sup> for the  $(6p_{1/2}$ - $5d_{5/2})$  one.

## 4. NEET probability

Inside the valleys of minimum mismatch, the probability reaches its asymptotic value around 10<sup>-14</sup> s. We have to make sure that the thermodynamic conditions remain stationary during this time so that the asymptotic value has been reached before the mismatch and other atomic physics related quantities have changed. If these conditions are fulfilled, we can use the asymptotic expression to calculate the NEET

rate in the plasma. On figure 2, we plotted the asymptotic value of the NEET probability as a function of the temperature for a density of  $10^{-1}$  g/cm<sup>3</sup>.

The calculation of the NEET rate from the asymptotic NEET probability needs to go beyond the average atom model. This calculation requires taking into account the complexity of the atomic spectra. When many thermally excited states become available, the number of configurations rises dramatically and a statistical approach must be used. In this case, an average atom description does not provide an accurate description of the atomic problem because the large number of configurations tends to split the average atom transition into many components with significantly various mismatches. However, in some cases, when the number of transitions is so high that the energy difference between two consecutive configurations is smaller than their width, a strong overlap takes place. Then, a statistical approach using a distribution of the configurations around the average transition is a good approximation.

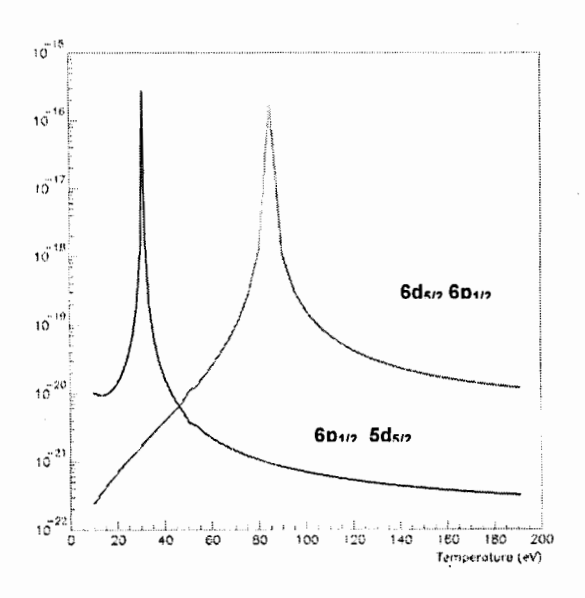


Figure 2. Asymptotic NEET probability versus temperature,  $\rho=0.1$  g/cm<sup>3</sup>, for the  $(6p_{1/2}-5d_{5/2})$  and  $(6d_{5/2}-6p_{1/2})$ .

#### 5. NEET and TEEN rates

From the asymptotic NEET probability, the NEET rate of isomer creation may be written as a sum over every initial atomic configuration  $\alpha$ :

$$\lambda_{NEET}(\rho,T_{e}) = \sum_{\alpha} P_{\alpha}(\rho,T_{e}) \frac{\left|\Gamma_{\alpha}\right|}{\hbar} \frac{\left|R_{\alpha,\beta}\right|^{2}}{\delta_{\alpha,\beta}^{2} + \left(\frac{\Gamma_{\alpha} + \Gamma_{\beta}}{2}\right)^{2}} \left(1 + \frac{\Gamma_{\beta}}{\Gamma_{\alpha}}\right)$$

where  $P_{\alpha}$  is the probability to find the  $\alpha$  configuration and  $\beta$  is the final atomic configuration after NEET has occurred.

The huge number of different configuration forbids any exact calculation. Thus the mismatch  $\delta_{\alpha,\beta}$  is described by a distribution over every possible configurations around the average atom configuration whose mismatch is  $\overline{\delta}$ . So, we replace the discrete summation over the real configurations by an integral on a statistically broadened averaged transition [12, 13, 14]. Thus we can write:

$$\lambda^{NEET}(\rho, T_{e}) = \int_{-\infty}^{+\infty} P_{\alpha}(\rho, T_{e}) \frac{\Gamma_{\alpha}}{\hbar} \frac{\left|R_{\alpha, \beta}\right|^{2}}{\delta_{\alpha, \beta}^{2} + \left(\frac{\Gamma_{\alpha} + \Gamma_{\beta}}{2}\right)^{2}} \left(1 + \frac{\Gamma_{\beta}}{\Gamma_{\alpha}}\right) \frac{1}{\sqrt{2\pi\sigma^{2}}} e^{-\frac{\left(\delta_{\alpha, \beta} - \bar{\delta}\right)^{2}}{2\sigma^{2}}} d\delta_{\alpha, \beta}$$

The energy variance  $\sigma$ , defined in reference [14], describes the dispersion of the electronic transition energy of real configurations around the average atom value.

If the energy variance is much larger than the collision widths  $\Gamma_{\alpha}$  and  $\Gamma_{\beta}$ , we may neglect the variations of the functions in every term under the integral except the first one and get:

$$\lambda^{NEET}(\rho, T_e) = \frac{2\pi}{\hbar} D_1 p_1 (1 - p_2) |R_{1,2}|^2 \frac{1}{\sqrt{2\pi\sigma^2}} e^{-\frac{\delta^2}{2\sigma^2}}$$

where D<sub>i</sub> is the i shell degeneracy.

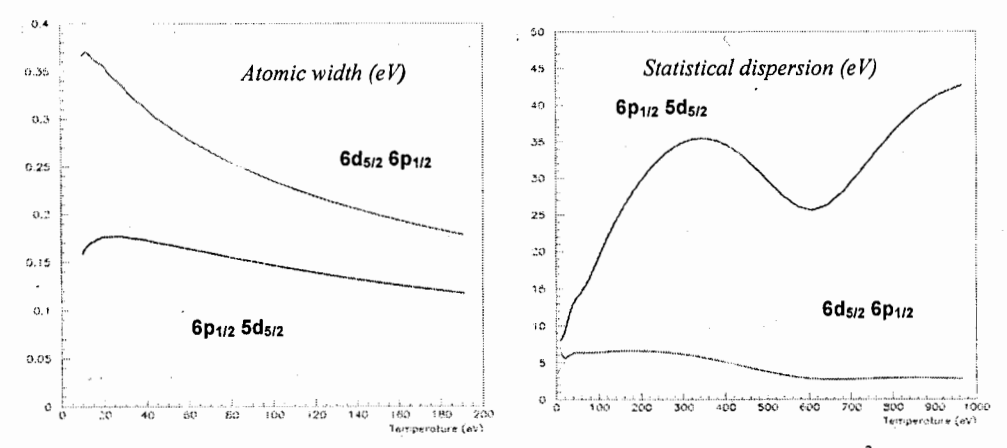


Figure 3 Atomic width and statistical dispersion versus temperature,  $\rho=0.1$  g/cm<sup>3</sup>, for the  $(6p_{1/2}-5d_{5/2})$  and  $(6d_{5/2}-6p_{1/2})$ 

We can observe that the expression of the NEET rate no longer depends on the atomic width but only on the statistical variance. The figure 3 shows the atomic widths and the statistical dispersions for both atomic transitions at  $\rho$ =0.1g/cm<sup>3</sup> as a function of temperature. We clearly see that the statistical spreading is one or two orders of magnitude higher than the atomic width.

Because we assume the thermodynamical equilibrium, the principle of the detailed balance allows calculating the inverse process of the NEET, the TEEN process or BIC for Bound Internal Conversion:

$$\lambda_{TEEN} = \frac{2J^f + 1}{2J_i + 1} \lambda_{NEET} \exp\left(-\frac{\Delta E}{kT}\right)$$

The figure 4 shows the maps of the NEET and TEEN rates for the first isomeric state of  $^{235}$ U. We clearly recognize the two favorable zones corresponding to  $(6p_{1/2}, 5p_{5/2})$  and  $(6d_{5/2}, 6p_{1/2})$ . For a given density the variations of the rates versus the temperature show large fluctuations. These variations come mainly from the evolution of the mismatch shown in figure 1. The experimental limits on the excitation rate, obtained in [6] and [7] are consistent with these calculations.

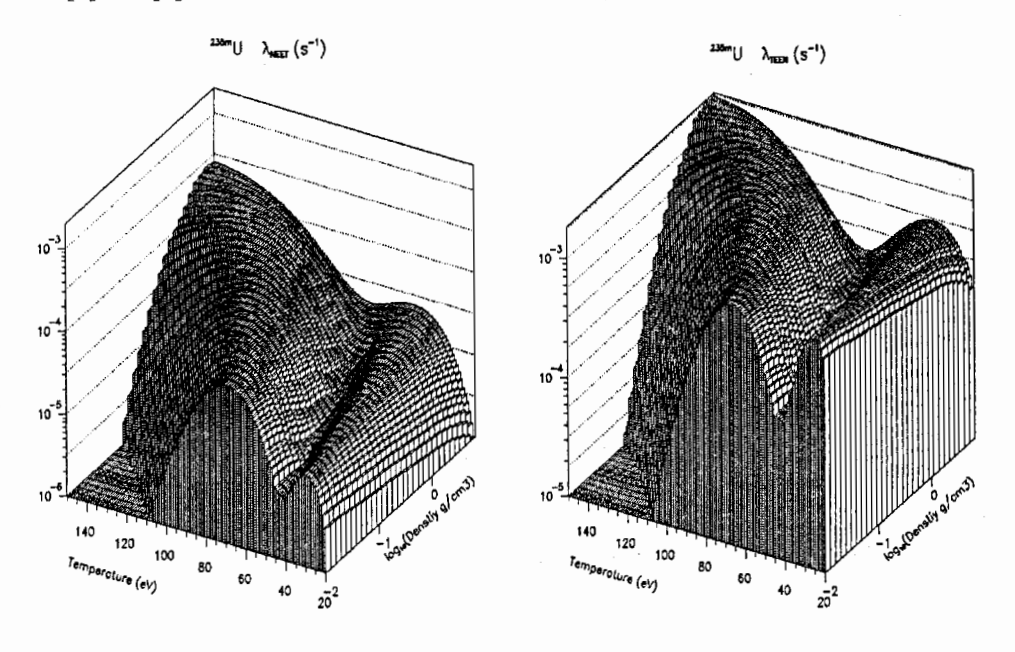


Figure 4 Maps of NEET and TEEN rates

## 6. Isomer lifetime in plasma

From the  $^{235}$ U NEET and TEEN rates we can determine the lifetime of the first isomeric state in plasma. Because the decay by internal conversion is the dominant channel ( $\alpha$ =  $10^{20}$ ) and the excitation energy of the isomer is very low, 76.8 eV, the ionization of low lying atomic shells may induce a drastic change in the half-life. On figure 5, the dashed line represents the lifetime where only the Internal Conversion is taken into account. The higher is the temperature, the higher is the lifetime. It increases by eight orders of magnitude when the temperature goes from 0 up to 70 eV. However, if we take into account the TEEN process the lifetime (solid curve) keeps rather constant until the effect of the resonant atomic transitions disappears.

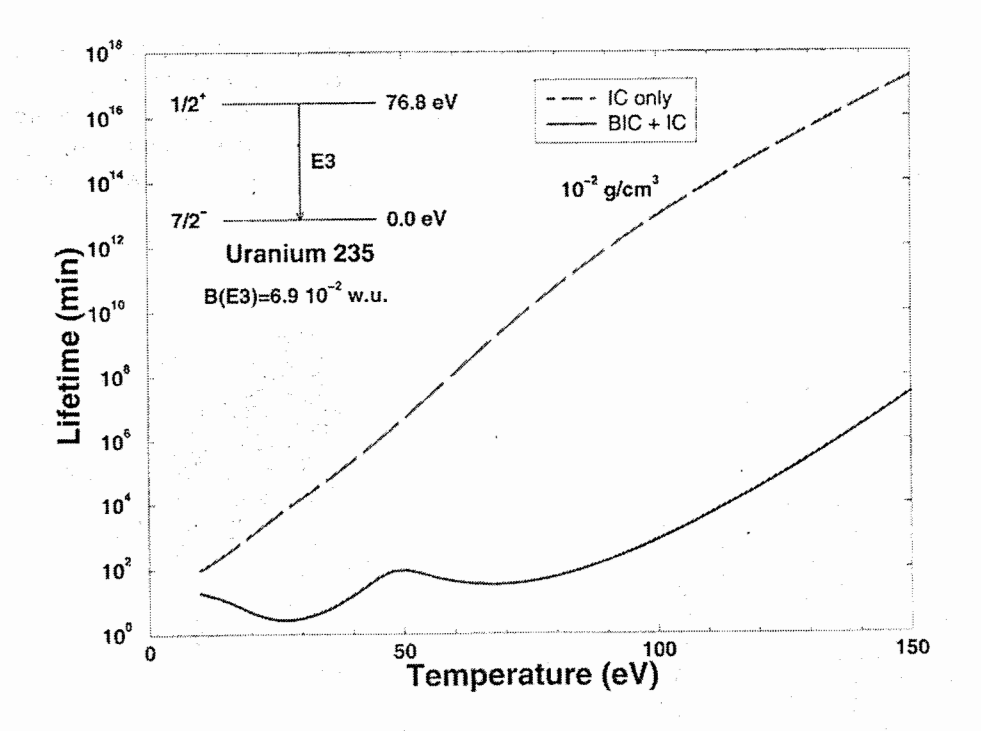


Figure 5 Lifetime of the first isomeric state of 235 U versus temperature

## 7. Conclusion

In this work, we exposed a calculation of the NEET and TEEN rates for the first isomeric state of <sup>235</sup>U in equilibrium plasma. We showed the influence of such processes on the lifetime of the isomeric state in plasma. Our calculation is in agreement with the experimental upper limits.

#### References

- 1. M. Morita, Progr. Theor. Phys. 49, 1574 (1973).
- 2. S. Kishimoto et al., Phys. Rev. Lett. 85, 1831 (2000).
- 3. K. Aoki et al., Phys. Rev. C64, 044609 (2001).
- 4. V Y.Izawa et al. Phys. Lett. 88B, 59 (1979).
- 5 R.V.Arutyunyan et al. Sov. J. Nucl. Phys. 53, 23 (1991).
- 6 V.Méot et al., CEA-R-5944 (2000)
- 7 G.Glaverie et al., Phys. Rev. C70, 044303 (2004).
- 8 P.Morel et al., Phys. Rev. A69, 063414 (2004).
- 9 G.Glaverie et al., Phys. Rev. C70, 044303 (2004).
- 10 B.F.Rozsnyai Phys. Rev. A5, 1137 (1972)
- 11 M.R.Harston and J.F.Chemin Phys. Rev. C59, 2462 (1999).
- 12 G. Faussurier et al., J. Quant. Radiat. Transfer Vol 58, 571 (1997)
- 13 G. Faussurier et al., Phys. Rev. E56, 3474 (1997).
- 14 G. Faussurier et al., Phys. Rev. E56, 3488 (1997).

# SEARCH FOR THE 6 KEV ISOMER EXCITATION AND DECAY IN A 181 TA PLASMA PRODUCED WITH A HIGH REPETITION RATE LASER.

F.GOBET, F.HANNACHI, M.M.ALÉONARD, J.F.CHEMIN, G. CLAVERIE, M.GERBAUX, G.MALKA, J.N.SCHEURER, M.TARISIEN

CENBG, CNRS-IN2P3-Université Bordeaux I, Domaine du Haut-Vigneau, 33170 Gradignan, France

F.BLASCO, F.DORCHIES, R.FEDOSEJEVS C. FOURMENT, J.J. SANTOS, D.DESCAMPS CELIA, Université Bordeaux 1, 351 Cours de la Libération 33405 Talence, France

#### V. MEOT AND P. MOREL

CEA/Service de Physique Nucléaire, B.P.12, 91680, Bruyères le Châtel, France

#### B. LIESFELD

IOQ, Friedrich Schiller University, Jena, Germany

#### L. ROBSON, S.HANVEY

Dept of Physics, University of Strathclyde Glasgow, G4 0NG, UK IOQ, Friedrich Schiller University, Jena, Germany

The possibility to excite the 6.2 keV, 6.8 µs isomer in <sup>181</sup>Ta within a plasma was studied with the high repetition rate laser available at the CELIA facility at Université de Bordeaux I. The laser is a 10mJ, 1kHz, 30fs Ti:sapphire laser. Excitation of the Ta isomer can be effective through electron excitation or photon absorption by the Ta nuclei inside the plasma produced in the interaction of the laser with solid Ta targets. We have, in a first step, characterized the photon production issued from the Bremsstrahlung of electrons for I=1-6 10<sup>16</sup> W.cm<sup>-2</sup> laser intensities. The photon spectrum extends up to 500 keV. The plasma expansion was also studied. We have used several set-ups to optimize the direct detection of the 6.2 keV gamma line which is a definite signature of the Ta de-excitation. This 6.8 µs isomer lifetime is short compared to nuclear physic electronic time scales and a special care is to be taken for the detection system in order to observe the gamma-line.

#### 1. Introduction

Nuclear excitations in plasmas have been the subject of many theoretical and experimental approaches, especially with the availability of high intensity lasers. These excitations can involve a coupling of the atomic and nuclear levels in

presence of the laser radiation. S.Matinyan made a survey of the direct use of a laser radiation for the study of low-energy nuclear physics phenomena [1]. A review of the main nuclear excitations as NEET, NEEC, photoexcitation and inelastic electron scattering in competition in a plasma was given by M.R.Harston and J.F. Chemin [2] and applied to the <sup>235</sup>U<sup>m</sup> isomer case.

Beyond these effects of the laser on the atomic/nuclear characteristics one may expect effects due to the plasma itself where electron-ions collisions and high flux of radiations are produced in the laser-solid target interaction. In the domain of femtosecond class lasers and I~10<sup>16</sup> W.cm<sup>-2</sup> intensities, hot electrons (10-500 keV) are produced and may excite, directly, low energy levels in nuclei or, indirectly, via photons produced by Bremsstrahlung (eventually through several Intermediary States (IS) higher in energy). In the noisy background of the laser-target interaction us lifetime isomers are ideal study cases since their decay can be observed after the laser pulse. The first isomeric state in <sup>181</sup>Ta at 6.2 keV is a good candidate with a lifetime of 6.8 µs. Evidence of the excitation of the isomer would be particularly interesting for subjects related to gamma-lasing or energy storage for example. A.V.Andreev [3,4] reported a large amount of excitation of the <sup>181</sup>Ta 6.2 keV isomer in two experiments with two different lasers. The 6.8 µs isomer population was estimated with an oscilloscope through the study of the scintillation detector electronic pulses rising above the background level or with a microchannel plate (MCP) coupled to a CCD camera. Both studies were conducted as a function of the time elapsed after the laser pulse (at least ~3 µs). Data were subtracted from similar measurements with a Tungsten target. Final results, obtained by fitting the 6 µs Ta isomer lifetime, lead to the excitation of  $(2 \pm 0.5) \times 10^4$  nuclei per laser shot  $(\tau = 200 \text{ fs})$  at I = 1-4 × 10<sup>16</sup>W.cm<sup>-2</sup> and  $(5 \pm 2) \times 10^7$   $(\tau = 1 \text{ ps})$  nuclei at I=3- $7 \times 10^{16}$  W.cm<sup>-2</sup> respectively. These large production rates cannot be explained by "classical" excitations due to electrons diffusion or photon resonant absorption on the Ta nuclei in the plasma. As regard the inelastic electron scattering excitation, the 6.2keV isomer can be excited, in this non-resonant process, by any electron with an energy above 6keV but the cross section is very low,  $\sigma = 10^{-31} cm^2$  for ~20keV electrons [5]; as regard the photon excitation, the cross section is higher,  $\sigma = 1.7 \times 10^{-18} cm^2$ , but the process is resonant and the energy width of the Ta isomer is  $\Gamma = 6.7 \times 10^{-11} eV$ . For a plasma volume of ~470  $\mu m^3$  (see further) and, with an estimate of 10<sup>10</sup> photons/keV/shot taken as a reference value, these considerations give  $N^* = (9 \pm 4) \times 10^{-3}$  isomer per laser shot for inelastic electron scattering and  $N^* = (10 \pm 5) \times 10^{-3}$  for photo-excitation. With these estimates in mind evidence for these excitations can only be produced with a high intensity laser with a very high repetition rate. Our intention is to search for the Ta excitation in a laser induced

plasma since A.V.Andreev results have not yet been confirmed. A first unsuccessful attempt to observe the 6.2 keV isomer excitation was done at the LUCA facility at CEA/Saclay [6] with a 20Hz, 800nm and 60fs laser. The availability of very high repetition rate laser at the CELIA facility at Université de Bordeaux I allowed a new attempt with a 1kHz Ti:sapphire laser, with a 10mJ energy and a 40 fs laser pulse duration.

We report here on the characterization of the photons produced in the interaction of the CELIA laser with the solid Ta target, in order to infer the electron spectrum as a function of the laser intensity. An attempt to measure the 6keV de-excitation, with different set-ups is also discussed.

## 2. Experimental set-ups

### 2.1. Laser performances

The CELIA Ti:sapphire laser delivers 10mJ pulses at a 1kHz repetition rate, with a wave length  $\lambda$ =800 nm. The Chirped Pulse Amplified beam is p-polarized; it is focused through a lens on a target located in the middle of the vacuum chamber. The pulse duration,  $\tau$ =40fs, was measured with a second order auto-correlator; the focal spot was  $\Phi$  = 10  $\mu m$  in diameter (at  $I_{max}/e$ ). Typical laser intensities used in this experiment were  $I\approx$  1-6 10<sup>16</sup> W.cm<sup>-2</sup>. The main pulse was preceded by a pre-pulse at 4ns with a contrast ratio of 6.10<sup>-5</sup> and the ASE contrast ratio was 3.10<sup>-7</sup>. These characteristics were measured carefully since they fix the pre-plasma conditions which influence strongly the laser-solid target interaction.

The high repetition rate imposes also to use computer driven motors for the target to have a fresh impact zone at each shot. The rotating Ta target was a 2 mm thick, 10cm diameter disc. The rotation was programmed for 50µm displacement between consecutive shots; with this value, the photons rates was steady from shot to shot.

# 2.1. Detection techniques for the photon spectra characterization

Various techniques have been implemented around the target to characterize the photon emission. The schematic set-up is presented on Fig.1. The laser incidence angle on the target could be changed. The results presented here are mainly for a 45° incidence angle. The 5.08cmx0.5cm NaI scintillation detector was surrounded by a shield of 5mm Cu and 5mm Pb defining only a 2cm aperture in the front face; a permanent magnet (not presented on the drawing) was positioned between the target and the NaI detector to avoid the contribution of electrons with energies below 1MeV. The data acquisition for this detector was triggered with the laser pulse; the energy collected in the NaI and the time signal relative to the laser trigger were registered as well as the signal of a photodiode looking at a laser beam leak before the compressor. This NaI was used as a monitor of the beam quality during the focus of the laser on

the Ta target. The photodiode was also used as a monitor in all other set-ups. The CCD camera was used to characterize the soft X-rays (1-20keV); several filters (C, Al) allowed the scanning of different energy bins. The NaI was also used to characterize hard X-rays (30-500 keV). Additional absorbers were set in front of the detector to avoid the pile-up of the high rate of low energy photons. The choice of absorbers was done by checking that, at the most, one photon was detected only each 10 shots. In addition to the X-rays characteristic studies, the plasma expansion speed was measured with two Langmuir Probes (LP) set inside the vacuum chamber at different angles.

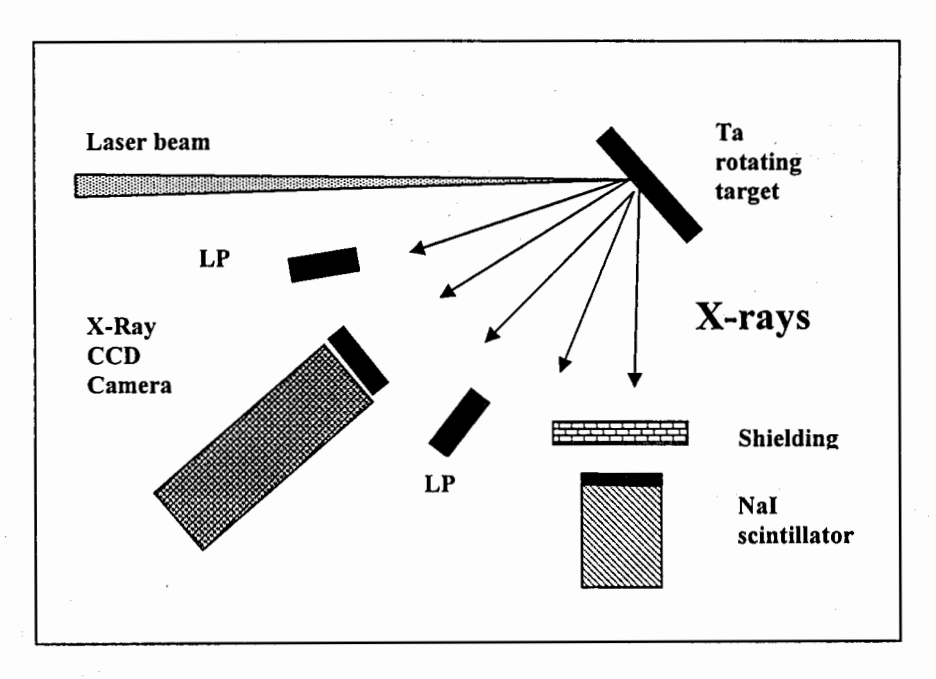


Figure 1. Schematic view of the experimental set-up for photon characterizations. LP is a Langmuir Probe to characterize the plasma.

# 2.3. Set-up for the 6.2keV isomer detection

We tried several set-up geometries to observe the 6keV isomer decay. The optimum configuration, to have less noise at low gamma-ray energies, is different from the one used by A.V. Andreev [2]. Our set-up is shown on Fig.2. The geometry is optimized to have the biggest solid angle for the NaI scintillator (with a Be entrance window). The NaI detector does not have a direct view of the bulk of the target. No front shielding of the NaI was used.

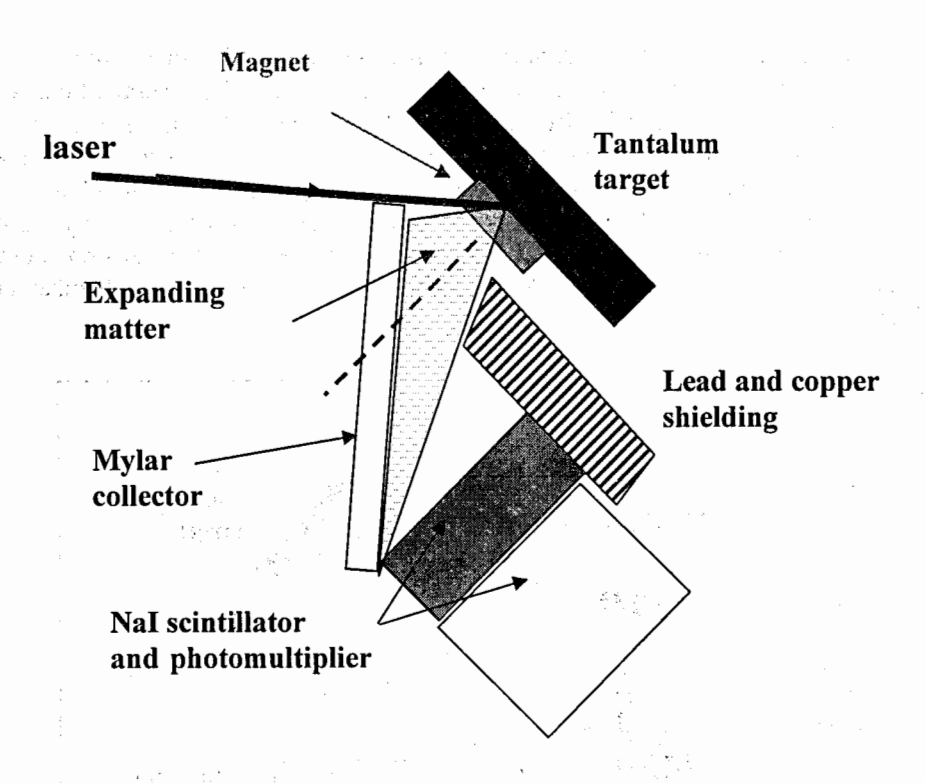


Figure 2. Schematic view of the detection geometry for the search of the 6keV isomer decay in the expanding Ta plasma. The NaI, as all other elements, is inside the vacuum chamber.

# 3. Characterization of the photon spectra and of the Ta nuclei number in the ablated matter

The soft X-rays energy distributions were measured at different laser intensities with the CCD camera (Fig.1). The study of the 6keV region was done using an Al filter ( $25\mu m$  thick). Associated X-ray spectra, corrected for efficiency and the filter absorption show a 2.5keV Maxwellian temperature in the region of 6keV photon energy [7]. This CCD allowed also estimating the number of X-rays photons produced around 6keV; the results are presented on Fig. 3. From these data there are  $\sim 2.10^5$  X-rays/keV/sr/shot. This is a too low value to expect the observation of the nuclear resonant photo-excitation in Ta, in our experimental conditions.

The characterization of the high energy photon spectra was performed using the NaI scintillator. A special care was taken to avoid pile-up detection. The initial photon energy distributions measured at different laser intensities have been unfolded to take account of the absorbers and of the response function of the NaI detector.

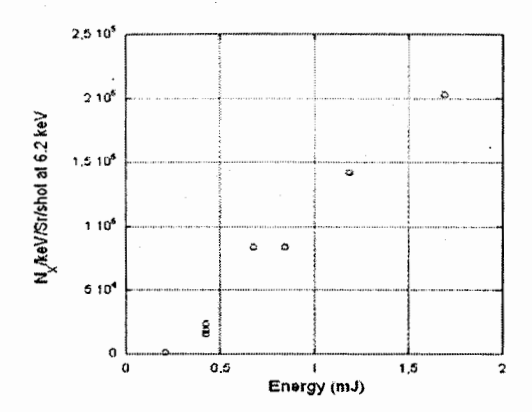


Figure 3: Number of X-rays in the 6keV energy region as a function of the laser energy on the target, as deduced from the CCD camera measurements.

The final results presented in Figure 4 show an increase in the temperature of the photon energy distributions when the laser intensity is increased. The distributions have different shapes with the development of a higher energy component for intensities on the target greater than 2.10<sup>16</sup>W.cm<sup>-2</sup>. Clearly the photon energies are higher than those predicted for the plasma emission in Ref.[8], this higher energy component can be explained with the onset of the preplasma or related to a change in the interaction such as vacuum heating [7].

A measure of the number of ablated Ta nuclei was done by collecting the matter on a  $50\,\mu m$  Mylar foil set parallel to the Ta target. This foil was then analyzed with the Rutherford BackScattering technique (RBS) with 2.3MeV <sup>4</sup>He particles at the Van de Graaff accelerator at CENBG. Figure 5 presents the measured number of ablated Ta nuclei as a function of the laser intensity. The number of Ta ions estimated from the Langmuir probe data are also presented on the same figure, in the hypothesis of a mean effective charge  $Z^*=10$  [7]. The ablated Ta nuclei number is a crude maximum value of the "possible" excited nuclei. A scaling law seems to emerge, but a more detailed analysis is needed to conclude.

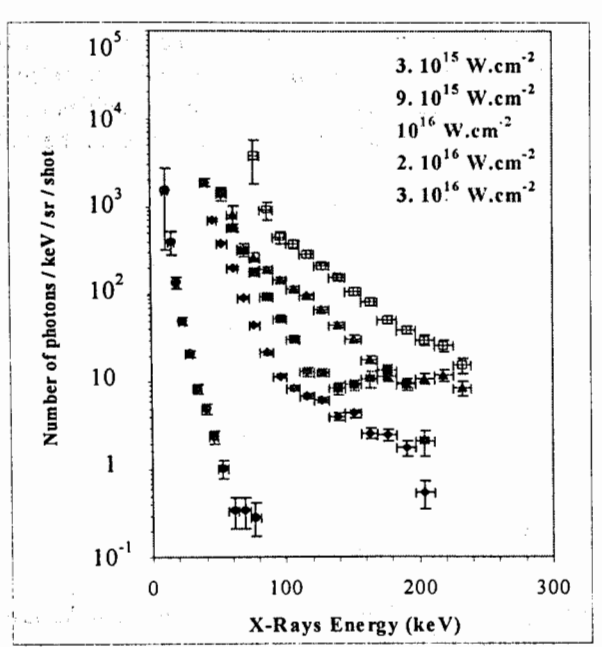


Figure 4: Photon energy distributions as a function of the laser intensity (in W.cm<sup>-2</sup>). These spectra are unfolded for the NaI response function and corrected for the presence of absorbers in front of the detector.

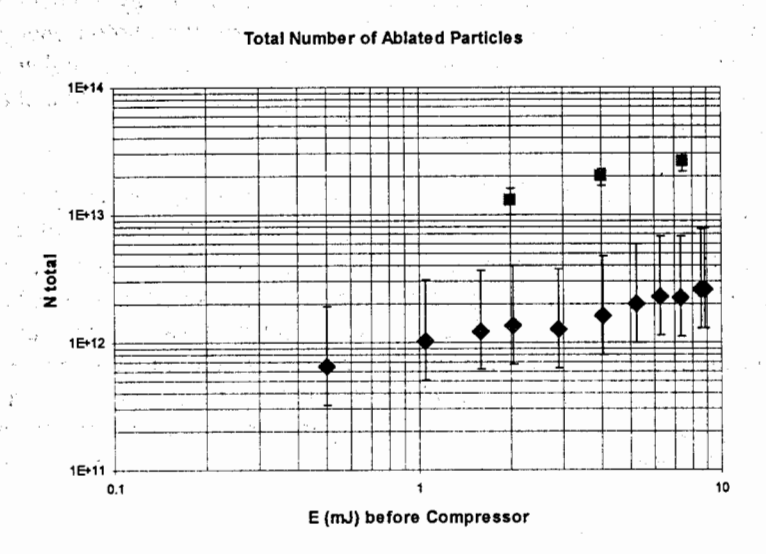


Figure 5. Evolution as a function of the laser energy: a) (squares) of the number of ablated Ta nuclei as deduced from RBS measures; b) (diamonds) of the number of Ta ions in the plasma deduced from the Langmuir probes assuming a 0.86 sr emission cone angle and a Ta average charge of 10.

# 4. Search for the 6keV isomer decay

The set-up shown in Fig.2 has been used to search for the 6keV decay of the  $^{181}$ Ta isomer. The photomultiplier high voltage was switched on just after the laser pulse. An electronic gate triggered the acquisition  $10\,\mu s$  after the laser pulse in order to let the electronic and the scintillator recover from the high radiation flux (electrons, photons) emitted at the instant of interaction. Events occurring within an  $18\,\mu s$  time window were collected. Even with these precautions background signals are still present and extend beyond 10~keV as can be seen on Fig. 6. These data were taken at a laser intensity of I  $\sim 2.5~10^{16}~\text{W.cm}^{-2}$  and result from a sequence of  $\sim 4~000~000$  shots.

This figure presents also a comparison of the hard photon spectra for a Ta target and a Tungsten target differing by only one Z unit. In this comparison one expects similar "background" spectra. This is not the case at low energy the noise is very different on the two targets. Hence, no comparison of these two targets is possible under these conditions at the contrary of the hypothesis done by A.V. Andreev [4] to infer its conclusions. We have not been able in this experiment to measure the excitation of the Ta target.

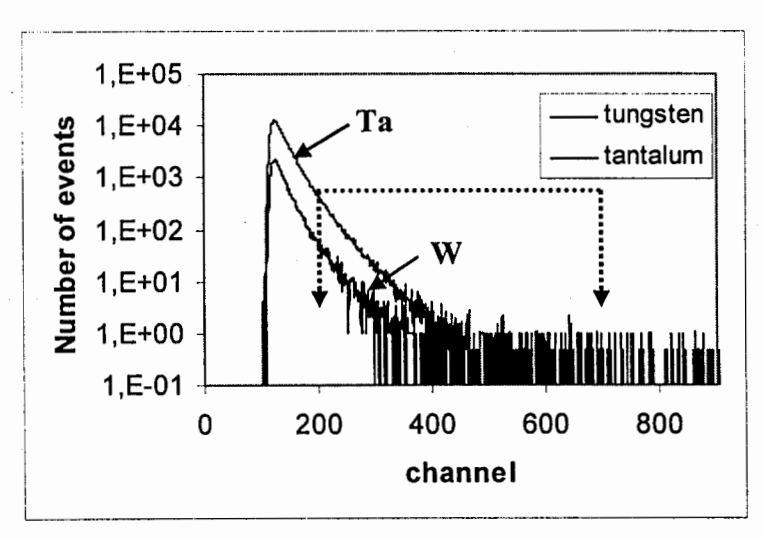


Figure 6.Photon spectra measured with a Ta and a W targets. The energy region between the dotted arrows is the 6keV region of interest.

#### 5. Discussion and conclusion

We have done a set of experiments to characterize the interaction of a 40fs high repetition rate laser and to clarify the experimental conditions for a search of the

excitation of the 6keV isomer in <sup>181</sup>Ta. We have measured the properties of the soft and hard X-rays as a function of the laser intensity. We measured also the velocity of the expansion of the plasma. All these informations conduct to a very low probability for the isomer excitation by photon resonant excitation. Within the focal spot we have ~1.5 10<sup>19</sup> Ta nuclei per cm² and per shot in the ablated matter. An X-rays amount of ~2.10<sup>5</sup> photon/keV/sr/shot (Fig. 3) in the 6keV region lead to an estimate of 0.17 isomer per 10<sup>6</sup> laser shots due to nuclear photo-excitation. This is impossible to observe in our experiment. Concerning the electron inelastic scattering, the probability to excite this isomer with electrons is also very low due to the process cross-section. More analysis is needed to obtain an estimate of the contributing electron number. The energy distribution of the electrons will be deduced from GEANT simulations reproducing the hard X-ray spectra. In any case we need to find experimental techniques which allow to avoid the detection of the prompt and very intense flux of radiation produced at the interaction time.

# Acknowledgements

This work was supported by the Region Aquitaine under contract #20040208004A.

#### References

- 1- S. Matinyan; Physics Reports 298, 199 (1998)
- 2- M.R. Harston and J.F. Chemin; Phys.Rev. C 59, 2462 (1999)
- 3- A.V. Andreev et al.; JETP Letters 69, 371 (1999)
- 4- A.V. Andreev et al.; JETP,91, 1163 (2000)
- 5- V.S. Letokhov and E.A. Yukov; Laser Physics, 4 382 (1994)
- 6- J.F.Chemin; Bilan d'activité GIAS, CEA Internal Report 2001.
- 7- R.Fedosejevs et al. 32<sup>nd</sup> European Physical Society Plasma Physics Conference, Tarragona, Spain, June 27-July 1st, 2005.
- 8- A.V. Andreev and R.A.Chalykh, Hyperfine Interactions 143, 13 (2002).

# EFFECT OF SURFACE CLEANING ON DECAY OF LOW ENERGY NUCLEAR ISOMERS EXCITED DURING FEMTOSECOND LASER-PLASMA INTERACTION

A.B.SAVEL'EV, V.M.GORDIENKO, I.M.LACHKO, A.A.RUSANOV, D.S.URYUPINA, and R.V.VOLKOV

International Laser Center and Faculty of Physics,
M.V.Lomonosov Moscow State University, Leninskie Gory, 119992, Moscow, Russia
Fax: +7(095)9393113, e-mail: ab savelev@phys.msu.ru

Decay of low energy nuclear states excited during femtosecond laser action onto the surface of a target can be much influenced by surface composition. We consider how surface cleaning could affect nuclear decay through electronic conversion (IC) process. We show that surface cleaning leads to prominent increase in charge and energy of bulk ions, eliminating signal from light ions (hydrogen). This could be used for deep IC blocking and also might help IC electrons detection.

#### 1. Introduction

During past years nuclear physics using ultra short laser pulses became one of the most "hot" and intensively investigated areas of super strong laser-matter interactions [1, 2]. A wide range of nuclear processes have been observed experimentally: from nuclear fusion and fission to photonuclear excitation and positron production. The primary source for impinging these reactions is electron acceleration up to 1 MeV and above by laser field in plasma. This happens if light intensity exceeds ~10<sup>19</sup> W/cm<sup>2</sup>. Though in the plasma produced upon irradiation of a target surface by a femtosecond laser pulse with a moderate intensity of  $10^{16}$  -  $10^{17}$  W/cm<sup>2</sup>, the electron temperature reaches 1 keV and the average energy of hot electrons is 5 - 20 keV. This hot electron component and its x-ray emission are also capable of initiating nuclear processes [1]. Among them isomeric low energy level excitation seems the most interesting one because of both fundamental physics involved and a wide set of possible applications [3, 4, 5]. Even for low energy levels of stable isotopes their characteristics could be still unclear or as yet unknown (for example only calculations exists for both lifetime and conversion coefficient of 201Hg 1.56 keV nuclear level). Usually, still fewer data are known for metastable isotopes. This means that excitation in hot dense laser plasma could provide for new methods of nuclear spectroscopy of low energy nuclear levels.

The most probable channels of decay of excited nuclei are the gamma decay and the internal electronic conversion (IC). For low energy nuclear isomeric levels the probability of the latter one exceeds the radiative transition probability by an order of magnitude and even more, depending on the energy of the nuclear transition and its multipolarity. Population depletion of electron atomic shells in plasma should result in a decrease in the total IC coefficient  $\alpha$  and an increase in the lifetime of the isomeric nuclear state. I.M.Band and co-authors [6] discussed this phenomenon in the case of

single ion in 1970. Experimental data were obtained for  $^{57}$ Fe with ion charges of 19-25 [7] and  $^{125}$ Te with ion charges up to 48 [8]. In [9, 10] we discussed the feasibility of IC blocking in the case of 1.561 keV nuclear level of  $^{201}$ Hg isotope excited under femtosecond laser plasma interaction. The measurements of  $\gamma$ -decay rate of the low-energy nuclear state in tantalum (E $\gamma$ =6.238 keV, T1/2=6.05  $\mu$ s), excited by irradiating of the target with 200 fs and  $2\cdot10^{16}$  W/cm² laser pulses was reported in [5], while IC electrons detection has not been accomplished yet.

To detect electrons emerging from IC decay of a low energy nucleus excited in hot dense plasma one needs to avoid signals coming from plasma negative particles such as electrons and negative ions. The most effective way to distinguish between IC electrons and plasma particles is time-of-flight detection with electrostatic energy separator. In fact, time-of-flight of fast plasma electrons with energies of few keV is much shorter than excited low energy nuclear level lifetime (typically greater than 10 ns). The most interfering signal comes from fast negative ions (mostly hydrogen) [11], having the same energy and comparable time-of-flight as few keV electrons from IC nuclear decay.

Ion bunches formation under interaction of ultra-short laser pulses with solid targets to date attracts considerable attention. Under moderate intensities (below  $10^{17} \text{W/cm}^2$ ), plasma ions are mainly accelerated by the ambipolar quasi-electrostatic field appearing due to the charge separation at the plasma-vacuum interface [12,13,14,15]. This field is generated by both thermal and hot electrons, and the energy spectrum of accelerated ions clearly exhibits two components usually referred to as the "slow" and "fast" ions [16,17]. Under usual experimental conditions, the target is covered with a thin surface layer consisting of oxides, hydrocarbons and water molecules. Previous investigations showed [18,19] that mainly protons and partially carbon ions are accelerated at the plasma-vacuum boundary by hot electrons. The cleaning of target surface from contaminating layer by either the resistive heating [19,20,21], ion sputtering [22] or pulsed laser cleaning [18,23] leads to acceleration of ions of target main substance.

In this paper we consider how surface cleaning could affect nuclear decay through electronic conversion process. First case is IC inhibition due to high ionic states of ion in plasma. Using clean surface one can obtain higher ionization states at the instant of plasma creation and nuclear excitation as well as prolonged ionization freezing due to higher ions velocities. Besides highly energetic negatively charged hydrogen ions emerged from femtosecond laser-plasma interaction prevent IC electrons to be detected by electrostatic time resolved technique. Surface cleaning nearly eliminates signal from all kind of hydrogen ions.

# 2. Experimental setup

The diagram of experimental setup is shown in Fig.1. The p-polarized 616-nm radiation from the femtosecond dye-laser system, delivering pulses with a 200-fs duration and energy of 0,5 mJ [24], was focused onto the target at an angle of 45 degrees, providing the peak intensity at the target of  $3 \cdot 10^{16}$  W/cm<sup>2</sup>. The energy density

of 10 ps ASE prepulse was less than 0.2 J/cm². To clean target surface we used the radiation of XeCl excimer laser ( $\tau_p$ =30ns, E=20mJ,  $\lambda$ =308nm, W=3J/cm²), which passed ahead of femtosecond laser pulse by 100 $\mu$ s. The energy of cleaning laser pulse and time delay between cleaning and femtosecond laser pulses were chosen from our previous experiments [18]. The cleaning laser pulse was focused in spot with 500  $\mu$ m diameter in the target area coinciding with focal spot of femtosecond radiation. We used tungsten target in our experiments. The target was placed in the vacuum chamber with the residual-gas pressure not higher than 2·10<sup>-5</sup> Torr. After each laser shot the target was shifted by 100  $\mu$ m.

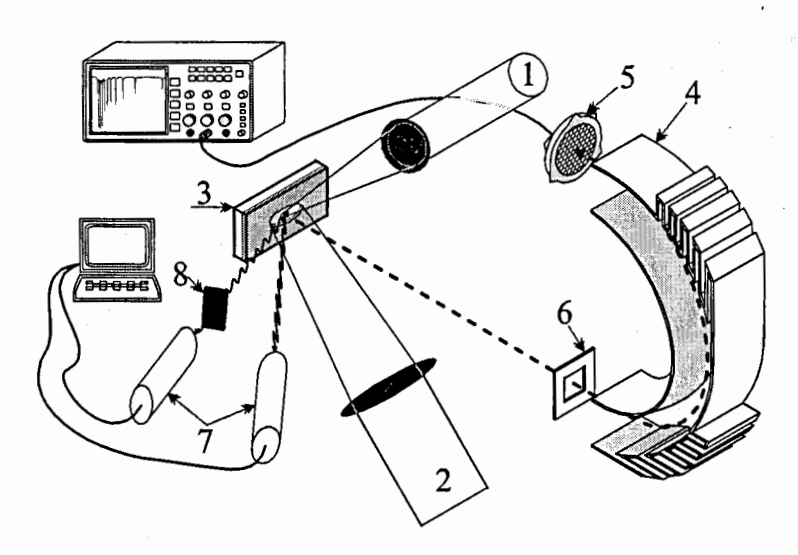


Fig. 1. Diagram of the experimental setup: 1 - femtosecond laser pulse, 2 - cleaning laser pulse, 3 - target (Si or W), 4 - electrostatic mass spectrometer, 5 - micro-channel plate, 6 - aperture, 7 - Nal(Tl) x-ray detectors, 8 - x-ray filters.

Ion currents from the plasma were detected in the line of target normal by the electrostatic time-of-flight spectrometer, described in detail in [25]. This spectrometer consisted of the semi-cylindrical analyzer including the chevron micro-channel plate (MCP), which served as a detector of ions. The full distance between the target and MCP was 62 cm. Each ion trace, detected at a certain voltage on the plates of the analyzer (which will be hereafter called "the analyzing voltage"), was treated with the time-of-flight technique. For every negative peak in the MCP signal, corresponding to a certain instant of the detection (i.e. time of ion flight), we determined the ion energy E and mass-to-charge ratio E0. With E1 was a constant of the formulae:

$$t = e\sqrt{\frac{M}{Z}}\sqrt{\frac{k}{2U}} \quad \text{sec,}$$

$$E = kUZ \quad \text{eV}$$
(1)

where U is the analyzing voltage, t is the time of ion flight, e is the electron charge;  $k=3.9\pm0.4~{\rm eV/V}$  is the constant determined from the geometry of the analyzer. The analyzing voltage was varied from 0.1 to 8.5 kV, thus ensuring the detection of ions with the values of energy-to-charge ratio E/Z of  $0.4-33~{\rm keV}$ . The relative energy resolution of the spectrometer was equal to 8% FWHM. The solid angle of registration was  $8\cdot10^{-4}$  steradian.

Jointly with ionic current measurements we registered hard x-ray yield by means of two channel analyzer based on pair of NaI(Tl) detectors with different X-ray bandpass filters (Al, Be). The measurements of hard x-ray permit us to estimate hot electron temperature in each laser shot [26]. We experimentally observed that these quantities are nearly the same in both cases being equal to  $\gamma$ =10<sup>-6</sup> % and  $E_e^{(hot)}$ =7±2 keV, respectively. Thus, we conclude that the pulsed laser cleaning strongly changes only the elemental composition of plasmas and does not influence the properties of hot electrons.

## 3. Experimental results

Figure 2 shows typical ionic currents from tungsten plasmas registered by electrostatic spectrometer. One can see that with increasing energy per charge mean ion charge also increases. For ion energy per charge of 1.8 keV (figure 2a) W ions with charge from 1+ to 7+ were registered. For energy of 10.1 keV per charge (fig. 2b) ion charge increases up to 26+. The maximum charge of W ions registered in our experiments reaches of 29+ (ionization potential ~800eV). The maximum energy of registered ions reaches 980 keV. Besides, ionic currents contain small amount of carbon, oxygen and hydrogen ions. The full amount of contaminant ions does not exceed of 2.5% from all ions. Among all contaminant's ions fully stripped ions are observed (ionization potential of O<sup>8+</sup> ion is 870 eV, ionization potential of C<sup>6+</sup> ion is 490 eV). Figure 2 also shows ionic currents from uncleaned tungsten target (fig. 2d). Comparing signals from uncleaned and cleaned target, one can easily reveal the following striking changes in the current from the front of the cleaned target: (i) an essential increase in the main substance ion energy, (ii) broadening of the charge distribution, (iii) growth of the mean charge, (iv) presence of the deeply ionized ions.

In order to reconstruct the full energy spectrum of ions for each ion charge, we registered ion traces for the spectrometer analyzing voltage varying in the range from 0.1 to 8.5 kV. This corresponds to ion energies per charge from 0.4 to 33 keV. At each value of the analyzing voltage at least 20 ion traces have been collected. For every peak in an ion trace, obtained at a fixed value of voltage, the ratio M/Z was unambiguously (one for each peak) determined using Eq.1. After obtaining the ion charge Z, we found the ion energy and then calculated the integral under the peak value of the ion trace and averaged the result over all laser shots at a fixed analyzing voltage.

Figure 3 shows energy spectra of of tungsten ions for charges of 2,9,19,24. One can easily distinguish two components: slow and fast ions. One can also notice that

ions with small charges are accelerated mainly by thermal electrons while ions having big charges are accelerated by hot electrons.

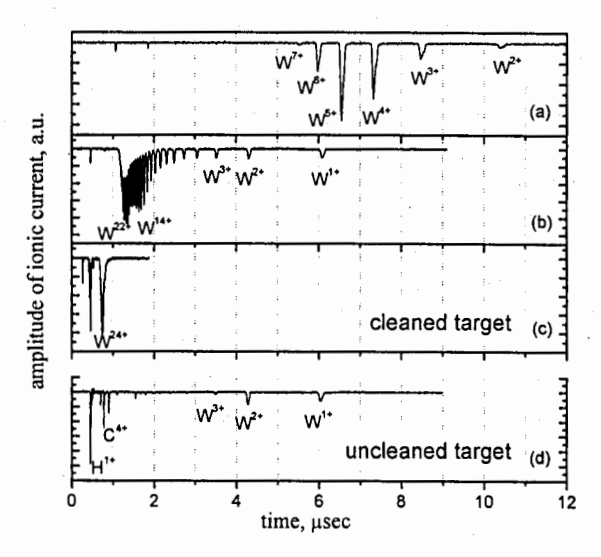


Fig. 2. Typical ionic currents from tungsten target (a, b, c - cleaned target, d - uncleaned target;  $a - E_{ion}/Z = 1.8 \text{ keV}$ , b,  $d - E_{ion}/Z = 10.1 \text{ keV}$ , c -  $E_{ion}/Z = 28 \text{ keV}$ .

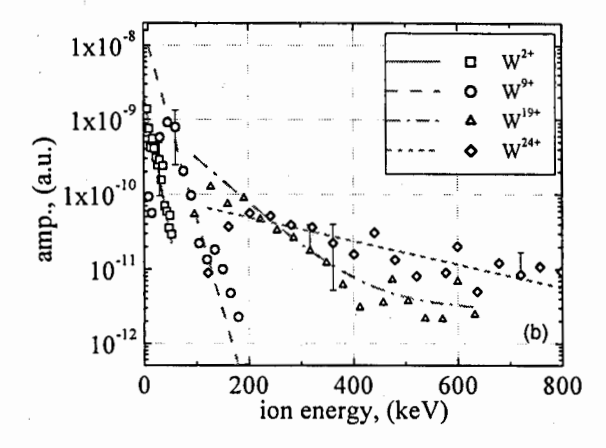


Fig. 3. Energy spectra of ions from tungsten plasma and its exponential fit.

The energy  $E_i$  gained by an ion with a charge Z during its acceleration at the plasma-vacuum interface is proportional to the mean energy of plasma electrons  $E_e$ : In the case of the plasma with the 1D Maxwellian electron population the energy spectrum of ions with the charge Z can be approximated by the exponential curve [12,13,14,15,17]:

$$f_i(E_i) \propto \exp\left\{-E_i/2ZE_e^{(thermal,hot)}\right\},$$
 (2)

where  $E_e^{\text{(thermal)}}$  and  $E_e^{\text{(hot)}}$  are the mean energies of thermal and hot electrons, respectively. In addition, traveling from the plasma to the MCP detector, the ion recombines; as a consequence, the charge state of ions at the instant of detection is different from that at the instant of the ion acceleration in the plasma. Therefore, the mean energies of electrons  $E_e$  can not be directly determined from the energy spectra of ions with the given charge Z. This fact is illustrated by Fig. 4, which presents the dependences of the mean energy and mean energy-to-charge ratio of slow ions on their charges at the instant of detection. Although all the ions of different charges gain approximately the same energy per charge during the acceleration [4], the subsequent recombination proceeds faster in the case of slower ions, inasmuch as they occur in the higher electron-density region and the time of their flight to the detector is longer. Indeed, from Fig. 4 one can see that the mean ion energy increases with the charge, while the mean ion energy per charge decreases with charge as a result of recombination. Increasing of energy-to-charge ratio for tungsten ions with charge more then 8+ caused by acceleration of such ions by hotter part of thermal electrons.

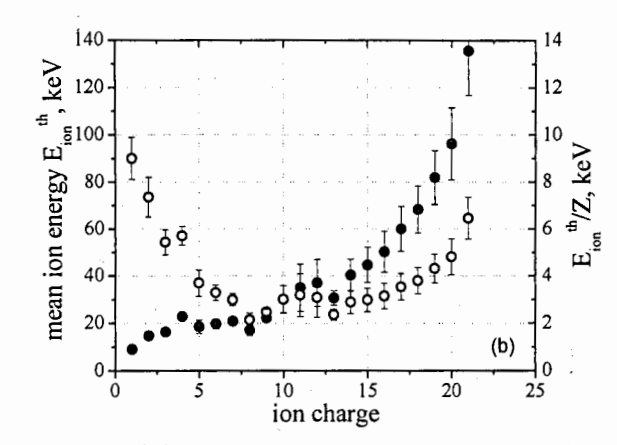


Fig. 4. Mean energy of slow ions (•) and their mean energy-to-charge ratio (o) as functions of the ion charge at the instant of detection for the tungsten target.

At the same time by fitting the energy spectra of the fast ions with the exponential function we found that  $E_e^{(hot)}$  does not depend on the charge (see Fig. 5). At the average, the value of  $E_e^{(hot)}$  is equal to  $5.6\pm1.2~\rm keV$  for tungsten plasma (see dashed horizontal line in Fig.5). This value well agreed with value of hot electron energy obtained from x-ray measurements. Thus, the fast ions really gain the same energy per charge and the measured charge distribution of fast ions is equal to that occurring in the plasma at the instant of acceleration. The charge spectrum of fast ions is shown in Fig. 6.

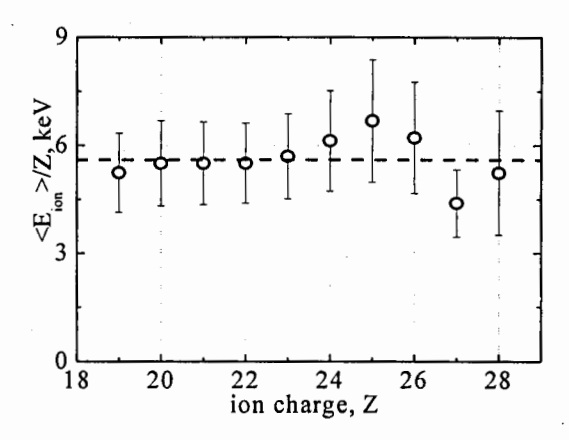


Fig. 5. Mean energy-to-charge ratio of fast ions as a function of the ion charge (dashed straight line corresponds to hot electron energy average value, see text.

### 4. Numerical simulation of plasma dynamics

To describe plasma expansion we used two numerical codes. First one models the interaction of power ultrashort laser pulse with a solid target [27]. The code takes into account laser-radiation absorption at the moving plasma-vacuum interface, the ionization kinetics, flux-limited Spitzer and ballistic thermal conductivity, electron-ion heat exchange and hydrodynamic plasma expansion. Input parameters of the code are the intensity, wavelength, polarization and duration of the laser pulse as well as the elemental composition and density of the target. All the calculations were made for the input parameters meeting the experimental conditions. Code permits us to consider plasma dynamics on a sub-picosecond time scale.

To model the process of ions recombination during plasma expansion we used the second numerical code [28]. This code calculates hydrodynamic plasma expansion into vacuum or low-pressure neutral gas on the nanosecond time scale, taking into account the ionization and recombination kinetics, thermal conductivity and electron-ion heat exchange. It uses the results from the previous code [27] as an input data. Both codes do not include hot electrons since their contribution to the plasma energy balance does not exceed one percent in our experimental conditions [29].

So our consecutive numerical simulation allows us to investigate spatial and temporal profiles of electron temperature, ion concentration and mean charge of ions in plasma and far from plasma. Finally, to estimate ion charge distribution we exploited Saha equation. Saha equation is valid for the equilibrium-state plasma and in our case it predicts wider charge distribution. Since we experimentally found that fast ions do not recombine during plasma expansion and their charge distribution repeats plasma charge distribution then we can compare fast ions charge distribution with charge distribution obtained from Saha equation. We calculated charge distribution for

electron temperature corresponding to the laser pulse maximum and for ion density in the area of fast ions acceleration, i.e. plasma corona.

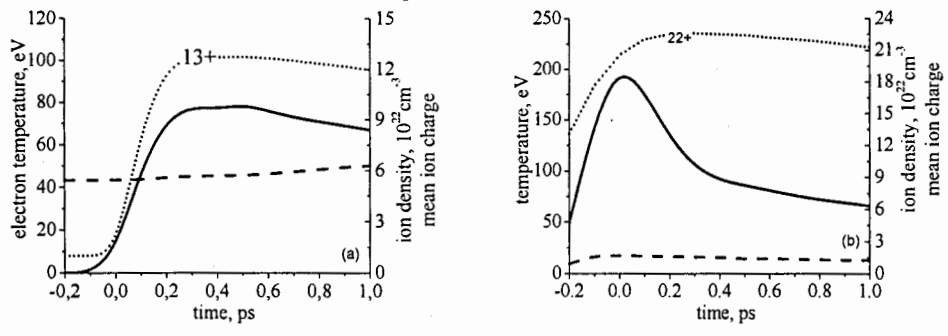


Fig. 6. Temporal profiles of ion concentration (dashed line), electron temperature (solid line) and mean ion charge (dotted line) in tungsten plasma at the target surface (a) and at a plasma depth of 60 nm (b).

Firstly we considered spatial and temporal changes of electron temperature, mean ion charge and ion concentration for the instant of laser pulse interaction with target. The results of calculation of temporal dynamics of T<sub>e</sub>, n<sub>ion</sub> and Z at the target surface (x=0) and deeper into the target (-60 nm) are shown in figure 6. One can see that ions at the target surface gain mean charge of 22+ while deeper into the target ion mean charge reaches only 13+. We assume that hot electrons accelerate mainly ions situated over the target surface, i.e. in the area of hot electron acceleration. The result of calculation of ions recombination during plasma expansion is presented in fig.7a. Here one can see the dependence of mean ion charge on ion velocity: fast ions do not recombine during expansion and their experimentally measured mean charge is as high as 23+.

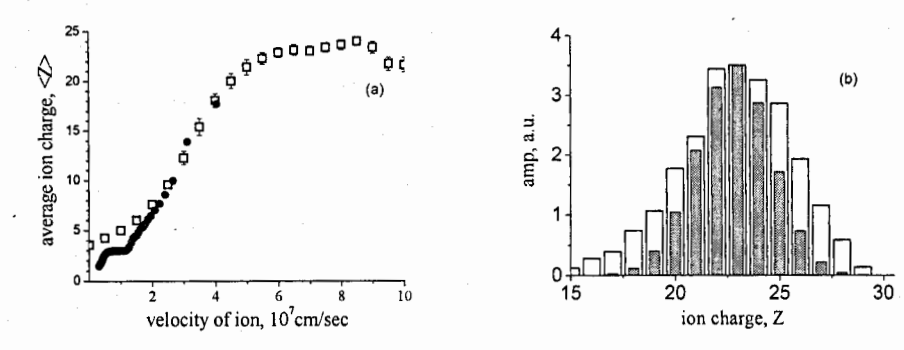


Fig. 7. Average ion charge of W ions as a function of the ion velocity ( $\square$  - experimental data,  $\bullet$  - calculated data) (a) and charge distribution of fast ions (open columns - experimental data, gray columns - calculated data) (b).

The results of calculation of ion charge distribution are shown in figure 7b. Experimentally measured charge distribution of fast ions is wider then calculated one. Broadening on the low charge (left) side of distribution can be easily understand from recombination of small part of highly charged ions. At the same time, the distribution broadening on the high charge side can not be attributed to any income from impact ionization. Alternatively, high ionization multiplicity of part of tungsten ions can be connected with barrier suppression ionization at the target surface by electrostatic ambipolar field. Such ionization mechanisms was considered in [19] for ions flying out from rear side of a target irradiated by fs laser pulse with intensity more than  $10^{19}$ W/cm². Our estimations show that ambipolar field can exceed field in the ion up to 28+ ion of tungsten [30].

#### 5. Concluding remarks

Our experiments revealed strong dependence of ionic current from laser-produced femtosecond plasma on the presence of contamination (or oxide) layer at the top of the target. With relation to internal conversion decay of low energy nuclear levels excited in plasma such a dependence could be crucial at various aspects. From one hand by surface cleaning one can achieve more bulk ions (possessing low energy nuclear state) in hot plasma region thus enhancing excited nuclei yield. Moreover, as it follows from our experiments, at cleaned surface the interaction of hot electrons with bulk ions becomes more efficient — more bulk ions are located in the same plasma volume as hot electrons are. This also should lead to an increase in the number of excited nuclei.

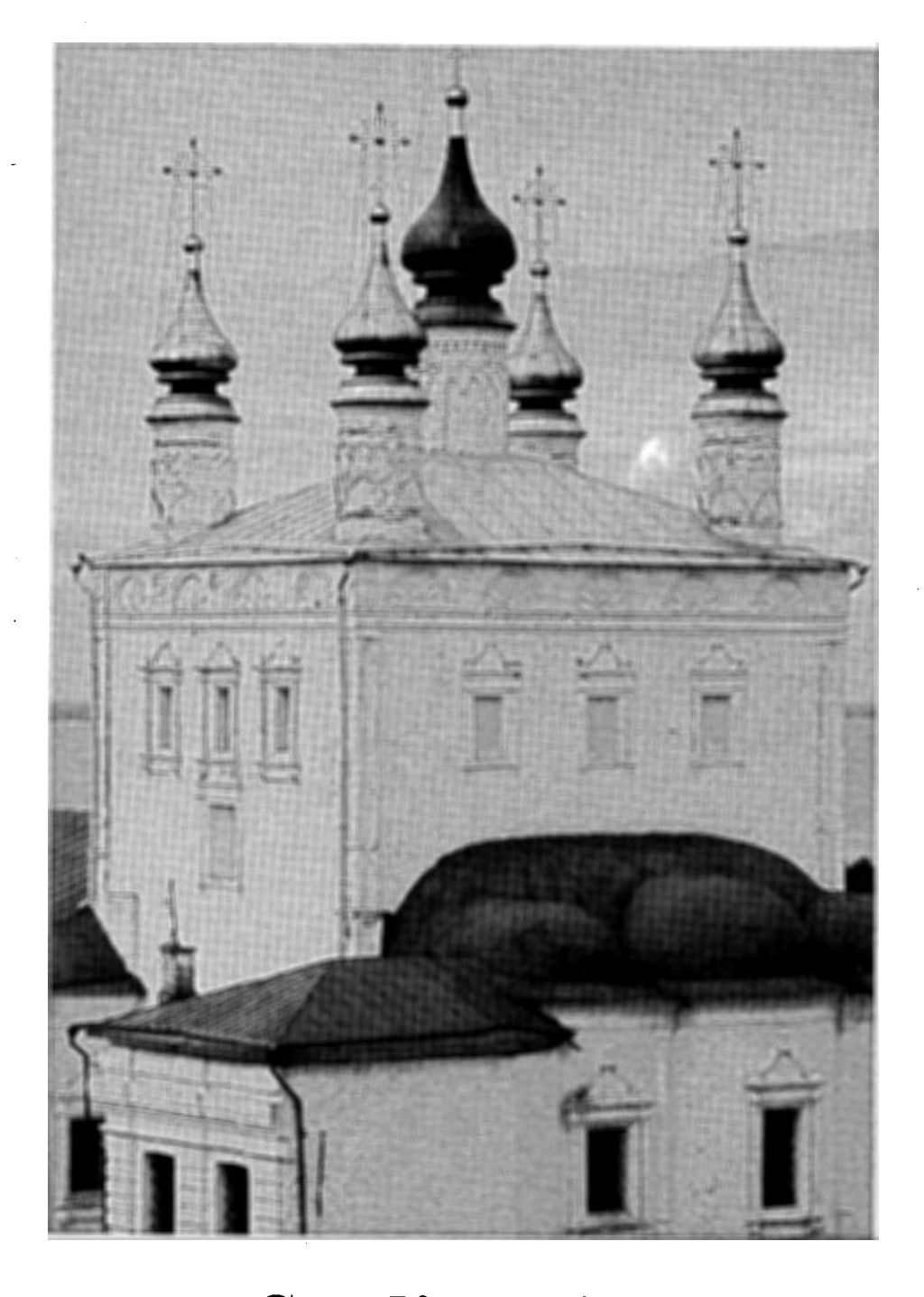
From another hand fast light ions, which come mostly from contamination layer have time-of-flight that is comparable to the low energy nuclear level life-time. Thus elimination of contaminant layer greatly decreases the "noise" signal from negative ions. It is this signal mostly preventing IC electrons detection by electrostatic time-of-light separator in the case of <sup>57</sup>Fe or <sup>181</sup>Ta isomeric levels. Finally the observed increase in the charge multiplicity of fast bulk ions could enhance IC blocking giving rise to gamma decay events. The appropriate candidate to observe this phenomenon could be <sup>201</sup>Hg isomeric state.

# Acknowledgements

This work was supported by ISTC-EOARD (grant 2651p) and Russian Fund for Basic Research (grant 04-02-16341a), I.M.L. was also supported by INTAS (grant 03-55-1982).

#### References

- 1A.V. Andreev, V.M.Gordienko, A.B.Savel'ev, Quantum electronics, 31 941 (2001).
- 2 K. W. D. Ledingham, P. McKenna, R. P. Singhal, Science, 300 1107 (2003).
- 3 A.V. Andreev, V.M. Gordienko, A.M.Dykhne, et al., JETP Lett., 66 331 (1997).
- 4 A.V. Andreev, V.M.Gordienko, A.B.Savel'ev, Laser Physics, 10 557 (2000).
- 5 A.V. Andreev, R.V.Volkov, V.M. Gordienko, et al., JETP Lett., 69 371 (1999); JETP, 91 1163 (2000).
- 6 I.M. Band, L.A. Sliv, and M.B. Trzhaskovskaya, Nucl. Phys., A156 170 (1970).
- 7 W.R. Phillips, J. Copnell, D. W. Banes, et al., Phys.Rev, A47 3682 (1993).
- 8 F. Attalah, M. Aiche, J.F. Chemin, et. al, Phys. Rev. Lett., 75 1715 (1995); Phys. Rev., C.55 1665 (1997).
- 9 A.V.Andreev, V.M.Gordienko, A.B.Savele'v, et al, Quantum Electronics, 31 567 (2001).
- 10 A.V. Andreev, O.V. Chutko, A.M. Dykhne, et al, Hyperfine interactions, 143 23 (2002).
- 11 R.V. Volkov, V.M.Gordienko, I.M.Lachko, et al, JETP Lett., 76 171 (2002).
- 12 A.V. Gurevich, L.V. Pariiskaya, L.P. Pitaevski, JETP, 49 647 (1965).
- 13 A.V. Gurevich, A.P. Mestserkin, JETP, 80 1811 (1981).
- 14 P. Mora, Phys. Rev. Lett., 90 185002 (2003).
- 15 M. Passoni, V.T. Tikhonchuk, M. Lontano and V.Yu. Bychenkov, Phys. Rev., E69, 026411 (2004).
- 16 L.M. Wickens, J.E. Allen, Phys. Rev. Lett., 41 243 (1978).
- 17 V.F.Kovalev, V.Yu. Bychenkov, Phys. Rev. Lett., 90 185004 (2003).
- 18 R.V. Volkov, D.M. Golishnikov, V.M. Gordienko, et al, Quantum Electronics, 33 981 (2003).
- 19 M. Hegelich, S. Karsch, G. Pretzler, et al, Phys. Rev. Lett., 89 085002 (2002).
- 20 F. Begay, D.W. Forslund, Phys. Fluids, 25 1675-1685 (1982).
- 21 M. Zepf, E.L. Clark, F.N. Beg, et al, Phys. Rev. Lett., 90 064801 (2003).
- 22 M. Allen, P.K. Patel, A. Mackinnon, et al, Phys. Rev. Lett., 93 265004 (2004).
- 23 R. Dinger, K. Rohr, H. Weber, J.Phys.D: Appl.Phys., 17 1707 (1984).
- 24 R.V. Volkov, V.M.Gordienko, M.S. Dzhidzhoev, et al, Quantum Electronics, 27 1081 (1997).
- 25 V.M. Gordienko, I.M. Lachko, P.M. Mikheev, et al, Plasma Phys. Control. Fusion, 44 2555 (2002).
- 26 R.V.Volkov, S.A.Gavrilov, D.M.Golishnikov, et al, Quantum Electronics, 31 241 (2001).
- 27 V.M. Gordienko, M.A. Joukov, A.B. Savel'ev et al, in: Application of High Field and Short Wavelength Sources, p.155 (Plenum Press, New York, 1998).
- 28 A.A. Rusanov, A.B. Savel'ev, Laser Physics, 14 1466 (2004).
- 29 A. Varanavicius, T.V. Vlasov, R.V. Volkov, et al, Quantum Electronics, 30 523 (2000).
- 30 R.V. Volkov, V.M.Gordienko, I.M.Lachko, et al, JETP Lett., 81 708 (2005).



Studies with Mössbauer techniques

# EXPERIMENTAL OBSERVATION OF LASER-INDUCED EFFECTS IN CaF<sub>2</sub>:Eu<sup>3+</sup> SINGLE CRYSTALS

## FARIT VAGIZOV1,2

<sup>1</sup>Physics Department, Texas A&M University, College Station, Texas 77840, USA <sup>2</sup>Kazan State University, Kazan 420008, Russia

ROMAN KOLESOV<sup>1,3</sup>, SILVIU OLARIU<sup>1,4</sup>, and OLGA KOCHAROVSKAYA<sup>1,3</sup>

<sup>3</sup>Institute of Applied Physics of the Russian Academy of Sciences, Nizhny Novgorod, 603600, Russia <sup>4</sup>National Institute of Physics and Nuclear Engineering, 077125 Magurele, Bucharest, Romania

In search of laser-induced effects caused by changes in the hyperfine interaction due to electronic excitations, Mössbauer spectra of  ${\rm CaF_2:Eu^{3^+}}$  single crystals were recorded. A Nd:YLF laser was used to illuminate the  ${\rm CaF_2:Eu^{3^+}}$  sample with 527 nm laser radiation, and fluorescence and absorption optical spectra were recorded. The Mössbauer spectrum observed in the presence of the laser radiation showed a reduction of the central peak intensity and an appearance of weak shoulder at the right wing of the resonance line. The latter might correspond to a certain contribution from the europium ions in the excited state  $^5D_0$ . However the amplitude of this shoulder was less than the value of experimental error (±0.1 %), while reduction of the central peak intensity was about 0.15 %. Therefore, we attribute the observed Mossbauer spectrum transformations mainly to the decrease of the recoil-free fraction as the temperature grows due to laser heating. The statistical significance of the electronic excitation effect under 1.2 W laser irradiation is not yet sufficient.

#### 1. Introduction

One of the most interesting and rapidly developing fields in quantum optics and laser physics deals with interference phenomena in multilevel coherently-driven atomic systems. They include electromagnetically induced transparency, lasing without inversion, and ultra-slow group velocity of light [1]. It would be very attractive to extend these ideas into two new directions, namely to the nuclear matter and to the novel range of wavelength of radiation shorter than 1Å where no coherent sources of radiation are available today.

Recently, a new spectroscopic technique was proposed in [2], which deals with modifications of the Mössbauer spectra under the action of laser radiation. The modifications can appear as a suppression of gamma-ray absorption, the appearance of additional or vanishing of existing lines in a Mössbauer spectrum, changes in linewidths and line positions, and additional splitting of the lines.

The laser-induced spin transition is a well-known phenomenon in the coordination chemistry of solids [3]. It occurs in various types of transition metal ion-activated compounds, demonstrating light-sensitive electronic structural transformation accompanied by substantial changes of magnetic and optical properties, as well as drastic modifications of Mössbauer absorption spectra. These changes can be

interpreted in terms of the laser-induced redistribution of the population of vibronic sublevels of high- (HS) and low-spin (LS) states.

There is also another type of compounds attractive for observation of laser-induced effect by means of Mössbauer spectroscopy. These are so-called Jahn-Teller crystals, where the configurational instability due to the Jahn-Teller effect can also result in many metastable electronic states, which can be populated by laser radiation. In Ref. [4] the experimental observation of laser-induced changes of the Mössbauer spectrum of a MgO:Fe<sup>2+</sup> single crystal was reported. It was initially suggested that the changes were caused by the modification of relaxation processes among electronic sublevels of the Fe<sup>2+</sup> ion due to the laser-induced change of energy separation between them. Subsequent work [5] has shown that after laser irradiation, the position of the Mössbauer line was changing in time as a decaying oscillation of well-defined frequency. This oscillation of the Mössbauer line was attributed to the vibration of the sample induced by the laser pulse [5].

The alkaline-earth fluoride crystals doped with Eu ions are very attractive objects to be used for proof-of-principle experiments on laser control of nuclear transitions. The spectroscopy of europium-doped fluoride crystals has been thoroughly investigated [6-8]. The Eu<sup>3+</sup> multiplets of the  ${}^5D_j$  term have absorption transitions in the visible region. One of them,  ${}^5D_l$ , has an absorption line at 527 nm which is very suitable for pumping with commercial Nd:YLF laser. The f-f interconfigurational transitions are well shielded from the lattice, giving relatively long fluorescent lifetimes and sharp atomic-like spectral lines even at room temperature. The lifetime of the  ${}^5D_0$  level is of order of several milliseconds. As a result, a detectable population of the  ${}^5D_0$  level can be reached at a moderate laser power due to the pumping of the  ${}^5D_l$  level.

The hyperfine interaction between a nucleus and the surrounding electronic shell depends on the properties of the electronic state, and therefore the changes of electronic state population will affect the shape of the Mössbauer spectrum. Thus, the laser control of the populations of the atomic states could be used, in principle, to influence the properties of the nuclear gamma-ray transitions in a determined way. Recently the shape of the Mössbauer spectrum of 21.5 keV transition of <sup>151</sup>Eu<sup>3+</sup> nuclei in a CaF<sub>2</sub> lattice was calculated, assuming that a population of the excited electronic state is maintained by optical pumping [9]. As up to now these theoretical predictions have not been verified experimentally, in this work we have studied the laser induced modifications of CaF<sub>2</sub>: <sup>151</sup>Eu Mössbauer spectra experimentally.

# 2. Experimental

The CaF<sub>2</sub> crystals containing EuF<sub>3</sub> were grown by a Bridgman-type technique. The Eu<sup>3+</sup> ions readily substitute into CaF<sub>2</sub> without altering the overall cubic symmetry of the lattice. However the rare-earth atoms substituting for calcium must be charge-compensated by an additional fluoride interstitial. The main sites seen spectroscopically have tetragonal and cubic symmetry. The tetragonal site has been identified as having a fluoride in the nearest-neighbor interstitial position, and the cubic site must be charge-compensated by an excess fluoride at a distant location. As-

grown crystals were colored a light violet because of the presence of  $\mathrm{Eu}^{2+}$  ions. The  $\mathrm{Eu}^{2+}/\mathrm{Eu}^{3+}$  ratio for them was about 3, as it was determined from Mössbauer measurement (Fig. 1a). The divalent species is created through the reduction of some of the  $\mathrm{Eu}^{3+}$  during the growth process. To increase the concentration of the  $\mathrm{Eu}^{3+}$  centers the samples were annealed at 800 °C in air. The sample annealing leads to an increase of the number of trivalent Eu ions (Fig. 1b). However, after the annealing the  ${}^5D_0 \rightarrow {}^7F_J$  fluorescent line intensity decreased significantly in comparison with the as-grown crystal fluorescence. The tightly-bound nature of the oxygen-compensated centers results in the significantly different optical properties of the  $\mathrm{Eu}^{3+}$  ions from those typically observed for an isolated europium centers in as-grown crystal. Therefore all measurements were performed on as-grown crystals of  $\mathrm{CaF_2}$  with a europium concentration about 2 % by weight.

All crystals used in the experiments were transparent plates with aperture 7x8 mm<sup>2</sup>, and the thickness was of about 0.5 mm. To avoid overheating, the sample crystal was mounted using metal-impregnated grease on a copper holder, and its temperature was monitored by a thermocouple.

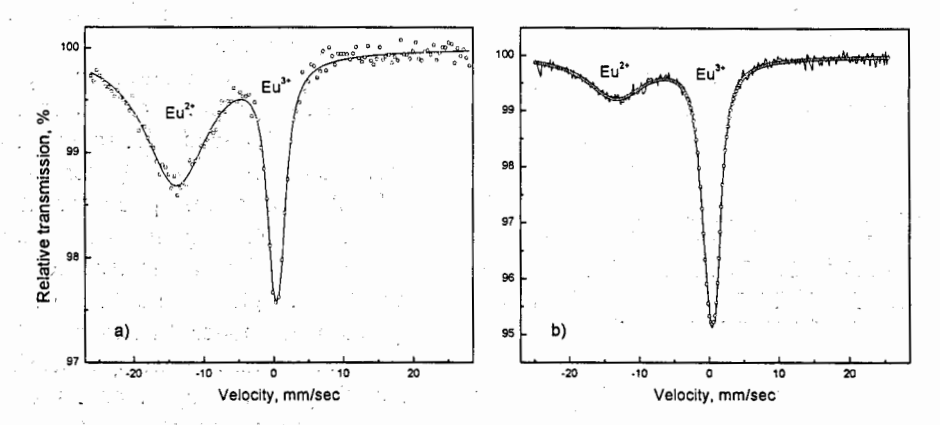


Fig. 1. CaF<sub>2</sub>:Eu Mössbauer spectra, a) as-grown, b) annealed at 700 °C.

Mössbauer spectra were recorded with a Wissel Mössbauer spectrometer operating in a constant acceleration mode. The source used for measurements was <sup>151</sup>Sm in a SmF<sub>3</sub> matrix at room temperature. A symmetrical saw-tooth velocity signal was used and the baseline distortion was corrected by folding the double spectrum. The isomer shift was determined relative to EuF<sub>3</sub>, and the velocity scale was calibrated using metallic iron at room temperature.

A Nd:YLF laser (Photonics Industries, model GM30-527) was used to illuminate the CaF<sub>2</sub>:Eu<sup>3+</sup> absorber. It was capable of delivering up to 1.5 W of CW power at 527 nm, and could also be Q-switched with a repetition rate from a single pulse up to 10 kHz. The pulse duration was about 250 ns. The laser beam was focused onto the sample down to a spot about 6-7 mm in diameter corresponding to the aperture used in the Mössbauer experiment. The fluorescence and absorption optical spectra were

recorded with an HR2000 Spectrometer (Ocean Optics). The wavelength resolution was 0.1 nm. The lifetime measurements were performed with a digital oscilloscope (Textronix, model TDS544).

#### 3. Results and discussion

# 3.1. Results of optical and Mössbauer measurements

To observe laser induced effects caused by changes in the hyperfine interaction due to electronic excitation, one should have samples possessing suitable optical and

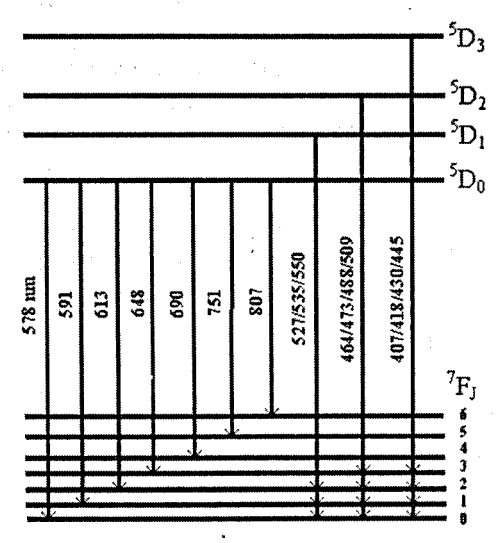


Fig. 2. The energy-level diagram of the  ${}^{7}F_{J}$  and  ${}^{5}D_{J}$  multiplets in CaF<sub>2</sub>:Eu<sup>3+</sup>. The transition wavelengths are taken from [10].

Mössbauer properties. The optical active centers should have a sharp optical resonance that can be efficiently driven by laser radiation, and these centers must possess Mössbauer nuclei with high recoilless factor. A CaF<sub>2</sub> crystal doped with Eu<sup>3+</sup> ions meets these requirements.

The  $4f^6$  configuration, appropriate for trivalent europium, consist of more than three thousand electronic states. Four multiplets of the  $^5D_J$  term (with J=0,1,2,3) have absorption transitions in the visible region. The ground multiplet is  $^7F_0$  and fluorescence to all the  $^7F_J$  multiplets could be observed. Typically, the optical transitions of Eu $^3$ + are weak because of the spin selection rule. They could only be observed due to intermediate coupling effects that mix states of the same J but different L

and S. Crystal-field J-mixing of higher-lying states also occurs [7]. In Fig. 2 the energy-level diagram of the levels of the  $^7F_J$  and  $^5D_J$  multiplets in CaF<sub>2</sub>:Eu<sup>3+</sup> is presented.

The absorption spectra of the as-grown  $CaF_2:Eu^{3+}$  crystal in the spectral region corresponding to the  ${}^7F_J \rightarrow {}^5D_0$  and  ${}^7F_J \rightarrow {}^5D_1$  optical transitions is shown in Fig. 3. The  ${}^7F_J \rightarrow {}^5D_0$  transition is spin-forbidden, and the optical absorption at 578 nm is very weak, as can be seen from Fig. 3a. The absorption at 527 nm corresponds to the  ${}^7F_J \rightarrow {}^5D_I$  transitions, and it is much stronger that the absorption at 578 nm.

The excitation of the  ${}^5D_1$  state leads to a strong fluorescence radiation from the  ${}^5D_0$  state with 578 nm wavelength (Fig. 4a). According to the lifetime measurements, the lifetime of the  ${}^5D_0$  state in the our CaF<sub>2</sub>:Eu<sup>3+</sup> single crystal was of the order of 2 msec (Fig. 4b).

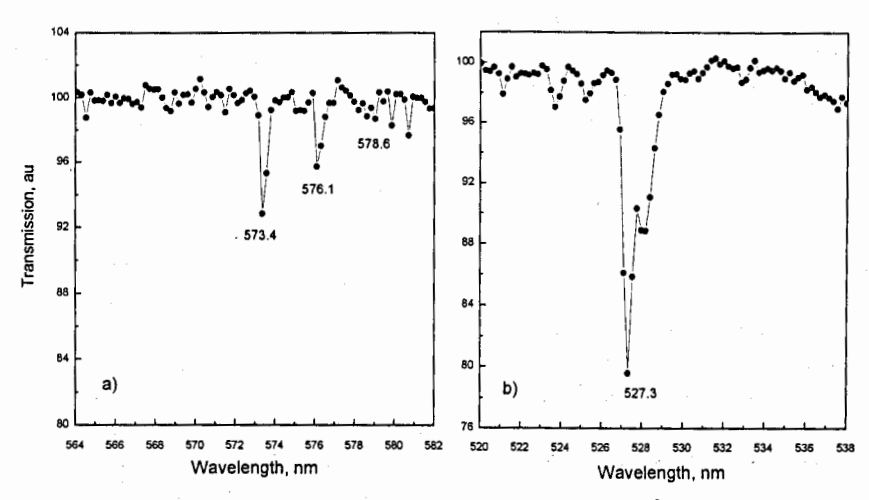


Fig. 3. The optical absorption spectra of the as-grown CaF<sub>2</sub>:Eu<sup>3+</sup> single crystal: a) Absorption at the  ${}^{7}F_{J} \rightarrow {}^{5}D_{0}$  transition, b) absorption at the  ${}^{7}F_{J} \rightarrow {}^{5}D_{1}$  transition.

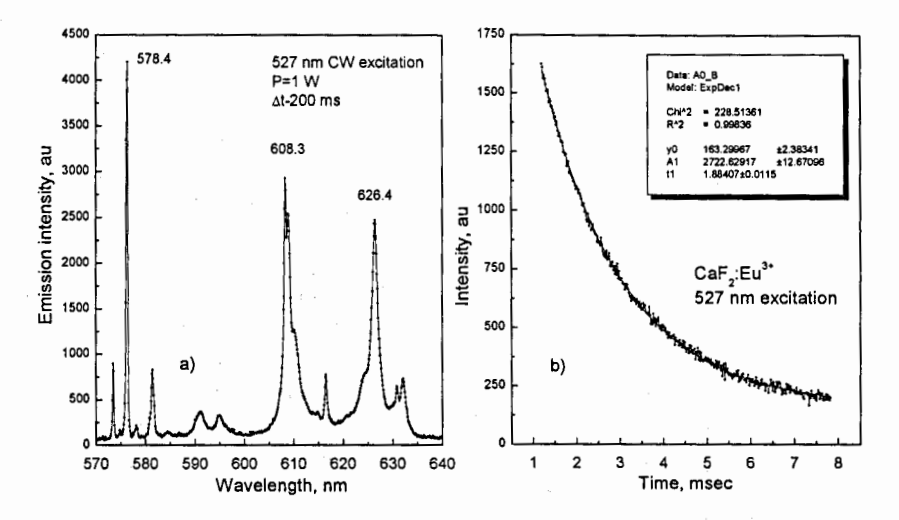


Fig. 4. a) Fluorescence spectrum of the CaF<sub>2</sub>:Eu<sup>3+</sup> single crystal in the region of  ${}^5D_0 \rightarrow {}^7F_0$ ,  ${}^7F_1$  transitions under 527 nm excitation, b) decay of the  ${}^5D_0$  excited state.

The room temperature <sup>151</sup>Eu Mössbauer spectra of the as-grown CaF<sub>2</sub>:Eu crystal consist of two lines corresponding to di- and trivalent states of Eu ions (Fig. 1a). The isomer shift values for the Eu<sup>3+</sup> ( $\delta = 0.38$  mm/sec) and Eu<sup>2+</sup> ( $\delta = -13.99$  mm/sec)

centers are consistent with other Mössbauer measurements. In order to estimate the Debye temperature of  $Eu^{3+}$  sites in the  $CaF_2$  crystal, Mössbauer spectra at 295 and 345 K were recorded. The observed temperature shift of the  $Eu^{3+}$  line agrees with calculation based on the Debye model, with the Debye temperature  $\theta_D$  =340K.

# 3.2. Predicted modifications of 151 Eu Mössbauer spectra in CaF2

The contribution to the Mössbauer spectrum due to the Eu<sup>3+</sup> ions in the  $^5D_0$  state is mixed with the regular Mössbauer spectrum of the Eu<sup>3+</sup> ions in the ground state  $^7F_0$ , so that the final shape of the Mössbauer spectrum depends on the fraction of ions in the excited state. That is why we should determine the magnitude of the quadrupole splitting and isomer shift corresponding to the electronic excited state  $^5D_0$ . The values of quadrupole constant and isomer shift of the electronic ground state  $^7F_0$  are available from a Mössbauer measurements and high-resolution laser spectroscopy data.

The electric field gradient of the electrons acts on the nucleus and produces a

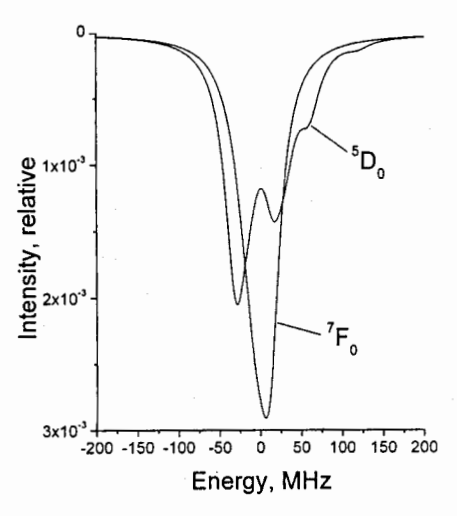


Fig. 5. Comparison of Mössbauer spectra of Eu<sup>3+</sup> nuclei in CaF<sub>2</sub> when the atoms are either in the ground state  ${}^{7}F_{0}$  or in the excited electronic state  ${}^{5}D_{0}$ , assuming an isomer shift of 6 MHz.

hyperfine splitting. For a center of axial symmetry of Eu<sup>3+</sup> ion in CaF<sub>2</sub> this quadrupole interaction is described by a Hamiltonian having form [11,12]

$$H_Q = (P+P')[I_z^2 - I(I+1)/3],$$

where I is the angular momentum of the nucleus, P is the quadrupole constant and P is a pseudoquadrupole term due to a second-order magnetic contribution. Since we have considered 2 nuclear levels, namely the nuclear ground state g and the nuclear excited state e, and 2 atomic levels, namely the electronic ground state  ${}^{7}F_{0}$  and the electronic excited state  ${}^{5}D_{0}$ , we shall have 4 quadrupole constants, which we shall designate as  $P(g, {}^{7}F_{0})$ ,  $P(g, {}^{5}D_{0})$ ,  $P(e, {}^{7}P_{0})$ ,  $P(e, {}^{5}D_{0})$ , and 4 pseudoquadrupole constants, which we shell designate as  $P'(g, {}^{7}F_{0})$ ,  $P'(g, {}^{5}D_{0})$ . The hyperfine structure of the optical

absorption spectra of the Eu<sup>3+</sup> ions in CaF<sub>2</sub> has been measured with the aid of high-resolution laser spectroscopy, and the values of the quadrupole constants for the ground nuclear state of <sup>151</sup>Eu<sup>3+</sup>:CaF<sub>2</sub> are  $P(g, {}^7F_0) = 7.81$  MHz,  $P'(g, {}^7F_0) = 0.45$  MHz for the ground electronic state  ${}^7F_0$  and  $P(g, {}^5D_0) = -22.23$  MHz,  $|P'(g, {}^5D_0)| < 0.01$  MHz for the electronic excited state  ${}^5D_0$  [12]. Using the relations (2)-(5) of Ref. [9], the sums of

the quadrupole constants are then  $P(g, {}^{7}F_{\theta}) + P'(g, {}^{7}F_{\theta}) = 8.26$  MHz,

 $P(g, {}^{5}D_{0}) + P'(g, {}^{5}D_{0}) = -22.23$  MHz,  $P(e, {}^{7}F_{0}) + P'(e, {}^{7}F_{0}) = 5.40$  MHz,  $P(e, {}^{5}D_{0}) + P'(e, {}^{5}D_{0}) = -15.00$  MHz.

The Mössbauer isomer shift  $\Delta E_M$  existing between states  $^7F_0$  and  $^5D_0$  of the Eu<sup>3+</sup> ion can be calculated from the isotopic shift  $\Delta E_{opt}$  for the ground state  $^7F_0$  between the <sup>151</sup>Eu and <sup>153</sup>Eu nuclei using the relation [13]

$$\frac{\Delta E_M}{\Delta E_{opt}} = \frac{\Delta \langle r^2 \rangle_M}{\Delta \langle r_g^2 \rangle},$$

where  $\Delta \langle r^2 \rangle_M$  is the difference of the square of the nuclear radii for the 21.5 keV excited state and the ground nuclear state of <sup>151</sup>Eu and  $\Delta \langle r_g^2 \rangle$  is the difference of the square of the of the nuclear radii of the nuclei <sup>153</sup>Eu and <sup>151</sup>Eu, and where the mass shift contribution has been neglected. The optical isotopic shift  $\Delta E_{opt}$  for <sup>153</sup>Eu with respect to <sup>151</sup>Eu has been measured in EuCl<sub>3</sub>·6H<sub>2</sub>O and has the value  $\Delta E_{opt} = 0.15$  GHz [14],  $\Delta \langle r^2 \rangle_M = 19.2 \cdot 10^{-3}$  fm<sup>2</sup> [15] and  $\Delta \langle r_g^2 \rangle = 0.522$  fm<sup>2</sup> [16]. With these values we obtain  $\Delta E_M = 5.2$  MHz [9].

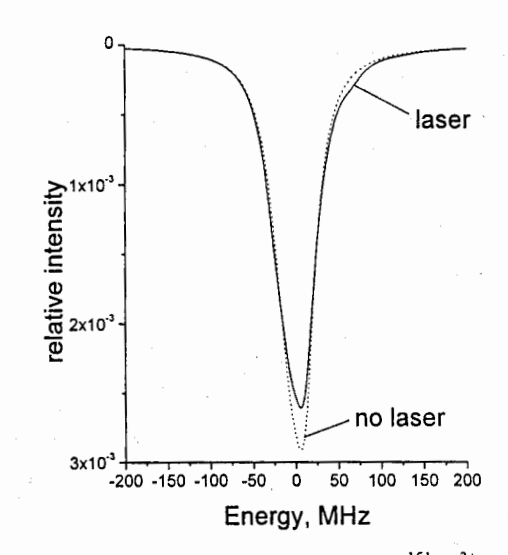


Fig. 6. Comparison of Mössbauer spectra of  $^{151}\text{Eu}^{3+}$  nuclei in  $\text{CaF}_2$  for a  $^5D_0$  population of 17 %, a linewidth of 16 MHz and an isomer shift of 6 MHz.

Using the intensities of the allowed  $\gamma$ -ray transitions between the nuclear hyperfine levels, the values of the quadrupole constants and the value of Mössbauer isomer shift, it is possible to obtain the Mössbauer spectrum for the case when the electrons are in the ground state  ${}^{7}F_{0}$ , and for the case when electrons are in the excited state  ${}^{5}D_{0}$  as shown in Fig. 5. In Fig. 6 the shape of the Mössbauer for the case in which a fraction of 17 % of the Eu<sup>3+</sup> ions are in the  ${}^{5}D_{0}$  state and the reference spectrum for which all

atoms are in the ground state  ${}^{7}F_{0}$  is presented. In Ref. [9] it was calculated that a population of 10 % in the excited electronic state produces a variation of the central peak of 1.9 %.

# 3.3. Laser induced effect in 151 Eu: CaF2 Mössbauer spectrum

We have excited the  ${}^5D_I$  electronic state of Eu $^{3+}$  ion by 527 nm laser radiation. To avoid laser-induced vibrations [4,5] we have used a Nd:YLF laser operating in CW mode. The life time of the  ${}^5D_I$  state is very short and its decay populates with high efficiency the  ${}^5D_0$  state, which has a lifetime of milliseconds. Since the predicted quadrupole coupling is considerably larger for the optical excited state  ${}^5D_0$  than the one for the ground state  ${}^7F_0$  [9], the quadrupole splitting in the Mössbauer subspectrum arising from this optical excited state should be correspondingly larger. As a result, we expect to observe in the Mössbauer spectrum a reduction of the height of the central peak and the appearance of a weak peak in the right wing of the main line [9]. The experimental  ${}^{151}$ Eu Mössbauer spectra of the as-grown CaF<sub>2</sub>:Eu single crystal taken under 527 nm laser excitation ("Laser On") and without excitation ("Laser Off") are shown in Fig. 7a. The difference between them is presented in Fig. 7b.

As can be seen from Fig. 7, the changes in the Mössbauer spectrum recorded in the presence of 527 nm laser radiation are similar to the changes of the Mössbauer spectrum shape predicted in Ref. [9]. The observed reduction of the central peak intensity was about 0.15 %, while the amplitude of the shoulder in the right wing of the resonance line was less than the value of experimental error ( $\pm 0.1$  %).

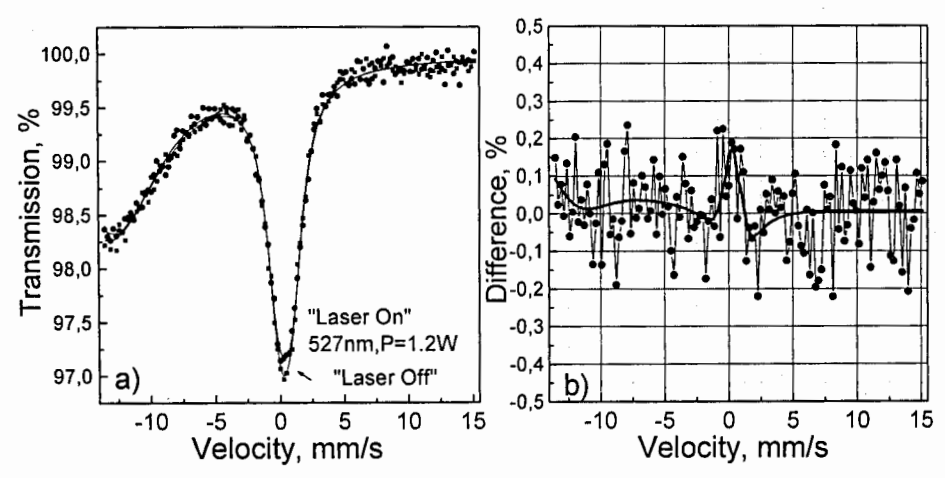


Fig. 7. a) "Laser On/Off" Mossbauer spectra of <sup>151</sup>Eu nuclei in as-grown CaF<sub>2</sub>:Eu single crystal; b) Difference between "Laser On/Off" Mössbauer spectra.

We estimated that the fraction of atoms excited in our experiments to the  ${}^5D_{\theta}$  state could lead to a reduction of the absorption line intensity comparable to that observed in

the Mössbauer spectra. However, there may be a different explanation of the observed laser-induced effects. Thus, the laser beam heats the sample, and according to temperature measurement the sample temperature was about 70 °C during the experiment. The temperature increase could lead to a decrease of the Mössbauer factor f, and consequently to a reduction of the central peak height. The thermal reduction of the Mössbauer line intensity is proportional to

s proportional to
$$f(T)/f(295) = e^{\frac{-6E_R(T-295)}{k_B\theta_D^2}}$$

where  $E_R = 2.64 \times 10^{-22} \text{ J}$  is the recoil energy for  $^{151}\text{Eu}$  nucleus,  $\theta_D$  is the Debye temperature,  $k_B$  - the Boltzmann constant. In the case of a sample temperature T=343 K and of a Debye temperature  $\theta_D = 340 \text{ K}$ , the Mössbauer factor ratio is equal to f(T)/f(295) = 0.93(3). Since the height of the central peak is 3 %, the difference between the Mössbauer line intensities for "Laser Off" (T=295 K) and "Laser On" ( $T\sim343 \text{ K}$ ) Mössbauer spectra due to thermal reduction of Mössbauer factor will be again of order of 0.15 %.

The thermal effects cannot lead to changes of Mössbauer line shape and to the appearance of additional lines. However, the statistical significance of the shoulder in the right wing of the resonance line reported in this work is not yet sufficient. Therefore, the thermal effects are regarded at this stage as the primary cause of the observed Mössbauer spectrum transformations. At the same time, the laser-induced changes reported in this paper contain a certain contribution from the europium ions in the excited state  $^5D_\theta$ .

#### 4. Conclusions

The changes in the Mössbauer spectrum recorded in the presence of 527 nm laser radiation are similar to the changes of the Mössbauer spectrum shape predicted in Ref. [9]. The observed reduction of central peak intensity was about 0.15 %, while the amplitude of the shoulder in the right wing of the resonance line was less than the value of the experimental error (±0.1 %). While we have searched laser-induced effects caused by changes in the hyperfine interaction due to electronic excitation, the reduction of the central peak intensity can be attributed to the decrease of the recoilfree fraction as the temperature increased due to laser-induced heating. The statistical significance of the electronic excitation effect under action of 1.2W laser is not yet sufficient. The more pronounced result of an electronic excitation effect may be obtained performing the experiment at low temperature (using a more effective cooling system) under the action of much stronger laser power on the sample with longer lifetime of <sup>5</sup>D<sub>0</sub> electronic state. An alternative way is to perform laser-Mössbauer experiment with synchrotron Mössbauer source in which active aperture can be reduced down to sub-millimeter size and, consequently, much higher laser intensity at the sample position can be achieved with moderate laser power.

#### Acknowledgments

This work was supported by the AFOSR, NSF, and CRDF. The authors are grateful to Yuri Rostovtsev for fruitful discussions and Elena Kuznetsova for help with manuscript preparation.

## References

- E.Arimondo, Prog. Opt. 35 (1996) 259; S.E.Harris, Phys. Today 50 (1997) 36;
   O.Kocharovskaya, Phys. Rep. 219 (1992) 175; M.O.Scully, Phys.Rep. 219 (1992) 191; C.Liu, Z.Dutton, C.H.Behroozi, L.V.Hau, Nature (London) 409 (2001) 490;
   D.F.Phillips, A.Fleischhauer, A.Mair, R.L.Walsworth, M.D.Lukin, Phys.Rev.Lett. 86 (2001) 783; M.O.Scully and M.S.Zubaity, Quantum Optics (Cambridge University Press, Cambridge, 1997).
- 2. O.Kocharovskaya, R.Kolesov, and Yu.Rostovtsev, Phys.Rev. Lett. 82 1999 3593.
- 3. P.Gutlich, Y.Garcia, T.Woike, Coord. Chem. Rev. 839 (2001) 219-221.
- 4. F. Vagizov, R. Kolesov, O. Kocharovskaya, J. Mod. Optics 51 (2004) 2579.
- 5. F.Vagizov, R.Kolesov, S.Olariu, Yu.Rostovtsev, and O.Kocharovskaya, Hyperfine Interactions, to be published.
- 6. L.R. Olsen, A.O. Wright, J.C. Wright, Rhys.Rev. B 53 (1996) 14135.
- 7. J.R. Wells, R.J. Reeves, Phys. Rev. B 64 (2001) 035102.
- 8. A.J. Silversmith, A.P. Radlinski, J.Phys. C: Solid State Physics 18 (1985) 4385.
- S.Olariu, R.Kolesov, F.Vagizov, and O.Kocharovskaya, J. Mod. Optics 52 (2005) 877.
- 10. W.Tian, R.S.Pandher, B.R.Reddy, J.Opt.Soc.Am. B 18 (2001) 1627.
- 11. A.J.Silversmith, A.P.Radlinski and N.B.Manson, Phys. Rev. B 34 (1986) 4854.
- 12. A.J.Silversmith and N.B.Manson, Phys. Rev. B 34 (1986) 7554.
- 13. S.Hufner, in *Mössbauer Isomer Shifts*, edited by G.K.Shenoy and F.E.Wagner (North-Holland, Amsterdam, 1978), p.203.
- 14. J.P.D.Martin, M.J.Sellars, P.Tuthill, et.al., J.Luminescence 78 (1998) 19.
- 15. G.M.Kalvius and G.K.Shenoy, At. Data Nucl. Data Tab. 14 (1974) 639.
- 16. P.Aufmuth, K. Heilig and A.Steudel, At. Data Nucl. Data Tab. 37 (1987) 455.

# THE INFLUENCE OF MAGNETIC FIELD DIRECTION ON THE RESONANT ABSORPTION OF LONG-LIVED ISOMER 109M AG GAMMA-RAYS

#### V.G.ALPATOV

State Scientific Center of Russian Federation Institute forTheoretical and Experimental Physics Moscow, Bol'shaya Cheremushkinskaya street 25, Russia

# YU.D.BAYUKOV, A.V.DAVYDOV, YU.N.ISAEV, G.R.KARTASHOV, M.M.KOROTKOV AND D.V.L'VOV

State Scientific Center of Russian Federation Institute for Theoretical and
Experimental Physics
Moscow, Bol'shaya Cheremushkinskaya Street 25, Russia

The experiments are described in which resonant absorption of <sup>109m</sup>Ag gamma-rays was revealed by influence of temperature, gravity and the changing of magnetic field dihection on gamma-ray resonant self-absorption in silver plates contained parent nuclide <sup>109</sup>Cd. The pair of Helmholtz rings was used for periodical compensation of vertical component of Earth's magnetic field. This caused the change of gamma-ray resonant absorption probability by 60 % for gamma-quanta emitted in horizontal direction at liquid helium temperature. Such effect was absent for gamma-rays emitted in vertical direction via the gravity influence on gamma-resonance and weak influence of magnetic field change in this case. The values of Mössbauer gamma-line broadening factor were estimated for single crystal as equal to 21<sup>+13</sup>-6 and for polycrystalline silver gamma-sources as equal to 22<sup>+25</sup>-8.

#### 1. Introduction

Atomic nuclei of silver isotops,  $^{107}$ Ag and  $^{109}$ Ag, have similar properties. Both nuclei have low-lying excited states with mean life times about 1 minute. This corresponds to the natural level width  $\sim 10^{-17}$  eV. The observation of Mössbauer absorption of gamma-rays emitted from these states is a very tempting goal because the resolution of Mössbauer spectrometer based on these isomers would be by  $\sim 8$  orders of magnitude better than in the case of the most widely used Mössbauer nuclide  $^{57}$ Fe. More of that the observation of Mössbauer effect with these nuclei would permit in principle to perform the experiments on the study some properties of induced gamma-emission and to estimate in particular the scale of the time interval between the registration of inducing and induced photons.

However the Mössbauer gamma-lines of silver isomers must be broadened by 10<sup>5</sup> – 10<sup>6</sup> times in accordance with existing theoretical conceptions. The main reasons of this broadening are the dipole-dipole interactions between the magnetic moments of excited nuclei and those of the neighbouring nuclei and of conduction electrons. First experiments on the Mössbauer excitation of 93.1 keV and 88 keV levels of <sup>107</sup>Ag and

<sup>109</sup>Ag correspondingly which were performed by ITEP group in 60-ths and 70-ths years of last century [1-3] using the method of resonant absorber activation by gamma-rays of strong gamma-source at low temperature confirmed as it would seem these theoretical predictions. However the conditions of these experiments do not permit to explain unambiguously the observed very low cross section of resonant gamma-ray absorption by the large gamma-line broadening solely. Gamma-sources for these experiments were fabricated using the irradiation of corresponding samples at cyclotrons and in reactor after which they could have the structure and the chemical composition differing from those of the resonant absorbers which were not exposed to such treatment. So the isomeric shift could play the role also.

In 1979 the work [4] was published in which the attempt was made (successive as it would seem) to observe the Mössbauer absorption of 88 keV gamma-rays of 109m Ag isomer by the new method. It consisted in the measurement of temperature dependence of gamma-ray yield from single crystal silver plate in which the parent nuclide 109Cd was introduced by thermodiffusion. When gamma-source was cooled from the room temperature to 77 K the detected gamma-ray intensity decreased in consequence of silver compression. At the further cooling to 4.2 K this compression must continue but in the much lower degree. One may calculate the result of this compression using the data on the temperature dependence of the compression coefficient which are known up to very low temperatures. However the observed decrease of gamma-ray intensity after the gamma-source cooling from 77 to 4.2 K turned out to be much larger than one could expect on the base of the data on silver compression. The authors of [4] ascribed the surplus weakening of gamma-ray intensity to the Mössbauer effect which is not observable practically at 77 K but must reveal itself at 4.2 K because the probability of recoilless emission (and absorption) is equal to 0.0535 for gamma-rays of 88 keV energy in silver metal at this temperature. The magnitude of surplus gamma-ray absorption corresponded to the Mössbauer gamma-line broadening factor equal to 30. Henceforth the analogous experiments were performed in USA [5-7] and the surplus gamma-ray absorption was observed also. The magnitudes of Mössbauer gamma-line broadening factor from the data of these experiments were lying in the range from 16 to 100. Note that not in one of these works one presented any explanation of the mysterious disappearance of dipole-dipole interactions.

# 2. The methods of new experiments by ITEP group

We have conducted a series of experiments in which the Mössbauer absorption of  $^{109m}$ Ag gamma-rays must be revealed at simultaneous influence on it of temperature, gravity and the direction of terrestrial magnetic field. Near the Earth surface the gravitational shift of  $^{109m}$ Ag gamma-resonance by the magnitude of the natural gammaline width takes place at the difference of vertical positions of emitting and absorbing nuclei equal to 1 micrometer. This means that one may observe the strong difference between resonant gamma-ray absorption in horizontal and vertical directions if the broadening factor of Mössbauer gamma-line is small. The Earth's magnetic field splits the Mössbauer gamma-line of  $^{109m}$ Ag by 14 components and the spacings between them exceeds the gamma-line natural width by  $\sim 10^6$  times. It is known that the relative

intensities of Zeeman hyperfine structure components depend on the angle  $\alpha$  between the direction of gamma-quantum emission and the magnetic field direction. This situation for  $^{109m}Ag$  isomer was analyzed in paper [8]. It is shown on the Fig. 1 how the probability of  $^{109m}Ag$  gamma-ray resonant absorption depends on the angle  $\alpha$ . The Earth's magnetic field in Moscow is directed downwards at the angle  $\sim 70^{\circ}$  with respect to the horizon. If one compensates the vertical component of Earth's magnetic field then the probability of resonant absorption of gamma-rays emitted in the horizontal direction would be increased by  $\sim 60$  %. For gamma-rays emitted vertically this effect would be much less as one may see on the Fig. 1

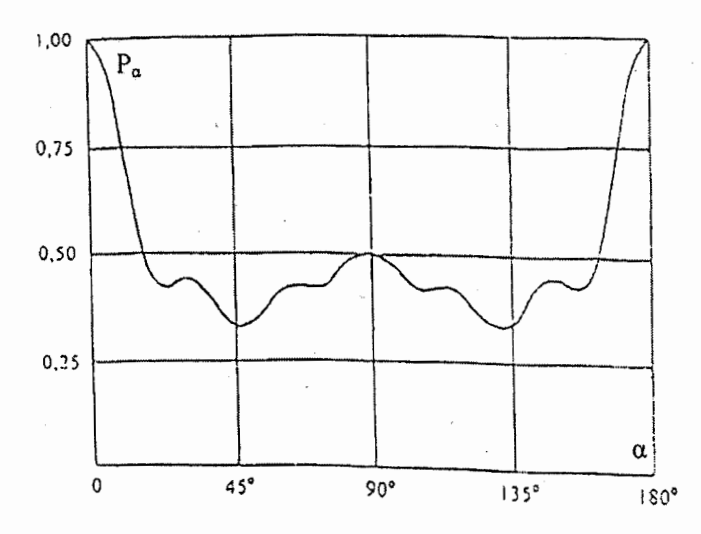


Figure 1. Factor  $P_{\alpha}$  proportional to the resonant absorption probability as a function of angle  $\alpha$  between the direction of gamma-quantum emission and that of magnetic field.

To observe all three appointed effects the experimental set-up was made which main part was a small cryostat permitting to cool the gamma-sources to the temperature of liquid nitrogen or liquid helium. The main gamma-source was a silver plate (single crystal in most cases) in which the parent nuclide <sup>109</sup>Cd was introduced by thermodiffusion. This gamma-source served simultaneously as a resonant gamma-ray absorber. The second nonresonant gamma-source on the base of <sup>241</sup>Am was used as the control one. It was a disc of chromatographic paper saturated with americium nitrate and packed hermetically into aluminium foil. Both gamma-sources were mounted on the bottom of cryostat helium volume which was inclined by the angle 45° with respect to the horizon. This permitted to detect gamma-rays in horizontal and vertical directions under the similar conditions by means of two germanium detectors. The pair of Helmholtz rings was mounted coaxially with the cryostat. One could use it to compensate the vertical component of

Earth's magnetic field at the site of gamma-sources. One of the set-up variants is described in our paper [9]. The version of the set-up used in our last experiments differs from that by using of high purity germanium detectors located at the distances of 40 cm from the sources, by presence of optical laser to observe and measure the possible turns of gamma-source plane which could be caused by deformations of inner cryostat parts at the temperature changes, and by some additional measures for decrease of such deformations. When one could expect the appearance of such deformations, for example at the temperature changes, then one has to use the ratio of silver and americium gamma-line intensities instead of their separate values. If the detector is located at the distance of 40 cm from the gamma-source then the change of this distance by 1 mm lead to the relative change of the detected gamma-ray intensity equal to 0.005. This value is comparable with the expected effect of resonant absorption. However if one would use the ratio R of silver and americium gamma-ray intensity then the relative change of R under the same conditions would be equal to  $2.5 \times 10^{-5}$  only even at the distance between two sources equal to 2 mm.

As it will be seen below the errors of our experimental results are rather large. This permits to use the approximate methods to extract from them the data about Mössbauer gamma-line broadening factor. At first we propose that cadmium is deposited in silver in two thin layers at the identical distances from both source plate surfaces equal to the mean values of real depth distribution. Then we determine this mean depth comparing the ratios of x-ray and gamma-ray intensities measured for silver gamma-source and for very thin source made by saturation of filter paper by <sup>109</sup>CdCl<sub>2</sub> solution with results of calculations for various values of mean depth using the known values of corresponding absorption coefficients. After that we find the value of gamma-ray resonant absorption cross section comparing the experimental value of relative effect of resonant absorption with its calculated values obtained for a set of cross section values and using the found mean depth of cadmium bedding. The cross section for the case of the emission of gamma-line along the direction of magnetic field at the absence of gamma-line broadening is equal to  $\sigma_{max} = \sim 8.5 \times 10^{-24}$  cm<sup>2</sup>. The gamma-line broadening factor is determined as the ratio of  $\sigma_{max}$  to the cross section value following from the experimental data.

The calculated value of the relative effect of  $^{109m}$ Ag gamma-ray resonant absorption in vertical direction under the conditions of our last experiments is equal to  $0.00004 \pm 0.00001$  and does not depend practically on the gamma-line broadening factor. This is explained by the increase of the way on which gamma-rays could experience a resonant absorption proportionally to the broadening factor and the simultaneous decrease of the resonant absorption cross section by the same degree.

# 3. The results of the experiments

The influence of magnetic field direction on the <sup>109m</sup>Ag gamma-ray resonant absorption cross section revealed itself firstly in our experiment [10]. All measurements at liquid helium temperature were performed in this work with Helmholtz rings switched on constantly that is under the optimal conditions for resonant absorption of gamma-rays emitted in the horizontal direction. The value of

Mössbauer gamma-line broadening factor was obtained in this work equal to  $2 \pm 1$ . If one interpret the same experimental data in such manner as it was made in the works [4-7], that is scorning the influence of magnetic field on the resonant absorption, one would obtain the value of broadening factor equal to  $35^{+19}_{-10}$ . This value is in good agreement with the results of works [4-7].

After this experiment we made three experiments more: two measurements with the same single crystal silver gamma-source and one with polycrystalline source. In all three cases the measurements were carrying out at three temperatures (room, 77 K and 4.2 K) in the mode of operation when Helmholtz rings were periodically switched on and off. The first experiment with single crystal source was performed as a main part of the INTAS project  $N_2$  97-31566. The relative effect of resonant absorption which revealed itself for horizontal direction at the transition from 77 K to 4.2 K turned out to be equal to  $0.00116 \pm 0.00080$ . The measured relative effect of switching Helmholtz rings on was equal to  $0.00113 \pm 0.00075$  for gamma-ray intensity change in horizontal direction and that for the vertical direction was equal to  $0.00006 \pm 0.00068$ . The full relative effect of resonant absorption in the horizontal directions may be determined from appointed value as  $0.0019 \pm 0.0013$ . Both results for the horizontal gamma-beam are in the mutual agreement and being united give the value of relative resonant absorption effect equal to  $0.00136 \pm 0.00068$ .

In the last experiments with polycrystalline and single crystal gamma-sources we couldn't see the effect of gamma-ray resonant absorption at cooling of gamma-sources from 77 K to the liquid helium temperature. More of that the weak increases of the counting rates were observed corresponding to both silver and americium gamma-rays in the horizontal and vertical directions. However the decrease of gamma-ray intensity must take place even in the absence of resonant absorption because of the silver compression at cooling. The absence of such decrease indicates that the cryostat inner part deformations took place apparently which were not observed by used methods. As a result of such deformation the gamma-sources could approach slightly to the detectors. One of the possible causes of this gamma-source displacement may be connected with the method of gamma-source fixing in the cryostat. The silver gammasources were soldered to the thin copper bottom of the helium volume and so the bimetallic pairs were formed which could bend without the displacement of very helium volume (we should observe such displacement) because of a large difference between the coefficients of temperature expansion of silver and copper at low temperature. However at the steady temperature state the appearance of additional deformations is impossible and one may attempt to observe the result of the magnetic field direction influence on the gamma-ray resonant absorption. The measurements performed at room temperature and at 77 K with both gamma-sources showed that the influence of magnetic field direction change on the detection efficiency of americium gamma-rays and silver x-rays was absent for both gamma-beams. For silver gammarays such influence was found for vertical gamma-beam were the relative effect turned out to be equal to  $0.00028 \pm 0.00013$ . This effect may be ascribed to influence of magnetic field on the carrier collection in Ge-detector. As the mean way of silver gamma-rays (88 keV) in germanium is essentially larger than that of americium gamma-rays (59.54 keV) and especially as that of x-rays (20-22 keV) the mean way

length for the carriers moving to the front electrode of the detector turns out to be the largest one just for the silver gamma-rays and the losses of the carriers on this way must be the largest in this case. In our detectors such carriers are the holes and the observed effect means that the probability of hole recombination in our detector is larger than that of electrons. The special measurements performed with constant magnet created the field  $\sim 1.3$  Oersted at the site of detector have shown that at some mutual orientations of magnet and detector the influence of magnetic field on the efficiency of the detector reached  $\sim 0.3$  %. The influence of magnetic field direction change on the efficiency of the horizontal gamma-beam detector was not observed because of the much smaller alteration of the magnetic field magnitude at its site than at the position of the vertical gamma-beam detector.

On the Fig. 2 the results are shown of the experiment with polycrystalline gamma-source. It is seen that the influence of magnetic field direction change on the detected intensity of  $^{109m}\mathrm{Ag}$  gamma-rays reveals itself clearly in the horizontal gamma-beam at the temperature of liquid helium. This influence told on both the number of counts corresponding to gamma-line 88 keV and the ratio R of count numbers of silver and americium gamma-lines. For the very americium gamma-line such influence is absent. It is absent also for both gamma-lines at the increased temperatures and under all conditions in the vertical gamma-beam. So there is every indication that resonant absorption of silver gamma-rays takes place in this case. The relative effects of the magnetic field direction influence on the  $^{109m}\mathrm{Ag}$  gamma-ray resonant absorption are equal for the number of counts of 88 keV gamma-line to 0.00048  $\pm$  0.00025 and for the value of ratio R - 0.00041  $\pm$  0.00034. The first, more precise, value corresponds to the relative effect of resonant absorption equal to 0.00079  $\pm$  0.00041. The Mössbauer gamma-line broadening factor is equal from here to  $22^{+25}_{-8}$ .

The data of the experiment with single crystal gamma-source are shown on the Fig. 3. They are less convincing at the first sight than the results of the experiment with polycrystalline gamma-source. Really, the measured with switching of Helmholtz rings ratio of silver gamma-ray intensities in the horizontal gamma-beam at the temperature of liquid helium does not differ from unity in the limits of errors. Note, however, that corresponding ratio for americium gamma-rays turned out in this case much higher than unity. This could take place owing to the drift phenomena in electronics. But if it is so that such drift could influence analogously on the intensity ratio of silver gamma-rays because intensities of both gamma-lines were measured simultaneously by the same detector. Therefore one has to use in this case the ratio of R values to find the influence of magnetic field direction. For this values such influence gave the relative effect equal to 0.00068 ± 0.00040 and the relative effect of resonant gamma-ray absorption is equal from here to 0.00113 ± 0.00066. So far as this experiment was performed with the same gamma-source as the experiment on the INTAS project one may unite both results. It gives the value  $0.00125 \pm 0.00047$ . This corresponds to the value of broadening factor equal to  $21_{-6}^{+13}$ .

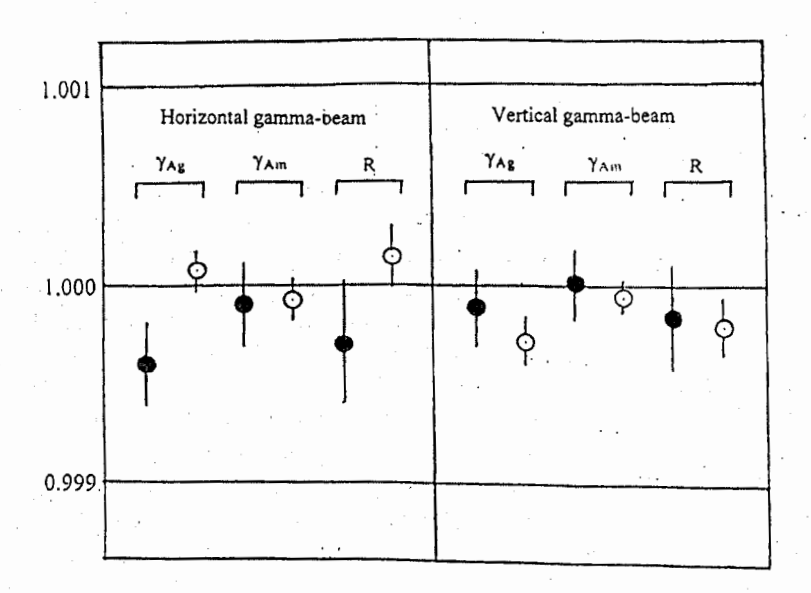


Figure 2. The results of the experiments with polycrystalline silver gamma-source and control <sup>24</sup> Am gamma-source. The gamma-ray intensity ratios are presented which were measured with Helmholtz rings switched on and off. The quantity R is the ratio of silver and americium gamma-ray intensities measured simultaneously by the same detector.

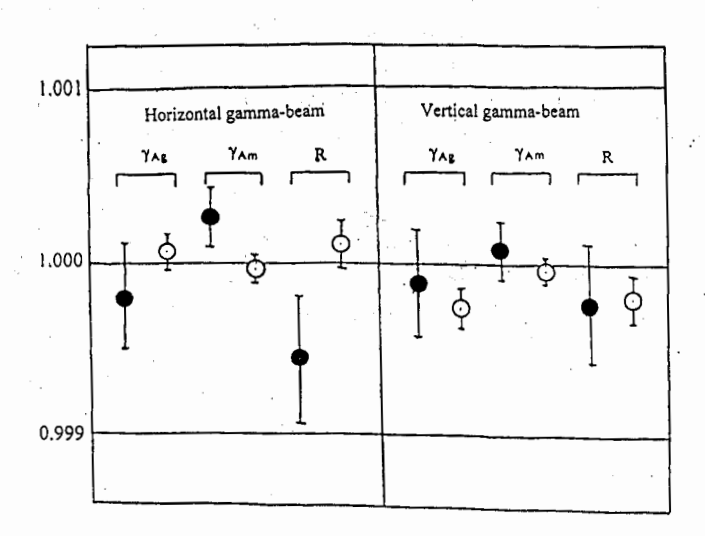


Figure 3. Results of the experiments with single crystal silver gamma-source and a control source of  $^{24l}$ Am. All designations are the same as on the foregoing figure.

#### 4. Conclusions

Thus in all experiments performed until now with gamma-sources made by thermodiffusive method of 109Cd introduction into silver the data were obtained indicating in any degree on the small broadening of 109m Ag Mössbauer gamma-line. However it is early vet to admit this fact definitively proved. The effects are small and the errors are large. The further more precise experiments are required. And if as result of these future experiments the conclusion about small gamma-line broadening would be confirmed it would lead to the important changes in theoretical conceptions connected with forming of long-lived isomer gamma-resonance. In particular the small Mössbauer gamma-line broadening would turn out to be the confirmation of the point of view presented in [12] in accordance with which the processes of gamma-ray emission and absorption are comparable by their durations with mean life time of the nuclei in corresponding excited states. Really, if gamma-quantum is emitted (and absorbed) during the time  $\sim \lambda/c$  ( $\lambda$  – wave length of gamma-radiation) as A.B.Migdal stated in his book [13] then the gamma-quantum energy would be a sum of the nuclear transition energy and the instantaneous value of dipole-dipole interaction energy which changes by the magnitude and by the sign but during the time much larger than  $\lambda c$ . The great broadening would be inevitable in this case. If gamma-quantum is emitted and absorbed "long" then one can put a question about some averaging mechanism of dipole-dipole interaction over the time of photon emission (absorption). If such mechanism will not be found within the framework of quantum electrodynamics then one has to postulate the insensitivity of the long emitted (absorbed) photon to such influence. It may be noted that the rather large spread of the broadening factor values from various experimental works may be connected with inhomogeneous isomeric shift related to the nonuniform distribution of cadmium over the gamma-source thickness. These distributions are most likely different in various gamma-sources

## Acknowledgments

Autors thank M-r V.E.Radko for his assistance in the measurements.

This work was supported by RFBR (grant № 03-02-17241). The first stage of experiments with single crystal silver was supported by INTAS (project № 97-31566).

#### References

- G. E. Bizina, A. G. Beda, N. A. Burgov and A. V. Davydov, Sov. JETP 45, 1408 (1963).
- 2. A. G. Beda, G. E. Bizina and A. V. Davydov, in: Problemy Yadernoi Fiziki I Fiziki Elementarnyh Chastiz (Problems of Nuclear Physics and Physics of Elementary Particles), Nauka, Moscow, 1975, p. 209 (in Russian).
- 3. V. G. Alpatov, A. G. Beda, G. E. Bizina et al., *Proceed. Intern. Conf. on Mössbauer Spectroscopy*, v. 1, Bucharest, Romania, 1977, p. 43 (in Russian).
- 4. W. Wildner and U. Gonser, J. de Phys. Coll. Suppl. 40, C2-47 (1979).
- 5. R. D. Taylor and G. R. Hoy, SPIE, 875, 126 (1988).
- 6. G. R. Hoy and R. D. Taylor, Quant. Spectrosc. Radiat. Transfer 40, 763 (1988).
- 7. S. Rezaie-Serej, G. R. Hoy and R. D. Taylor, Laser Physics 5, 240 (1995).
- 8. A. V. Davydov, Yu. N. Isaev and V. M. Samoylov, *Izvestia Rossiisk. Akad. Nauk, Seria Fiz; (Bull. of Russian Academy of Sciences Physics)* 61, 1747 (1997).
- 9. V. G. Alpatov, Yu. D. Bayukov, A. V. Davydov et al., *Pribory I Tehnika Experimenta (Instruments and Esperimental Technics)* **40**, 753 (1997).
- 10. V. G. Alpatov, Yu. D. Bayukov, V. M. Gelis et al., *Laser Physics* **10**, 955 (2000).
- 11. Final Report on the INTAS project № 97-31566.
- 12. A. V. Davydov, Yadernaya Fizika (Physics of Atomic Nuclei) 66, 2113 (2003).
- 13. A. B. Migdal, in: Kachestvennye Metody v Kvantovoi Teorii (Qualitative Methods in Quantum Theory) Nauka, Moscow, 1975, p. 92 (in Russian).

## COHERENT POPULATION TRAPPING IN RUBY AT ROOM TEMPERATURE

#### ROMAN KOLESOV

Department of Physics and Institute for Quantum Studies, Texas A&M University, College Station, Texas 77843-4242

Coherent population trapping in room-temperature ruby crystal is reported at Zeeman transitions of  $Cr^{3+}$ -ions under the action of an optical pulse train under the condition of Zeeman transition frequency being a multiple of pulse repetition rate in the train. The demonstrated technique allows one to study the influence of atomic coherence on the properties of resonant nuclear  $\gamma$ -ray transitions.

In recent years, attention was paid to a possibility of manipulating nuclear resonant properties with external electromagnetic radiation [1]. There are several reasons for that. The first one is that such studies allow one to understand better the electron-nuclear interactions in solids and, consequently, would result in obtaining new spectroscopic data about solids. In other words, a new type of spectroscopic technique can be developed if the influence of electronic excitations on nuclear properties is studied by means of nuclear resonant spectroscopy (Mössbauer spectroscopy). The second issue is that such a technique would result in obtaining  $\gamma$ -quanta with desired properties, for example, generation of ultrashort pulses of  $\gamma$ -radiation. The third instance is a possibility of exploiting the phenomenon of lasing without population inversion, well-known in conventional optics, to the problem of creating of a  $\gamma$ -ray laser. Though the latter is an extremely challenging task, the problem of  $\gamma$ -ray laser itself generates many interesting physical issues with potential applications in science and technology.

It is well-known that electronic surrounding of the nucleus strongly affects properties of resonant interaction of the latter with  $\gamma$ -radiation. Thus, if electronic surrounding is changed by some means, the hyperfine structure of nuclear  $\gamma$ -ray transitions would also alter in a more or less predictable way. The most efficient way of changing the properties of electronic surrounding is resonant optical excitation of electronic degrees of freedom of an ion or an atom. Such an excitation would lead to the appearance of the hyperfine structure of the excited electronic state in the Mössbauer spectrum. However, there is even more profound possibility of manipulating Mössbauer transitions, which allows one to study interference effects of  $\gamma$ -rays due to atomic coherence. In that way, one can realize electromagnetically induced transparency (EIT) and, possibly, lasing without inversion (LWI) in the  $\gamma$ -ray range.

Overall, the challenge is as follows. Suppose, we have a sample doped with ions exhibiting Mössbauer effect. Suppose also, that there is a possibility of exciting electronic coherence in those ions by some external means. Mössbauer spectroscopy can reveal interference effects in y-ray range arising due to this coherence.

So far, EIT in solids was studied only at very low temperatures in the optical range [2]. Under this condition, most optical transitions of impurities in solids are broadened *inhomogeneously*. Thus, it is possible to excite electronic coherence only in a small group of ions within the inhomogeneous linewidth. Typically, the number of ions participating in EIT is only 0.01-0.1% [2]. At the same time, all ions contribute to the Mössbauer spectrum of the substance. Thus, it is very difficult to extract the change in the Mössbauer spectrum caused by such small fraction of ions. In order to increase the number of ions in which the coherence is excited, it is natural to turn to room temperature solids in which most electronic transitions are broadened homogeneously. The latter leads to the fact that all ions interact with the external driving optical field responsible for the creation of the coherence. However, so far no experimental evidence of efficient coherence excitation in a considerable fraction of active centers in room-temperature solids was demonstrated.

In this paper, the first observation of coherent population trapping (CPT) in a ruby crystal is reported. Laser-induced fluorescence drops under the condition of two-photon resonance. The magnitude of that fluorescence decrease allows one to estimate the number of ions in which electronic coherence is excited. It is experimentally shown that the fraction of coherently prepared ions can be as high as several percent. Though Cr-ions in ruby are not Mössbauer-active, the presented proof-of-principle results demonstrate the way in which atomic coherence can be excited in Mössbauer-active ions, such as  $Fe^{3+}$  and  $Eu^{2+}$ . In that way, the effect of atomic coherence on the Mössbauer spectrum can be easily detected.

Before turning to the experimental results, we have to identify the class of solid-state materials in which the phenomena of EIT/CPT can be observed at room temperature. Only optical crystals doped with either rare-earth or transition metal ions possessing discrete electronic states within the bandgap of the host material will be considered. The class of ions, in which electron paramagnetic resonance (EPR) can be observed at room temperature, is of particular interest. It includes  $Cr^{3+}$ ,  $Eu^{2+}$ ,  $Fe^{3+}$ , and several others. The most important feature of those ions is that, when incorporated into a crystal, their first excited electronic state lies several thousands  $cm^{-1}$  above the ground one. Consequently, Orbach relaxation process [3] between the ground-state Zeeman or hyperfine sublevels is suppressed. As a result, the room temperature decoherence rate at the transitions between Zeeman/hyperfine sublevels can be as low as a few MHz. Some of those ions, namely,  $Cr^{3+}$ ,  $Eu^{2+}$ , and  $Gd^{3+}$ , offer very favorable optical properties as well. For the proof-of-principle experiment ruby, i.e.  $Cr^{3+}:Al_2O_3$ , is chosen because it has the simplest structure of electronic levels and because the properties of this crystal are studied very well.

Typical lifetimes of the excited optical states in solids are much longer than Zeeman decoherence rate. Thus, the population of so-called "dark" state of the medium (the one which does not interact with the incident radiation under the condition of two-photon resonance) cannot be accomplished by population decay from the upper optical state as in conventional CPT experiments in alkali metal vapors. However, one can remove population from the "bright" state (the one orthogonal to the "dark") in a pulsed regime with optical pulse duration being shorter or comparable

to the Zeeman decoherence rate. Thus, room-temperature CPT experiments should be pulsed. This situation is considered in the rest of the paper.

To understand how the  $\Lambda$ -system required for observation of CPT can be realized in ruby and how the condition of two-photon resonance can be fulfilled, let us consider the energy levels of  $Cr^{3+}$  in that crystal (see Fig.1). Its ground state is described by the following spin Hamiltonian:

$$H = g_{\parallel} B_{\parallel} S_z + g_{\perp} \mathbf{B}_{\perp} S_{\perp} + D(S_z^2 - S(S+1)/3),$$

with  $g_{\parallel}=1.982$  and  $g_{\perp}=1.987$  being the ground-state g-factors in the directions parallel and perpendicular to the crystal c-axis respectively,  $B_{\parallel}$  and  $B_{\perp}$  being the corresponding magnetic field components,  $2D=-11.47~GHz~(-0.38~cm^{-1})$  being the zero-field splitting of the ground state, and S=3/2 being the spin of  $Cr^{3+}$ . The width of both optical transitions is  $11~cm^{-1}$  while the total oscillator strength is  $7.5\cdot 10^{-7}$ .

In a situation when  $B \perp c$ -axis, the optical matrix elements indicated on

Fig.1. They are normalized so that the sum of their squares for each of the  $\sigma^{\pm}$  circular polarizations is unity. There are three pairs of  $\Lambda$ -systems: the one connecting  $G_1$  and  $G_2$ through  $E_1$  and  $E_2$ , another one connecting  $G_1$  and  $G_2$ through  $E_3$  and  $E_4$ , and the third one connecting  $G_3$  and  $G_1$  through  $E_1$  and  $E_2$ . For circularly polarized light the products of the optical matrix elements of both  $\Lambda$ -systems in each pair have the same sign, i.e. both A-systems tend to excite ground-state coherence in phase. This is not the case for linearly polarized light when the two  $\Lambda$ -systems in each pair tend to excite coherence with Zeeman exactly the opposite phase. Thus, CPT can be expected only under illumination by circularly polarized light. According to the above

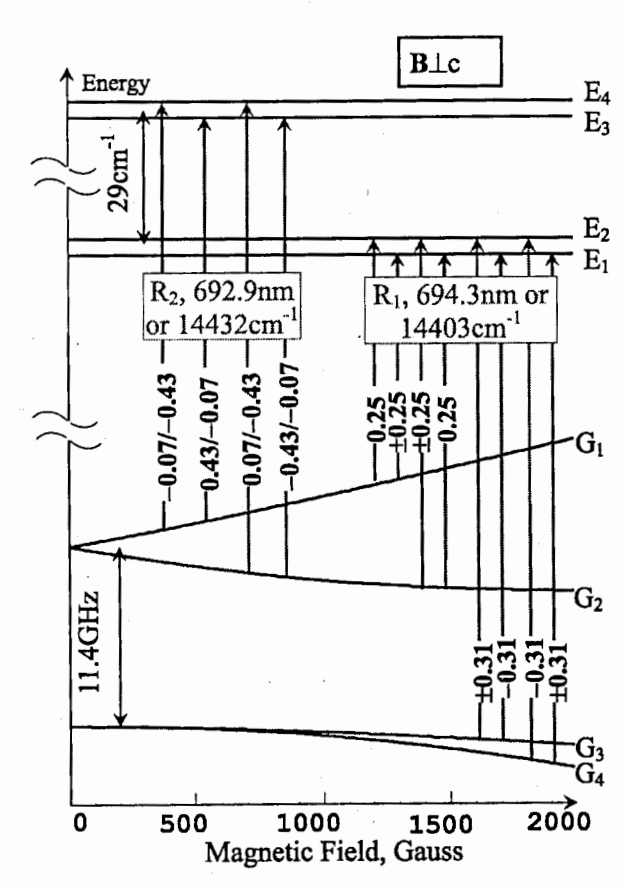


Fig. 1 Energy level structure and optical matrix element of R-lines of  $Cr^{3+}$ -ion in ruby

discussion, two independent CPT resonances can be expected for  $R_I$ -line and only one for  $R_I$ -line as long as two-photon resonance condition is fulfilled.

The latter condition can be realized in two ways. In the first one, the two-photon resonance is fulfilled when the crystal is illuminated with a nanosecond optical pulse interacting with both transitions forming a Λ-system. The CPT resonance is expected whenever the frequency of Zeeman transition is zero. This situation is analogous to the well-known Hanle effect. In the second case, CPT can be observed with a nanosecond train of ultrashort (picosecond) optical pulses whenever the frequency of Zeeman transition becomes multiple of the pulse repetition rate in the train. In both cases the frequency of Zeeman transition can be controlled by external magnetic field.

The experiments were performed on a  $3\times3\times5$  mm<sup>3</sup> dilute ruby crystal  $(0.002\% \text{ of } Cr^{3+})$  with c-axis being perpendicular to one of  $3\times5$  mm<sup>2</sup> sides (Scientific Materials Corp.) A homemade tunable Ti:Sapphire laser pumped by the doubled Nd:YLF pulsed laser could operate both in a nanosecond pulse regime (pulse duration  $\approx30$  ns FWHM) and in a mode-locked regime delivering  $\approx30$  ns pulse trains with repetition rate  $\approx260$  MHz. The typical output energy per pulse or per train was several

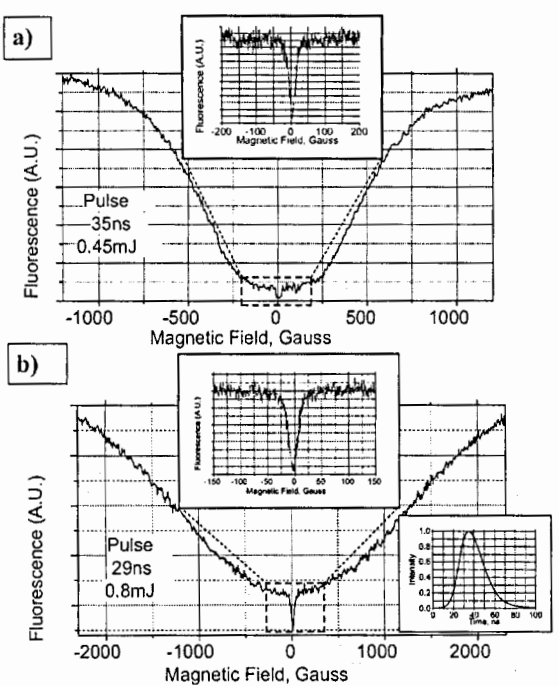


Fig.2. Fluorescence vs. magnetic field in a nanosecond pulse regime. Upper trace: laser is in resonance with  $R_1$ -line. Lower trace: laser is in resonance with  $R_2$ -line.

tenths of a mJ at a 100 Hz repetition rate. The laser polarization was linear. The typical shapes of pulses in both regimes are shown on the insets of Figs.2 and 3. The shape of the pulse train was taken with a 350 ps-risetime photodiode and a 500 MHz-bandwidth

oscilloscope. The duration of each individual pulse in the train was not measured, but it was presumably in the range of tens of picoseconds. The crystal was placed into a varying magnetic  $B \perp c$  -axis field with illuminated along its axis by laser pulses sent through a  $\lambda/4$ -plate and focused by an f=10 cm lens. The fluorescence, i.e. the excited state population, was detected as a function of slowly varying periodic magnetic field.

The experimental results for the case of nanosecond pulse

excitation for both  $R_1$  and  $R_2$  lines are shown in Fig.2. The spectra were averaged over several hundreds of magnetic field sweeps. In the case of  $R_1$ -line, there are two features present in the spectrum: the broad one with the plateau on the bottom and a

203

sharp one of much smaller amplitude. The smaller one corresponds to less than 0.5 % decrease in the fluorescence amplitude and has a width of 18 G. It corresponds to CPT resonance due to  $G_1 \leftrightarrow (E_1, E_2) \leftrightarrow G_2$   $\Lambda$ -system, thus its width in terms of frequency units is  $\approx 100 \ MHz$  since g-factor for  $G_1 \leftrightarrow G_2$  transition is  $\approx 4$ . The broad drop in fluorescence signal has an amplitude  $\approx 7.8 \%$ . Its FWHM is close to  $\approx 950 \ G$ . The presence of plateau at the bottom of that feature indicates that this is a CPT resonance in the  $G_3 \leftrightarrow (E_1, E_2) \leftrightarrow G_4$   $\Lambda$ -system with levels  $G_3$  and  $G_4$  being split very slowly as the magnetic field increases. Its width recalculated into frequency domain is  $\approx 40-50 \ MHz$ , i.e. this CPT resonance is, in fact, much sharper than the one corresponding to  $G_1 \leftrightarrow (E_1, E_2) \leftrightarrow G_2$   $\Lambda$ -system. This can be easily explained since  $G_3 \leftrightarrow G_4$  transition is magnetic-forbidden, thus the contribution due to dipole-dipole interaction with neighboring  $^{27}Al$  nuclei to the line broadening is much smaller than in the case of  $G_1 \leftrightarrow G_2$  transition. In turn, that interaction is known to be the most severe mechanism of broadening of EPR lines in ruby.

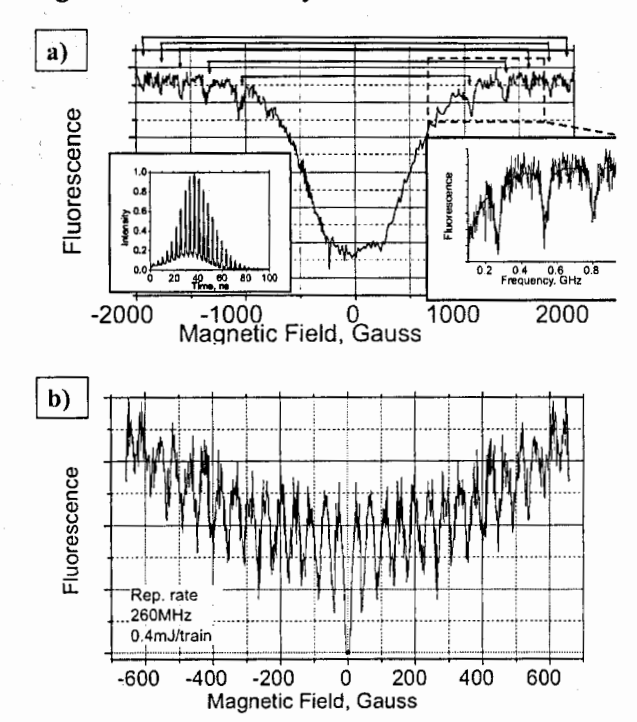


Fig. 3. Fluorescence vs. magnetic field in case of nanosecond trains of picosecond pulses. Upper trace: laser is in resonance with  $R_1$ -line. Lower trace: laser is in resonance with  $R_2$ -line.

For the  $R_2$ -line only one CPT resonance, represented by a sharp feature at the bottom of a smooth background, is observed. It has the same width of 18 G, thus it corresponds to  $G_1 \leftrightarrow (E_3, E_4) \leftrightarrow G_2$   $\Lambda$ -system. The decrease in the fluorescence is 3-4 % at the center of the resonance. The smooth background originates, probably, from level mixing in high magnetic fields and consequent change in the optical selection rules. That was confirmed by removing the  $\lambda/4$ -plate. With linearly polarized light all changes in the fluorescence disappeared, indicating no CPT for linear optical polarization, while the smooth background did not. This is a good confirmation that this broad feature has nothing to do with CPT.

The results for ultrashort pulse trains are shown in Fig.3. CPT resonances corresponding to  $G_1 \leftrightarrow (E_1, E_2) \leftrightarrow G_4$   $\Lambda$ -system of  $R_I$ -line are not equidistant because of nonlinear dependence of the levels  $G_3$  and  $G_4$  separation on the magnetic field strength. However, if recalculated into frequency domain, their positions exactly correspond to the harmonics of laser repetition rate (260 MHz). The widths of these resonances are in good agreement with the one obtained in a nanosecond pulse regime. CPT resonances corresponding to  $G_1 \leftrightarrow (E_1, E_2) \leftrightarrow G_2$   $\Lambda$ -system were not observed because of poor signal-to-noise ratio. The latter occurred due to very small amplitude of the CPT effect (<0.5 %) and rather unstable operation of the laser in a mode-locked regime.

For  $R_2$ -line 13 CPT resonances for both positive and negative sign of the magnetic field are detected (see Fig.3). This number is probably even bigger, but the range of magnetic field sweep was limited to 700 G in order to keep more data points at each resonance. The magnetic field separation between each pair of resonances is ≈45 G. This value corresponds to 252 MHz of frequency separation which is somewhat close to 260 MHz of laser repetition rate. The linewidth of each resonance corresponds rather well to the value of 18 G obtained in a nanosecond pulse regime.

The magnitude of the fluorescence drop was several percent. Thus, Zeeman coherence was excited in several percent of all chromium ions. If applied to Fe<sup>3+</sup>- or Eu<sup>2+</sup>-doped compounds, the proposed method would allow one to study the influence of Zeeman coherence on the Mössbauer spectra of these elements. One can expect the such effects as EIT and slow light in γ-ray range. Moreover, observation of CPT in a room-temperature solid medium is an important step towards applications of EIT/CPT-related effects in real devices.

The author is grateful to F. Vagizov, P. Hemmer, Y. Rostovtsev, E. Kuznetsova, and O.Kocharovskaya for stimulating discussions and to S.Lissotchenko for technical assistance. The work was supported by NSF and AFOSR.

#### References:

[1] O. Kocharovskaya, R. Kolesov, and Y. Rostovtsev, Phys. Rev. Lett., 82, 3593 (1999); R. Kolesov and E. Kuznetsova, Phys. Rev. B, 63, art. no. 184107 (2001); R. Kolesov, and Y. Rostovtsev, O. Kocharovskaya, Opt. Commun., 179, 537 (2000);

[2] A.V. Turukhin et al., Phys. Rev. Lett. 88, art. no. 023602 (2002); Y. Zhao, C.K. Wu, B.S. Ham, M.K. Kim, and E. Awad, Phys. Rev. Lett. 79, 641 (1997); C.J. Wei and N.B. Manson, Phys. Rev. A 60, 2540 (1999); P.R. Hemmer, A.V. Turukhin, M.S. Shahriar, and J.A. Musser, Opt. Lett. 26, 361 (2001); M. Phillips and H.L. Wang, Phys. Rev. Lett. 89, art. no. 186401 (2002); G.B. Serapiglia, E. Paspalakis, C. Sirtori, K.L. Vodopyanov, and C.C. Phillips, Phys. Rev. Lett. **84**, 1019 (2000). [3] R. Orbach, Proc. Roy. Soc. (London) **A264**, 458 (1961)

## MAGNETIC RADIOFREQUENCY QUANTUM BEAT APPROACH FOR TEST OF REVERSAL INVARIANCE OF THE ELECTROMAGNETIC INTERACTION IN 99RU

### A.V. MITIN, I.P. ANISKIN

Kazan State Technological University, K. Marx str.68 Kazan, 420015, Russia

Magnetic radiofrequency quantum beats, stimulated by gamma magnetic resonance for study of 90 keV M1-E2 mixed transition of <sup>99</sup>Ru is considered. The peculiarities of gamma magnetic resonance are coherent excitations of the interference between isomeric Rabi-states and temporal quantum beats also. This method has additional degrees freedom and therefore takes precedence over ordinary nuclear Faraday effect test of time-reversal invariance in <sup>99</sup>Ru. The analysis time-amplitude converter spectra in thin Mössbauer absorber (<sup>99</sup>Ru in iron) shows the strong dependence on relative phase factor between the individual multipole amplitudes of a mixed gamma transition.

#### 1. Introduction

The apparent violation of CP invariance in  $2\pi$  decay mode of the  $K_2^0$  has led Bernstein et al. [1] to bring attention to the fact that there is no substantial experimental evidence that the electromagnetic interaction of the strongly interacting particles is invariant under C and T. These authors show that strong violation of T invariance of the electromagnetic interaction may reveal itself, through higher order effects, as a T-noninvariant impurity of 0,1 to 1% in the amplitude of the nuclear gamma-decay matrix element. The invariance under T requires that the relative phase angle  $\alpha$  between the individual multipole amplitudes of a mixed gamma transition be either 0 or  $\pi$ . A finite value of  $\sin \alpha$  would be equal to the fraction of T-nonivariance amplitude presence.

The Mössbauer spectroscopy has broad applications for features and structures of solids and one may been employed to determine the time-reversal noninveriance in nuclear gamma decays as well [2, 3]. Meanwhile the coherent time-frequency magnetic gamma-resonance methods can investigate these effects by more direct way. Quantum beats induced by gamma magnetic resonance (GMR) [4-6] are depended on a phase of magnetic radiofrequency field. So, the phase factor  $\alpha$  between individual multipole amplitudes of mixed gamma transitions may change the gamma radiation absorption of quantum beat temporal harmonics [7].

In the given paper the example of the 90-kev M1-E2 mixed transition in <sup>99</sup>Ru in iron demonstrates opportunities and challenges of the time-frequency GMR method.

#### 2. Theory

Let us assume that the scattering and absorption of the gamma rays is done entirely by the nuclei of the absorber, so that electronic effects are neglected. Then the refraction index is given

$$n^{pp'} = \delta^{pp'} + \left(\frac{2\pi}{k^2}\right) NA^{pp'},\tag{1}$$

where  $A^{pp'}$  is the coherent forward scattering amplitude tensor;  $p = \pm 1$  determine left and right circular polarizations, N is the nuclei number into a volume unit,  $\delta^{pp'}$  is Kronecker symbol.

The gamma radiation intensity which passed the distance z may be described by the formula

$$P(z) = Sp\{\hat{\chi}(z)\},\tag{2}$$

where the polarization density matrix  $\hat{\chi}(z)$  satisfies the equation [8]:

$$\frac{d\hat{\chi}(z)}{dz} = ik \left( \hat{n}\hat{\chi}(z) - \hat{\chi}(z) \hat{n}^{\dagger} \right) \tag{3}$$

with the boundary condition

$$\hat{\chi}(z)\big|_{z=0} = \frac{1}{2} \left[ \hat{E} + \left( \bar{S}\hat{\sigma} \right) \right]. \tag{4}$$

Here the three parameters  $S_1$ ,  $S_2$  and  $S_3$  give the Poincare representation of the incident radiation polarization, and  $\hat{\sigma}_1$ ,  $\hat{\sigma}_2$  and  $\hat{\sigma}_3$  are Pauli matrices,  $\hat{E}$  is unit matrix.

So, we have gamma radiation intensity change in thin absorber

$$\Delta P = -\frac{4\pi}{k} Nz \operatorname{Im} Sp \left\{ \hat{A} \hat{\chi}(0) \right\}, \tag{5}$$

where the track of matrix  $\hat{A}\hat{\chi}(0)$  is taken on polarization states. In more detailed form

$$\Delta P = -s \sum_{M,M'} \sum_{p,p'} \sum_{e_1,g_1} \frac{\exp\left[i(M-M')(\Omega t + \varphi)\right]}{-L_{e_1g_1}^{(M)} + i} \times \hat{\chi}(0) \times$$
(6)

$$\times \left(\mu_{M,e_1g_1}^p - pq_{M,e_1g_1}^p \delta \exp\left(-i\alpha\right)\right) \left(\mu_{M',e_1g_1}^{p',\bullet} - p'q_{M',e_1g_1}^{p',\bullet} \delta \exp\left(i\alpha\right)\right)$$

$$\mu_{M,e_{i}g_{i}}^{p} = \sum_{e,g} d_{e_{i}e}^{(I_{e})} (\beta_{e}) (2L+1)^{\frac{1}{2}} \exp(ip\psi) d_{pM}^{(L)}(\theta) C(I_{g}LI_{e};gMe) d_{gg_{i}}^{(I_{g})}(-\beta_{g})$$
(6a)

$$q_{M,e_{1}g_{1}}^{p} = \sum_{e,g} d_{e,e}^{(I_{e})} (\beta_{e}) (2L+3)^{\frac{1}{2}} \exp(ip\psi) d_{pM}^{(L+1)}(\theta) C(I_{g}L+I_{e};gMe) d_{gg_{1}}^{(I_{g})}(-\beta_{g})$$
 (6b)

$$L_{e_1g_1}^{(M)} = a_e e_1 - a_g g_1 - M\Omega + D$$
(6c)

where  $\delta^2$  is mixing ratio E2/M1,  $\alpha$  is relative phase angle between the individual multipole amplitudes of a mixed M1-E2 gamma transitions.

Here r = e, g denotes excited and ground nuclear states, respectively and  $a_r$  and  $\beta_r$  are satisfied by equation system

$$\begin{cases} a_r \sin \beta_r = \omega_{1r}/2 \\ a_r \cos \beta_r = \omega_{0r} + \Omega \end{cases}$$
 (7)

where  $\omega_{0r}$ ,  $\omega_{1r}$  are Zeeman energy due to interaction of magnetic nuclear moments with constant or alternating magnetic fields in  $\Gamma_{exp}$  units, respectively.

We consider <sup>99</sup>Ru in case of iron, which magnetic hyperfine field is 500 kOe. Hence the amplification coefficient of radiofrequency magnetic field on nucleus is equal more than  $5 \cdot 10^3$ . The Larmor frequency in excited nuclear state  $\omega_{0e}/2\pi \approx 70$  MHz. Let us assume the frequency of alternating magnetic field is equal to Larmor frequency and so that  $\beta_e \approx 0$ ,  $\beta_e \approx \pi/2$ .

If in Kistner's experiments the magnitude member of the interference between MT- and E2- poles has been due to  $\cos \alpha$  then GMR inserts the  $\sin \alpha$  dependence and phase harmonics shifts.

We're considering results of numerical calculations to the next cases: natural polarization of gamma radiation, linear polarization of gamma radiation along to the radiofrequency field and transversely to the field.

The cases are interesting because of their experimental realization is the most convenient in practice.

In according to Eq. (6) we have:

$$\Delta P = -s \operatorname{Im} \sum_{M,M'} \sum_{p,p'} \sum_{e_{1},g_{1}} \frac{\exp\left[i(M-M')(\Omega t + \varphi)\right]}{-L_{e_{1}g_{1}}^{(M)} + i} \times \hat{\chi}(0) \times \left[\mu_{M,e_{1}g_{1}}^{p} \mu_{M',e_{1}g_{1}}^{p',\bullet} + pp'q_{M,e_{1}g_{1}}^{p} q_{M',e_{1}g_{1}}^{p',\bullet} - \left(\mu_{M,e_{1}g_{1}}^{p} p'q_{M',e_{1}g_{1}}^{p',\bullet} \exp(i\alpha) + \mu_{M',e_{1}g_{1}}^{p',\bullet} pq_{M,e_{1}g_{1}}^{p} \exp(-i\alpha)\right)\right]$$
(8)

To establish an effect we choose a terms depend on  $\alpha$ :

$$F = s\delta \operatorname{Im} \sum_{M,M'} \sum_{p,p'} \sum_{e_{1},g_{1}} \frac{\exp\left[i(M-M')(\Omega t + \varphi)\right]}{-L_{e_{1}g_{1}}^{(M)} + i} \times \hat{\chi}(0) \times \left(\mu_{M,e_{1}g_{1}}^{p} p' q_{M',e_{1}g_{1}}^{p^{*}} \exp(i\alpha) + \mu_{M',e_{1}g_{1}}^{p^{*}} pq_{M,e_{1}g_{1}}^{p} \exp(-i\alpha)\right) =$$

$$= s\delta \left[\sin(\alpha) \sum_{M,M'} \left\{\cos\left[(M-M')(\Omega t + \varphi)\right] \tilde{F}_{1}''(M,M') + \sin\left[(M-M')(\Omega t + \varphi)\right] \tilde{F}_{1}''(M,M')\right\} + \left(\cos(\alpha) \sum_{M,M'} \left\{\cos\left[(M-M')(\Omega t + \varphi)\right] \tilde{F}_{2}''(M,M') + \sin\left[(M-M')(\Omega t + \varphi)\right] \tilde{F}_{2}''(M,M')\right\}\right\}$$

$$+ \sin\left[(M-M')(\Omega t + \varphi)\right] \tilde{F}_{2}''(M,M')$$

$$\tilde{F}'_{1}(M,M') = -\frac{L_{e_{1}g_{1}}^{(M)}}{\left(L_{e_{1}g_{1}}^{(M)}\right)^{2} + 1} \sum_{e_{1},g_{1}} \sum_{p=\pm 1} \operatorname{Re} \chi^{pp'}(0) \left(\mu_{M,e_{1}g_{1}}^{p} p' q_{M',e_{1}g_{1}}^{p',*} - \mu_{M',e_{1}g_{1}}^{p',*} p q_{M,e_{1}g_{1}}^{p}\right) + \frac{1}{\left(L_{e_{1}g_{1}}^{(M)}\right)^{2} + 1} \sum_{e_{1},g_{1}} \sum_{p=\pm 1} \operatorname{Im} \chi^{pp'}(0) \left(\mu_{M,e_{1}g_{1}}^{p} p' q_{M',e_{1}g_{1}}^{p',*} - \mu_{M',e_{1}g_{1}}^{p',*} p q_{M,e_{1}g_{1}}^{p}\right) \tag{9a}$$

$$\tilde{F}_{1}'''(M,M') = \frac{L_{e_{1}g_{1}}^{(M)}}{\left(L_{e_{1}g_{1}}^{(M)}\right)^{2} + 1} \sum_{e_{1},g_{1}} \sum_{p=\pm 1} \operatorname{Im} \chi^{pp'}(0) \left(\mu_{M,e_{1}g_{1}}^{p} p' q_{M',e_{1}g_{1}}^{p'} - \mu_{M',e_{1}g_{1}}^{p'} p q_{M,e_{1}g_{1}}^{p}\right) + \frac{1}{\left(L_{e_{1}g_{1}}^{(M)}\right)^{2} + 1} \sum_{e_{1},g_{1}} \sum_{p=\pm 1} \operatorname{Re} \chi^{pp'}(0) \left(\mu_{M,e_{1}g_{1}}^{p} p' q_{M',e_{1}g_{1}}^{p'} - \mu_{M',e_{1}g_{1}}^{p'} p q_{M,e_{1}g_{1}}^{p}\right) \tag{9b}$$

$$\tilde{F}_{2}'(M,M') = -\frac{L_{e_{1}g_{1}}^{(M)}}{\left(L_{e_{1}g_{1}}^{(M)}\right)^{2} + 1} \sum_{e_{1},g_{1}} \sum_{p=\pm 1} \operatorname{Re} \chi^{pp'}(0) \left(\mu_{M,e_{1}g_{1}}^{p} p' q_{M',e_{1}g_{1}}^{p',\bullet} + \mu_{M',e_{1}g_{1}}^{p',\bullet} p q_{M,e_{1}g_{1}}^{p}\right) - \frac{1}{\left(L_{e_{1}g_{1}}^{(M)}\right)^{2} + 1} \sum_{e_{1},g_{1}} \sum_{p=\pm 1} \operatorname{Im} \chi^{pp'}(0) \left(\mu_{M,e_{1}g_{1}}^{p} p' q_{M',e_{1}g_{1}}^{p',\bullet} + \mu_{M',e_{1}g_{1}}^{p',\bullet} p q_{M,e_{1}g_{1}}^{p}\right) \tag{9c}$$

$$\tilde{F}_{2}'''(M,M') = -\frac{L_{\epsilon_{i}g_{1}}^{(M)}}{\left(L_{\epsilon_{i}g_{1}}^{(M)}\right)^{2} + 1} \sum_{\epsilon_{i},g_{1}} \sum_{p=\pm 1} \operatorname{Im} \chi^{pp'}(0) \left(\mu_{M,\epsilon_{i}g_{1}}^{p} p' q_{M',\epsilon_{i}g_{1}}^{p', \star} + \mu_{M',\epsilon_{i}g_{1}}^{p', \star} p q_{M,\epsilon_{i}g_{1}}^{p}\right) + \\
+ \frac{1}{\left(L_{\epsilon_{i}g_{1}}^{(M)}\right)^{2} + 1} \sum_{\epsilon_{i},g_{1}} \sum_{p=\pm 1} \operatorname{Re} \chi^{pp'}(0) \left(\mu_{M,\epsilon_{i}g_{1}}^{p} p' q_{M',\epsilon_{i}g_{1}}^{p', \star} + \mu_{M',\epsilon_{i}g_{1}}^{p', \star} p q_{M,\epsilon_{i}g_{1}}^{p}\right) \tag{9d}$$

The analyses concludes, that in general case we have only three harmonics with frequencies  $\Omega$ ,  $2\Omega$  and  $3\Omega$ . But in the cases of polarization gamma radiation, which we consider there is only  $2\Omega$ -harmonic. In according to Eq. (6) we can write:

$$F = s\delta \left( \sin(\alpha) \left\{ \sin[2(\Omega t + \varphi)] F_1'' + \cos[2(\Omega t + \varphi)] F_1' \right\} + \cos(\alpha) \left\{ \sin[2(\Omega t + \varphi)] F_2'' + \cos[2(\Omega t + \varphi)] F_2' \right\} \right)$$

$$(10)$$

Amplitude of  $\sin(\alpha)$  depends on factors  $F_1'$ ,  $F_1''$  and, respectively, amplitude of  $\cos(\alpha)$  depends on  $F_2'$ ,  $F_2''$ . As we can see (Figs. 1-4), factors  $F_1'$  and  $F_1''$  have a dispersion character, but factors  $F_2'$  and  $F_2''$  have a symmetrical character relative to the zero point of gamma spectrum. The complex different character of the behavior allows to in future pick out terms which are liable to T-nonivariance.

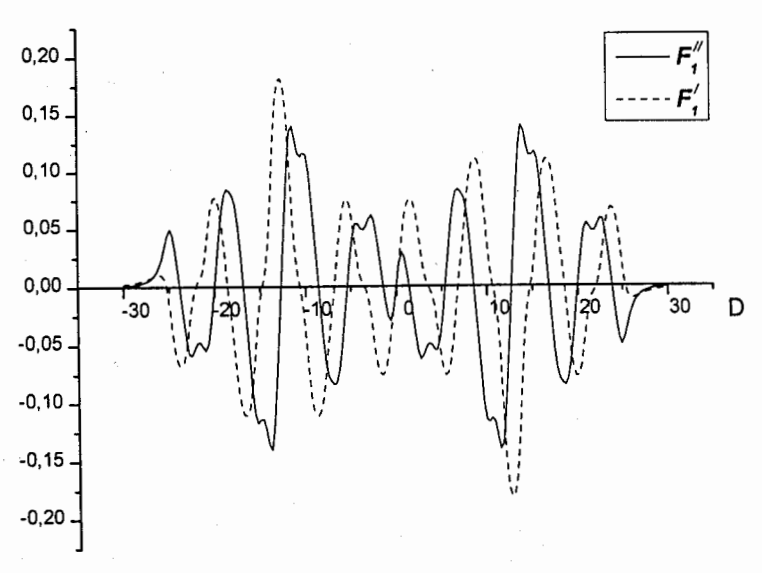


Figure 1. Amplitudes  $F'_1$  and  $F''_1$  in the case of natural polarization of gamma radiation.

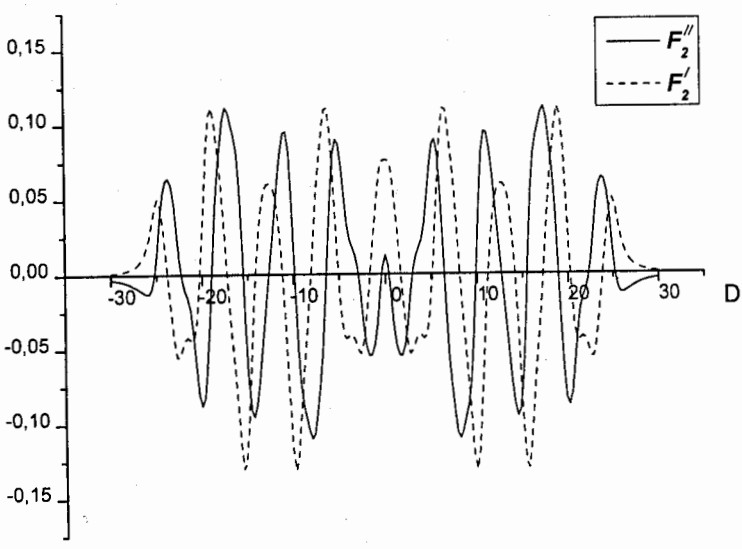


Figure 2. Amplitudes  $F_2'$  and  $F_2''$  in the case of natural polarization of gamma radiation.

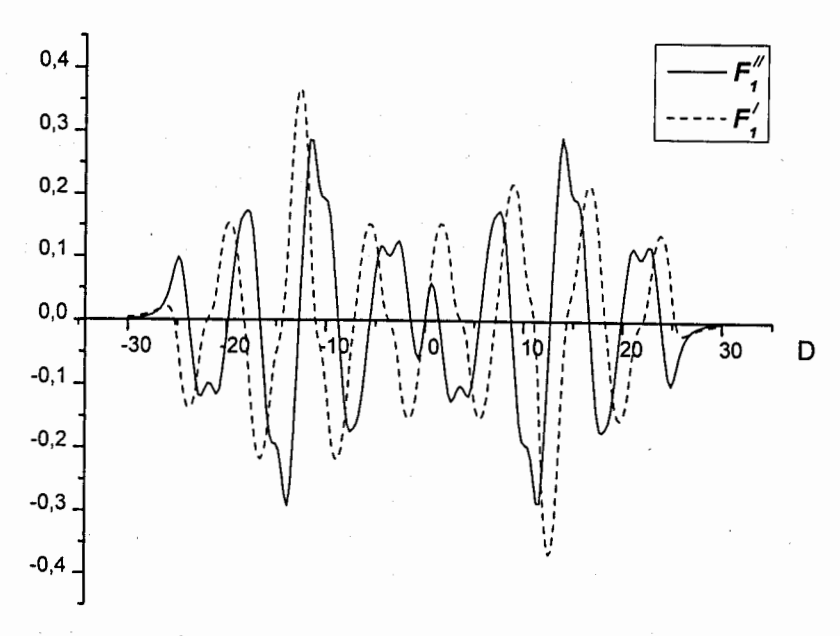


Figure 3. Amplitudes  $F_1'$  and  $F_1''$  in the case of linear polarization of gamma radiation transversely to the radiofrequency field.

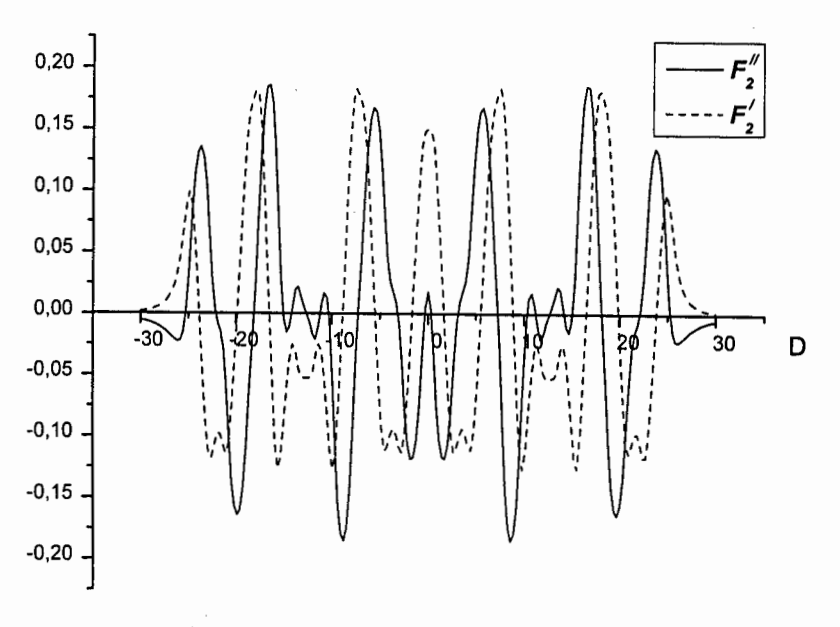


Figure 4. Amplitudes  $F_2'$  and  $F_2''$  in the case of linear polarization of gamma radiation transversely to the radiofrequency field.

#### 3. Conclusion

The offered method allows to combine phase temporal analysis with energy scanning. Thereby this method is more many-sided than the polarization scheme [3]. But this method has a number of difficulties of experimental character. Firstly, the stimulation of gamma magnetic resonance is carried out on the rather high frequency (70 MHz), and so the method of time-amplitude converter detection demands the nanosecond accuracy. The more suitable isomer with mixed valence is the object of future investigations.

#### References

- 1. J. Bernstein et al., Phys. Rev. 139, B1650 (1965).
- 2. O.C. Kistner, Phys. Rev. 144, 1022 (1966).
- 3. Blume and O.C. Kistner, Phys. Rev. 171, 417 (1968).
- 4. A.V. Mitin, In Proceedings of 5th Int. Conf. on Mössbauer Spectroscopy, Bratislava, Czechoslovakia, Part 3, p.615, 1973 (Praha, 1975).
- 5. A.V. Mitin, Phys. Lett. 84A, 278 (1981).
- 6. A.V. Mitin, V.Yu. Lubimov and E.K. Sadycov, JETP Lett. 81, 424 (2005).
- 7. A.V. Mitin, Doctoral Dissertation of Physics and Mathematics Sciences (Kazan, 1984), p.112.
- 8. A.V. Mitin, Phys. Stat. sol. **b53**, 93 (1972).

# RESONANT SCATTERING OF MÖSSBAUER PHOTONS UNDER THE CONDITIONS OF CONTROLLABLE QUANTUM INTERFERENCE

#### SADYKOV E.K., ARININ V.V., YURICHUK A.A.

Department of Physics, Kazan State University, Kremlyovskaya st. 18 Kazan, 420008, RUSSIA, esad@ksu.ru

#### VAGIZOV F.G.

Department of Physics, Kazan State University, Kremlyovskaya st. 18 Kazan, 420008, RUSSIA Department of Physics, Texas A&M University, College Station, TX, USA

In this report we focus on the Quantum Interference (QI) of gamma photons studied by the Mossbauer resonance scattering method. Actually this problem naturally arises in the investigation of the external control mechanisms of nuclear radiations. Undoubtedly the experimental observation of QI effects is a very important step towards solving the problems declared at this Workshop. That is why we consider various mechanisms and ways of preparation of a nuclear spin system in order to provide controlled QI. We propose the mechanism of state mixing under the "dynamical level-crossing" conditions in addition to well-known mechanisms of radiofrequency (RF) mixing of nuclear sublevels and mixing of states under the "level-crossing" conditions.

#### 1. Introduction

The interference - one of the basic principles of a quantum theory - displays itself in all microscopic physical processes. At the same time the specific conditions are needed the macroscopic consequences of interference in physical systems to be effective [1]. For example, such requirements are satisfied at Mossbauer scattering in the conditions of coherent dynamics of nuclear spin in resonant RF field. As will be shown below, QI leads to the redistribution of the elastic and Raman scattering intensities [2].

# 2. Resonant fluorescence of Mossbauer radiation in the regime of RF resonance in excited nuclear state.

Let's consider before three-level model system (Fig. 1a). The level 1 represents the ground state of the nucleus, and 2 and 3 - spin sublevels of the excited nuclear state. The strong RF field of frequency  $\omega_0$  ( $\omega_0 = \omega_{32} = \varepsilon_3 - \varepsilon_2$ ) is set up (in exact resonance to transition 2-3). The Mössbauer source radiation tuned (probably, with detuning) to

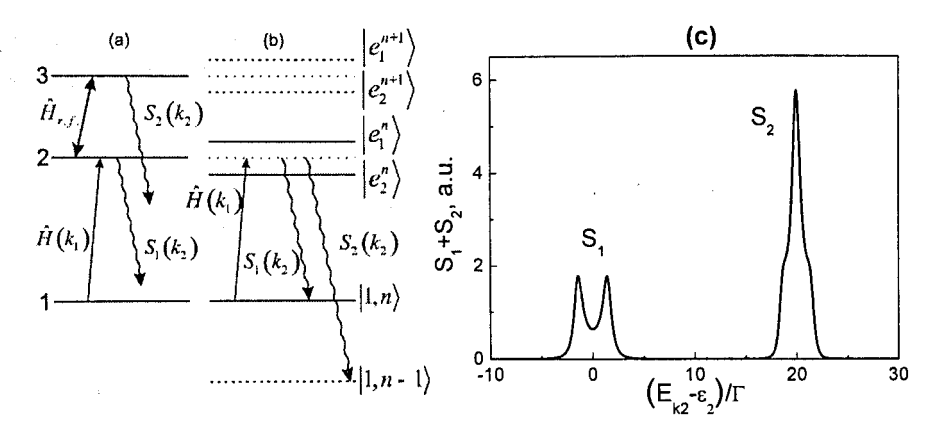


Fig.1. (a) Three-level model system; (b) Equivalent scheme using dressed states; (c) Expected spectra of resonant scattering ( $\Omega_r = 1.5$ ,  $\Gamma = 1$ ,  $E_{k0} = \varepsilon_2$  are used).

transition 1-2, and one may be considered as probe field. The Hamiltonian of such system looks as follows:

$$\hat{H} = \hat{H}_0 + \hat{H}_{r,f}^0 + \hat{H}_{r}^0 + \hat{H}_{r,f}^0 + \hat{H}_{r,f}^0 + \hat{H}_{r}(k), \tag{1}$$

where  $\hat{H}_0$  represents nuclear and hyperfine interactions,  $\hat{H}_{r,f}^0$  at  $\hat{H}_r^0$  - the operator of RF and gamma radiation fields,  $\hat{H}_{r,f}$  is  $\hat{H}_r(k)$  represent the nucleus interactions with RF field and with gamma quanta.

$$\hat{H}_0 = \sum_{i=1,3} \varepsilon_j a_j^{\dagger} a_j, \, \varepsilon_1 = 0; \, \hat{H}_{r,f}^0 = \omega_0 \hat{b}^{\dagger} \hat{b}; \quad \hat{H}_{\gamma}^0 = \sum_k \omega_k \hat{c}_k^{\dagger} \hat{c}_k \,, \tag{2}$$

$$\hat{H}_{r,f} = \Omega_0 \hat{b} \hat{a}_3^{\dagger} \hat{a}_2 + \Omega_0^{\dagger} \hat{b}^{\dagger} \hat{a}_2^{\dagger} \hat{a}_3, \tag{3}$$

$$\hat{H}_{\nu}(k) = A_{k}\hat{c}_{k}\hat{a}_{2}^{\dagger}\hat{a}_{1} + A_{k}^{\dagger}\hat{c}_{k}^{\dagger}\hat{a}_{1}^{\dagger}\hat{a}_{2}, \quad \omega_{k} = c_{0}k,$$
(4)

where  $\hat{a}_{j}^{+}$ ,  $\hat{a}_{j}$  and  $\varepsilon_{j}^{-}$  - creation and annihilation Fermi operators and energy of j-th state of H<sub>0</sub> (Fig.1a),  $\hat{b}^{+}$ ,  $\hat{b}$  and  $\hat{c}_{k}^{+}$ ,  $\hat{c}_{k}^{-}$  - creation and annihilation Bose operators of RF and gamma photon, respectively,  $A_{k}$   $\cup$   $\Omega_{0}$  - constants of interaction of gamma photon and RF photon with nucleus. Further we assume that  $\hbar=1$ ,  $c_{0}$  – velocity of light.

Let us consider first the pair of spin states interacting with strong RF field:

$$\sum_{j=2,3} \varepsilon_j \hat{a}_j^{\dagger} \hat{a}_j^{\dagger} + \omega_0 \hat{b}^{\dagger} \hat{b} + \Omega_0 \hat{a}_3^{\dagger} \hat{a}_2 \hat{b} + \Omega_0^{\dagger} \hat{a}_2^{\dagger} \hat{a}_3 \hat{b}^{\dagger}.$$
 (5)

The eigenstates of this Hamiltonian  $e_q^n(t)$ , q=1,2 are well known as dressed states [1]. The explicit expressions for  $e_q^n(t)$  are given below through basic states of  $\hat{H}_0$ ,  $\hat{H}_{r,f}^0$  for conditions of exact resonance:

$$e_1^n(t) = \exp\left(-iE_1^n t - in\omega_0 t\right) \frac{1}{\sqrt{2}} \left(-|2,n\rangle + \exp(i\varphi)|3,n-1\rangle\right),\tag{6}$$

$$e_2^n(t) = \exp\left(-iE_2^n t - in\omega_0 t\right) \frac{1}{\sqrt{2}} \left(\exp\left(-i\varphi\right) | 2, n\rangle + |3, n-1\rangle\right),\tag{7}$$

where  $|j,n\rangle = |j\rangle |n\rangle$ ,  $|n\rangle$  - n - photon state of RF field,  $\varphi$  - is defined by equality  $\Omega_0 = |\Omega_0| \exp(i\varphi)$ .

The states (6) and (7) can be classified also as quasienergy states [3] (steady states [4]). It means that time dependence of these states satisfies to relation:

$$e_q^n(t) = \exp\left(-iE_q^n t\right) \chi_q^n(t), \ \chi_q^n(t+T) = \chi_q^n(t), \tag{8}$$

where  $T = 2\pi/\omega_0$  - period of RF field,  $E_{1,2}^n = \mp |\Omega_0| \sqrt{n} + \varepsilon_2$  - quasienergy,  $|\Omega_0| \sqrt{n}$  - Rabi frequency. Classical RF field may be represented by coherent state [5] as linear combination of Fock states  $|\alpha\rangle = \exp(-|\alpha|^2/2) \sum_{n=0}^{\infty} \frac{\alpha^2}{\sqrt{n!}} |n\rangle$ , where  $|\alpha| = \overline{n} = \sum_{n=1}^{\infty} nP(n)$  is large. The Poisson's distribution P(n) describes the population of Fock states  $|n\rangle$  and it has sharp maximum at  $n \approx \overline{n}$ . In this case we can describe the effect of classical RF field on spin states by expressions (6) and (7) with a high degree of accuracy when  $n \approx \overline{n}$ .

Further we will use scattering amplitudes as second order perturbation on interaction  $\hat{H}(k)$  [6]. The "dressed" states are used as basic states. The exact account of RF influence is achieved by using of the "dressed" states.

$$A_{i,f} \sim \sum_{q} \int_{0}^{\infty} dt \exp(-\Gamma t/2) \langle f(t) | \hat{H}_{r}(\vec{k}_{2}) | e_{q}^{n}(t) \rangle \langle e_{q}^{n}(0) | \hat{H}_{r}(\vec{k}_{1}) | i(0) \rangle, \quad (9)$$

where  $\Gamma$  – natural width of Mossbauer level,  $|i(0)\rangle = |i(t=0)\rangle = |1\rangle |n\rangle |k_1\rangle$  and  $|f(t)\rangle = \exp(-iE_f t)|1\rangle |n'\rangle |k_2\rangle$  - initial and final states of system, with total energies  $E_i = \varepsilon_1 + n\omega_0 + E_{k1}$  and  $E_f = \varepsilon_1 + n'\omega_0 + E_{k2}$ ,  $k_1$  and  $k_2$  are wave vectors of incident and scattered gamma quantum.

The probability of Mossbauer scattering is described by following expression:

$$S_{i,f} \sim \int dE_{k_i} |A_{i,f}|^2 \delta(E_f - E_i) f_L(E_{k_i} - E_{k_0}). \tag{10}$$

In this expression energy conservation law for whole system is taken into consideration and averaging over photon energies from Mossbauer source  $E_{k1}$  is curried out using line form function (ordinary of Lorenth type)  $f_L(E_{k1} - E_{k0})$ . Here  $E_{k0}$  - is energy of source corresponding to maximum of this function.

In Fig.1b the scheme of resonant scattering of photons in dressed states representation at  $E_{k0} = \varepsilon_2$  is presented. We shall consider transitions (9) with n' = n and n' = n - 1 corresponding to elastic scattering  $(S_1)$  and Raman scattering  $(S_2)$ . The following transition amplitudes describe these two processes:

$$A_{\ln k_2, \ln k_1} \sim \sum_{q} \int_{0}^{\infty} dt \left\langle 1, n, k_2 \left| \hat{H}\left(\vec{k}_2\right) \right| e_q^n(t) \right\rangle \left\langle e_q^n(0) \left| \hat{H}\left(\vec{k}_1\right) \right| 1, n, k_1 \right\rangle e^{iE_{k2}t + in\omega_0 t - \Gamma t/2}, \tag{11}$$

$$A_{1nk_{1},1(n-1)k_{2}} \sim \sum_{q} \int_{0}^{\infty} dt \langle 1, n-1, k_{2} | \hat{H}(\vec{k}_{2}) | e_{q}^{n}(t) \rangle \langle e_{q}^{n}(0) | \hat{H}(\vec{k}_{1}) | 1, n, k_{1} \rangle e^{-\Gamma t/2 + iE_{k2}t + i(n-1)\omega_{0}t}.$$
(12)

Substituting amplitudes of (11) and (12) in (10) and making executed integration on energy of an initial photon, we have spectral forms of elastic and Raman scattering (at  $E_{k0} = \varepsilon_2$ ).

$$S_{1}(k_{2}) = S_{k_{1n,k_{2n}}} - \left| \frac{1}{ip - \Omega_{r}} + \frac{1}{ip + \Omega_{r}} \right|^{2} f_{L}(E_{k_{2}} - \varepsilon_{2}) \left| \langle 1 | \hat{H}(k_{2}) | 2 \rangle \langle 2 | \hat{H}(k_{1}) | 1 \rangle \right|^{2}, \quad (13)$$

$$S_{2}(k_{2}) = S_{k_{1n,k_{2n-1}}} - \left| \frac{1}{ip - \Omega_{r} - \omega_{0}} - \frac{1}{ip + \Omega_{r} - \omega_{0}} \right|^{2} \times , \quad (14)$$

$$\times f_{L}(E_{k_{2}} - \varepsilon_{2} - \omega_{0}) \left| \langle 1 | \hat{H}(k_{2}) | 3 \rangle \langle 2 | \hat{H}(k_{1}) | 1 \rangle \right|^{2}$$

$$p = -i(E_{k2} - \varepsilon_2) + \Gamma/2$$
,  $\Omega_r = |\Omega_0|\sqrt{\overline{n}}$  - Rabi frequency of RF field.

In Fig.1c the expected spectrum  $S_1(k_2) + S_2(k_2)$  under the assumption that matrix elements of transitions 1-2 and 1-3 are equal is presented. It is easy to see that in the (13) and (14) expressions the interference has constructive and destructive character at small values of  $\Omega_r$ . In particular,  $S_2$  tends to zero as  $\Omega_r$  tends to zero. However with growth of  $\Omega_r$  (namely at  $\Omega_r > \Gamma/2$ ) the character of the interference in the (13) and (14) expressions under the same conditions ( $E_{k0} = \varepsilon_2$ ) is reversed. Now, at enough large values of  $\Omega_r$  the intensity of Raman line becomes more than the intensity of the elastic scattering line. The ratio of line intensities is defined as  $I_2/I_1$  where  $I_2$  and  $I_1$  - the areas under lines  $S_2$  and  $S_1$ . The dependence  $I_2/I_1$  versus  $\Omega_r$  is shown in Fig.2a. When the value  $I_2/I_1$  exceeds unit (it means that in conditions under discussion the nucleus excited to sublevel 2 prefers to emit gamma photon from a level 3) the Raman scattering instead of the elastic scattering takes place. Such preference in a nuclear

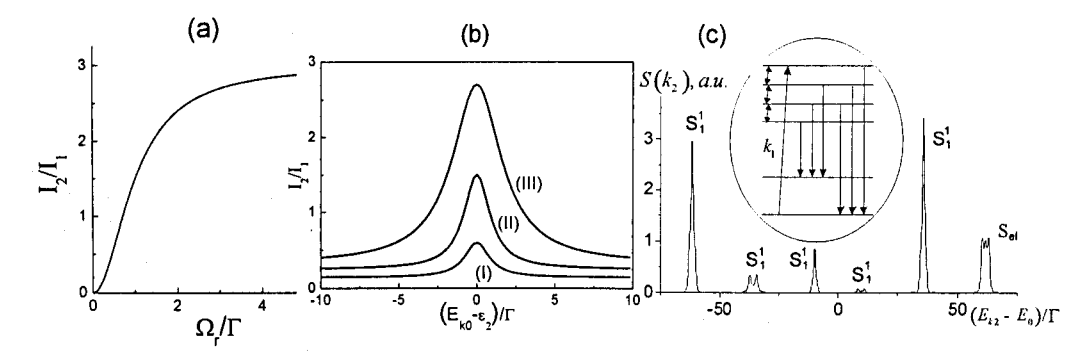


Fig.2. a) Ratio of line intensities; b) (I)  $\Omega_r = 0.5$ ; (II)  $\Omega_r = 1$ ; (III)  $\Omega_r = 3$ ; c) Expected spectrum of resonant scattering on isotope Fe<sup>57</sup> in condition of the RF resonance on excited nuclear state; E<sub>0</sub>-the energy of Mossbauer level. The probing Mossbauer line is tuned to the sixth line of the Zeeman sextet, S<sub>el</sub> - the line of elastic scattering,  $(S_1^1, S_1^2)$ ,  $(S_2^1, S_2^2)$  and  $S_3$  - Raman lines of the first, second and third order respectively.

scattering channel has been named by us as "valve" effect (intuitively the relation  $I_2/I_1$  should asymptotically tend to unit with growth of  $\Omega$ , ). This result indicates that at enough large values of  $\Omega$ , the intensity of the elastic scattering decreases because of destructive interferences of amplitudes (at the same time the Raman intensity increases as a result of a constructive interference). The effect of the interference is maximal at  $E_{k0} = \varepsilon_2$ , in this case interfering terms in (13) and (14) are comparable in value. The detuning of equality  $E_{k0} = \varepsilon_2$  decreases the "valve" effect value, and the dependence of  $\left(I_2/I_1\right)$  versus the probe photon energy,  $E_{k0}$ , has resonant character (Fig.2b).

The "valve" effect value monotonously depends on value  $\Omega_r/\Gamma$ , as it is shown in Fig.2a. However, when the  $\Omega_r/\Gamma$  increases the total intensity of scattering  $(I_1+I_2)$  quickly decreases. It is worth noting that first of all this circumstance must be taken into account at experimental realization of this effect. Thus, the optimal condition of experiment looks as  $\Omega_r \sim \Gamma$ . This is a condition of the phase-correlated excitation by one photon of two dressed states, which interference underlies the phenomenon under discussion.

Let us now consider the scheme with number of levels more than three suitable for isotope  $Fe^{57}$ . In this case there is a necessity to take into account that the intensities of hyperfine Mossbauer transitions are different and have various angular dependences. It is worth to note that the "valve" effect will take place even this case, if driving field mixes sublevels of the excited state of a nucleus. The intensity of elastic scattering will be reduced (at  $\Omega_r > \Gamma/2$ ) due to destructive interference. The intensity of Raman lines increases, if the odd number of RF photons participates in forming of the Raman line and decreases at even number of photons. In Fig.2c the expected effect for isotope  $Fe^{57}$  is presented.

Next, we shall discuss what is the relation between the effect under discussion and other RF effects in Mossbauer spectroscopy described earlier [7,8]. The purpose of the first works in this field has consisted in study of quasienergy structures of the Mossbauer spectra, proposed for the first time in work [7]. Such structure in absorption spectra was observed in works [9] and [10]. These experiments have the direct relation to QI effect discussed here. The possibility to observe by Mossbauer effect the coherent nuclear spin dynamics (for isotope Fe<sup>57</sup>) in magnetic materials has been shown in these works. One is the main condition for realization of the effect discussed above. Moreover the results of works [9] and [10] have showed, that values of Rabi frequencies necessary for observing the "valve" effect can be realized in case of isotope Fe<sup>57</sup> in magnetically ordered systems. From experimental spectra [9] it is easy to estimate the amplitude of RF hyperfine field induced on a nucleus as  $h_1 = 88 \text{ kOe}$ , one corresponds to Rabi frequency  $\Omega_r = 1.5$  used in Fig.2c.

Let's note that in Mossbauer absorption spectra (at least, in approach of a thin absorber) there is not a reason to expect the QI effects for the given (RF) mechanism of excitation. Indeed, according to the optical theorem, the absorption cross section is represented as an imaginary part of forward scattering amplitude, and the absorption spectrum depends linearly (instead of quadratic dependence) on amplitude of scattering and an interference between the split amplitudes does not arise. Therefore in works [7,8] the QI effect could not appear. As to early theories of resonant scattering of Mossbauer radiation in the regime of RF nuclear spin dynamics [6,11,12], the QI effects were not accented in them.

# 3. Resonant fluorescence of Mossbauer radiation in the conditions of nuclei spin levels anticrossing.

Effects considered above arise due to the mixing of basis states 2 and 3 by RF field (see (6) and (7)). Analogous mixing of the states takes place also in conditions of level crossing if there is a small static interaction between crossing levels. For example, at simultaneous action of Zeeman and axial quadrupole hyperfine interactions the crossing states  $|-3/2\rangle$  and  $|1/2\rangle$  (Fe<sup>57</sup>, see Fig.3a) may be mixed by small nonaxial quadrupole interaction [13]. As a result we have new linear combinations of these states:  $\Psi_1 = \left(\left|-3/2\right\rangle + \left|1/2\right\rangle\right)/\sqrt{2} = \left(\left|M_1\right\rangle + \left|M_2\right\rangle\right)/\sqrt{2}$ , and  $\Psi_2 = \left(\left|-3/2\right\rangle - \left|1/2\right\rangle\right)/\sqrt{2} = \left(\left|M_1\right\rangle - \left|M_2\right\rangle\right)/\sqrt{2}$  which have different energies  $E_{1,2} = E_c \pm \Delta$  at a "crossing" point ("anticrossing" effect, Fig.3b). Here  $E_c$ —energy of the "crossing" point,  $\Delta$ —the shift of energy depending on mixing parameter. It may be shown easily that the effects of quantum interference in resonant scattering spectra are possible also in this case.

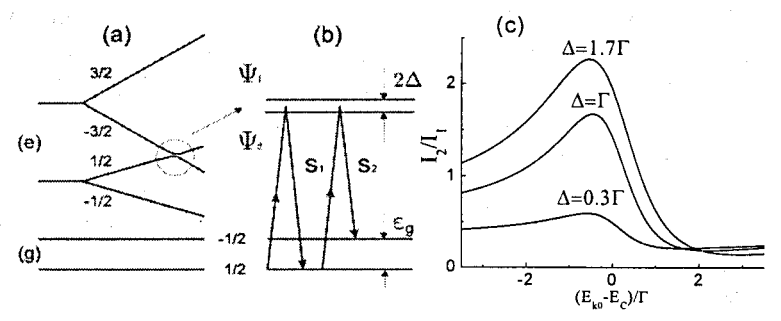


Fig. 3. (a) Level anticrossing scheme; (b) Equivalent scheme using mixed states; (c)  $I_2/I_1$  versus the initial quantum energy.

Let's consider scattering process, which starts from the ground state  $m_1 = |1/2\rangle$ , as the simplest case (Fig.3b). The amplitude of resonance scattering looks analogous to (9). For the elastic scattering channel we have:

$$A_{m_1 \to m_1} \sim i \langle m_1 | \hat{H}_{\gamma}(k_2) | M_2 \rangle \langle M_2 | \hat{H}_{\gamma}(k_1) | m_1 \rangle \left( \frac{1}{ip' + \Delta} + \frac{1}{ip' - \Delta} \right). \tag{15}$$

For inelastic channel (which is ended on a sublevel  $m_2 = |-1/2\rangle$ ) we have:

$$A_{m_{1} \to m_{2}} \sim i \langle m_{2} | \hat{H}_{y}(k_{2}) | M_{1} \rangle \langle M_{2} | \hat{H}_{y}(k_{1}) | m_{1} \rangle \left( \frac{1}{i p' + \Delta + \varepsilon_{g}} - \frac{1}{i p' - \Delta + \varepsilon_{g}} \right) + ,$$

$$+ i \langle m_{2} | \hat{H}_{y}(k_{2}) | M_{2} \rangle \langle M_{2} | \hat{H}_{y}(k_{1}) | m_{1} \rangle \left( \frac{1}{i p' - \Delta + \varepsilon_{g}} + \frac{1}{i p' - \Delta + \varepsilon_{g}} \right)$$

$$(16)$$

here  $\varepsilon_g$  — splitting of a ground state of a nucleus,  $p' = -i(E_{\vec{k}_2} - E_c) + \Gamma/2$ .

Probabilities of scattering are given by formula (10) of previous section:

$$S_1 \sim \sum_{\sigma_1, \sigma_2} \left| A_{m_1 \to m_1} \right|^2 f_L \left( E_{k_2} - E_c \right),$$
 (17)

$$S_2 \sim \sum_{\sigma_1, \sigma_2} \left| A_{m_1 \to m_2} \right|^2 f_L \left( E_{k_2} - E_c + \varepsilon_g \right)$$
 (18)

for a elastic scattering and for inelastic one. We note, that the averaging over polarization is supposed in (17) and (18) for unpolarized Mossbauer source.

The amplitude (15), as well as in a case (13) reduces due to destructive interference for a line  $S_1$  (for  $\Delta > \Gamma/2$ ) while expression (16) displays both destructive and constructive interference.

The ratio of inelastic and elastic line intensities  $I_2/I_1$  may be considered as a measure of quantum interference again. The dependence of this ratio versus the initial quantum energy for different values of  $\Delta$  is presented in Fig.3c. The asymmetry of this curve is explained by different type (constructive and destructive) of interference terms in the amplitude of inelastic scattering. The dependence of  $I_2/I_1$  versus the splitting  $\Delta$  (Fig.3c) behaves analogously to a case of the RF mixing (it increases monotonically with the increasing  $\Delta$ ). The dependence of total scattering intensity  $(I_1 + I_2)$  versus  $\Delta$  is completely analogous to the RF mixing case, i.e. this sum quickly decreases with the increasing  $\Delta$ .

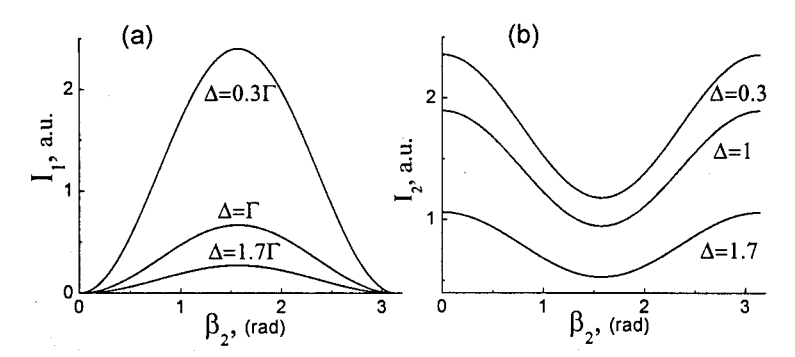


Fig. 4. Angular dependence of intensities for (a) elastic line  $I_1$  and (b) inelastic line  $I_2$ .

Unlike to the preceding three-level abstract example, in this "anticrossing" case we deal with concrete nucleus Fe<sup>57</sup>, and that is why the angular dependence of the matrix elements  $\langle m_i | H_{\gamma}(k_i) | M_l \rangle$  must be taken into consideration. The ratio of intensities  $I_2 / I_1$  depends only on a direction of scattered gamma photons (angle  $\beta_2$ ). One does not depend on the direction of absorbed quantum (angle  $\beta_1$ ). The intensities of lines  $I_1$  and  $I_2$  as functions of  $\beta_2$  are shown in Fig.4.

# 4. "Dynamical" anticrossing.

Let's return to RF dynamics of Mossbauer spins. Now we will consider the nonresonant RF fields with the amplitude comparable or larger than the external constant magnetic field. The hyperfine field in this case (we mean Mössbauer atoms in magnetic material) consists of constant field and alternating field with large amplitude. One of the interesting situations is the case when there is no constant field and the hyperfine field is rotating as whole in plane. The nuclear spin wave functions (quasienergy states (QS)) now look as [14] (we mean further  $^{57}$ Fe and  $\omega_0^I=0$ ):

$$\Psi_{M'} = e^{-iE_{M'}t} \sum_{M=-3/2}^{3/2} d_{MM}^{3/2} (\beta_{3/2}) |3/2, M\rangle \exp[i(M-M')\omega t - iM\psi], \qquad (19)$$

$$E_{M'} = -\omega M' - M' \left( \left( \omega_0^I - \omega \right)^2 + \left( \omega_1^I \right)^2 \right)^{1/2}, \quad \beta_I = arctg \left[ \omega_1^I / \left( \omega_0^I + \omega \right) \right], \quad I - \text{nuclear spin, } \omega_I^I$$

and  $\omega_0^I$  - Larmour frequencies corresponding to alternating (RF) and constant parts of hyperfine field, M', M - magnetic quantum numbers in rotating and laboratory systems, respectively,  $\psi$  - phase of RF field.

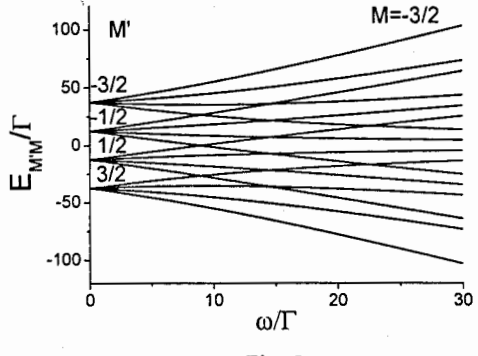
We can see from (19) that each QS identified by M' is a linear combination of basic (Zeeman) substates M with different time-dependent exponents. In the Fig.5 the energy parameters of the whole set of QS  $E_{M'M} = E_{M'} + \omega (M' - M)$  are shown as functions of field rotation frequency  $\omega$ . There are level-crossing points of different types: 1) at frequency satisfying  $3\omega = \sqrt{\omega_1^2 + \omega}$  in laboratory system (with transition rules  $\Delta M' = \pm 1$  and  $\Delta M = \pm 3$ ); 2) at  $2\omega = \sqrt{\omega_1^2 + \omega}$  ( $\Delta M' = \pm 1$  and  $\Delta M = \pm 2$ ); 3) at  $3\omega = 2\sqrt{\omega_1^2 + \omega}$  ( $\Delta M' = \pm 2$ ). The crossing point frequencies may be interpreted as resonance conditions in rotating laboratory system.

In context of this paper, the level crossing in rotating field is of interest as a model leading to dynamical anticrossing effect in analogy with the static anticrossing effect considered above. The question is, is there any perturbation, which leads to the anticrossing effect in this case? It may be easily shown that in case 2) the non-axial quadrupole interaction  $H_{\delta} = \delta(\hat{I}_{+}^2 + \hat{I}_{-}^2)$  may serve as such small perturbation. The problem is solved using the perturbation theory for a degenerate case (at crossing frequencies). One needs to diagonalize the matrix consisting of elements which have to be calculated in the space of periodic functions (in composite Gilbert space).

$$\left\langle \left\langle \Psi_{M^{*}}(\vec{r},t)H_{\delta}\Psi_{M^{*}}(\vec{r},t)\right\rangle \right\rangle \equiv \left(\frac{1}{T}\right)\int_{-T/2}^{T/2} \int \Psi_{M^{*}}(\vec{r},t)H_{\delta}\Psi_{M^{*}}(\vec{r},t)d\vec{r}dt, \qquad (20)$$

T is the period of RF field.

The calculation of matrix elements must be curried out at values of QS parameters corresponding to the crossing point of second type:  $\omega_0 = 0$ ,  $\omega = \omega_1/\sqrt{3}$ , a  $\beta_{3/2} = \pi/3$ . So, we have:



$$\left\langle \left\langle \Psi_{M_{1}}\left(\vec{r},t\right)H_{\delta}\Psi_{M_{2}}\left(\vec{r},t\right)\right\rangle \right\rangle =$$

$$=\begin{bmatrix}
0 & \frac{3}{4}\delta & 0 & 0 \\
\frac{3}{4}\delta & 0 & 0 & 0 \\
0 & 0 & 0 & \frac{3}{4}\delta \\
0 & 0 & \frac{3}{4}\delta & 0
\end{bmatrix} . (21)$$

New eigenstates (and energies) are:

$$\begin{split} \Psi_{1}' &= e^{-i\frac{3\delta}{4}t} \left( \Psi_{-1/2} - \Psi_{-3/2} \right), \quad \Psi_{2}' &= e^{i\frac{3\delta}{4}t} \left( \Psi_{-1/2} + \Psi_{-3/2} \right), \\ \Psi_{3}' &= e^{i\frac{3\delta}{4}t} \left( \Psi_{3/2} - \Psi_{1/2} \right), \quad \Psi_{4}' &= e^{-i\frac{3\delta}{4}t} \left( \Psi_{3/2} + \Psi_{1/2} \right). \end{split} \tag{22}$$

It must be noted that in all expressions (22) only the crossing substates are mixing. In this case the state  $\Psi'_i$  includes the linear combination of the crossing substates multiplied by common time exponent. All other terms in  $\Psi'_i$  are the linear combinations of the substates oscillating with different frequencies. In this case the influence of  $H_{\delta}$  is negligible.

We see from (21) that the anticrossing of QS pairs ( $\Psi_{-3/2}$  with  $\Psi_{-1/2}$  and  $\Psi_{3/2}$  with  $\Psi_{1/2}$ ) is possible. In each case we have two new functions  $\Psi'_i$  with close energies. So, the possibility of exciting of these two states by single quantum in phase correlated way may be realized in this case again. At the same time the anticrossing of  $\Psi_{-1/2}$  with  $\Psi_{1/2}$  is not possible.

The peculiarities discussed for the scheme of resonant scattering of gamma - photons are equally valid for a spontaneous emission of nucleus in above mentioned conditions if the another method of phase correlated "population" of excited states is used instead of initial gamma quantum.

### Acknowledgments

Work supported by grants RFBR №04-02-16939, CRDF CGP RP1-2560-KA-03 and NIOKR RT 06-6.1-2003/2005(F).

#### References

- 1. M.O. Scully, M.S. Zubairy, Quantum Optics, Cambridge University Press, 1997.
- 2. E.K. Sadykov, A.A. Arinin, F.G. Vagizov, JETP Lett. (2005) (accepted).
- 3. H. Sambe, Phys. Rev. A7, 2203 (1973).
- 4. Jon H. Shirley, Phys. Rev. 138, B979 (1965).
- 5. Ya. Perina, Coherence of the light, MIR Press, Moscow (1974).
- Sh.Sh. Bashkirov, A.L. Beljanin, E.K. Sadykov, Phys. Status Solidi (b) 93, 437 (1979).
- 7. M.N. Hack, M. Hammermesh, Nuovo Cimento 19, 546 (1961).
- 8. H. Gabriel, Phys. Rev. 184, 359 (1969).
- 9 F.G. Vagizov, Hyp. Int. 61, 1359 (1990).
- 10. I. Tittonen, M. Lippmaa, E. Ikonen et al, Phys. Rev. Lett. 69, 2815 (1992).
- 11. A.M. Afanasev, P.A. Alexandrov, S.S. Yakimov, Preprint of Atom Energy Institute, #3337/9, 24 (1980).
- 12. A.V. Mitin, Phys. Lett. 84A, 283 (1981).
- 13. R. Coussement and G. Neyens, Hyp. Int. 107, 307 (1997).
- F.G. Vagizov, R.A. Manapov, E.K. Sadykov, L.L. Zakirov, Hyp.Int., 116, (1998) 91.

# **AUTHOR INDEX**

A.J., T. 60	T.i. 3.6 45 01
Adam, J. 68	Litz, M. 45, 91
Agee, F. J. 9	L'vov, D.V. 191
Alpatov, V.G. 191	Liesfeld, B. 162
Aléonard, M.M. 162	Matsuura, A.Y. 9,
Aniskin, I.P. 206	Matthies, A. 110
Arinin, V.V. 213	Malka, G. 162
Bayukov, Yu.D. 191	Mazur, V. M. 105
Bigan, Z. M. 105	McDaniel, P. 99
Blasco, F. 162	Merkel, G. 45, 91
Carroll, J. J. 15, 45, 56, 68, 85, 91	Méot, V. 153, 162
Chemin, J.F. 162	Mitin, A.V. 206
Claverie, G. 162	Morel, P. 153, 162
Collins, C.B. 99	Olariu, S. 181
Davydov, A.V. 191	Pereira, N.R. 91
Descamps, D. 162	Propri, R. 56
Dorchies, F. 162	Pouvesle, J.M. 99
Dzyublik, A.Ya. 145	Ratis, Yu.L. 130
Fedosejevs, R. 162	Rivlin, L.A. 23
Fourment, C. 162	Robson, L. 162
Gareev, F.A. 130	Roberts, H. 45
Gerbaux, M. 162	Rusanov, A.A. 171
Gordienko, V.M. 171	Sadykov, E.K. 213
Gobet, F. 162	Santos, J.J. 162
Gohlke, D. 56	Savel'ev, A.B. 171
Gosselin, G. 153	Samartsev, V.V. 35,
Gogny, D. 153	Scheurer, J.N. 162
Hannachi, F. 162	Shabalin, E. P. 68
Hanvey, S. 162	Simochko, D. M. 105
Helba, M. 45	Strilchuk, N.V. 99
Isaev, Yu.N. 191	Tarisien, M. 162
Izosimov, I.N. 115	Tkalya, E.V. 65
Karamian, S. A. 56, 68, 85	Trifonov, P. N. 105
	Trzhaskovskaya, M.B. 121
Kalachev, A.A. 35	- · · · · · · · · · · · · · · · · · · ·
Kamanin, D.V. 110	Uryupina, D.S. 171
Karpeshin, F.F. 121	Vagizov, F.G. 181, 213
Kartashov, G.R. 191	Volkov, R.V. 171
Kirischuk, V.I. 99, 105	Younes, W. 153
Kolesov, R. 181, 200	Yurichuk, A.A. 213
Kocharovskaya, O. 181	Zadernovsky, A.A. 27
Korotkov, M.M. 191	Zheltonozhsky, V.A. 99, 105
Kulagin, E. N. 68	Zhidkova, I.E. 130
Lachko, L.M. 171	And the second second

## Научное издание

## **Isomers and Quantum Nucleonics**

Proceedings of the 7th AFOSR Workshop

## Изомеры и квантовая нуклеоника

Труды 7-го рабочего совещания

E15,18-2006-24

Сборник отпечатан методом прямого репродуцирования с оригиналов, предоставленных оргкомитетом.

Ответственные за подготовку сборника к печати С. А. Карамян, Е. А. Черепанов.

Получено 17.02.2006. Подписано в печать 27.03.2006. Формат 70 × 100/16. Бумага офсетная. Печать офсетная. Усл. печ. л. 18,2. Уч.-изд. л. 21,02. Тираж 200 экз. Заказ № 55268.

Издательский отдел Объединенного института ядерных исследований 141980, г. Дубна, Московская обл., ул. Жолио-Кюри, 6. E-mail: publish@pds.jinr.ru www.jinr.ru/publish/